Effects of Electrode Rotation and Co-reactant Identity on Electrogenerated Chemiluminescence

Submitted by

Noah Kebede

Bachelor of Forensic Science (Hons)

A thesis submitted in total fulfilment

of the requirements for the degree of

Doctor of Philosophy

Department of Chemistry and Physics

School of Molecular Sciences

College of Science, Health and Engineering

La Trobe University

Victoria, Australia

January 2020

Contents

Abstract

The work in this thesis explores both fundamental and applied aspects of electrochemiluminescence (ECL). Chapter 1 presents an outline of the background theory relating to ECL and surveys the literature relevant to the thesis. In chapter 2, a series of aliphatic tertiary amines (HEPES, POPSO, EPPS and BIS-TRIS) commonly used to buffer the pH in biological experiments, were examined as alternative, non-toxic co-reactants for the electrogenerated chemiluminescence (ECL) of tris(2,2′-bipyridine)ruthenium(II) ($[Ru(bpy)_3]^{2+}$). These were found to be very attractive as "multi-tasking" reagents, serving not only as co-reactants, but also fulfilling the roles of pH buffer and supporting electrolyte thus significantly simplifying the overall ECL analysis. Sub-nanomolar detection limits were obtained for $[Ru(bpy)_3]^{2+}$ in the presence of BIS-TRIS, making this species a valuable option for co-reactant ECL-based bioanalytical applications.

Chapters 3 and 4 explored more fundamental aspects of co-reactant and annihilation ECL respectively, looking at the effects of electrode rotation on several co-reactant and annihilation ECL systems. These studies uncovered a novel "critical rotation rate" phenomenon in systems in organic media, where an increase in current and ECL intensities was observed as the rotation rate increased until a certain rotation rate was reached (the critical RPM). At rates faster than this critical RPM, a decrease of ECL intensities (both co-reactant and annihilation) was observed even though the currents generated from these systems continued to increase. These unusual results were interpreted as reflecting the kinetics of the ECL reaction under study and it was shown that the critical RPM could be used to estimate the rate constant for the homogeneous electron transfer reaction leading to the excited state, in some cases. Tuneable multiplexed emission from the $Ru(bpy)_3(PF)_6$/$Ir(ppy)_3$ annihilation ECL system was also demonstrated using a RRDE for the first time.

Statement of Authorship

Except where reference is made in the text of the thesis, this thesis contains no material published elsewhere or extracted in whole or in part from a thesis accepted for the award of any other degree or diploma. No other person's work has been used without due acknowledgment in the main text of the thesis. This thesis has not been submitted for the award of any degree or diploma in any other tertiary institution.

This work was supported by an Australian Government Research Training Program Scholarship.

Signature 

Noah Kebede

14 January 2020

Publications

N. Kebede, P. S. Francis, G. J. Barbante and C. F. Hogan, ***Electrogenerated chemiluminescence of tris(2,2' bipyridine)ruthenium(II) using common biological buffers as co-reactant, pH buffer and supporting electrolyte.*** Analyst, **2015**, 140, 7142–7145

Acknowledgements

I would firstly like to thank my supervisor, Assoc. Prof. Conor Hogan for all of the support and guidance you have provided me throughout my entire candidature. Thank you for your patience and understanding, even at times where I may or may not be deserving of it. Thank you for nurturing me and allowing me to grow not only as an analytical scientist but as a leader within a group of very talented scientists. Thank you for the opportunity to travel around Australia and the world presenting my work and providing some life experiences and lessons I will never forget. Without you, I would not be the scientist I am today. Thank you for believing in me.

I would also like to thank my co-supervisor Prof. Paul Francis and Deakin University. Without the combined efforts of Conor, Paul, La Trobe University and Deakin University, I would never have the funding available to me to even partake in a PhD. A special thanks to Dr Gregory Barbante. We first met when I was a starry eyed honours student in Deakin University. You convinced me to go further beyond and apply for a PhD candidature. You helped me through my honours project and you helped me through the latter stages of my candidature after I returned from medical setbacks and surgery. Thank you to Darryl Huntington and Robert Polglase for helping engineer modifications to my custom built faraday cage and custom built Teflon RRDE cell lid.

To my fellow students in the chemistry department, especially my fellow Hogan Heroes, thank you for always being there to lend me a helping hand in the lab or answer all my stupid questions (and yes there were some really stupid ones) and just making me feel as I was a part of the family. To my fellow Hogan Heroes, both past and present, I am so thankful that I was able to spend some of the most enjoyable years of my career with so many wonderful and intelligent people. I had a hell of a lot of fun and I hope you guys did to.

Lastly I would like to thank my friends and family, especially my Mum and Dad. You were there from the moment of my existence, showering me with unconditional love and support. I can never thank you enough for the sacrifices that the two of you have made in the name of making my life a better one. I'm extremely lucky and proud to have parents like you. Even though the vast majority of my friends and family didn't understand what the hell I was doing for all these years, I thank you all for pushing me through the highs and lows brought about by my candidature. I couldn't have finished without all of your support. If I have missed anyone I sincerely apologise and thank you all from the bottom of my heart. Forever.

List of Tables

List of Figures

Chapter 1: Introduction

1.1 Electrochemistry

Electrochemical methods are an important and highly useful category of analytical technique within the field of analytical chemistry which provides simple, selective and sensitive forms of analysis.[1] Electrochemistry can be branched into two different categories: potentiometric techniques and dynamic electrochemical (potentiostatic) techniques.[1]

Potentiometric techniques are zero current techniques. Potentiometric analysis is often used for the determination of ionic species and is performed by measuring a potential generated between two electrodes.[1] Apart from their use in analysis, dynamic electrochemical techniques (such as voltammetry and chronoamperometry) are used to acquire qualitative information about electrochemical reactions such as the redox potential and the kinetics. A potential is applied to an electrode in order to drive a redox reaction and the resulting current or charge is measured usually using a three electrode electrochemical cell setup.

1.1.1 Dynamic electrochemical techniques

While there are numerous dynamic electrochemical techniques (e.g. AC voltammetry, pulsed voltammetry and stripping analysis),[1] cyclic voltammetry (CV) and chronoamperometry are two of the most commonly used electrochemical techniques in analytical chemistry.[1]

CV involves the application of a triangular potential waveform (Figure 1.1a) to an immersed working electrode (the electrode where the reaction takes place) in solution.[1] Alongside the working electrode, a reference electrode is used to facilitate control of the electrochemical potential. To close the electrical circuit, a counter electrode, made from an

inert material that will not interfere with the electrochemical reaction, allows current to flow between the working and counter electrodes in a conventional three electrode cell system.[1]

In a CV experiment, the potential is scanned from an initial potential (E_1) and at the end of its linear sweep (E_2), the direction of the potential scan is reversed, usually returning to E_1. The current that is produced as a result of the potential sweep is measured using a potentiostat. A graph for current vs. potential (the current generated between the working and counter electrode) is then plotted and is referred to as a cyclic voltammogram (Figure 1.1b).[1]

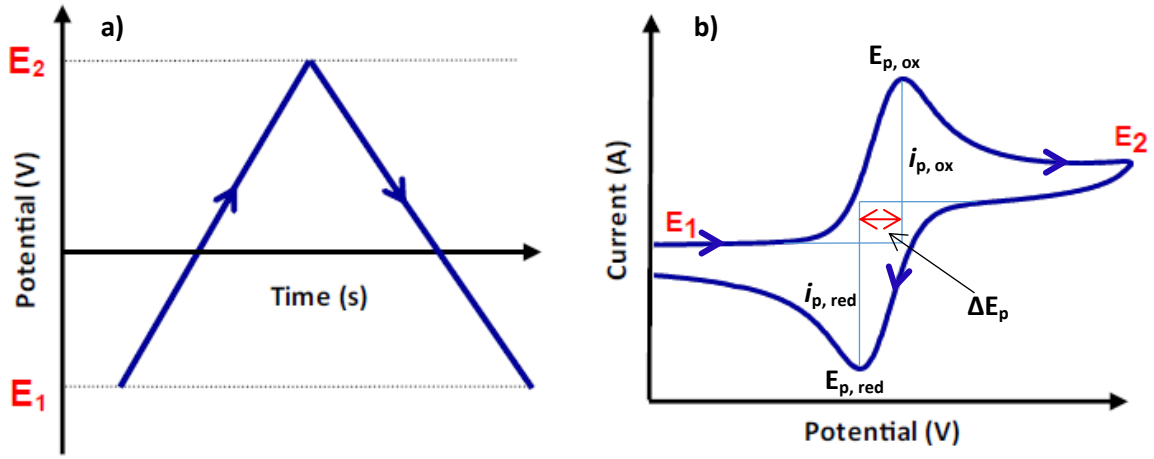

Figure 1.1: Triangular waveform (a) applied to a working electrode resulting in the typical reversible cyclic voltammogram (b) for a one-electron transfer, where E_1 and E_2 are the lower and upper potential limits, E_p and i_p indicates peak potential and current respectively. Arrows indicate the direction of scan

For a redox couple to be defined as chemically reversible, the ratio between the Faradaic current generated when oxidation occurs at the electrode surface ($i_{p,ox}$), and during reduction ($i_{p,red}$), should be equal. For an electrochemical reaction to be electrochemically reversible, the difference between the peak potentials, $E_{p,ox}$ and $E_{p,red}$ should be 59/n mV (where n represents the number of transferred electrons). However this value may vary due to ohmic effects or slow heterogeneous kinetics.[1]

Varying the time scale of the experiment by performing multiple scans or varying the scan rate, gives further information on the stability of the generated species and the possible existence of side reactions. The Randles-Sevcik equation (Eqn. 1.1) highlights the relationship between the current peak height and the square root of the scan rate where i_p is the peak current (in amperes), A is the electrode area (cm^2), C is the analyte concentration, n is the number of electrons transferred, F is Faraday's constant (96485 C mol^{-1}), ν is the scan rate (V s^{-1}), D is the analyte diffusion coefficient (cm^2 s^{-1}), R is the ideal gas constant (8.314 J mol^{-1} K^{-1}) and T is the absolute temperature (K).

$$i_p = 0.4463AC(nF)^{\frac{3}{2}}\left(\frac{\upsilon D}{RT}\right)^{\frac{1}{2}} \qquad \textbf{Eqn. 1.1}$$

Apart from quantitative analysis, CV can also be used for a variety of applications including determining rate constants, formal potentials, diffusion coefficients, reaction mechanisms, and the number of transferred elections in a redox reaction.

Chronoamperometry is another electrochemical technique and is performed by stepping the potential of the working electrode (i.e. a square waveform, see Figure 1.2a) and the resulting current is monitored as a function of time (Figure 1.2b).[1] This current reflects the change in the concentration of the electroactive species at the electrode surface upon oxidation/reduction. The diffusion layer at the electrode will continually grow over time until either the bulk solution has been completely oxidised/reduced or when the experiment has ended.

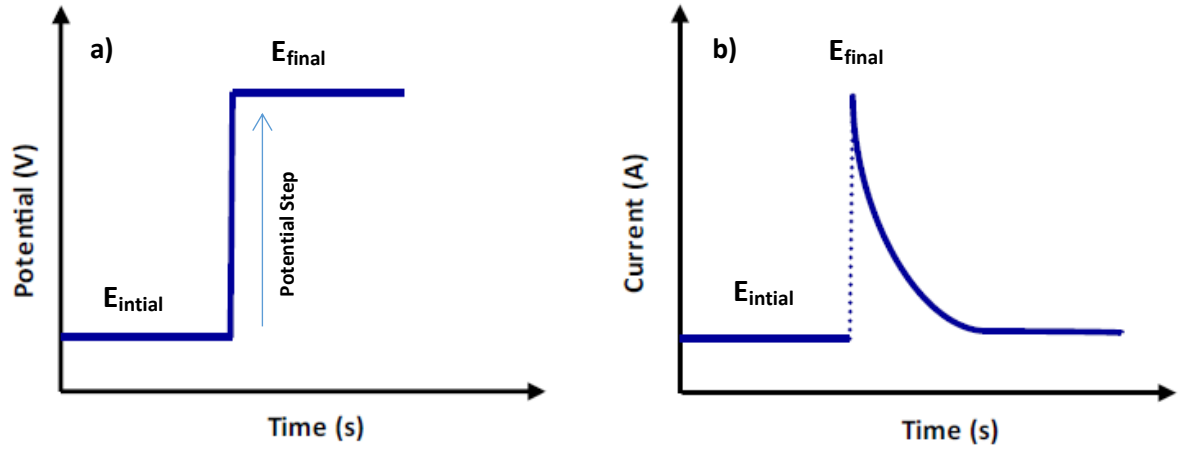

Figure 1.2: Square waveform showing the stepping from one potential to another (a), and the resulting chronoamperometric response (b)

$$i(t) = \frac{\mathrm{n}FACD^{1/2}}{\pi^{1/2}t^{1/2}} \qquad \textbf{Eqn. 1.2}$$

Although chronoamperometry does not provide the same amount of qualitative information cyclic voltammetry can, chronoamperometry can still provide valuable quantitative information. This is due to the fact that concentration is directly proportional to current, as highlighted by the Cottrell equation (Eqn. 1.2), where *i(t)* is current at a specific time, n is the number of electrons transferred, F is Faraday's constant (96485 C/mol), A is the electrode area (cm^2), C is the concentration (mol/cm^3), D is the diffusion coefficient (cm^2/s) and t is the time (s). The diffusion coefficient of the system can be calculated using the Cottrell equation if the concentration is known.

1.1.2 Mass transfer

In every electrochemical system, a Faradaic current is generated from the electrolysis of electroactive species in the system at the working electrode. This current is dependent on the rate of mass transfer (the net movement of species within a solution towards the electrode) and charge transfer kinetics. Mass transfer occurs by a combination of diffusion

(the spontaneous movement of material down a concentration gradient), migration (the movement of charged particles within an electric field applied through the solution) or convection (the movement of the solution species generated by stirring or other means).

$$J_j(x) = -D_j \frac{\partial C_j(x)}{\partial x} - \frac{zC_jF}{RT} D_j C_j \frac{\partial \phi(x)}{\partial x} + C_j V(x) \qquad \textbf{Eqn. 1.3}$$

The Nernst-Planck equation (Eqn. 1.3) describes the total flux (total mass transfer) of material within a solution towards the electrode where *J* represents flux (in mol cm^{-2} s^{-1}), *D* is the diffusion coefficient (cm/s^2), C is the concentration for the species (mol/cm^3), ϕ is the electrostatic potential and *v(x)* represents the hydrodynamic velocity (cm sec^{-1}). The blue highlighted section of the Nernst-Planck equation relates to diffusion governed by Fick's first law. The green highlighted section relates to migration and the yellow highlighted section relates to convection.

Convection within an electrochemical system can have an enormous effect in enhancing the generated current within the system. Due to this effect, control of the movement of solution is critical for the accurate analysis of the voltammetric response in electrochemical systems.

Performing experiments in quiescent (non-moving) solutions can reduce or completely remove convection effect on the recorded current. Alternatively, the controlled stirring/pumping of the electrochemical system, known as forced convection, is a method for electrochemists to increase mass transport in a controlled way from regular convection.

Electrochemical techniques such as CV and chronoamperometry[1] are generally performed under quiescent conditions. The effects of convection are generally negligible within quiescent solutions if the timescales of these experiments are short. However convective interference such as external vibrations or temperature can affect quiescent solutions during longer timescale experiments and this is where a problem arises. Experiments that require longer timescales, such as steady-state electrochemistry, will always be under the effects of convection even if performed under quiescent conditions. Hence the use of forced convection is required to induce a controlled and uniform flow of solution that can minimise the effect of convection on the generated current.[1]

Many electroanalytical methods that can control the flow of solution have been reported in literature.[2–7] Collectively these methods are referred to as hydrodynamic voltammetry. Rotating disk electrode (RDE)[1,8–13] and rotating ring-disk electrode (RRDE)[14–21] are examples of the most commonly used hydrodynamic voltammetric methods for generating stable and steady-state laminar flow conditions for the analysis of electrode reaction kinetics.[11,12,20–31]

1.1.3 Levich equation

In 1952, Benjamin Levich was the first to propose a theory that describes the mass transport occurring at a RDE.[8,9] As the RDE rotates, laminar flow is induced in the bulk solution resulting in the continual refreshment of solution particles at the electrode surface. As the bulk solution continues to be influenced by the effects of forced convection, solution near the electrode surface, known as the hydrodynamic boundary layer, appears stagnant as this solution layer rotates with the electrode. The hydrodynamic boundary layer is typically 300-400 µm thick within aqueous solutions rotated at a moderate rate (approx. 1000 µm). The thickness of the hydrodynamic boundary layer (δ_H) can be approximated (Eqn. 1.4) where υ represents the kinematic viscosity of the solution and ω is the angular rotation rate.

$$\delta_H = 3.6\left(\frac{\upsilon}{\omega}\right)^{\frac{1}{2}} \qquad \textbf{Eqn. 1.4}$$

However, as ions or molecules enter the hydrodynamic boundary layer (under the effects of convection induced by the RDE) and approach the diffusion layer, diffusion rather than convection now has greater influence over the mass transport of the ion/molecule towards the surface of the electrode. The thickness of the diffusion layer (δ_f) can be approximated (Eqn. 1.5) where (D_f) represents the diffusion coefficient of the molecule or ion. Typically the diffusion layer in aqueous systems is approximately twenty times thinner than the hydrodynamic boundary layer.

$$\delta_f = 1.61 D_f^{\frac{1}{3}} \upsilon^{\frac{1}{6}} \omega^{-\frac{1}{2}} \qquad \textbf{Eqn. 1.5}$$

Levich was the first to develop an equation that accounts for the effect on the current response of both convection and diffusion observed in RDE systems and is referred to simply as the Levich equation[1,8] (Eqn. 1.6) where i_L represents the cathodic limiting current, C_o is the concentration of the electroactive species, F is the Faraday constant (96485 C/mol), A the area of the electrode and D is the diffusion coefficient of the molecule or ion.

$$i_L = 0.0620 nFAD^{\frac{1}{3}} \upsilon^{-\frac{1}{6}} C_o \omega^{\frac{1}{2}} \qquad \textbf{Eqn. 1.6}$$

A Levich study is typically carried out by performing repeated voltammetric experiments using an RDE (or RRDE) over a wide range of rotation rates. Typically, a Levich study reveals that the current generated in an electrochemical system with a half-reaction solely controlled by mass transport is directly proportional to the square root of the rotation rate (Figure 1.3). Therefore the current generated at any potential in a Levich study

should linearly vary with rotation rate. A plot of the current observed against the square root of the rotation rate is referred to as a Levich plot (Figure 1.3b).

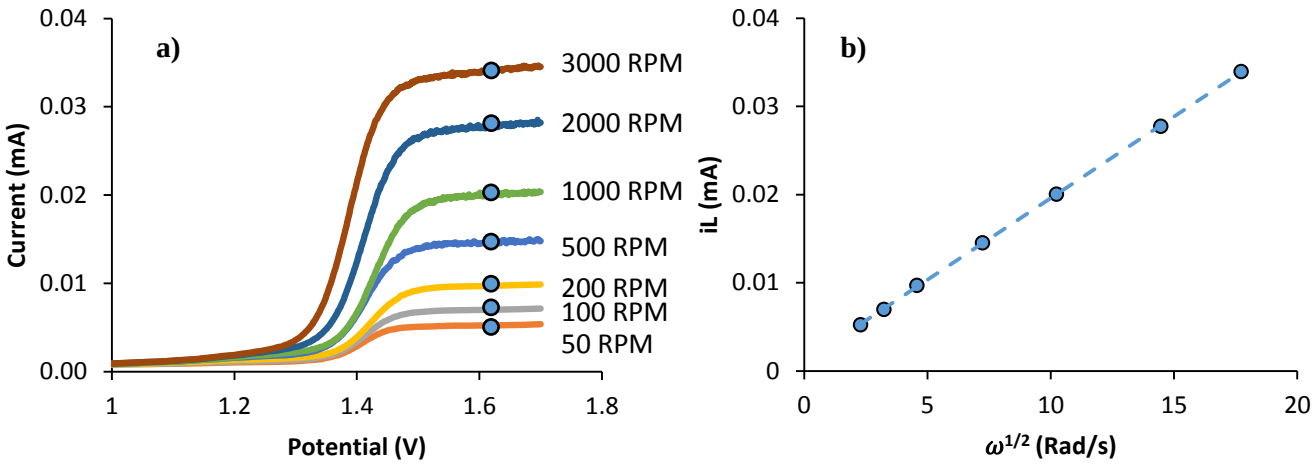

Figure 1.3: a) RDE voltammograms at various rotation rates. b) The Levich plot of generated currents against the square root of the rotation rate

Regardless of rotation rate, the mass transport controlled cyclic voltammogram (Figure 1.3a) will appear sigmoidal if the half reaction of the system is simple and reversible and not hindered by slow kinetics or coupled chemical reactions. A Levich study can also describe kinetic and mass transport parameters (e.g. the standard rate constant (k°) and the diffusion coefficient) when a combination of sluggish kinetics and mass transport limits the rate of the half-reaction of the system. A shift in the plateau of mass transport current away from the standard electrode potential ($E°$) is observed in systems that possess sluggish kinetics compared to systems with facile kinetics. To reach this current plateau, higher potentials are required for systems that exhibit sluggish kinetics

1.1.4 Koutecky-Levich equation

The reciprocal of the Levich equation (Eqn. 1.7) is an alternative way of displaying the data acquired from a Levich study. Plotting this reciprocal (the reciprocal of the current against the reciprocal of the square root of the rotation rate) is called a Koutecky-Levich plot.[1,12] Figure 1.4 shows an example of a Koutecky-Levich plot with the corresponding *i*L vs rotation rate; and *i*L vs square root rotation rate plots for comparison.

$$\frac{1}{i_L} = \frac{1}{0.0620nFAD^{\frac{2}{3}}\upsilon^{-\frac{1}{6}}C_o\omega^{\frac{1}{2}}} \qquad \textbf{Eqn. 1.7}$$

Similar to a Levich plot, data will be displayed linearly with an intercept at the origin (if the system studied is simple and reversible). However, a positive ordinate intercept in the Koutecky-Levich plot may indicate that the system is limited by sluggish kinetics.

$$\frac{1}{i} = \frac{1}{i_k} + \frac{1}{0.0620nFAD^{\frac{2}{3}}\upsilon^{-\frac{1}{6}}C_o\omega^{\frac{1}{2}}} \qquad \textbf{Eqn. 1.8}$$

The Koutecky-Levich equation, Equation 1.8, denotes a linear $1/i$ against $1/\omega^{1/2}$ plot with an ordinate intercept of $1/i_k$, which represents the kinetic current of the system (where no mass transport limitations are present). Experimentally, i_k can be determined by measuring the kinetic current over several selected overpotentials along a voltammogram.

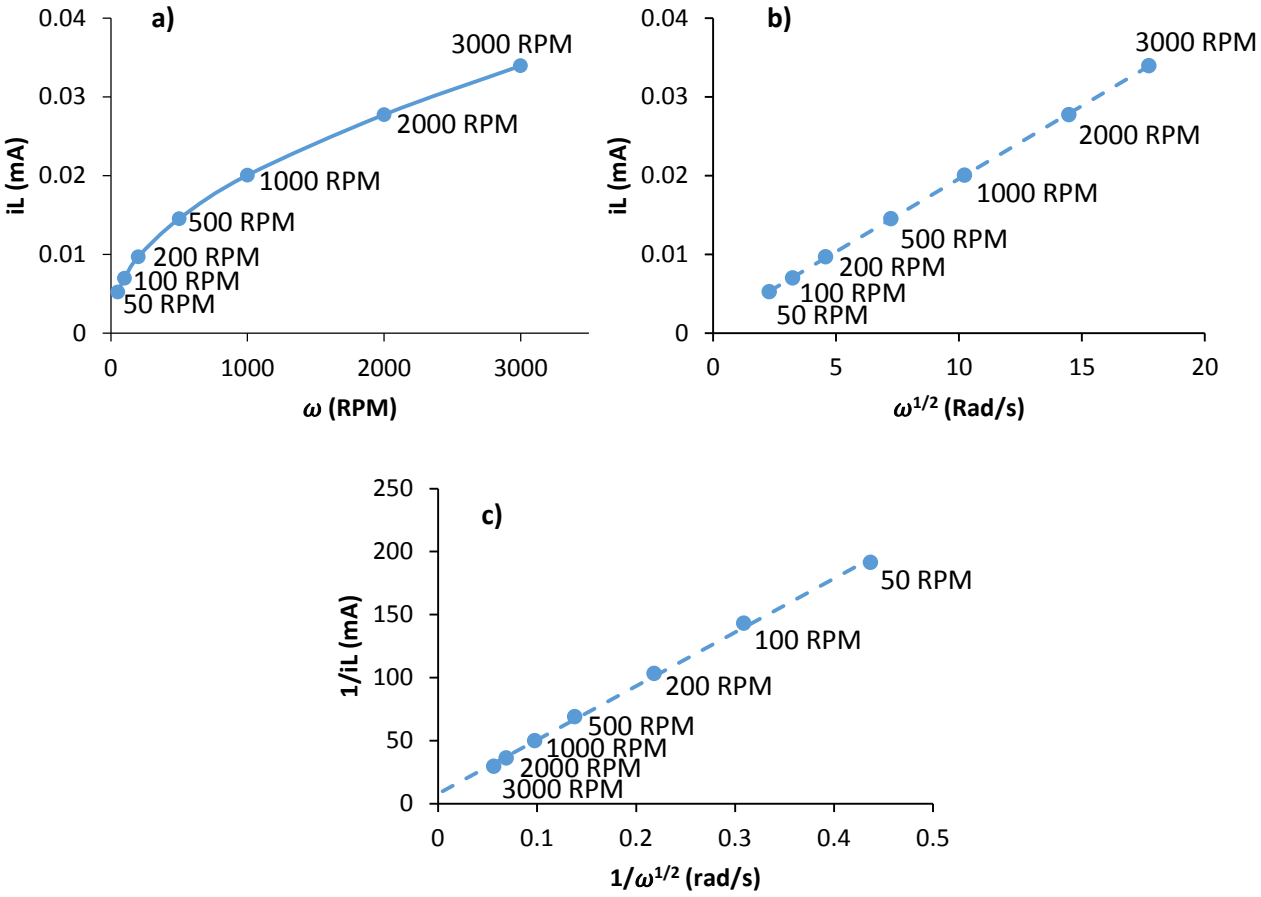

Figure 1.4: A comparison of plots where a) represents a simple limiting current versus rotation rate plot; b) Levich plot; c) Koutecky-Levich plot

1.1.5 Rotating ring-disk electrodes

A generator-collector electrode comprises of two parallel working electrodes, where an analyte (e.g. reaction [1.1]) undergoes either an oxidation or a reduction at the generator electrode, while a single potential is simultaneously applied to the collector electrode to promote reduction or oxidation of the product at the generator electrode, typically back to the starting analyte (see reaction [1.2]).

$$A \pm e^{-} \rightleftharpoons B \quad \textbf{[1.1]}$$

$$B \pm e^{-} \rightleftharpoons A \quad \textbf{[1.2]}$$

Collection efficiency (N) is an important parameter in the use of generator-collector systems. Eqn. 1.9 illustrates collection efficiency, where I_{col} denotes the collector electrode current and I_{gen} the generator electrode current. Typically, the higher the value of the collection efficiency, the greater the sensitivity within the system is, leading to more accurate results. Therefore a large collection current is desirable.

$$N = -\frac{I\text{col}}{I\text{gen}} \quad \textbf{Eqn. 1.9}$$

A generator electrode that is completely surrounded by the collector electrode is one way to increase the collection efficiency of the system. Less of the generated species is able to escape back into the bulk solution, allowing for most of the generated species to be collected by the collector electrode. Another way to increase the collection efficiency of the system is to direct the flow of the generated species (via convection or limiting diffusion to one dimension) towards the collector electrode, allowing for most of the generated species to be collected by the collector electrode. Reducing the inter electrode gap between the electrodes however will have the greatest positive effect on the collection efficiency.

There are many varied applications in the use of generator-collector systems. Systems where homogeneous kinetics occurs after an electrochemical reaction can be analysed using generator-collector electrodes.[19,20,32–36] This is accomplished by measuring I_{col} as a function of I_{gen}. Information regarding the mechanism of systems can also be deduced.[11] Detection of analytic concentrations at a micromolar level,[37] the investigation of the dissolution of the generator electrode[38,39] and the analysis of ion transport across phase junctions[40,41] are examples of other applications of generator-collector systems.

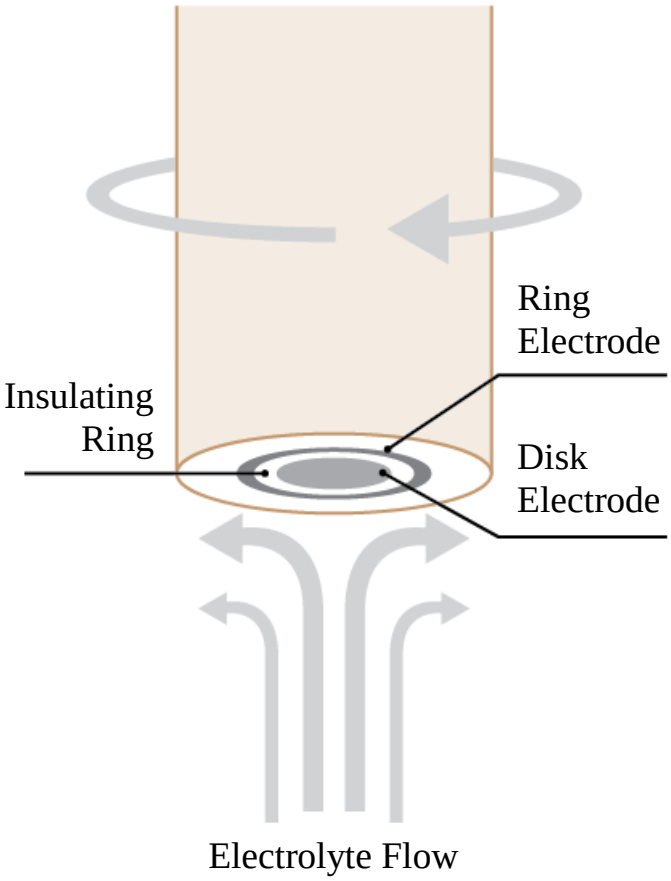

Figure 1.5: Representation of the flow of electrolyte under the rotation of a RRDE

Over the years, numerous generator-collector electrode systems comprising of varying electrode configurations and modes of analyte transportation between the generator and collector have been proposed. Nekresov and co-workers in 1959 proposed the first and perhaps most commonly used generator-collector electrode system within analytical chemistry, the rotating ring-disk electrode (RRDE).[14] The RRDE was then extensively studied over many years by Albery and co-workers.[16–20,42–60] A RRDE (Figure 1.5) consists of a RDE that is surrounded by a ring electrode. The small gap between the ring electrode and disk electrode consists of an insulating material that separates the two electrodes from each other.[11,32]

Convective flow of bulk solution towards the centre of the disk electrode is induced by the rotation of a submerged RRDE (Figure 1.5). Bulk solution containing electroactive

species formed at the disk electrode (if the disk electrode was used as the generator electrode) is then transported radially from the centre of the disk to the ring electrode via centrifugal forces. If a suitable potential is applied at the ring, the electroactive species that was swept can be "collected" at the ring electrode and another electrode reaction may occur, altering the measured ring current.

Unlike other generator/collector electrode systems, such as interdigitated band electrodes, the presence of a ring (collector electrode) on a RRDE does not affect the processes occurring at the disk (generator) electrode due to hydrodynamic constraints. A distinct disadvantage of the use of RRDEs however is their sensitivity is usually much lower than other generator-collector electrode systems such as the aforementioned interdigitated band systems.

Compared to the usual electrochemical results obtained from a single working electrode setup, more dimensions are used to represent the results obtained from a RRDE experiment since RRDE experiments involve two potentials (E_{disk} and E_{ring}) and two currents (I_{disk} and I_{ring}).[1]

Coupled with a bi-potentiostat, there are numerous common techniques that can be performed using a RRDE. By applying an appropriate constant potential, an analyte is oxidised/reduced to yield the corresponding product or intermediates at the generator electrode, while a second constant potential held at the ring electrode will promote another electrochemical reaction involving the oxidation/reduction products or intermediates. The current-potential curve observed at the ring electrode can indicate the products formed when a constant potential is applied to the disk electrode. The analyte of interest can provide transient shielding of the ring current during electrolysis when the potential applied across the disk electrode is stepped up to a point where the species is adsorbed.

At least one of the electrodes of each of the above mentioned techniques are held at a constant potential for the duration of the experiment. Simultaneously applying time-varying controlling waveforms to both the ring and disk electrodes will significantly increase the applicability and sensitivity of the RRDE system.[61,62]

1.2 Electrochemiluminescence

1.2.1 Photoluminescence

Luminescence is the emission of light without the simultaneous production of heat from the excited state of a molecule or atom.[63] Through a number of different luminescent processes, such as photoluminescence (PL), chemiluminescence (CL), or electrochemiluminescence (ECL), light can be emitted. PL is the emission of light from a molecule following photoexcitation. PL is typically classified as fluorescence (where emission arises from a singlet excited state where all the electrons have paired spins) and phosphorescence (where emission arises from triplet excited states in which one set of electron spin are unpaired).[64]

First proposed by Aleksander Jablonski in 1935, the Jablonski diagram illustrates these photochemical processes.[64] In a Jablonski diagram the singlet ground state is represented by S_0, the first electronic state by S_1, and the second electronic state by S_2. At each of these electronic levels are vibrational energy levels where an excited molecule (that has undergone light absorption) can exist within. Typically through light absorption, molecules are excited up to the higher vibrational levels of S_1 or S_2. The lifetimes of these excited vibrational states are very short (in the range of picoseconds) however. Through internal conversion and vibrational relaxation (usually occurring within 10^{-12} seconds), the excited vibration states of the molecule rapidly decays to the lowest vibrational energy level of S_1.

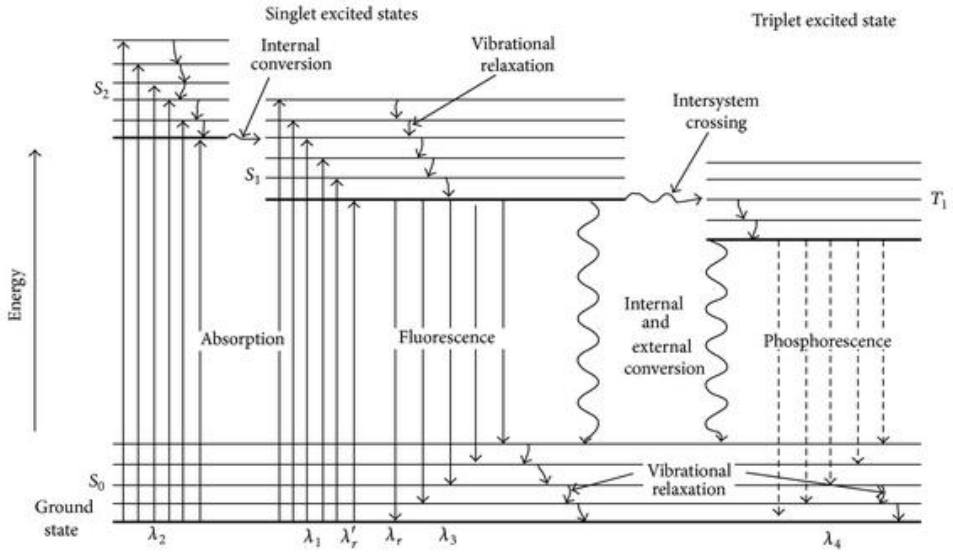

Figure 1.6: Jablonski diagram showing possible transitions both radiative and non-radiative. Adapted from Fereja *et al.*[65]

Fluorescence occurs when the promoted electron decays from the S_1 to the S_0 energy state in a relatively short time frame (10^{-9} – 10^{-7} seconds). Due to this very small time frame, internal conversion occurs before emission. Fluorescent emission of an excited molecule always occurs from the lowest vibrational level of a singlet excited state, therefore the emitted photon energy is lower than the energy of the photon required to excite the molecule. The energy difference between the excitation and emission of the molecule is referred to as the Stokes shift (Figure 1.7).[64] Alternatively, instead of emitting a photon, excited molecules can convert excitation energy into heat allowing it to return back down to its ground state.

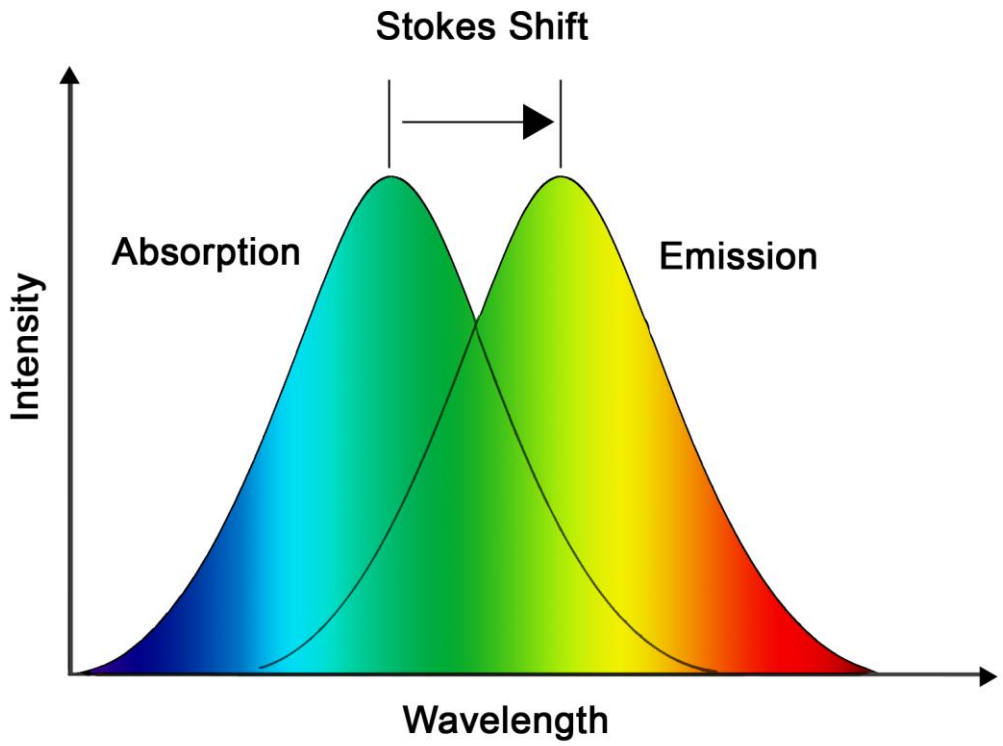

Figure 1.7: Illustration of the Stokes shift

Phosphorescence occurs when the excited electron from the S_1 state undergoes spin conversion and is converted into the forbidden triplet excited state, T_1. The transition from a singlet to a triplet state is known as intersystem crossing (ISC) and it is less probable to occur than singlet to singlet transitions. ISC occurs when there is significant coupling between the S_1 and T_1 states. Following ISC, the excited molecule undergoes vibrational relaxation to emit a photon and return to its ground state. ISC can compete with fluorescent emission but is unable to compete with vibrational deactivation from higher vibrational levels of the excited singlet state. Compared to fluorescence, phosphorescence has a much longer time scale (10^{-6} – 10 seconds) since it is a forbidden transition.

1.2.2 Chemiluminescence

CL (the emission of ultraviolet, visible or infrared light from a chemical reaction), was one of the initial six sub-classes of luminescence proposed by Wiedermann.[66] In 'direct' CL, a redox reaction between two molecules creates an electronically excited species that emits a photon upon relaxing to its ground state (reactions [1.3] and [1.4]).[67]

$$A + B \rightarrow C^* + \text{Products} \quad \textbf{[1.3]}$$

$$C^* \rightarrow C + h\nu \quad \textbf{[1.4]}$$

Indirect or sensitised CL occurs when the electronically excited species transfers its energy to a suitable luminophore, which then becomes the emitting species.[67] Either way, once the emitting species is excited, the emission process is identical to other modes of luminescence and it is considered to be spontaneous.

As the amount of light emitted from the electronically excited intermediate is directly related to the concentration of the reacting species,[67] CL is an attractive option for chemical detection. As an analytical tool, CL has many advantages, such as high signal-to-background ratio, as there is no need for an excitation light source, and increased selectivity due to the relatively low number of chemical reactions that can undergo CL.[68] Another inherent advantage of CL is that the instrumentation required for its generation and measurement is relatively inexpensive,[68] because unlike other spectroscopic detection methods (such as spectrophotometry and fluorescence), there is no need for light sources, optical fibres and monochromators.[69]

1.2.3 Electrochemiluminescence

ECL, in contrast to CL, is the emission of light from the excited products of a chemical reaction, where at least one reactant is generated electrochemically.[70–72] The first detailed ECL studies were described by Hercules,[73] Visco *et al.*[74] and Bard *et al.*[75] in the mid-

1960's; however, there are reports of light emission during electrolysis that date back to the 1920's.[76]

Compared to CL, ECL systems have the advantage of spatial and temporal control due to the emission of light concentrated close to the electrode, and enhanced sensitivity due to the regeneration of the active form of some reagents at the electrode surface. Temporal control over the ECL emission can allow for reactions (such as enzyme-catalysed reactions) to take place before emission can occur. Spatial control over the ECL emission can increase the signal-to-background ratio within the system by situating the electrode surface (the source of the ECL emission) close to the detector as well as examining multiple reaction mechanisms within the same ECL system.[77] ECL can also provide the highly selective generation of excited species by varying the applied electrode potential, unlike the non-specific chemical excitation with CL. Similar to CL, ECL does not require a light source or monochromator so attendant problems observed in fluorescent methods, such as scattering and auto-fluorescence, are not present within ECL systems.[78,79]

1.2.4 Annihilation ECL pathway

ECL can be produced through two different mechanistic pathways: the annihilation and co-reactant pathway. The annihilation pathway was the first to be studied extensively; however it does not have as many uses as the co-reactant ECL pathway for analytical applications.

$$A \rightarrow A^{\bullet +} + e^{-} \quad \textbf{[1.5]}$$

$$A \rightarrow A^{\bullet -} - e^{-} \quad \textbf{[1.6]}$$

$$A^{\bullet +} + A^{\bullet -} \rightarrow A + A^{*} \quad \textbf{[1.7]}$$

$$A^{*} \rightarrow A + h\nu \quad \textbf{[1.8]}$$

In the annihilation pathway (shown in reactions [1.5]-[1.8]), oxidised and reduced forms of the luminophore are both generated at the electrode surface when a potential step or sweep is applied at the electrode. A ground and excited state of the luminophore are then formed from the interaction between the oxidised and reduced forms of the luminophore. This excited state then emits a photon in order for it to relax back to its ground state.

$$\Delta G = nF(E°_{Donor} - E°_{Acceptor}) \qquad \textbf{Eqn. 1.10}$$

The free energy, ΔG, of the annihilation reaction between the oxidised and reduced forms of the luminophore can be calculated using Eqn. 1.10 where $E°_{Donor}$ represents the formal potential of the ground state reduction and $E°_{Acceptor}$ represents the formal potential of the ground state oxidation. For systems to be "energy sufficient" for annihilation ECL emission to occur, the ΔG of the reaction must be greater than or equal to the energy required to generate the electronically exited state of the luminophore.

The annihilation pathway would be an attractive analytical method due to its simplicity as only a luminophore, a solvent and a supporting electrolyte are required to generate annihilation ECL. However, in order to oxidise and reduce a luminophore, the solvent used in the system must have a large potential window.[1,71,72,78,80–82] Unfortunately, aqueous solvents tend not to have a large enough potential window (between approximately -0.2 V and 1.3 V vs Ag/AgCl) for annihilation ECL to occur, which limits the analytical application of annihilation ECL.[1,71,72,78,80–82]

1.2.5 Co-reactant ECL pathway

Co-reactant ECL, unlike annihilation ECL, is typically generated with a one-directional potential scan or step at the electrode in the presence of both a luminophore and a co-reactant. A co-reactant is defined as a species that can interact with the oxidised or reduced form of a luminophore after the co-reactant is oxidised or reduced. At the electrode

surface, the luminophore and the co-reactant can simultaneously be oxidised or reduced when a potential is applied across the electrode. In “oxidative-reductive” co-reactant ECL systems, the luminophore and co-reactant are oxidised at the electrode surface to produce an oxidised state of the luminophore and radical cation of the co-reactant. This radical cation breaks down to produce a strongly reducing intermediate which then interacts with and reduces the oxidised luminophore to generate light. Alternatively in “reductive-oxidative” co-reactant ECL systems, both the luminophore and co-reactant are reduced at the electrode surface. Strongly oxidising intermediates of the co-reactant are produced instead and go on to oxidise the reduced form of the luminophore to produce light.

The use of a co-reactant has numerous advantages over the use of annihilation ECL. Unlike annihilation ECL, co-reactant ECL can be performed in either organic or aqueous environments since it does not require a wide cathodic potential window. Co-reactant ECL is also more desirable than the use of the annihilation pathway if the oxidised or reduced forms of the analyte are not stable enough for annihilation ECL emission. Furthermore, the co-reactant pathway can generate ECL emissions from some fluorescent compounds that contain only a reversible reduction or oxidation. Through the use of oxidative-reductive ECL, the co-reactant pathway can reduce the effects oxygen quenching can have over the intensity of the emission (an issue that discourages annihilation ECL) and allows for ECL analysis within an oxygen rich environment.

The solubility, electrochemical properties, stability, kinetics, ECL background and quenching effect of a compound must be taken into account for it to be determined as a suitable co-reactant.[78] The co-reactant should also be easily oxidised or reduced at the electrode surface. Commercially available ECL instruments have become widely used in the field of bio-analytical chemistry due to their sensitivity, dynamic range, precision and

tolerance of sample matrices. All commercially available ECL instrumentation these days generates ECL intensities using the co-reactant ECL pathway.

1.2.6 Oxalate ($C_2O_4^{2-}$) system

The first reported case of co-reactant ECL was reported by Bard *et al.* using the oxalate ion ($C_2O_4^{2-}$) acting as the co-reactant in the presence of tris(2,2'-bipyridine)ruthenium(II) ($[Ru(bpy)_3]^{2+}$) acting as the luminophore.[83] Upon oxidation within an aqueous solution, instead of an oxidant, oxalate produces a strong reductant ($CO_2^{\bullet-}$).[72,80,81,83–85] The mechanism for this co-reactant ECL system is shown below (reactions [1.9]-[1.15]).

$$[Ru(bpy)_3]^{2+} - e^- \rightarrow [Ru(bpy)_3]^{3+} \quad \textbf{[1.9]}$$

$$[Ru(bpy)_3]^{3+} + C_2O_4^{2-} \rightarrow [Ru(bpy)_3]^{2+} + C_2O_4^{\bullet-} \quad \textbf{[1.10]}$$

$$C_2O_4^{\bullet-} \rightarrow CO_2^{\bullet-} + CO_2 \quad \textbf{[1.11]}$$

$$[Ru(bpy)_3]^{3+} + CO_2^{\bullet-} \rightarrow [Ru(bpy)_3]^{2+*} + CO_2 \quad \textbf{[1.12]}$$

$$[Ru(bpy)_3]^{2+} + CO_2^{\bullet-} \rightarrow [Ru(bpy)]^{+} + CO_2 \quad \textbf{[1.13]}$$

$$[Ru(bpy)_3]^{3+} + [Ru(bpy)]^{+} \rightarrow [Ru(bpy)_3]^{2+*} + [Ru(bpy)_3]^{2+} \quad \textbf{[1.14]}$$

$$[Ru(bpy)_3]^{2+*} \rightarrow [Ru(bpy)_3]^{2+} + h\nu \quad \textbf{[1.15]}$$

In this mechanism, the oxidised ruthenium complex oxidises oxalate to form the radical $C_2O_4^{\bullet-}$ (reactions [1.9] and [1.10]). This radical then degrades, forming a strongly reducing carbon dioxide radical ($CO_2^{\bullet-}$) (reaction [1.11]). At this point, ECL could occur from two pathways. In the favoured pathway, $CO_2^{\bullet-}$ reduces the oxidised ruthenium complex, $[Ru(bpy)]^{3+}$, to form an excited state (reaction [1.12]) where it will emit light to return to its ground state (reaction [1.15]). In the other pathway, $CO_2^{\bullet-}$ reduces the un-oxidised ruthenium complex, $[Ru(bpy)_3]^{2+}$, to form a reduced ruthenium complex $[Ru(bpy)]^{+}$

(reaction [1.13]) which will then react with the oxidised ruthenium complex in a similar fashion to annihilation ECL to form an excited state (reaction [1.14]).[1,78,81,82,86] While theoretically possible, there is no evidence to suggest that the second pathway actually occurs. Over the years, numerous applications of the co-reactant ECL detection of oxalate or the use of oxalate in an ECL application have been developed and documented.[87–93]

1.2.7 Tripropylamine (TPA) system

While oxalate was the first co-reactant reported and to be studied extensively, there are many other co-reactants in existence. While primary and secondary amines can also act as suitable co-reactants for co-reactant ECL, the intensities observed when tertiary amines are used as co-reactants are by far superior.[1,71,78,80–82,86] Aromatic and quaternary amines however do not elicit ECL intensities.[82] Knight and Greenway determined that electron donating substituents attached to a nitrogen attached to the α-carbon of an amine generally increases the ECL intensity observed within the system due to stabilisation of the radical intermediate of the co-reactant.[94] Lower ECL intensities are usually observed however if electron withdrawing substituents (hydroxyl, halogen and carboxy groups for example) are attached to amines due to these substituents destabilising the radical intermediate of the co-reactant. Amines are also likely to exhibit lower ECL activity if the amine structure is not planar in geometry post oxidation, hindering the production of the co-reactant radical.

The $[Ru(bpy)_3]^{2+}$/tripropylamine (TPA) system, like the $[Ru(bpy)_3]^{2+}/C_2O_4^{2-}$ co-reactant ECL system, is an oxidative-reductive co-reactant ECL system.[86,95–98] Noffsinger and Danielson were the first to study and report on $[Ru(bpy)_3]^{2+}$ CL in the presence of aliphatic amines in 1987.[97] Following Bard *et al.* and their work involving $[Ru(bpy)_3]^{2+}$ co-reactant ECL emission using oxalate as the co-reactant[83] as well as Noffsinger and Danielson's research, Leland and Powell introduced TPA in 1990 as a suitable co-reactant for $[Ru(bpy)_3]^{2+}$ co-reactant ECL.[96] Blackburn *et al*. subsequently developed ECL detection for

immunoassays and DNA probe assays where $[Ru(bpy)_3]^{2+}$ and TPA are used as the label and co-reactant respectively.[98] Even though TPA co-reactant ECL is still widely studied, the reaction mechanism is still not fully understood. There are several proposed parallel mechanisms, but none are absolute.[1,72,80–82]

$$[Ru(bpy)_3]^{2+} - e^- \rightarrow [Ru(bpy)_3]^{3+} \quad \textbf{[1.16]}$$

$$TPA - e^- \rightarrow TPA^{\bullet+} \quad \textbf{[1.17]}$$

$$TPA^{\bullet+} \rightarrow TPA^{\bullet} + H^+ \quad \textbf{[1.18]}$$

$$[Ru(bpy)_3]^{3+} + TPA^{\bullet} \rightarrow [Ru(bpy)_3]^{2+}* + \text{other products} \quad \textbf{[1.19]}$$

$$[Ru(bpy)_3]^{2+}* \rightarrow [Ru(bpy)_3]^{2+} + h\nu \quad \textbf{[1.20]}$$

In one of the proposed mechanisms (reactions [1.16]-[1.20] and Figure 1.8a), $[Ru(bpy)_3]^{2+}$ and TPA are simultaneously oxidised at the electrode surface to form $[Ru(bpy)_3]^{3+}$ and $TPA^{\bullet+}$ respectively. $TPA^{\bullet+}$ then deprotonates to form a strongly reducing intermediate, $TPA^{\bullet}$, that then goes on to reduce $[Ru(bpy)_3]^{3+}$ to produce the excited state of the luminophore which then relaxes back down to its ground state via the emission of a photon. An alternative reaction mechanism for the ECL emission of $[Ru(bpy)_3]^{2+}$ in the presence of TPA is highlighted by Figure 1.8b where the strongly reducing intermediate of the co-reactant, $TPA^{\bullet}$, reduces the ground $[Ru(bpy)_3]^{2+}$ state to form $[Ru(bpy)_3]^{+}$ which then goes on to react with $[Ru(bpy)_3]^{3+}$ resulting in the generation of the excited state which can relax back down to its ground state by emitting a photon.

In the reaction mechanism shown in Figure 1.8c, only $[Ru(bpy)_3]^{2+}$ is oxidised at the electrode. The oxidation of TPA occurs not at the electrode but from the interaction between TPA and the $[Ru(bpy)_3]^{3+}$ generated at the electrode surface. This mechanism isn't typically favoured when low concentrations of $[Ru(bpy)_3]^{2+}$ is present within the system.

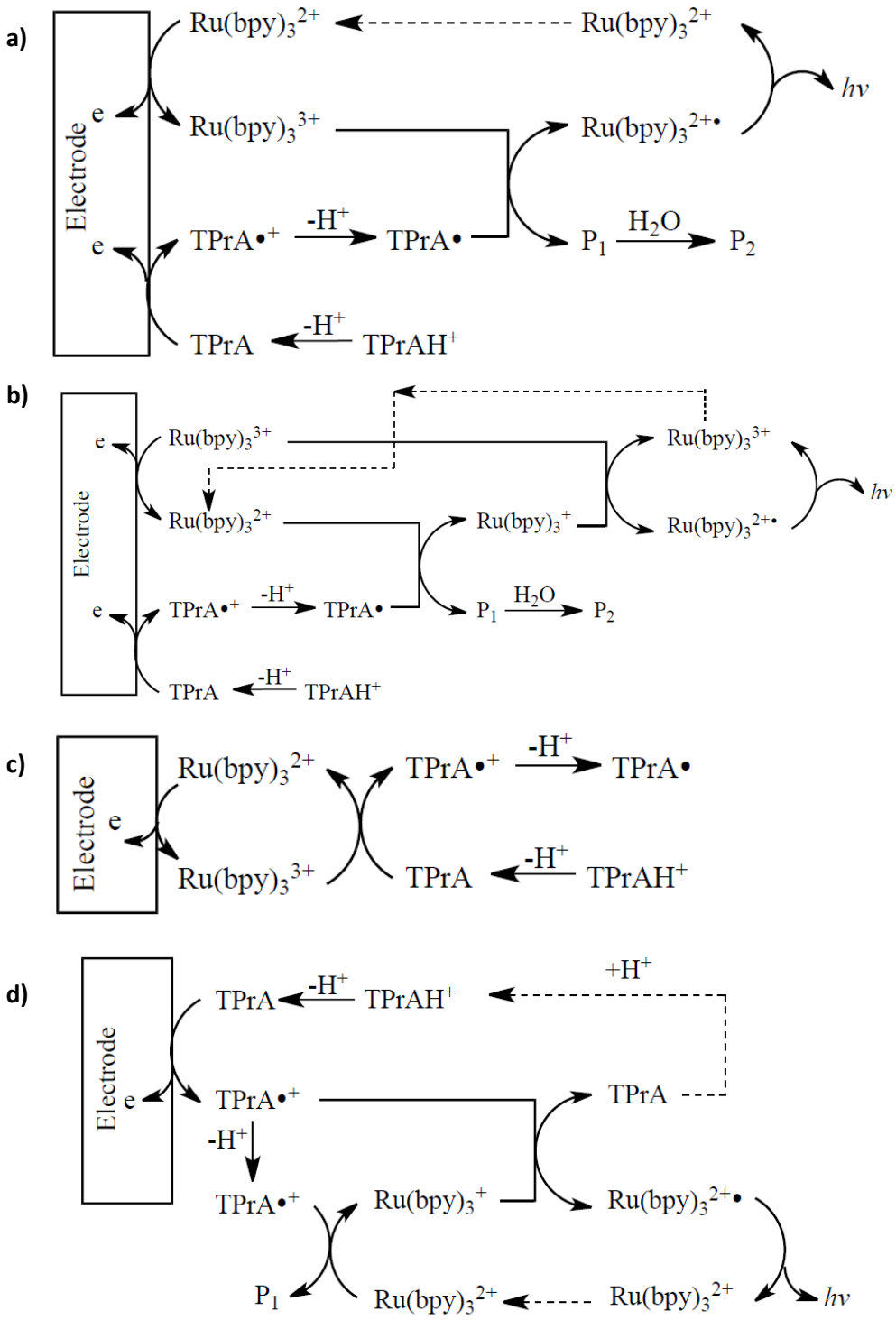

Figure 1.8: Proposed reaction mechanisms of the $[Ru(bpy)_3]^{2+}$/TPA co-reactant ECL system. Adapted from Miao *et al.*[86]

Unlike the reaction mechanism shown in Figure 1.8c, only TPA, not $[Ru(bpy)_3]^{2+}$, is oxidised on the electrode surface in the reaction mechanism shown in Figure 1.8d to generate $TPA^{\bullet+}$ and $TPA^{\bullet}$. $TPA^{\bullet}$ and $[Ru(bpy)_3]^{2+}$ reacts to form $[Ru(bpy)_3]^{+}$. The excited state is then formed when $[Ru(bpy)_3]^{+}$ reacts with $TPA^{\bullet+}$. Low oxidation potential ECL can be achieved using this reaction mechanism where low potentials can be applied to solely oxidise the TPA co-reactant and not $[Ru(bpy)_3]^{2+}$.

Currently, TPA is the most widely used ECL co-reactant and has become very important for commercial applications due to the wide variety of applications that are possible with its use.[99–145] However, there are several issues relating to the use of TPA as a co-reactant. Firstly, TPA is a toxic and volatile tertiary amine that is not readily soluble in water. To attain high sensitivity, high concentrations (~100 mM) of TPA are required.[81,82,94] The material of the working electrode also has a severe effect on the $[Ru(bpy)_3]^{2+}$ ECL intensities generated when TPA is used as a co-reactant (for example, intensities generated using Pt electrodes are only 10% of the those at Au electrodes).[146] As a direct result of these disadvantages, alternative co-reactants have been studied and proposed in literature.

1.2.8 2-(Dibutylamino)ethanol (DBAE) system

2-(Dibutylamino)ethanol (DBAE), displaying a mechanism similar to that of TPA, was introduced by Liu *et al.* in 2007 as an environmentally safer alternative than TPA for $[Ru(bpy)_3]^{2+}$ co-reactant ECL.[146] At Au and Pt electrodes, the $[Ru(bpy)_3]^{2+}$/DBAE co-reactant system elicited ECL intensities 10 and 100 times greater than those observed in $[Ru(bpy)_3]^{2+}$/TPA systems under identical conditions respectively. However, only under specific conditions did DBAE elicit intensities greater than TPA when a glassy carbon working electrode was used.[146] Typically electron withdrawing substituents, such as hydroxyl groups, decrease observed ECL intensities. However the hydroxyl group that DBAE possess has a catalytic effect on the oxidation of the co-reactant which increases the ECL intensities.

DBAE is also far less toxic and volatile than TPA making DBAE safer for analytical use and environmental disposal, while lower concentrations of DBAE are more effective than TPA at higher concentrations. Preparing aqueous DBAE solutions is much easier compared to preparing aqueous TPA solutions since DBAE has the greater solubility in aqueous media. Due its many advantages over the use of TPA, DBAE has been incorporated in methods used for the quantitative analysis of many substances, such as tetracyclines[147] and dopamine[148] and has found increasing use in a wide variety of applications.[149–167]

1.2.9 NADH system

Nicotinamide adenine dinucleotide, more specifically its reduced form NADH, can be used as a suitable co-reactant as NADH contains a tertiary amine group. The $[Ru(bpy)_3]^{2+}$/NADH co-reactant ECL system follows a similar mechanistic reaction to both the $[Ru(bpy)_3]^{2+}$/TPA and $[Ru(bpy)_3]^{2+}$/DBAE co-reactant ECL systems. NADH is widely used in bioanalytical applications and bioprocesses. ECL detection of biological species is possible by coupling the biological species with the dehydrogenase enzyme responsible for the reduction of the NAD^+ cation into NADH.[168]

In 1993, a flow injection analysis method for the detection of glucose was first proposed by Martin and Nieman[169] where glucose dehydrogenase enzyme reduces NAD^+ cation into NADH. NADH then interacts with $[Ru(bpy)_3]^{2+}$ immobilised on a Nafion film coated platinum electrode to produce detectable CL emissions. Later, Martin and Nieman developed flow injection electrochemiluminescent biosensors capable of quantifying glucose, ethanol and lactate via the immobilisation of dehydrogenase in cation exchange polymers like Nafion and Eastman AQ.[170] Since then, using NADH as the co-reactant, many ECL biosensors have been developed for the quantitative determination of glucose.[171–178] Ethanol, alcohol dehydrogenase and L-glutamic acid biosensors have also been developed incorporating NADH.[179–181]

1.2.10 Other oxidative-reductive co-reactant systems

Peptides and amino acids can also be used as suitable co-reactants for co-reactant ECL because they both contain amine groups. The detection of both peptides and amino acids, while acting as the co-reactant, has been successfully exploited in capillary electrophoretic detection.[182–185] Notably with proline acting as the co-reactant/analyte, a microchip capillary electrophoresis-ECL system consisting of a poly(dimethylsiloxane) layer on an indium titanium oxide electrode was developed.[186]

Alkaloids such as morphine, heroin, codeine and dextromethorphan can also act as co-reactants in the presence of a luminophore as they each contain tertiary amines.[187,188] Even though they have similar structures, the ECL intensities generated when using morphine is approximately 95% and 78% lower than those generated when codeine or heroin are used respectively due to the phenol groups (acting as an electron withdrawing group) present within pseudomorphine, whereas the respective methoxy and acetyl groups present in codeine and heroin blocks reactions that lead to the reduction of $[Ru(bpy)_3]^{2+}$ ECL intensities. The ECL detection of pesticides and other pharmaceuticals has been successfully implemented into many applications.[189–198]

Nucleic acids could also be used as co-reactants. Using a thin film of $[Ru(bpy)_2(PVP)_{10}]^{2+}$ metallopolymer (where PVP = poly(vinyl pyridine)), an ECL detection method for DNA was developed by Dennany and co-workers.[199,200] To generate ECL within this system, Ru^{3+} (formed from the oxidation of Ru^{2+} sites within the metallopolymer) oxidises guanine to form guanine radicals, generating ECL. Detection of bio-activated genotoxicity was then developed involving the ECL from the $[Ru(bpy)_2(PVP)_{10}]^{2+}$ metallopolymer in the presence of a ultrathin DNA film.[201] Label free ECL DNA detection was later developed incorporating a CNT/ Nafion/$[Ru(bpy)_3]^{2+}$ film coated glassy carbon electrode.[202]

Pyruvate cannot solely act as a co-reactant for $[Ru(bpy)_3]^{2+}$ ECL due to the difficulty involved with oxidising pyruvate. However in the presence of Ce^{3+}, pyruvate can indeed act as a co-reactant and illicit $[Ru(bpy)_3]^{2+}$ ECL emissions.[85] For pyruvate to act as a co-reactant within this system, Ce^{3+} is oxidised to form Ce^{4+} which can then oxidise pyruvate allowing for ECL to be generated. The quantitative ECL detection of pyruvate in the presence of Ce^{3+} was later proposed by Knight and Greenway.[203] Co-reactant ECL of formic acid and formaldehyde,[204] mono and polyhydric alcohols,[205] various ketones[206] and Vitamin C and its derivatives[207–213] have also been reported within literature.

1.2.11 Reductive-oxidative co-reactant systems

As mentioned previously, in "reductive-oxidative" co-reactant ECL systems, both the luminophore and co-reactant are simultaneously reduced at the electrode surface. Strong oxidising intermediates of the co-reactant are produced which then goes on to oxidise the reduced form of the luminophore producing light.

$$S_2O_8^{2-} + e^- \rightarrow SO_4^{\bullet-} + SO_4^{2-} \quad \textbf{[1.21]}$$

$$[Ru(bpy)_3]^{2+} + e^- \rightarrow [Ru(bpy)_3]^{+} \quad \textbf{[1.22]}$$

$$[Ru(bpy)_3]^{+} + SO_4^{\bullet-} \rightarrow [Ru(bpy)_3]^{2+*} + SO_4^{2-} \quad \textbf{[1.23]}$$

$$[Ru(bpy)_3]^{2+} + SO_4^{\bullet-} \rightarrow [Ru(bpy)_3]^{3+} + SO_4^{2-} \quad \textbf{[1.24]}$$

$$[Ru(bpy)_3]^{3+} + [Ru(bpy)_3]^{+} \rightarrow [Ru(bpy)_3]^{2+} + [Ru(bpy)_3]^{2+*} \quad \textbf{[1.25]}$$

$$[Ru(bpy)_3]^{2+*} \rightarrow [Ru(bpy)_3]^{2+} + h\nu \quad \textbf{[1.26]}$$

The $[Ru(bpy)_3]^{2+}$/peroxydisulfate ($S_2O_8^{2-}$) system was the first reductive-oxidative co-reactant system reported in literature.[214] Initially, the $[Ru(bpy)_3]^{2+}/S_2O_8^{2-}$ system could only be performed within organic or acetonitrile/H_2O mixed solutions due to the fact that in reductive-oxidative systems, a potential more negative than -1.2 V vs Ag/AgCl needs to be

applied to generate ECL. See reactions [1.21]-[1.26] for the mechanism of the $[Ru(bpy)_3]^{2+}$/ $S_2O_8^{2-}$ co-reactant system.

Emissions from the $[Ru(bpy)_3]^{2+}$/ $S_2O_8^{2-}$ co-reactant system in an aqueous environment is problematic because applying such negative potentials produces hydrogen bubbles at the electrode surface, severely affecting the ECL intensity emitted. To minimise this problem, Xu and Dong used carbon paste electrodes which has an extended cathodic potential window and were able to generate stable ECL intensities from the $[Ru(bpy)_3]^{2+}$/ $S_2O_8^{2-}$ system in a purely aqueous environment.[215] Bismuth working electrodes were later proved capable of producing stable ECL emissions of the $[Ru(bpy)_3]^{2+}$/ $S_2O_8^{2-}$ system in an aqueous environment due to the electrodes' large overpotential for hydrogen evolution.[216]

Interestingly, when potentials more negative than -0.6 V were applied at carbon paste electrodes, the reaction between $[Ru(bpy)_3]^{2+}$ and oxygen generated a small detectable ECL emission in an aqueous solution.[215] Typically O_2 was viewed as a quenching species in $[Ru(bpy)_3]^{2+}$ ECL but this is a system where O_2 now actively promotes ECL emissions from $[Ru(bpy)_3]^{2+}$. Later Cao *et al.* observed ECL intensities from the reaction between $[Ru(bpy)_3]^{2+}$ and O_2 species when potentials more negative than -0.4 V was applied at a glassy carbon electrode.[217] Strong $[Ru(bpy)_3]^{2+}$ ECL emissions with O_2 was acting as the co-reactant was also observed when a potential window of 1.5 V to -1.0 V was applied to a glassy carbon electrode coated with a $[Ru(bpy)_3]^{2+}$/Nafion film.[218]

$$[Ru(bpy)_3]^{2+} + e^- \rightarrow [Ru(bpy)_3]^{+} \quad \textbf{[1.27]}$$

$$H_2O_2 + e^- \rightarrow OH^{\bullet} + OH^- \quad \textbf{[1.28]}$$

$$[Ru(bpy)_3]^{+} + OH^{\bullet} \rightarrow [Ru(bpy)_3]^{2+*} + OH^- \quad \textbf{[1.29]}$$

$$[Ru(bpy)_3]^{2+*} \rightarrow [Ru(bpy)_3]^{2+} + h\nu \quad \textbf{[1.30]}$$

When reduced, peroxides (such as hydrogen peroxide) can also act as co-reactants in reductive-oxidative systems (reactions [1.27]-[1.30]) since they produce reactive oxidising agents.[219] ECL is quenched significantly when a high concentration of H_2O_2 is present within the system.

1.2.12 Generation of ECL using rotating electrodes

RDEs and RRDEs have been extensively used to study the mechanisms and kinetics of electrochemical reactions of various systems,[61,62,220–233] however there have been very few studies adapting RDE/RRDE instrumentation to ECL detection. In 1968, Maloy *et al.*[234] reported the use of a platinum RRDE to generate ECL from the pyrene-N,N,N′,N′-tetramethyl-*p*-phenylenediamine (P-TMPD) system. Digital simulations were then performed to predict the effect of electrode rotation rate and the kinetics of the annihilation reaction of 9,10-diphenylanthracene (DPA) would have on the ECL intensity.[235,236] Maloy and Bard then went on to determine the ECL efficiencies from several ECL systems (DPA, DPA-TMPD, rubene and P-TMPD) using a RRDE.[237]

Tokel-Takvoryan *et al.* in 1973 reported the determination of the ECL efficiency of $[Ru(bpy)_3]^{2+}$ using a RRDE.[238] A study on the 9,10-dichloro-9,10-dihydro-9,10-diphenylanthracene ($DPACl_2$) annihilation ECL system was performed by Boto and Bard using an RRDE.[239] Ziebig *et al.* using a platinum RRDE, performed studies on the ECL intensities generated from five derivatives of 1-amino-3-anthryl-(9)-propane.[240]

ECL studies on various dihydropyridine derivatives, disulfides, aromatic sulfochlorides, sulfones and sulfonic ethers were performed by Pragst and various co-workers using an RDE.[241–246] Pastore *et al.* reported on the ECL intensities generated from the luminol/H_2O_2 and luminol/O_2 systems using an RDE.[247] More recently, ECL emissions from

$[Ru(bpy)_3]^{2+}$, luminol and N-(4-aminobuthyl)-N-ethyl-isoluminol was reported on by Juknelevicius *et al.* using a gold RDE at a single rotation rate.[248]

1.3 Project Aims and Outline

The work presented in chapter 2 of this thesis, aims to discover novel and environmentally safe co-reactants for co-reactant ECL as well as expand on the fundamental knowledge of several co-reactant ECL systems. Chapter 2 reports the examination of a series of aliphatic tertiary amines used to buffer the pH in biological experiments, as alternative, non-toxic co-reactants for the ECL of $[Ru(bpy)_3]^{2+}$ with the interesting prospect of also simultaneously serving as the pH buffer and electrolyte within the aqueous environment. Chapters 3 and 4 describes a mechanistic study of several different co-reactant ECL systems (chapter 3), and annihilation ECL systems (chapter 4) under rotation using an RDE and RRDE electrochemical setup as well as documenting the unusual effect rotation has on the ECL generated within these systems.

1.4 References

1 A. Bard and L. Faulkner, *Electrochemical Methods-Fundamentals and Applications*, John Wiley & Sons, New York, 2000.

2 D. C. Johnson, S. G. Weber, A. M. Bond, R. M. Wightman, R. E. Shoup and I. S. Krull, *Anal. Chim. Acta*, 1986, **180**, 187–250.

3 I. E. Henley, K. Yunus and A. C. Fisher, *J. Phys. Chem. B*, 2003, **107**, 3878–3884.

4 H. Gunasingham and B. Fleet, *Anal. Chem.*, 1983, **55**, 1409–1414.

5 J. V. Macpherson and P. R. Unwin, *Anal. Chem.*, 1999, **71**, 2939–2944.

6 C. Hagan and L. A. Coury, *Anal. Chem.*, 1994, **66**, 399–405.

7 K. W. Pratt and D. C. Johnson, *Electrochim. Acta*, 1982, **27**, 1013–1021.

8 V. Levich, *Physicochemical Hydrodynamics*, Prentice-Hall, Upper Saddle River NJ, 1964.

9 Z. Galus, C. Olson, H. Y. Lee and R. N. Adams, *Anal. Chem.*, 1962, **34**, 164–166.

10 S. Bruckenstein and T. Nagai, *Anal. Chem.*, 1961, **33**, 1201–1209.

11 S. Bruckenstein and B. Miller, *Acc. Chem. Res.*, 1977, **10**, 54–61.

12 S. Treimer, A. Tang and D. C. Johnson, *Electroanalysis*, 2002, **14**, 165–171.

13 W. Albery and R. Bell, *Proc. Chem. Soc.*, 1963, 169–170.

14 A. Frumkin, L. Nekrasov, B. Levich and J. Ivanov, *J. Electroanal. Chem.*, 1959, **1**, 84–90.

15 F. Dalton, *Interface Mag.*, 2016, **25**, 50–59.

16 W. J. Albery, *Trans. Faraday Soc.*, 1966, **62**, 1915–1919.

17 W. J. Albery and S. Bruckenstein, *Trans. Faraday Soc.*, 1966, **62**, 1920–1931.

18 W. J. Albery, S. Bruckenstein and D. T. Napp, *Trans. Faraday Soc.*, 1966, **62**, 1932–1937.

19 W. J. Albery, S. Bruckenstein and D. C. Johnson, *Trans. Faraday Soc.*, 1966, **62**, 1938–1945.

20 W. J. Albery and S. Bruckenstein, *Trans. Faraday Soc.*, 1966, **62**, 1946–1954.

21 W. Albery and M. Hitchman, *Ring-Disc Electrodes*, Clarendon Press, London, 1971.

22 S. Marcotte, D. Villers, N. Guillet, L. Roué and J. P. Dodelet, *Electrochim. Acta*, 2004, **50**, 179–188.

23 E. Higuchi, H. Uchida and M. Watanabe, *J. Electroanal. Chem.*, 2005, **583**, 69–76.

24 H. A. Gasteiger, S. S. Kocha, B. Sompalli and F. T. Wagner, *Appl. Catal. B Environ.*, 2005, **56**, 9–35.

25 Y. Garsany, O. A. Baturina, K. E. Swider-Lyons and S. S. Kocha, *Anal. Chem.*, 2010, **82**, 6321–6328.

26 L. Geniès, R. Faure and R. Durand, *Electrochim. Acta*, 1998, **44**, 1317–1327.

27 G. Brisard, N. Bertrand, P. N. Ross and N. M. Marković, *J. Electroanal. Chem.*, 2000, **480**, 219–224.

28 T. J. Schmidt, U. A. Paulus, H. A. Gasteiger and R. J. Behm, *J. Electroanal. Chem.*, 2001, **508**, 41–47.

29 U. A. Paulus, T. J. Schmidt, H. A. Gasteiger and R. J. Behm, *J. Electroanal. Chem.*, 2001, **495**, 134–145.

30 U. A. Paulus, A. Wokaun, G. G. Scherer, T. J. Schmidt, V. Stamenkovic, N. M.

Markovic and P. N. Ross, *Electrochim. Acta*, 2002, **47**, 3787–3798.

31 S. Durón, R. Rivera-Noriega, P. Nkeng, G. Poillerat and O. Solorza-Feria, *J. Electroanal. Chem.*, 2004, **566**, 281–289.

32 L. N. Nekrasov, *Faraday Discuss. Chem. Soc.*, 1973, **56**, 308–316.

33 K. Aoki, K. Tokuda and H. Matsuda, *J. Electroanal. Chem. Interfacial Electrochem.*, 1977, **79**, 49–78.

34 A. C. Fisher and R. G. Compton, *J. Appl. Electrochem.*, 1991, **21**, 208–212.

35 C. G. Phillips and H. A. Stone, *J. Electroanal. Chem.*, 1997, **437**, 157–165.

36 D. Menshykau, M. Cortina-Puig, F. J. del Campo, F. X. Muñoz and R. G. Compton, *J. Electroanal. Chem.*, 2010, **648**, 28–35.

37 S. E. C. Dale, A. Vuorema, E. M. Y. Ashmore, B. Kasprzyk-Horden, M. Sillanpää, G. Denuault and F. Marken, *Chem. Rec.*, 2012, **12**, 143–148.

38 H. Sasaki and M. Maeda, *J. Electrochem. Soc.*, 2010, **157**, C414–C418.

39 H. Sasaki, M. Miyake and M. Maeda, *J. Electrochem. Soc.*, 2010, **157**, E82–E87.

40 R. W. French, Y. Chan, P. C. Bulman-Page and F. Marken, *Electrophoresis*, 2009, **30**, 3361–3365.

41 M. Y. Vagin, A. A. Karyakin, A. Vuorema, M. Sillanpää, H. Meadows, F. J. Del Campo, M. Cortina-Puig, P. C. B. Page, Y. Chan and F. Marken, *Electrochem. commun.*, 2010, **12**, 455–458.

42 W. J. Albery, *Trans. Faraday Soc.*, 1971, **67**, 153–160.

43 W. J. Albery, J. S. Drury and M. L. Hitchman, *Trans. Faraday Soc.*, 1971, **67**, 161–165.

44 W. J. Albery, J. S. Drury and M. L. Hitchman, *Trans. Faraday Soc.*, 1971, **67**, 166–169.

45 W. J. Albery, J. S. Drury and M. L. Hitchman, *Trans. Faraday Soc.*, 1971, **67**, 2162–2166.

46 W. J. Albery, J. S. Drury and A. P. Hutchinson, *Trans. Faraday Soc.*, 1971, **67**, 2414–2418.

47 W. J. Albery and J. S. Drury, *J. Chem. Soc. Faraday Trans. 1 Phys. Chem. Condens. Phases*, 1972, **68**, 456–464.

48 S. Bruckenstein, K. Tokuda and W. J. Albery, *J. Chem. Soc. Faraday Trans. 1 Phys. Chem. Condens. Phases*, 1977, **73**, 823–829.

49 W. J. Albery, R. G. Compton and A. R. Hillman, *J. Chem. Soc. Faraday Trans. 1 Phys. Chem. Condens. Phases*, 1978, **74**, 1007–1019.

50 W. J. Albery and A. R. Hillman, *J. Chem. Soc. Faraday Trans. 1 Phys. Chem. Condens. Phases*, 1979, **75**, 1623–1634.

51 W. J. Albery, M. G. Boutelle, P. J. Colby and A. R. Hillman, *J. Chem. Soc. Faraday Trans. 1 Phys. Chem. Condens. Phases*, 1982, **78**, 2757–2763.

52 W. J. Albery and E. J. Calvo, *J. Chem. Soc. Faraday Trans. 1 Phys. Chem. Condens. Phases*, 1983, **79**, 2583–2596.

53 W. J. Albery and A. R. Mount, *J. Chem. Soc. Faraday Trans. 1 Phys. Chem. Condens. Phases*, 1989, **85**, 1181–1188.

54 W. J. Albery and A. R. Mount, *J. Chem. Soc. Faraday Trans. 1 Phys. Chem. Condens. Phases*, 1989, **85**, 1189–1198.

55 W. J. Albery and A. R. Mount, *J. Chem. Soc. Faraday Trans. 1 Phys. Chem. Condens. Phases*, 1989, **85**, 3717–3724.

56 W. J. Albery and S. Bruckenstein, *Trans. Faraday Soc.*, 1966, **62**, 2584–2595.

57 W. J. Albery and S. Bruckenstein, *Trans. Faraday Soc.*, 1966, **62**, 2596–2606.

58 W. J. Albery, *Trans. Faraday Soc.*, 1967, **63**, 1771–1781.

59 W. J. Albery, M. L. Hitchman and J. Ulstrup, *Trans. Faraday Soc.*, 1968, **64**, 2831–2840.

60 W. J. Albery, M. L. Hitchman and J. Ulstrup, *Trans. Faraday Soc.*, 1969, **65**, 1101–1112.

61 S. Vesztergom, M. Ujvári and G. G. Láng, *Electrochem. commun.*, 2012, **19**, 1–4.

62 S. Vesztergom and G. G. Lang, *Instrum. Sci. Technol.*, 2013, **41**, 82–95.

63 D. C. Harris, *Quantitative Chemical Analysis*, W. H. Freeman and Company, New York, 6th Edn., 2003.

64 J. R. Lakowicz, *Principles of Fluorescence Spectroscopy*, Springer US, Boston, MA, 2006.

65 T. H. Fereja, A. Hymete and T. Gunasekaran, *ISRN Spectrosc.*, 2013, **2013**, 1–12.

66 E. Wiedemann, *Ann. der Phys. und Chemie*, 1888, **270**, 446–463.

67 N. W. Barnett and P. S. Francis, *Encycl. Anal. Sci.*, 2005, 506–511.

68 D. A. Skoog, F. J. Holler and T. A. Nieman, *Principles of Instrumental Analysis*, Harcourt Brace & Company, Orlando, USA, 5th edn., 1998.

69 A. Roda, M. Guardigli, E. Michelini, M. Mirasoli and P. Pasini, *Anal. Chem.*, 2003,

75, 462 A-470 A.

70 L. Hu and G. Xu, *Chem. Soc. Rev.*, 2010, **39**, 3275–3304.

71 R. J. Forster, P. Bertoncello and T. E. Keyes, *Annu. Rev. Anal. Chem.*, 2009, **2**, 359–385.

72 W. Miao, *Chem. Rev.*, 2008, **108**, 2506–2553.

73 D. M. Hercules, *Science*, 1964, **145**, 808–809.

74 R. E. Visco and E. A. Chandross, *J. Am. Chem. Soc.*, 1964, **86**, 5350–5351.

75 K. S. V Santhanam and A. J. Bard, *J. Am. Chem. Soc.*, 1965, **87**, 139–140.

76 N. Harvey, *J. Phys. Chem.*, 1928, **33**, 1456–1459.

77 Meso Scale Discovery, http://www.mesoscale.com/, (accessed 7 April 2018).

78 A. J. Bard, *Electrogenerated Chemiluminescence*, CRC Press, New York, 2004.

79 A. J. Bard, J. D. Debad, J. K. Leland, G. B. Sigal, J. L. Wilbur and J. N. Wohlsatdter, *Encyclopedia of Analytical Chemistry*, John Wiley & Sons, Ltd, Chichester, UK, 2006.

80 R. Pyati and M. M. Richter, *Annu. Rep. Prog. Chem., Sect. C Phys. Chem.*, 2007, **103**, 12–78.

81 M. M. Richter, *Chem. Rev*, 2004, **104**, 3003–3036.

82 W.-Y. Lee, *Mikrochim. Acta*, 1997, **127**, 19–39.

83 M. M. Chang, T. Saji and A. J. Bard, *J. Am. Chem. Soc.*, 1977, **99**, 5399–5403.

84 X.-B. Yin, S. Dong and E. Wang, *TrAC Trends Anal. Chem.*, 2004, **23**, 432–441.

85 I. Rubinstein and A. J. Bard, *J. Am. Chem. Soc.*, 1981, **103**, 512–516.

86 W. Miao, J.-P. Choi and A. J. Bard, *J. Am. Chem. Soc.*, 2002, **124**, 14478–14485.

87 T. M. Downey and T. A. Nieman, *Anal. Chem.*, 1992, **64**, 261–268.

88 N. Egashira, H. Kumasako and K. Ohga, *Anal. Sci.*, 1990, **6**, 903–904.

89 D. J. Walton, S. S. Phull, D. M. Bates, J. P. Lorimer and T. J. Mason, *Ultrasonics*, 1992, **30**, 186–191.

90 D. R. Skotty and T. A. Nieman, *J. Chromatogr. B Biomed. Sci. Appl.*, 1995, **665**, 27–36.

91 W.-Y. Lee and T. A. Nieman, *Anal. Chem.*, 1995, **67**, 1789–1796.

92 D. R. Skotty, W.-Y. Lee and T. A. Nieman, *Anal. Chem.*, 1996, **68**, 1530–1535.

93 F. Jameison, R. I. Sanchez, L. Dong, J. K. Leland, D. Yost and M. T. Martin, *Anal. Chem.*, 1996, **68**, 1298–1302.

94 A. W. Knight and G. M. Greenway, *Analyst*, 1996, **121**, 101R.

95 D. R. Deaver, *Nature*, 1995, **377**, 758–760.

96 J. K. Leland and M. J. Powell, *J. Electrochem. Soc.*, 1990, **137**, 3127.

97 J. B. Noffsinger and N. D. Danielson, *Anal. Chem.*, 1987, **59**, 865–868.

98 G. F. Blackburn, H. P. Shah, J. H. Kenten, J. Leland, R. A. Kamin, J. Link, J. Peterman, M. J. Powell, A. Shah and D. B. Talley, *Clin. Chem.*, 1991, **37**, 1534–1539.

99 W. Cao, J. Liu, X. Yang and E. Wang, *Electrophoresis*, 2002, **23**, 3683–3691.

100 W. Miao and A. J. Bard, *Anal. Chem.*, 2003, **75**, 5825–5834.

101 R. Okabe, K. Nakatsuka, M. Inaba, T. Miki, H. Naka, H. Masaki, A. Moriguchi and Y. Nishizawa, *Clin. Chem.*, 2001, **47**, 1410–1414.

102 M. Ohlin, M. Silvestri, V. A. Sundqvist and C. A. Borrebaeck, *Clin. Diagn. Lab. Immunol.*, 1997, **4**, 107–111.

103 B. Weber, A. Bayer, P. Kirch, V. Schlüter, D. Schlieper and W. Melchior, *J. Clin. Microbiol.*, 1999, **37**, 2639–2647.

104 M. P. de Baar, K. H. van der Horn, J. Goudsmit, A. de Ronde and F. de Wolf, *J. Clin. Microbiol.*, 1999, **37**, 63–67.

105 L. Kobrynski, L. Tanimune, N. A. Pawlowski, S. D. Douglas and D. E. Campbell, *Clin. Diagn. Lab. Immunol.*, 1996, **3**, 42–46.

106 R. Sapin, V. Le Galudec, F. Gasser, M. Pinget and D. Grucker, *Clin. Chem.*, 2001, **47**, 602–605.

107 D. Novick, B. Schwartsburd, R. Pinkus, D. Suissa, I. Belzer, Z. Sthoeger, W. F. Keane, Y. Chvatchko, S. H. Kim, G. Fantuzzi, C. A. Dinarello and M. Rubinstein, *Cytokine*, 2001, **14**, 334–342.

108 S. V. Sennikov, S. V. Krysov, T. V. Injelevskaya, A. N. Silkov, L. V. Grishina and V. A. Kozlov, *J. Immunol. Methods*, 2003, **275**, 81–88.

109 A. W. Butch, D. Crary and M. Yee, *Clin. Biochem.*, 2002, **35**, 143–145.

110 A. Haese, R. T. Dworschack, S. P. Piccoli, L. J. Sokoll, A. W. Partin and D. W. Chan, *Clin. Chem.*, 2002, **48**, 944–947.

111 M.-T. Chiang, M.-C. Lu and C.-W. Whang, *Electrophoresis*, 2003, **24**, 3033–3039.

112 P. B. Luppa, S. Reutemann, U. Huber, R. Hoermann, S. Poertl, S. Kraiss, S. von Bülow and D. Neumeier, *Clin. Chem. Lab. Med.*, 1998, **36**, 789–796.

113 M. Sánchez-Carbayo, M. Mauri, R. Alfayate, C. Miralles and F. Soria, *Clin. Biochem.*,

1999, **32**, 395–403.

114 X.-H. N. Xu, R. B. Jeffers, J. Gao and B. Logan, *Analyst*, 2001, **126**, 1285–1292.

115 O. Hetland and K. Dickstein, *Clin. Chem.*, 1998, **44**, 1348–1350.

116 J. Ishii, T. Ishikawa, J. Yukitake, Y. Nagamura, M. Ito, J. H. Wang, Y. Kato, S. Hiramitsu, S. Inoue, T. Kondo, S. Morimoto, M. Nomura, Y. Watanabe and H. Hishida, *Clin. Chim. Acta.*, 1998, **270**, 183–188.

117 P. O. Collinson, B. Jørgensen, C. Sylvén, M. Haass, F. Chwallek, H. A. Katus, M. Müller-Bardorff, U. Derhaschnig, M. M. Hirschl and R. Zerback, *Clin. Chim. Acta*, 2001, **307**, 197–203.

118 E. Moreau, J. Philippé, S. Couvent and G. Leroux-Roels, *Clin. Chem.*, 1996, **42**, 1450–1453.

119 J. H. Tai, M. S. Ewert, G. Belliot, R. I. Glass and S. S. Monroe, *J. Virol. Methods*, 2003, **110**, 119–127.

120 K. N. Reetoo, S. A. Osman, S. J. Illavia, J. E. Banatvala and P. Muir, *J. Virol. Methods*, 1999, **82**, 145–156.

121 R. Boom, C. Sol, J. Weel, Y. Gerrits, M. de Boer and P. Wertheim-van Dillen, *J. Clin. Microbiol.*, 1999, **37**, 1489–1497.

122 Y. Namba, M. Usami and O. Suzuki, *Anal. Sci.*, 1999, **15**, 1087–1093.

123 S. J. Wu, E. M. Lee, R. Putvatana, R. N. Shurtliff, K. R. Porter, W. Suharyono, D. M. Watts, C. C. King, G. S. Murphy, C. G. Hayes and J. W. Romano, *J. Clin. Microbiol.*, 2001, **39**, 2794–2798.

124 S. J. Stevens, M. B. Vervoort, A. J. van den Brule, P. L. Meenhorst, C. J. Meijer and J.

M. Middeldorp, *J. Clin. Microbiol.*, 1999, **37**, 2852–2857.

125 R. A. Collins, L.-S. Ko, K. Y. Fung, L.-T. Lau, J. Xing and A. C. H. Yu, *Biochem. Biophys. Res. Commun.*, 2002, **297**, 267–274.

126 B. van Gemen, R. van Beuningen, A. Nabbe, D. van Strijp, S. Jurriaans, P. Lens and T. Kievits, *J. Virol. Methods*, 1994, **49**, 157–167.

127 T. E. Schutzbank and J. Smith, *J. Clin. Microbiol.*, 1995, **33**, 2036–2041.

128 J. H. Kenten, S. Gudibande, J. Link, J. J. Willey, B. Curfman, E. O. Major and R. J. Massey, *Clin. Chem.*, 1992, **38**, 873–879.

129 R. A. Collins, L.-S. Ko, K.-Y. Fung, K.-Y. Chan, J. Xing, L.-T. Lau and A. C. H. Yu, *Biochem. Biophys. Res. Commun.*, 2003, **300**, 507–515.

130 S. Shan, L.-S. Ko, R. A. Collins, Z. Wu, J. Chen, K.-Y. Chan, J. Xing, L.-T. Lau and A. C.-H. Yu, *Biochem. Biophys. Res. Commun.*, 2003, **302**, 377–383.

131 I. Miyashiro, C. Kuo, K. Huynh, A. Iida, D. Morton, A. Bilchik, A. Giuliano and D. S. Hoon, *Clin. Chem.*, 2001, **47**, 505–512.

132 C. D. O'Connell, A. Juhasz, C. Kuo, D. J. Reeder and D. S. Hoon, *Clin. Chem.*, 1998, **44**, 1161–1169.

133 K. Fukuda, K. Takahashi, Y. Iwata, N. Mori, K. Gonda, T. Ogawa, K. Osonoe, M. Sato, S.-I. Ogata, T. Horimoto, T. Sawada, M. Tashiro, K. Yamaguchi, S.-I. Niwa and S. Shigeta, *J. Clin. Microbiol.*, 2001, **39**, 419–429.

134 B. Taback, A. D. Chan, C. T. Kuo, P. J. Bostick, H. J. Wang, A. E. Giuliano and D. S. Hoon, *Cancer Res.*, 2001, **61**, 8845–8850.

135 D. S. B. Hoon, C. T. Kuo, S. Wen, H. Wang, L. Metelitsa, C. P. Reynolds and R. C.

Seeger, *Am. J. Pathol.*, 2001, **159**, 493–500.

136 R. S. Lanciotti and A. J. Kerst, *J. Clin. Microbiol.*, 2001, **39**, 4506–4513.

137 M. D. de Jong, J. F. Weel, T. Schuurman, P. M. Wertheim-van Dillen and R. Boom, *J. Clin. Microbiol.*, 2000, **38**, 2568–2573.

138 H. J. Stern, R. D. Carlos and T. E. Schutzbank, *Clin. Biochem.*, 1995, **28**, 470–3.

139 B. D. Muegge and M. M. Richter, *Anal. Chem.*, 2002, **74**, 547–550.

140 R. Y. Lai, M. Chiba, N. Kitamura and A. J. Bard, *Anal. Chem.*, 2002, **74**, 551–553.

141 K. Yamaguchi, T. Sawada, S. Yamane, S. Haga, K. Ikeda, R. Igata-Yi, K. Yoshiki, M. Matsuoka, H. Okabe, Y. Horii, Y. Nawa, R. W. Waltrip and K. M. Carbone, *Ann. Clin. Biochem.*, 2001, **38**, 348–355.

142 O. E. Khorkova, K. Patel, J. Heroux and S. Sahasrabudhe, *J. Neurosci. Methods*, 1998, **82**, 159–166.

143 P. Stieber, R. Molina, D. W. Chan, H. A. Fritsche, R. Beyrau, J. M. G. Bonfrer, X. Filella, T. G. Gornet, T. Hoff, W. Jäger, G. J. van Kamp, D. Nagel, K. Peisker, L. J. Sokoll, F. Troalen, M. Untch and I. Domke, *Clin. Chem.*, 2001, **47**, 2162–2164.

144 H. E. van Ingen, D. W. Chan, W. Hubl, H. Miyachi, R. Molina, L. Pitzel, A. Ruibal, J. C. Rymer and I. Domke, *Clin. Chem.*, 1998, **44**, 2530–2536.

145 T. Seck, I. Diel, H. Bismar, R. Ziegler and J. Pfeilschifter, *Bone*, 2002, **30**, 217–222.

146 X. Liu, L. Shi, W. Niu, H. Li and G. Xu, *Angew. Chem. Int. Ed. Engl.*, 2007, **46**, 421–424.

147 Z. Guo and P. Gai, *Anal. Chim. Acta*, 2011, **688**, 197–202.

148 L. Xue, L. Guo, B. Qiu, Z. Lin and G. Chen, *Electrochem. commun.*, 2009, **11**, 1579–

1582.

149 X.-M. Chen, G.-H. Wu, J.-M. Chen, Y.-Q. Jiang, G.-N. Chen, M. Oyama, X. Chen and X.-R. Wang, *Biosens. Bioelectron.*, 2010, **26**, 872–876.

150 G. A. Crespo, G. Mistlberger and E. Bakker, *J. Am. Chem. Soc.*, 2012, **134**, 205–207.

151 S. Wang, J. Milam, A. C. Ohlin, V. H. Rambaran, E. Clark, W. Ward, L. Seymour, W. H. Casey, A. A. Holder and W. Miao, *Anal. Chem.*, 2009, **81**, 4068–4075.

152 S. Wang, J. Wei, T. Hao and Z. Guo, *J. Electroanal. Chem.*, 2012, **664**, 146–151.

153 Q.-H. Wei, Y.-F. Lei, Y.-N. Duan, F.-N. Xiao, M.-J. Li and G.-N. Chen, *Dalt. Trans.*, 2011, **40**, 11636–11642.

154 S. Parveen, W. Zhang, Y. Yuan, L. Hu, M. R. H. Shah Gilani, A. ur Rehman and G. Xu, *J. Electroanal. Chem.*, 2013, **688**, 45–48.

155 S. Wu, Z. Zhou, L. Xu, B. Su and Q. Fang, *Biosens. Bioelectron.*, 2014, **53**, 148–153.

156 M. Sentic, M. Milutinovic, F. Kanoufi, D. Manojlovic, S. Arbault and N. Sojic, *Chem. Sci.*, 2014, **5**, 2568–2572.

157 X. Jiang, W. Ding and C. Luan, *Can. J. Chem.*, 2013, **91**, 656–661.

158 M.-J. Li, Y.-Q. Shi, T.-Y. Lan, H.-H. Yang and G.-N. Chen, *J. Electroanal. Chem.*, 2013, **702**, 25–30.

159 J. L. Delaney, E. H. Doeven, A. J. Harsant and C. F. Hogan, *Anal. Chim. Acta*, 2013, **790**, 56–60.

160 Z. Guo, T. Hao, L. Shi, P. Gai, J. Duan, S. Wang and N. Gan, *Food Chem.*, 2012, **132**, 1092–1097.

161 T. Hu, X. Liu, S. Liu, Z. Wang and Z. Tang, *Anal. Chem.*, 2014, **86**, 3939–3946.

162 Y. Lei, Y. Lin, Y. Zheng, M. Dai, K. Wang and X. Lin, *Electroanalysis*, 2013, **25**, 1388–1394.

163 S. Sun, F. Li, F. Liu, X. Yang, J. Fan, F. Song, L. Sun and X. Peng, *Dalt. Trans.*, 2012, **41**, 12434–12438.

164 S. Sun, Y. Yang, F. Liu, J. Fan, J. Kehr, L. Sun and X. Peng, *Dalt. Trans.*, 2010, **39**, 8626–8630.

165 S. Sun, Y. Yang, F. Liu, J. Fan, X. Peng, J. Kehr and L. Sun, *Dalt. Trans.*, 2009, 7969–7974.

166 S. Sun, Y. Yang, F. Liu, Y. Pang, J. Fan, L. Sun and X. Peng, *Anal. Chem.*, 2009, **81**, 10227–10231.

167 E. K. Walker, D. A. Vanden Bout and K. J. Stevenson, *Langmuir*, 2012, **28**, 1604–1610.

168 S. Kumar and S.-M. Chen, *Sensors*, 2008, **8**, 739–766.

169 A. F. Martin and T. A. Nieman, *Anal. Chim. Acta*, 1993, **281**, 475–481.

170 A. F. Martin and T. A. Nieman, *Biosens. Bioelectron.*, 1997, **12**, 479–489.

171 R. Lei, X. Wang, S. Zhu and N. Li, *Sensors Actuators B Chem.*, 2011, **158**, 124–129.

172 G. Guo, Q. Chen and X. Chen, *Sci. China Chem.*, 2011, **54**, 1777–1781.

173 M. Milutinovic, S. Sallard, D. Manojlovic, N. Mano and N. Sojic, *Bioelectrochemistry*, 2011, **82**, 63–68.

174 C. Zhang, J. Xu, W. Ma and W. Zheng, *Biotechnol. Adv.*, 2006, **24**, 243–284.

175 H. N. Choi, S. H. Yoon, Y.-K. Lyu and W.-Y. Lee, *Electroanalysis*, 2007, **19**, 459–465.

176 L. Deng, L. Zhang, L. Shang, S. Guo, D. Wen, F. Wang and S. Dong, *Biosens. Bioelectron.*, 2009, **24**, 2273–2276.

177 A. Bergel, J. Souppe and M. Comtat, *Anal. Biochem.*, 1989, **179**, 382–388.

178 D. Jiang, L. Zhang, F. Liu, C. Liu, L. Liu and X. Pu, *RSC Adv.*, 2016, **6**, 19676–19685.

179 L. Zhang, Z. Xu, X. Sun and S. Dong, *Biosens. Bioelectron.*, 2007, **22**, 1097–1100.

180 T. Jia, Z. Cai, X. Chen, Z. Lin, X. Huang, X. Chen and G. Chen, *Biosens. Bioelectron.*, 2009, **25**, 263–267.

181 X. Lin, Q. Wang, S. Zhu, J. Xu, Q. Xia and Y. Fu, *RSC Adv.*, 2016, **6**, 45829–45834.

182 X. Wang and D. R. Bobbitt, *Anal. Chim. Acta*, 1999, **383**, 213–220.

183 D. R. Bobbitt, W. A. Jackson and H. P. Hendrickson, *Talanta*, 1998, **46**, 565–572.

184 H. P. Hendrickson, P. Anderson, X. Wang, Z. Pittman and D. R. Bobbitt, *Microchem. J.*, 2000, **65**, 189–195.

185 M. T. Chiang and C. W. Whang, *J. Chromatogr. A*, 2001, **934**, 59–66.

186 H. Qiu, J. Yan, X. Sun, J. Liu, W. Cao, X. Yang and E. Wang, *Anal. Chem.*, 2003, **75**, 5435–5440.

187 G. M. Greenway, A. W. Knight and P. J. Knight, *Analyst*, 1995, **120**, 2549–2552.

188 J. L. Adcock, C. J. Barrow, N. W. Barnett, X. A. Conlan, C. F. Hogan and P. S. Francis, *Drug Test. Anal.*, 2011, **3**, 145–160.

189 Y. Li, C. Wang, J. Sun, Y. Zhou, T. You, E. Wang and Y. Fung, *Anal. Chim. Acta*, 2005, **550**, 40–46.

190 Y. Yuan, H. Li, S. Han, L. Hu and G. Xu, *Talanta*, 2011, **84**, 49–52.

191 H. Yoshida, K. Hidaka, J. Ishida, K. Yoshikuni, H. Nohta and M. Yamaguchi, *Anal. Chim. Acta*, 2000, **413**, 137–145.

192 Q. Song, G. M. Greenway and T. McCreedy, *Analyst*, 2001, **126**, 37–40.

193 Z. Lin and G. Chen, *Talanta*, 2006, **70**, 111–115.

194 G. M. Greenway and P. J. Knight, *Anal. Proc. Incl. Anal. Commun.*, 1995, **32**, 251–253.

195 S. J. L. Dolman and G. M. Greenway, *Anal. Commun.*, 1996, **33**, 139–141.

196 A. W. Knight and G. M. Greenway, *Anal. Commun.*, 1996, **33**, 171–174.

197 P. Liang, R. I. Sanchez and M. T. Martin, *Anal. Chem.*, 1996, **68**, 2426–2431.

198 G. A. Forbes, T. A. Nieman and J. V Sweedler, *Anal. Chim. Acta*, 1997, **347**, 289–293.

199 L. Dennany, R. J. Forster and J. F. Rusling, *J. Am. Chem. Soc.*, 2003, **125**, 5213–5218.

200 L. Dennany, C. F. Hogan, T. E. Keyes and R. J. Forster, *Anal. Chem.*, 2006, **78**, 1412–1417.

201 M. So, E. G. Hvastkovs, J. B. Schenkman and J. F. Rusling, *Biosens. Bioelectron.*, 2007, **23**, 492–498.

202 H. Wei, Y. Du, J. Kang and E. Wang, *Electrochem. commun.*, 2007, **9**, 1474–1479.

203 A. W. Knight and G. M. Greenway, *Analyst*, 1995, **120**, 2543–2547.

204 L. Hu, H. Li, S. Han and G. Xu, *J. Electroanal. Chem.*, 2011, **656**, 289–292.

205 X. Chen, M. Sato and Y. Lin, *Microchem. J.*, 1998, **58**, 13–20.

206 K. Uchikura, *Anal. Sci.*, 1999, **15**, 1049–1050.

207 X. Chen and M. Sato, *Anal. Sci.*, 1995, **11**, 749–754.

208 X. Sun, Y. Niu, S. Bi and S. Zhang, *Electrophoresis*, 2008, **29**, 2918–2924.

209 F. Takahashi and J. Jin, *Luminescence*, 2008, **23**, 121–125.

210 M. Zorzi, P. Pastore and F. Magno, *Anal. Chem.*, 2000, **72**, 4934–4939.

211 F. Takahashi and J. Jin, *Anal. Bioanal. Chem.*, 2009, **393**, 1669–1675.

212 Y. Yuan, H. Li, S. Han, L. Hu, S. Parveen and G. Xu, *Anal. Chim. Acta*, 2011, **701**, 169–173.

213 Y. Liao, R. Yuan, Y. Chai, Y. Zhuo, Y. Yuan, L. Bai, L. Mao and S. Yuan, *Biosens. Bioelectron.*, 2011, **26**, 4815–4818.

214 H. S. White and A. J. Bard, *J. Am. Chem. Soc.*, 1982, **104**, 6891–6895.

215 G. Xu and S. Dong, *Electroanalysis*, 2000, **12**, 583–587.

216 L. Hu, H. Li, S. Zhu, L. Fan, L. Shi, X. Liu and G. Xu, *Chem. Commun.*, 2007, 4146.

217 W. Cao, G. Xu, Z. Zhang and S. Dong, *Chem. Commun.*, 2002, 1540–1541.

218 L. Zheng, Y. Chi, Q. Shu, Y. Dong, L. Zhang and G. Chen, *J. Phys. Chem. C*, 2009, **113**, 20316–20321.

219 J.-P. Choi and A. J. Bard, *Anal. Chim. Acta*, 2005, **541**, 141–148.

220 T. Lopes, J. Chlistunoff, J.-M. Sansiñena and F. H. Garzon, *Int. J. Hydrogen Energy*, 2012, **37**, 5202–5207.

221 J. L. Reyes-Rodríguez, F. Godínez-Salomón, M. A. Leyva and O. Solorza-Feria, *Int. J. Hydrogen Energy*, 2013, **38**, 12634–12639.

222 K. Ono, Y. Yasuda, K. Sekizawa, N. Takeuchi, T. Yoshida and M. Sudoh, *Electrochim. Acta*, 2013, **97**, 58–65.

223 S. Vesztergom, M. Ujvári and G. G. Láng, *Electrochim. Acta*, 2013, **110**, 49–55.

224 S. Tsuneyasu, K. Ichihara, K. Nakamura and N. Kobayashi, *Phys. Chem. Chem. Phys.*, 2016, **18**, 16317–16324.

225 S. Tsuneyasu, T. Ichikawa, K. Nakamura and N. Kobayashi, *ChemElectroChem*, 2017, **4**, 1731–1735.

226 A. Damjanovic, M. A. Genshaw and J. O. Bockris, *J. Phys. Chem.*, 1966, **70**, 3761–3762.

227 M. A. Genshaw, A. Damjanovic and J. O. Bockris, *J. Phys. Chem.*, 1967, **71**, 3722–3731.

228 A. Damjanovic, M. A. Genshaw and J. O. Bockris, *J. Electrochem. Soc.* , 1967, **114**, 466–472.

229 A. Damjanovic, M. A. Genshaw and J. O. Bockris, *J. Electrochem. Soc.*, 1967, **114**, 1107–1112.

230 L. S. Marcoux, R. N. Adams and S. W. Feldberg, *J. Phys. Chem.*, 1969, **73**, 2611–2614.

231 P. Krishnan, T.-H. Yang, S. G. Advani and A. K. Prasad, *J. Power Sources*, 2008, **182**, 106–111.

232 F. Jaouen, *J. Phys. Chem. C*, 2009, **113**, 15433–15443.

233 R. J. Fealy and J. I. Goldsmith, *J. Phys. Chem. C*, 2012, **116**, 13133–13142.

234 J. T. Maloy, K. B. Prater and A. J. Bard, *J. Phys. Chem.*, 1968, **72**, 4348–4350.

235 J. T. Maloy, K. B. Prater and A. J. Bard, *J. Am. Chem. Soc.*, 1971, **93**, 5959–5968.

236 J. T. Maloy, *Comput. Chem. Instrum.*, 1972, **2**, 241–260.

237 J. T. Maloy and A. J. Bard, *J. Am. Chem. Soc.*, 1971, **93**, 5968–5981.

238 N. E. Tokel-Takvoryan, R. E. Hemingway and A. J. Bard, *J. Am. Chem. Soc.*, 1973, **95**, 6582–6589.

239 K. Boto and A. J. Bard, *J. Electroanal. Chem.*, 1975, **65**, 945–962.

240 R. Ziebig, H.-J. Hamann, W. Jugelt and F. Pragst, *J. Lumin.*, 1980, **21**, 353–366.

241 F. Pragst and B. Kaltofen, *J. Electroanal. Chem. Interfacial Electrochem.*, 1980, **112**, 339–345.

242 F. Pragst, *J. Electroanal. Chem. Interfacial Electrochem.*, 1981, **119**, 315–330.

243 F. Pragst, B. Kaltofen, J. Volke and J. Kuthan, *J. Electroanal. Chem. Interfacial Electrochem.*, 1981, **119**, 301–314.

244 F. Pragst and B. Kaltofen, *Electrochim. Acta*, 1982, **27**, 1181–1191.

245 F. Pragst and M. Von Löwis, *J. Electroanal. Chem. Interfacial Electrochem.*, 1982, **133**, 173–182.

246 F. Pragst and M. Niazymbetov, *J. Electroanal. Chem. Interfacial Electrochem.*, 1986, **197**, 245–264.

247 P. Pastore, G. Favaro, A. Gallina and R. Antiochia, *Ann. di Chim. (Rome, Italy)*, 2002, **92**, 271–280.

248 D. Juknelevicius, L. Mikoliunaite, A. Ramanaviciene and A. Ramanavicius, *Chem. Pap.*, 2017, **71**, 905–912.

Chapter 2: ECL of $[Ru(bpy)_3]^{2+}$ Using Common Biological Buffers as the Co-reactant, pH Buffer and Supporting Electrolyte

2.1 Introduction

ECL is the emission of light from the excited products of a chemical reaction, where at least one reactant is generated electrochemically.[1–3] The first detailed studies of ECL were described by Hercules[4] and Bard *et al*.[5] in the mid-1960s; however, reports of light emission during electrolysis date back to the 1920s[6]. In 1972, Tokel and Bard described the ECL of $[Ru(bpy)_3]^{2+}$ via annihilation between oxidised and reduced forms of the complex in acetonitrile.[7] Bard's group also demonstrated the first co-reactant ECL (using oxalate),[8] before Leland and Powell introduced tri-n-propylamine (TPA) in 1990.[9] Blackburn *et al*. subsequently adopted this system for ECL detection in immunoassays using $[Ru(bpy)_3]$-based labels.[10]

TPA remains by far the most widely used co-reactant for ECL,[3,11–19] and the $[Ru(bpy)_3]^{2+}$/TPA system is currently employed in the vast majority of commercially available ECL instrumentation and methods.[1,20] TPA is an effective co-reactant for $[Ru(bpy)_3]^{2+}$ ECL, but there are several well-known problems associated with its use. Most importantly, TPA is highly toxic (LD50 oral: 98 mg/Kg, LC50 inhalation: 1500 mg/m^3) and quite volatile. It is destructive to the mucous membrane and upper respiratory tract system of the human body and can be fatal if inhaled. While some of the luminophores used in ECL are also toxic, this is less of a problem because they are used in far lower concentrations. TPA is not readily soluble in water, but relatively high concentrations (~100 mM) are required to attain the highest sensitivity.[11–13] Furthermore, the intensity of $[Ru(bpy)_3]^{2+}$ ECL with TPA as the co-reactant strongly depends on the working electrode material (for example, intensities generated using Pt electrodes are only 10% of the those at Au electrodes).[21]

Not surprisingly, there has been considerable interest in the development of alternatives to TPA for co-reactant ECL.[21,22] Most notably, Liu *et al*.[21] introduced 2-(dibutylamino)ethanol (DBAE) as a safer co-reactant for $[Ru(bpy)_3]^{2+}$ ECL. Under certain circumstances, such as at relatively low co-reactant concentrations when using glassy carbon working electrodes, DBAE gave greater ECL intensities than TPA, but under other conditions, the novel co-reactant is not as effective. Han *et al*.[22] subsequently examined a series of tertiary amines and ethanolamines, and reported that N-butyldiethanolamine performed better than DBAE at lower co-reactant concentrations, but unfortunately, it is more toxic than DBAE.

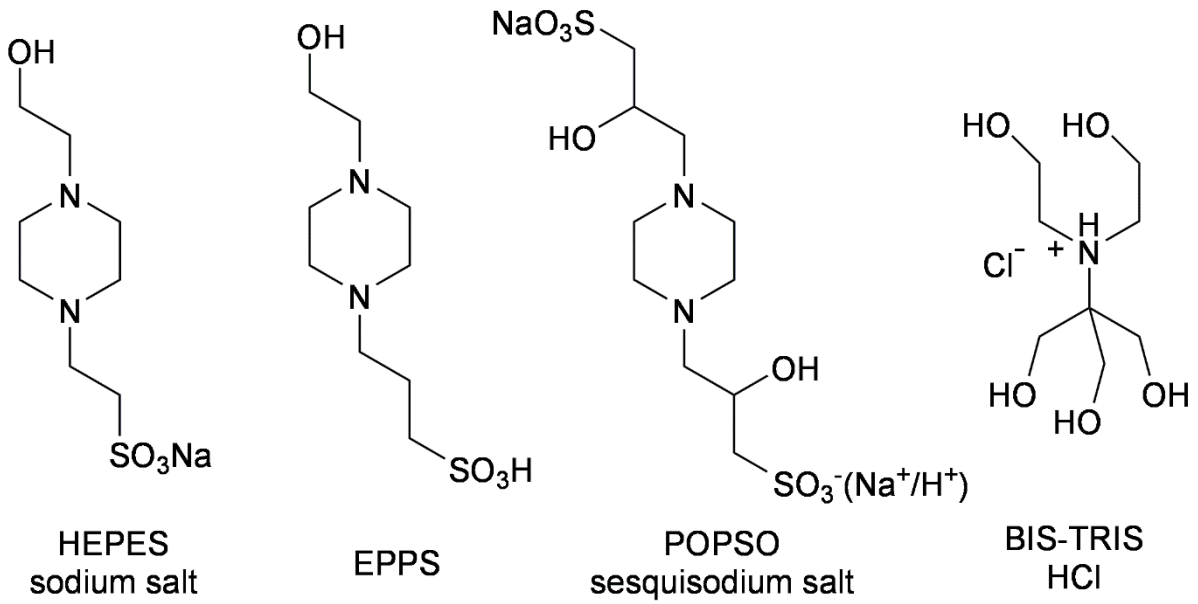

Figure 2.1: Biological buffers examined in this study containing aliphatic tertiary amine/ethanolamine groups: N-(2-hydroxyethyl)piperazine-N′-(2-ethane-sulfonic acid) sodium salt (HEPES sodium salt); *N*-(2-hydroxythyl)piperazine-*N*′-(3-propanesulfonic acid) (EPPS); piperazine-N,N′-bis(2-hydroxypropanesulfonic acid) sesquisodium salt (POPSO sesquisodium salt); and 2-bis(2-hydroxyethyl)amino-2-(hydroxymethyl)-1,3-propanediol hydrochloride (BIS-TRIS HCl)).

Several commonly used laboratory buffers (Figure 2.1) possess similar chemical structures to previously investigated tertiary amine and ethanolamine co-reactants.[16,17] Moreover, Leland and Powell[9] reported that when triethanolamine and 1,4-piperazinediethanesulfonic acid (PIPES) were used as co-reactants with $[Ru(bpy)_3]^{2+}$, the ECL intensity was 53% and 31% of that using TPA, respectively. Later, a study exploring the co-reactant ability of a number of biological buffers in the presence of an electrolyte[23] showed that such species could elicit ECL from $[Ru(bpy)_3]^{2+}$. In this work we have carried out a detailed study of the potential of several common laboratory buffers as alternative co-reactants for $[Ru(bpy)_3]^{2+}$ ECL. These buffers are a sub-set of those referred to as 'biological' buffers, or 'Good' buffers, after the pioneering work on these substituted glycine and *N*-substituted taurine molecules by Good and co-workers.[24–26] Importantly, the following criteria used by Good et al. in the development of these buffers[25] are also highly desirable properties for ECL co-reactants, particularly in bioanalytical applications: (i) they should be readily soluble in water and should not be able to permeate biological membranes; (ii) they should alter the ionic strength of the system as little as possible; (iii) their pKa should be influenced as little as possible by their concentration, temperature and the ion composition of the medium; (iv) they should not be subject to enzymatic or non-enzymatic changes; (v) they should not be able to absorb light at wavelengths longer than 230 nm; (vi) they should be easily manufactured and purified; and finally (vii) they should be non-toxic and cost effective.

In this study, four 'Good' buffers that possess aliphatic tertiary amine/ethanolamine groups (Figure 2.1) were examined as alternative, non-toxic co-reactants for $[Ru(bpy)_3]^{2+}$ ECL, with the interesting prospect of also simultaneously serving as the pH buffer and electrolyte within the aqueous environment. A buffer for ECL-based bioanalysis, which performs multiple functions (co-reactant/buffer/electrolyte) would significantly simplify the

analytical procedure, reducing the variability associated with adding numerous components to a sample. Moreover, this simplicity would reduce the probability of a reagent interfering with interactions between biomolecules in immunoassays or DNA probe analysis. Finally, replacing the electrolyte with the co-reactant offers the possibility of migrationally enhanced ECL signals.

2.2 Experimental

2.2.1 Chemicals and materials

Unless otherwise stated, deionised water (Sartorius Stedim biotech arium® pro VF Ultrapure Water System, 18.2 MΩ cm, Germany) and analytical grade reagents were used. The Good buffers shown in Figure 2.1: BIS-TRIS hydrochloride, POPSO sesquisodium salt, EPPS, and HEPES sodium salt were obtained from Sigma-Aldrich (NSW, Australia). Tris(2,2´-bipyridine)ruthenium(II) chloride hexahydrate ($[Ru(bpy)_3]Cl_2.6H_2O$, 99%) was purchased from Strem Chemicals (MA, USA). In the examination of optimum pH the buffers were each prepared at 0.1 M, with 1 μM $[Ru(bpy)_3]^{2+}$. Useful pH range: BIS-TRIS HCl: pH 5.8-7.2; POPSO sesquisodium salt: pH 7.2-8.5; HEPES sodium salt: pH 6.8-8.2; EPPS: pH 7.3-8.7. The pH was adjusted using 0.1 M HCl or 0.1 M NaOH.

2.2.2 Instrumentation

The pH of the working solutions was measured using an MEP Instruments Metrohm 827 pH Lab pH meter and an MEP Instruments Metrohm 6.0228.010 pH electrode. A CH instruments (TX, USA) electrochemical workstation was used to perform cyclic voltammetry experiments (660E) with CHI660e software. A custom built light-tight faraday cage encased the electrochemical cell, which consisted of a cylindrical glass cell with a quartz window base and a Teflon cover with a spill tray. A conventional three-electrode configuration was used, comprising a glassy carbon (3 mm diameter) working electrode shrouded in Teflon (CH

Instruments, Austin, TX, USA), a 1 cm^2 gold wire auxiliary electrode and a Ag/AgCl (3 M KCl) reference electrode (CH Instruments, Austin, TX, USA). The working electrode was polished with alumina slurry (0.3 µm) on a felt pad, rinsed with water and acetone and dried while under a steady stream of nitrogen. The surface of the working electrode was then positioned at a reproducible distance (~2 mm) from the bottom of the cell for detection. The ECL intensity was measured with a photomultiplier tube (PMT) (model 98285B; Electron Tubes, Ruislip, UK), biased at 500 V using a PM28B power supply (Electron Tubes). The PMT signal was amplified using a TA-GI-74 Ames Photonics amplifier (model D7280) and acquired using the auxiliary channel of the potentiostat. Cyclic voltammetry (CV) was performed over the 0 V to 1.5 V range at a scan rate of 0.05 V/s while the ECL signal was simultaneously recorded.

2.3 Results and Discussion

2.3.1 'Good' buffer as a co-reactant

We initially examined the co-reactant ECL intensity of 1 µM $[Ru(bpy)_3]^{2+}$ with each of the four amines shown in Figure 2.1 and TPA at a concentration of 10 mM in aqueous solution, using a phosphate buffer to control the pH and serve as the electrolyte (Figure 2.2). The ECL intensity using the biological buffers as co-reactants was between 13% and 48% of that observed when using TPA.

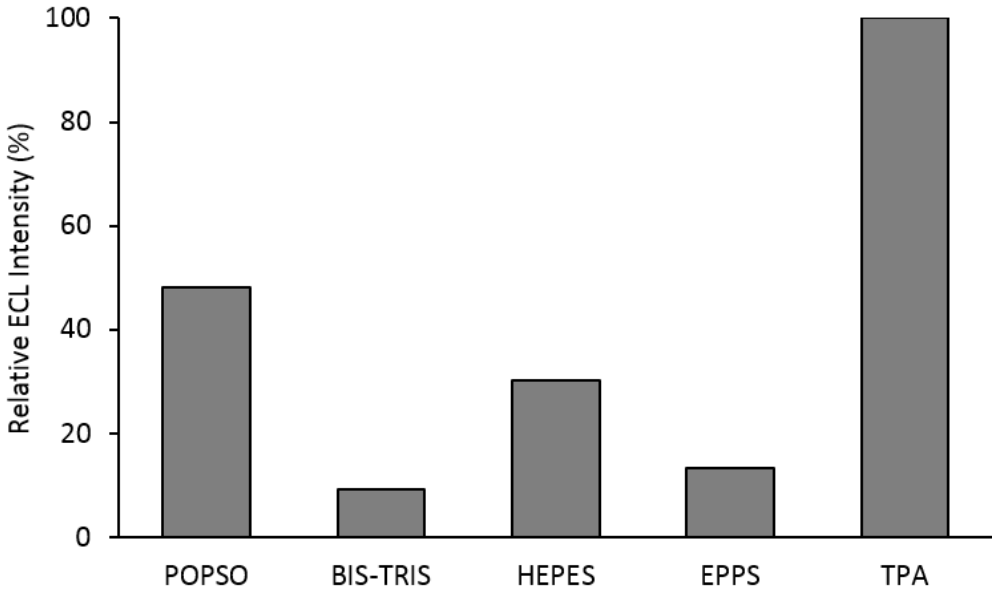

Figure 2.2: Relative ECL intensities for the four amines shown in Figure 2.1, with $[Ru(bpy)_3]^{2+}$ compared to that of TPA, under conventional co-reactant ECL conditions, in 0.1 M phosphate buffer (pH 7). The co-reactant concentration was 10 mM in each case and the concentration of the ruthenium complex was 1 μM.

2.3.2 'Good' buffer as a co-reactant, buffer and electrolyte

Having shown that these amines can act as efficient co-reactants, we examined the possibility that they could also simultaneously serve as the buffer and the electrolyte in solution (which is not feasible with TPA). The voltammetric and corresponding co-reactant ECL signals for aqueous solutions containing only $[Ru(bpy)_3]^{2+}$ and each of these tertiary-amine 'Good' buffers (i.e. no additional buffer or electrolyte) is shown in Figure 2.3. Under the conditions at which the experiment was conducted, Figure 2.3 shows that HEPES sodium salt generated the highest $[Ru(bpy)_3]^{2+}$ ECL intensity compared to the other buffers used in this study.

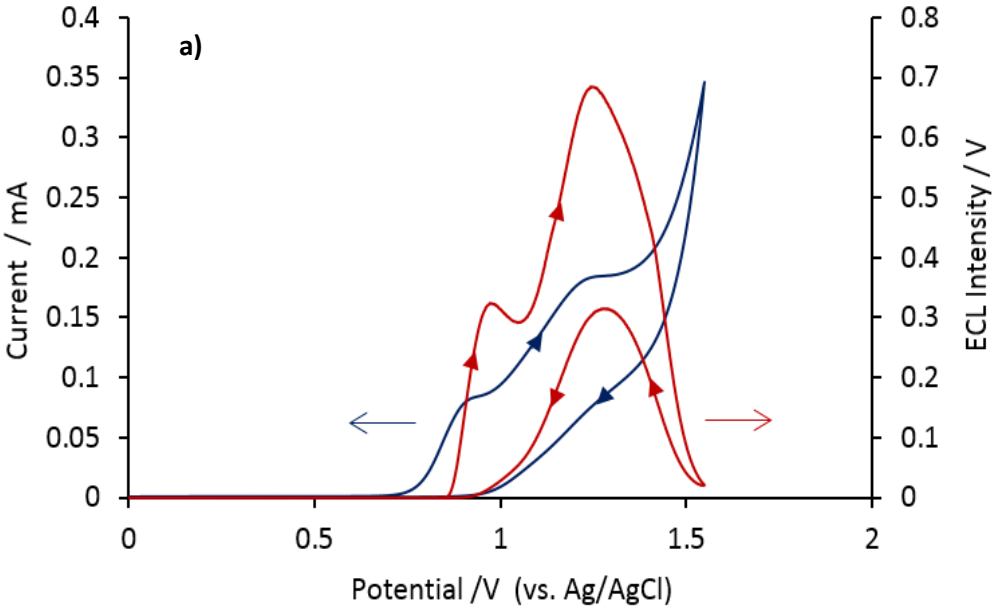
a)
Current / mA
ECL Intensity / V
Potential /V (vs. Ag/AgCl)
0.4
0.35
0.3
0.25
0.2
0.15
0.1
0.05
0
0.8
0.7
0.6
0.5
0.4
0.3
0.2
0.1
0
0
0.5
1
1.5
2

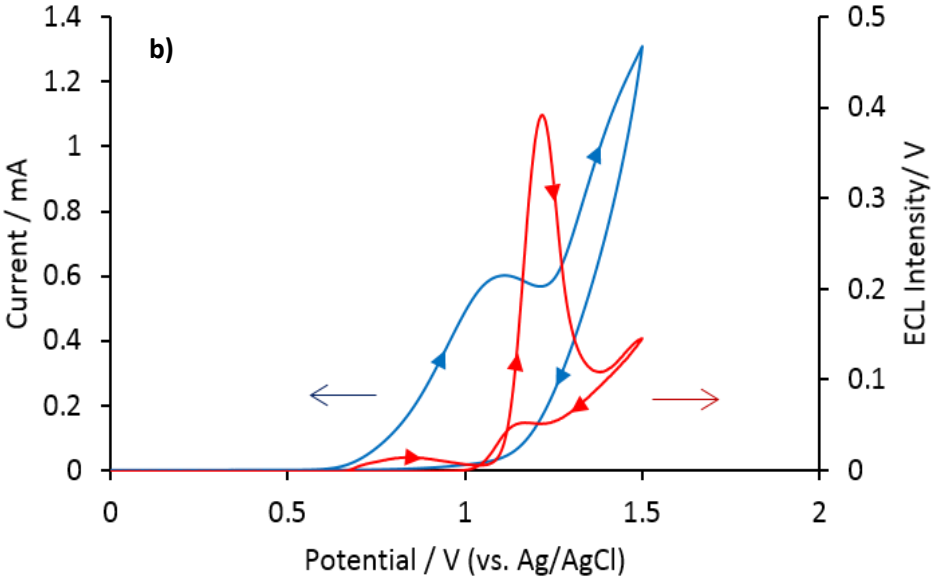
b)
Current / mA
ECL Intensity/ V
Potential / V (vs. Ag/AgCl)
1.4
1.2
1
0.8
0.6
0.4
0.2
0
0.5
0.4
0.3
0.2
0.1
0
0
0.5
1
1.5
2

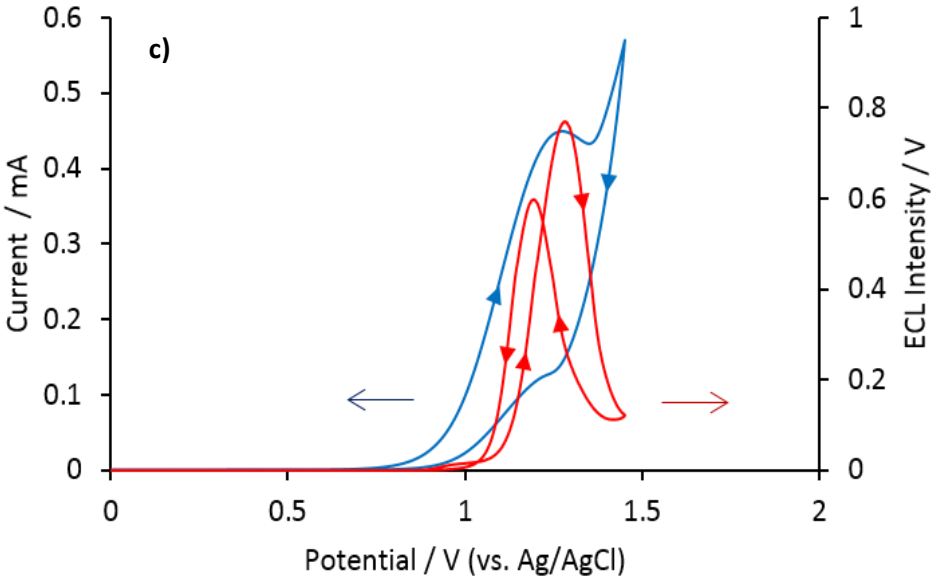

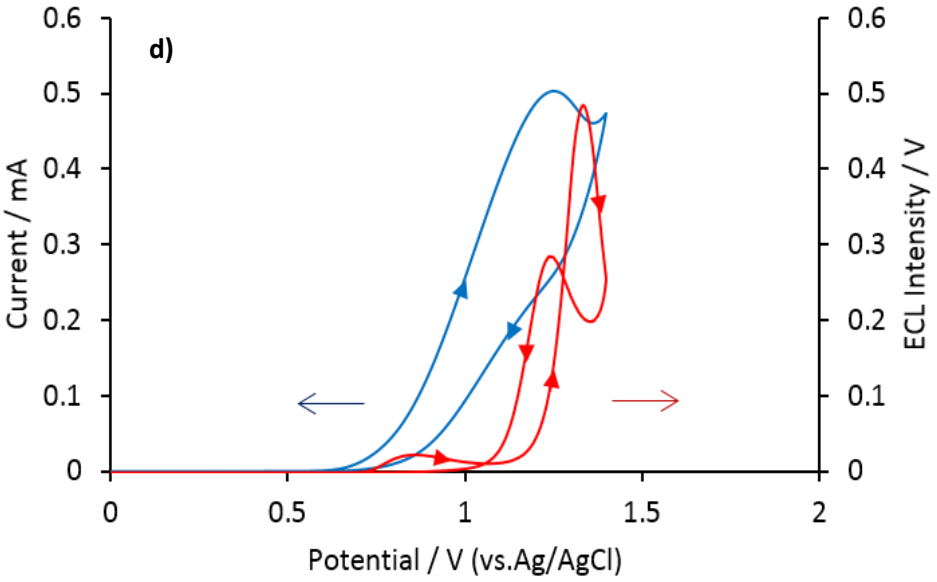

Figure 2.3: Cyclic voltammogram (blue) and the corresponding ECL intensity (red) of 1 μM $[Ru(bpy)_3]^{2+}$ in (a) 0.1 M BIS-TRIS hydrochloride, (b) 0.1 M POPSO sesquisodium salt, (c) 0.1 M HEPES sodium salt, and (d) 0.1 M EPPS, where each tertiary amine reagent was used as the co-reactant, buffer and electrolyte.

2.3.3 Effect of pH

The ECL intensity of $[Ru(bpy)_3]^{2+}$ (1 μM) with each aqueous biological buffer was examined across the useful pH range of the buffer (Figure 2.4). Under these conditions, the optimum pH for co-reactant ECL was 5.8 for BIS-TRIS HCl, 8.4 for POPSO sesquisodium salt, 8.2 for HEPES sodium salt and 8.3 for EPPS. As shown in Figure 2.4, the peak ECL intensities for $[Ru(bpy)_3]^{2+}$ with biological buffer as co-reactant, buffer and electrolyte increased in the order: POPSO sesquisodium salt (0.39 V) < EPPS (0.43 V) < BIS-TRIS HCl (0.69 V) < HEPES sodium salt (0.77 V). These ECL signals were lower than that obtained with TPA (at its optimal pH) as co-reactant and a phosphate buffer/electrolyte (9.98 V), but as shown on page 62, the use of these tertiary amine buffers can still provide sufficiently low detection limits for many biological assays. Moreover, they offer a useful alternative in terms of the safety and simplicity of sample preparation.

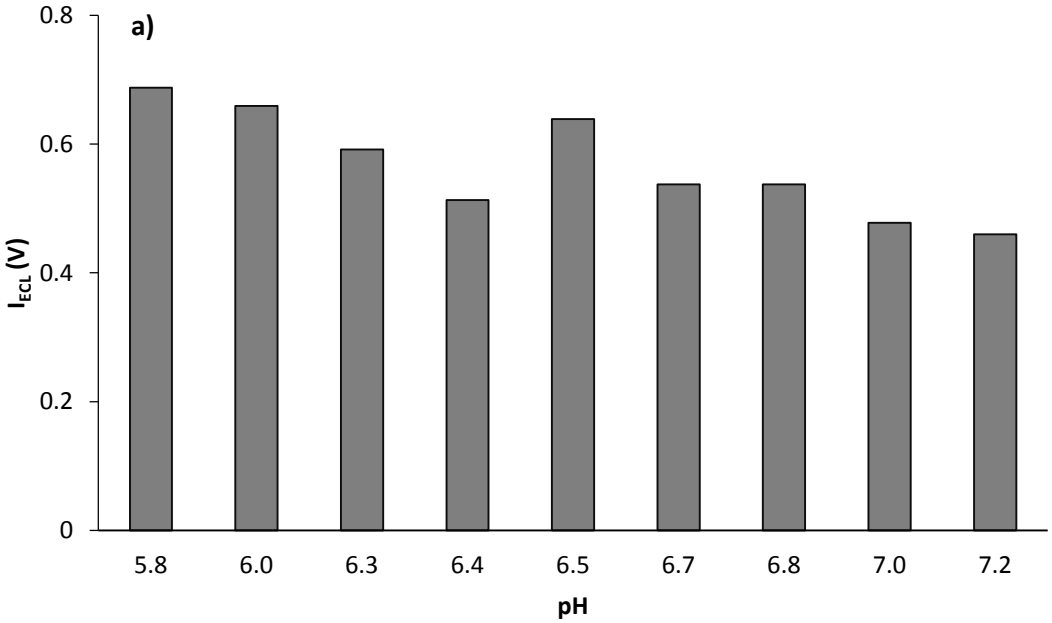

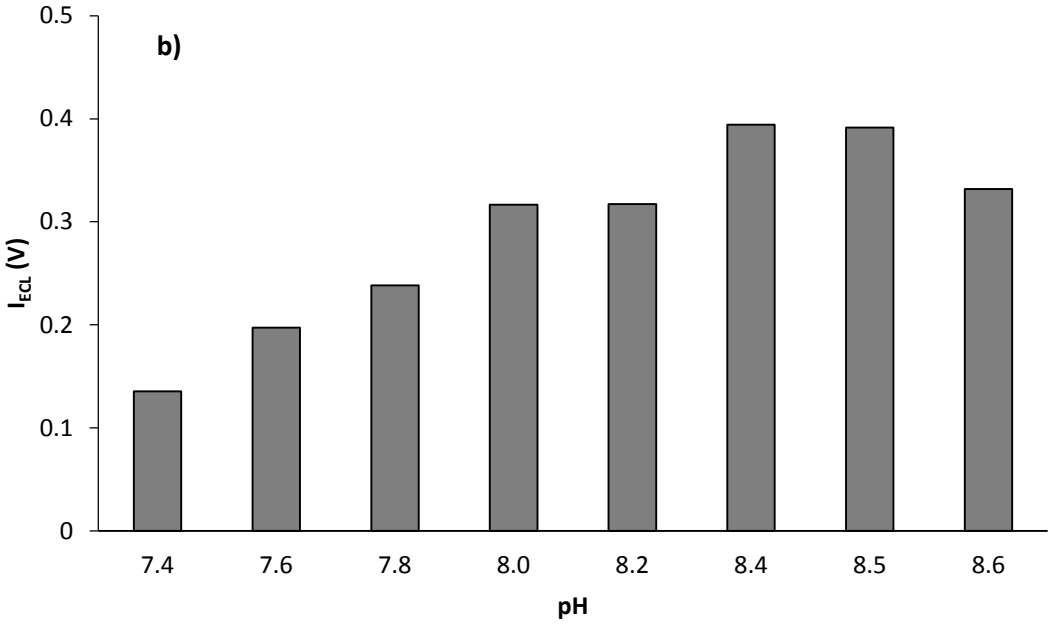
b)
0.5
0.4
0.3
0.2
0.1
0
I_{ECL} (V)
7.4
7.6
7.8
8.0
8.2
8.4
8.5
8.6
pH

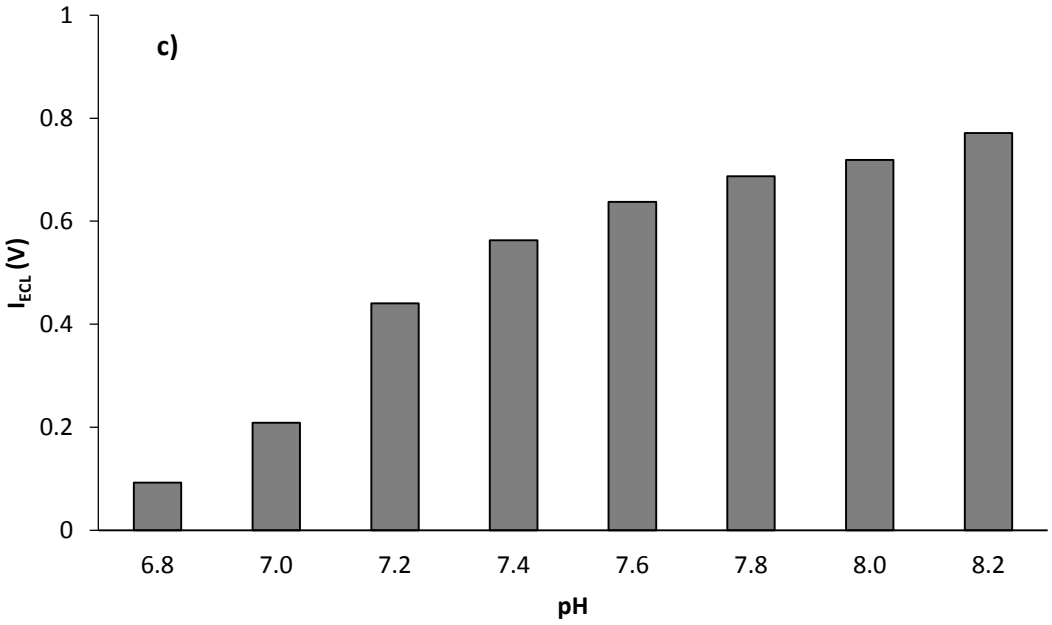
c)
1
0.8
0.6
0.4
0.2
0
I_{ECL} (V)
6.8
7.0
7.2
7.4
7.6
7.8
8.0
8.2
pH

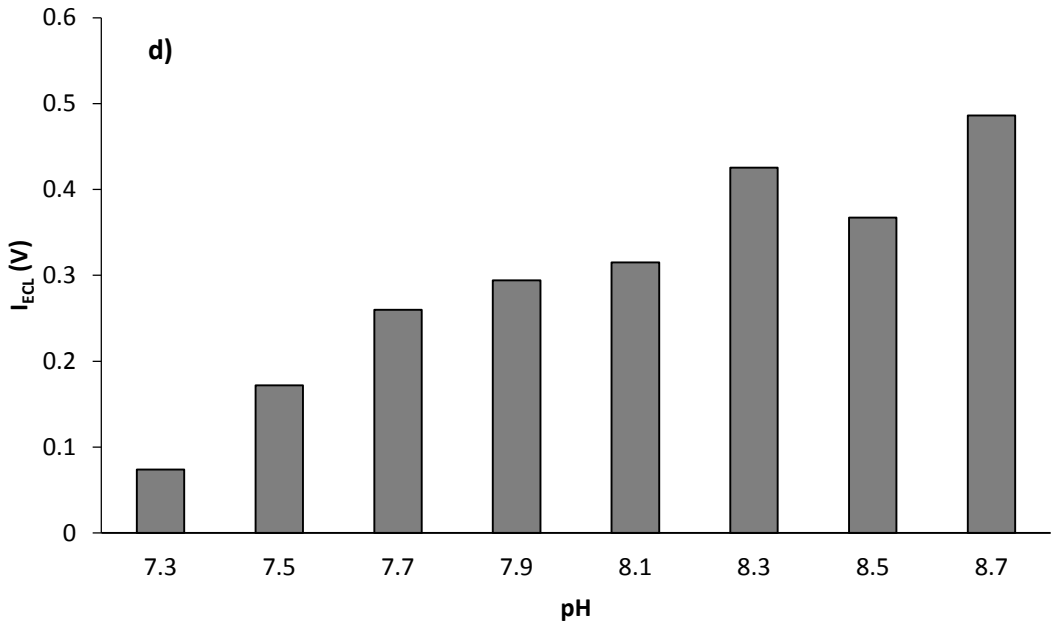

Figure 2.12: Peak ECL intensities generated from 1 µM $[Ru(bpy)_3]^{2+}$/0.1 M biological buffer, obtained through cyclic voltammetry at a scan rate of 0.05 V/s within the useful pH range of each buffer used in the study where a) BIS-TRIS hydrochloride; b) POPSO sesquisodium salt; c) HEPES sodium salt; d) EPPS are used as the co-reactant, buffer and electrolyte simultaneously.

2.3.4 The mechanism of co-reactant ECL of $[Ru(bpy)_3]^{2+}$ and tertiary amine biological buffers

Considering the similarity in the chemical structure of the biological buffers under investigation (Figure 2.1) to that of the aliphatic tertiary amine/ethanolamine co-reactants such as TPA and DBAE, a mechanism for the ECL of $[Ru(bpy)_3]^{2+}$ with these four biological buffers can be confidently drawn from previous investigations.[27,28] Although the reaction may proceed simultaneously via several pathways,[27] under conditions involving low concentrations of the luminophore and relatively high concentrations of the co-reactant in aqueous solution, the dominant pathway can be illustrated as follows:

$$[Ru(bpy)_3]^{2+} - e^- \rightarrow [Ru(bpy)_3]^{3+} \quad \textbf{[2.1]}$$

$$B - e^- \rightarrow B^{\bullet+} \quad \textbf{[2.2]}$$

$$B^{\bullet+} \rightarrow B^{\bullet} + H^+ \quad \textbf{[2.3]}$$

$$[Ru(bpy)_3]^{3+} + B^{\bullet} \rightarrow [Ru(bpy)_3]^{2+*} + \text{other products} \quad \textbf{[2.4]}$$

$$[Ru(bpy)_3]^{2+*} \rightarrow [Ru(bpy)_3]^{2+} + h\nu \quad \textbf{[2.5]}$$

In the above mechanism, both $[Ru(bpy)_3]^{2+}$ and the tertiary-amine biological buffer (B) are oxidised at the electrode surface forming $[Ru(bpy)_3]^{3+}$ and a radical cation of the buffer. This radical cation becomes deprotonated and the neutral radical reduces $[Ru(bpy)_3]^{3+}$, enabling the formation of the excited $[Ru(bpy)_3]^{2+*}$, which emits a photon to return to the ground state. With this in mind, the lower co-reactant ECL intensities from the four biological buffers (Figure 2.2) compared to that of TPA can in part be rationalised. Three of the biological buffers (EPPS, POPSO and HEPES) are diamines. The CV of each system shows relatively large cathodic current, indicative of significant side reactions at the electrode surface. In the case of diamines, it is possible that their oxidation generates intermediates that contain both an oxidative amine cation radical ($B^{\bullet+}$) and a reductive amine free radical ($B^{\bullet}$), leading to intramolecular reactions that consume the key intermediates required to generate the excited state (i.e. reaction [2.4]). Han *et al.*[22] previously reported that monoamines DBAE and N-butyldiethanolamine gave greater co-reactant ECL intensities than the closely related diamine molecules such as *N,N,N′,N′*-tetrakis-(2-hydroxyethyl)ethylenediamine[22].

The difference in ECL intensity using BIS-TRIS HCl as a co-reactant compared to TPA (or DBAE) is more difficult to explain. Subtle changes in co-reactant structure can have a dramatic effect on ECL intensity.[29] Under specific experimental conditions, certain

aliphatic tertiary amines containing one or two β-hydroxyl substituents (DBAE[21] or N-butyldiethanolamine[22]) have been found to be more effective co-reactants than TPA, but triethanolamine (containing three β-hydroxyl substituents) gave lower ECL intensities than DBAE.[22,29]

2.3.5 Determination of $[Ru(bpy)_3]^{2+}$ using BIS-TRIS simultaneously as co-reactant, buffer and electrolyte

An ECL intensity versus $[Ru(bpy)_3]^{2+}$ concentration calibration plot is shown in Figure 2.5, where 0.1 M BIS-TRIS HCl served as co-reactant, buffer and electrolyte, revealed a detection limit of 0.2 nM (based on a signal-to-noise (S/N) of 2). Obtaining sub-nanomolar detection limits for $[Ru(bpy)_3]^{2+}$ employing a biological buffer as co-reactant, buffer and electrolyte opens up new possibilities for immunoassays, DNA probe assays and cellular imaging applications, in which the use of the toxic and volatile TPA can be avoided.

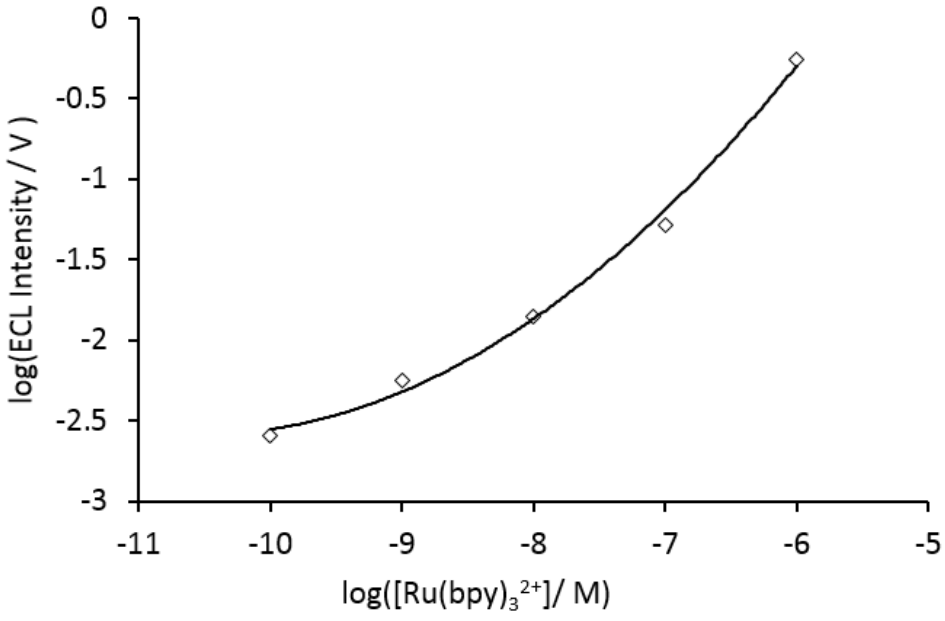

Figure 2.5: Log-log plot of the ECL intensity of various concentrations of $[Ru(bpy)_3]^{2+}$ in the presence of 0.1 M BIS-TRIS (at pH 5.8). Each point represents the average peak ECL intensity observed for three scans.

2.4 Conclusion

The results presented show that the aliphatic tertiary amine/ethanolamine 'Good' buffers can be employed as multitasking reagents in ECL-based assays; serving as co-reactant, buffer and electrolyte in ECL systems (using $[Ru(bpy)_3]^{2+}$ as the luminophore) over a wide pH range. Although the biological buffers give lower ECL intensities compared with TPA, this is compensated for by ease of sample preparation due to their higher aqueous solubility and the simplicity advantage of requiring fewer reagents. Moreover, their lower volatility and considerably lower toxicity allow for a safer and more environmentally friendly analysis and waste disposal. Therefore, although these buffers are not likely to replace traditional ECL co-reactants such as TPA, they do provide a useful alternative for certain applications where exceedingly low detection limits are not required.

2.5 References

1. L. Hu and G. Xu, *Chem. Soc. Rev.*, 2010, **39**, 3275–3304.
2. R. J. Forster, P. Bertoncello, and T. E. Keyes, *Annu. Rev. Anal. Chem. (Palo Alto. Calif).*, 2009, **2**, 359–85.
3. W. Miao, *Chem. Rev.*, 2008, **108**, 2506–2553.
4. D. M. Hercules, *Science*, 1964, **145**, 808–809.
5. K. S. V Santhanam and A. J. Bard, *J. Am. Chem. Soc.*, 1965, **87**, 139–140.
6. R. T. Dufford, D. Nightingale, and L. W. Gaddum, *J. Am. Chem. Soc.*, 1927, **49**, 1858–1864.
7. N. E. Tokel and A. J. Bard, *J. Am. Chem. Soc.*, 1972, **94**, 2862–2863.
8. I. Rubinstein and A. J. Bard, *J. Am. Chem. Soc.*, 1981, **103**, 512–516.
9. J. K. Leland and M. J. Powell, *J. Electrochem. Soc.*, 1990, **137**, 3127–3131.
10. G. F. Blackburn, H. P. Shah, J. H. Kenten, J. Leland, R. A. Kamin, J. Link, J. Peterman, M. J. Powell, A. Shah, D. B. TaHey, S. K. Tyagi, E. Wilkins, T.-G. Wu, and R. J. Massey, *Clin. Chem.*, 1991, **37**, 1534–1539.
11. A. W. Knight and G. M. Greenway, *Analyst*, 1996, **121**, 101R.
12. W.-Y. Lee, *Mikrochim. Acta*, 1997, **127**, 19–39.
13. M. M. Richter, *Chem. Rev*, 2004, **104**, 3003–3036.
14. A. W. Knight, *TrAC Trends Anal. Chem.*, 1999, **18**, 47–62.
15. E. H. Doeven, E. M. Zammit, G. J. Barbante, C. F. Hogan, N. W. Barnett, and P. S. Francis, *Angew. Chemie Int. Ed.*, 2012, **51**, 4354–4357.

16. G. J. Barbante, P. S. Francis, C. F. Hogan, P. R. Kheradmand, D. J. D. Wilson, and P. J. Barnard, *Inorg. Chem.*, 2013, **52**, 7448–7459.

17. G. J. Barbante, C. F. Hogan, A. Mechler, and A. B. Hughes, *J. Mater. Chem.*, 2010, **20**, 891.

18. T. Joshi, G. J. Barbante, P. S. Francis, C. F. Hogan, A. M. Bond, G. Gasser, and L. Spiccia, *Inorg. Chem.*, 2012, **51**, 3302–3315.

19. T. Joshi, G. J. Barbante, P. S. Francis, C. F. Hogan, A. M. Bond, and L. Spiccia, *Inorg. Chem.*, 2011, **50**, 12172–12183.

20. X. Zhou, D. Zhu, Y. Liao, W. Liu, H. Liu, Z. Ma, and D. Xing, *Nat. Protoc.*, 2014, **9**, 1146–59.

21. X. Liu, L. Shi, W. Niu, H. Li, and G. Xu, *Angew. Chemie Int. Ed.*, 2007, **46**, 421–424.

22. S. Han, W. Niu, H. Li, L. Hu, Y. Yuan, and G. Xu, *Talanta*, 2010, **81**, 44–47.

23. J.-P. Choi, Dissertation, University of Texas, 2003.

24. N. E. Good, G. D. Winget, W. Winter, T. N. Connolly, S. Izawa, and R. M. M. Singh, *Biochemistry*, 1966, **5**, 467–477.

25. N. E. Good and S. Izawa, *Methods Enzymol.*, 1972, **24**, 53–68.

26. W. J. Ferguson, K. I. Braunschweiger, W. R. Braunschweiger, J. R. Smith, J. J. McCormick, C. C. Wasmann, N. P. Jarvis, D. H. Bell, and N. E. Good, *Anal. Biochem.*, 1980, **104**, 300–10.

27. W. Miao, J.-P. Choi, and A. J. Bard, *J. Am. Chem. Soc.*, 2002, **124**, 14478–14485.

28. C. M. Hindson, G. R. Hanson, P. S. Francis, J. L. Adcock, and N. W. Barnett, *Chemistry (Easton).*, 2011, **17**, 8018–8022.

29. G. J. Barbante, N. Kebede, C. M. Hindson, E. H. Doeven, E. M. Zammit, G. R. Hanson, C. F. Hogan, and P. S. Francis, *Chem. - A Eur. J.*, 2014, **20**, 14026–14031.

Chapter 3: Rotating Disk Co-Reactant ECL

3.1 Introduction

The first detailed studies of ECL were described by Hercules[1] and Bard *et al*.[2] in the mid-1960s; however, reports of light emission during electrolysis date back to the 1920s.[3] In 1972, Tokel and Bard described the ECL of $[Ru(bpy)_3]^{2+}$ via annihilation between oxidised and reduced forms of the complex in acetonitrile.[4] Bard's group also demonstrated the first co-reactant ECL (using oxalate),[5] before Leland and Powell introduced tri-n-propylamine (TPA) in 1990.[6]

Over the last 40 years, ECL has become a useful analytical detection method and has been developed and applied to many various areas including food and water analysis, clinical diagnostics and detection of bio-warfare agents.[7,8] The majority of ECL systems investigated and reported in the literature involve solutions containing freely diffusing species where the emission of light occurs from the reaction layer close to the electrode surface. Films that have been attached chemically or otherwise immobilised on the surface of an electrode have also been reported to generate ECL.[9]

The analytical applications of ECL can be divided into approaches where either the co-reactant or the luminophore is detected. The detection of co-reactants such as tertiary amines has been successfully exploited in analytical methods including high-performance liquid chromatography, capillary electrophoresis, flow injection analysis and micro total analysis systems.[8] Alternatively, with a co-reactant in excess, ECL offers the highly sensitive detection of biomolecules that are labelled with a luminophore, such as tris(2,2′-bipyridine)ruthenium(II) ($[Ru(bpy)_3]^{2+}$), and has been successfully applied to commercial immunoassay systems.[8] Compared to chemiluminescence, ECL has the advantage of facilitating spatial and temporal control over the luminescent reaction due to the

emission of light being localised at the surface of the electrode. In comparison with fluorescence, it offers enhanced sensitivity due to low background and regeneration of the active form of the luminophore at the electrode surface.[7]

As ECL is an electrochemical methodology, ECL intensities are limited by the rate of diffusion of the reacting species to the electrode surface.[10–12] Therefore, a method to enhance the rate of mass transport could prove advantageous in the advancement of future ECL based applications and methods. A solution to this problem could come in the form of the use of a rotating disk electrode (RDE) instead of the use of a conventional non-rotating working electrode. As the RDE turns, solution containing the hydrodynamic boundary layer is swept away from the centre of the electrode due to the centrifugal force generated from the rotation of the RDE. Bulk solution is then transported upwards, perpendicular to the electrode surface, so that it can replace the now displaced boundary layer resulting in the laminar flow of solution, containing our ECL reactants, towards and across the electrode.

This flow of solution (which can be controlled by the electrode rotation rate) can quickly achieve conditions where steady-state current is observed, controlled by convective mass transport rather than diffusion alone. This is unlike the case where experiments are conducted under quiescent conditions, where the transient current and/or light intensities generated are limited by diffusion

While there has been extensive study of the electrochemistry, kinetics and mechanisms of various systems using an RDE or RRDE,[13–25] there have been very few studies adapting RDE instrumentation to ECL detection.[26–28] Juknelevicius *et al.*[28] investigated ECL emission from $[Ru(bpy)_3]^{2+}$, luminol and *N*-(4-aminobuthyl)-*N*-ethyl-isoluminol using an RDE found an increase of ECL intensities observed when these systems

were rotated, however all experiments in their study were set at a single rotation rate of 2000 RPM.

The aim of this study was to not only adapt the RDE for ECL measurements of various co-reactant ECL systems under rotation, but also to perform detailed rotation rate studies of the ECL intensities generated from these co-reactant ECL systems, an aspect that has not been previously reported in the literature. Investigating how these co-reactant ECL systems behave under a range of rotation rates may lead to the further advancement in existing and future ECL based applications and methods. Thus, we show that RDE-ECL can be an important tool for fundamental studies of ECL systems.

3.2 Experimental

3.2.1 Chemicals and materials

Unless otherwise stated, deionised water (Sartorius Stedim biotech arium® pro VF Ultrapure Water System, 18.2 MΩ cm, Germany) and analytical grade reagents were used. Dry acetonitrile was distilled from CaH_2. Tris(2,2′-bipyridine)ruthenium(II) hexafluorophosphate ($Ru(bpy)_3(PF_6)_2$, 97%), [4,4′-*bis*(1,1-dimethylethyl)-2,2′-bipyridine-*N*1,*N*1′]*bis*[2-(2-pyridinyl-*N*)phenyl-C]iridium(III) hexafluorophosphate ($[Ir(dtbbpy)(ppy)_2][PF_6]$), [4,4′-*bis*(1,1-dimethylethyl)-2,2′-bipyridine-*N*1,*N*1′]*bis*[3,5-difluoro-2-[5-(trifluoromethyl)-2-pyridinyl-*N*]phenyl-C]iridium(III) hexafluorophosphate ($(Ir[dF(CF_3)ppy]_2(dtbpy))PF_6$), tris[2-(4,6-difluorophenyl)pyridinato-C^2,N]iridium(III) ($Ir(dF\text{-}ppy)_3$), tripropylamine (TPA), 2-(dibutylamino)ethanol (DBAE) and tetrabutylammonium hexafluorophosphate (NBu_4PF_6) were all purchased from Sigma-Aldrich (NSW, Australia). Tris(2,2´-bipyridine)ruthenium(II) chloride hexahydrate ($[Ru(bpy)_3]Cl_2.6H_2O$, 99%) was purchased from Strem Chemicals (MA, USA). Structures for the luminophores and co-reactants used in this study are shown in Figure 3.1.

3.2.2 Photophysics

Characterisation of $Ru(bpy)_3(PF_6)_2$, $[Ir(dtbbpy)(ppy)_2][PF_6]$, $(Ir[dF(CF_3)ppy]_2(dtbpy))PF_6$ and $Ir(dF\text{-}ppy)_3$ were performed by collecting absorption spectra using a Cary Series UV−visible spectrophotometer (Agilent) with a 1 cm path length quartz cuvette, 1 nm spectral bandwidth, 0.1 s signal averaging time, 0.25 nm data interval and a 150 nm/min scan rate. In this work, 0.02 mM samples of $Ru(bpy)_3(PF_6)_2$, $[Ir(dtbbpy)(ppy)_2][PF_6]$, $(Ir[dF(CF_3)ppy]_2(dtbpy))PF_6$ and $Ir(dF\text{-}ppy)_3$were prepared in distilled acetonitrile. A blank solvent was used to baseline (T100%) correct the spectrometer while blocking the detector from the light-beam zero (T0%) corrected the spectrometer.

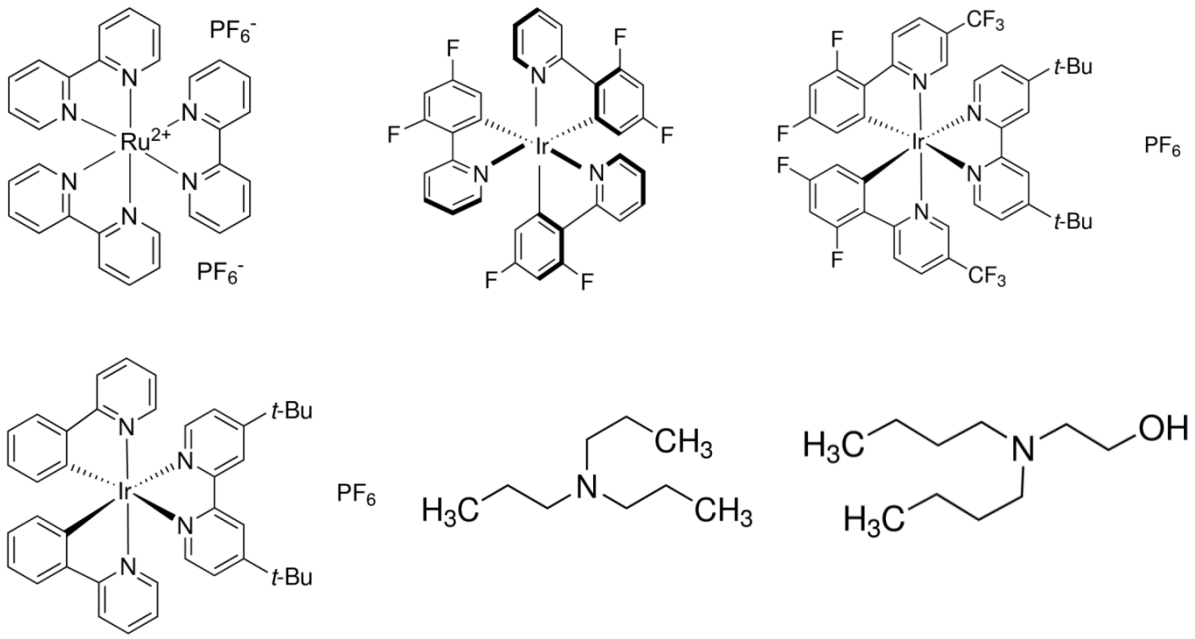

Figure 3.1: Luminophores and co-reactants used in this study from left to right: $Ru(bpy)_3(PF_6)_2$, $Ir(dF\text{-}ppy)_3$, $(Ir[dF(CF_3)ppy]_2(dtbpy))PF_6$, $[Ir(dtbbpy)(ppy)_2][PF_6]$, TPA and DBAE

Steady-state emission spectra were collected on a Nanolog (HORIBA Jobin Yvon IBH) spectrometer using a 1 cm four-sided quartz cuvette, 2 nm band pass and an increment of 1 nm. An integration time of 0.2 seconds was used for 0.02 mM solutions. To excite the complexes, a 450 W xenon-arc lamp was used in conjuncture with a 1200 g/mm grating blazed at 330 nm excitation monochromator and a 1200 g/mm grating blazed at a 500 nm emission monochromator. A liquid nitrogen-cooled Symphony II (model SII-1LS-256-06) charged couple device (CCD) was used to detect the light emission from these complexes. Long pass filters were used on the emission side to block the excitation scatter peaks and spectra were corrected for wavelength dependent variation in source intensity, gratings and detector response.

3.2.3 Electrochemistry and Electrochemiluminescence

A CH instruments (TX, USA) electrochemical workstation (CHI660B) potentiostat was used to perform cyclic voltammetry experiments with CHI660B software. Levich and Koutecky-Levich studies were performed with the use of an RRDE-3A Rotating Ring Disk Electrode Apparatus (ALS Co., Ltd, Japan). The electrochemical cell consisted of a glass cell with a quartz window base and Teflon cover with a spill tray. A conventional three-electrode configuration consisting of a 1 cm^2 silver-wire quasi reference electrode, a 1 cm^2 gold wire auxiliary electrode and a 3 mm diameter glassy-carbon rotating disk working electrode (with an area of 0.071 cm^2) shrouded in Teflon (ALS Co., Ltd, Japan) was used. The RDE was polished on a felt pad containing 0.3 μm alumina slurry and rinsed with water and acetone. The RDE was then dried under a steady stream of nitrogen (N_2).

Aqueous solutions of $[Ru(bpy)_3]Cl_2.6H_2O$ were prepared at varying concentrations in 0.1 M phosphate buffer solution at pH 7 in the presence of a tertiary amine co-reactant, either TPA or DBAE. Organic solutions of $Ru(bpy)_3(PF_6)_2$, $[Ir(dtbbpy)(ppy)_2][PF_6]$, $(Ir[dF(CF_3)ppy]_2(dtbpy))PF_6$ and $Ir(dF\text{-}ppy)_3$ of varying concentrations in the presence of TPA were prepared in freshly distilled acetonitrile and 0.1 M NBu_4PF_6 added as supporting electrolyte. Oxygen was removed from the solutions by bubbling vigorously with N_2 for 5 min, followed by lightly blanketing the solution with N_2 during the experiments. Potentials were referenced against a Ag/Ag^+ wire quasi reference electrode. The surface of the rotating disk electrode was positioned at a reproducible distance (~2 mm) from the bottom of the cell for detection.

Levich and Koutecky-Levich studies were performed using cyclic voltammetry at various rotation rates at a scan rate of 0.01 V/s, while the ECL signal was simultaneously recorded. ECL signals were detected using a liquid nitrogen cooled Symphony II (model SII-1LS-256-06) CCD, with an integration time of 0.9965 s, coupled via an FL-3000

fibre-optic adapter and a fibre optic bundle to the underside of a custom-built light-tight Faraday cage (see supplementary information Figures S1 and S2). The pH of the solutions used in the pH study was adjusted using triflic acid and measured using an MEP Instruments Metrohm 827 pH Lab pH meter (coupled with a MEP Instruments Metrohm 6.0228.010 pH electrode).

3.3 Results and Discussion

3.3.1 Basic spectroscopic and electrochemical properties

The photoluminescence, UV-VIS absorption and electrochemical characteristics of the complexes were first evaluated. The absorbance and photoluminescence spectra of the luminophores used in the study are shown in Figures 3.2 and 3.3 respectively. Figure 3.2 shows that the ruthenium complex has a significantly higher absorbance in the visible region of the spectrum compared to the iridium complexes, while Figure 3.3 illustrates the range of emission colours of the complexes used in the study. The electrochemical and spectroscopic properties of each complex is summarised in Table 3.1.

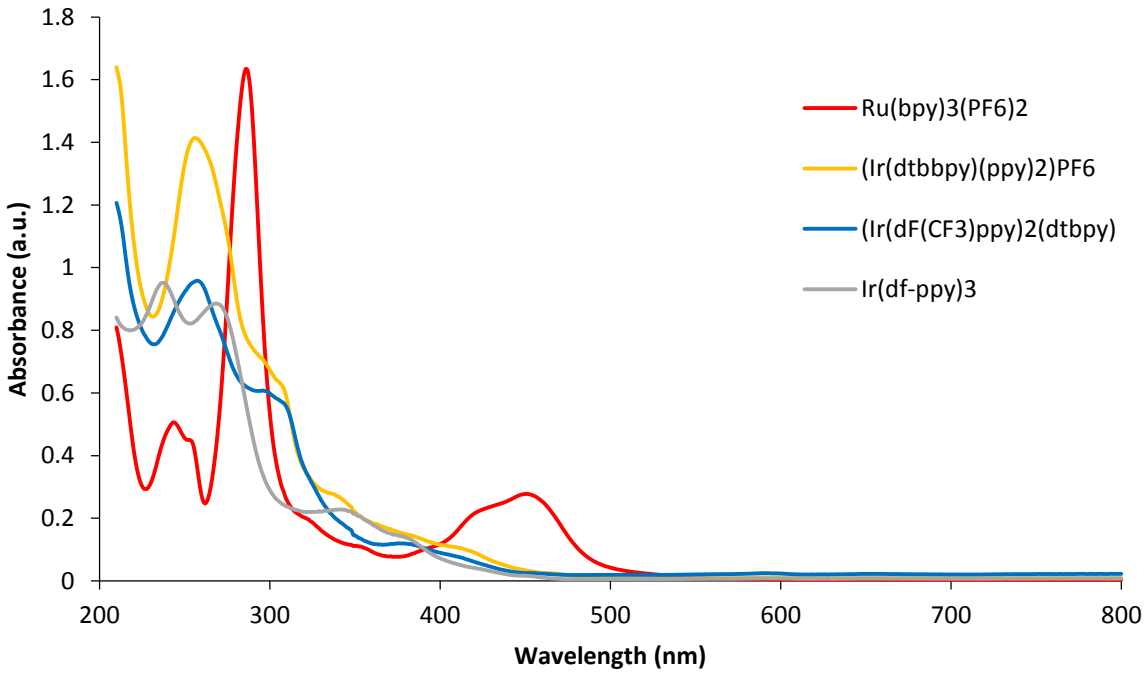

Figure 3.2: Absorbance spectra of 2 µM samples of $Ru(bpy)_3(PF_6)_2$, $[Ir(dtbbpy)(ppy)_2][PF_6]$, $Ir(dF\text{-}ppy)_3$ and $(Ir[dF(CF_3)ppy]_2(dtbpy))PF_6$

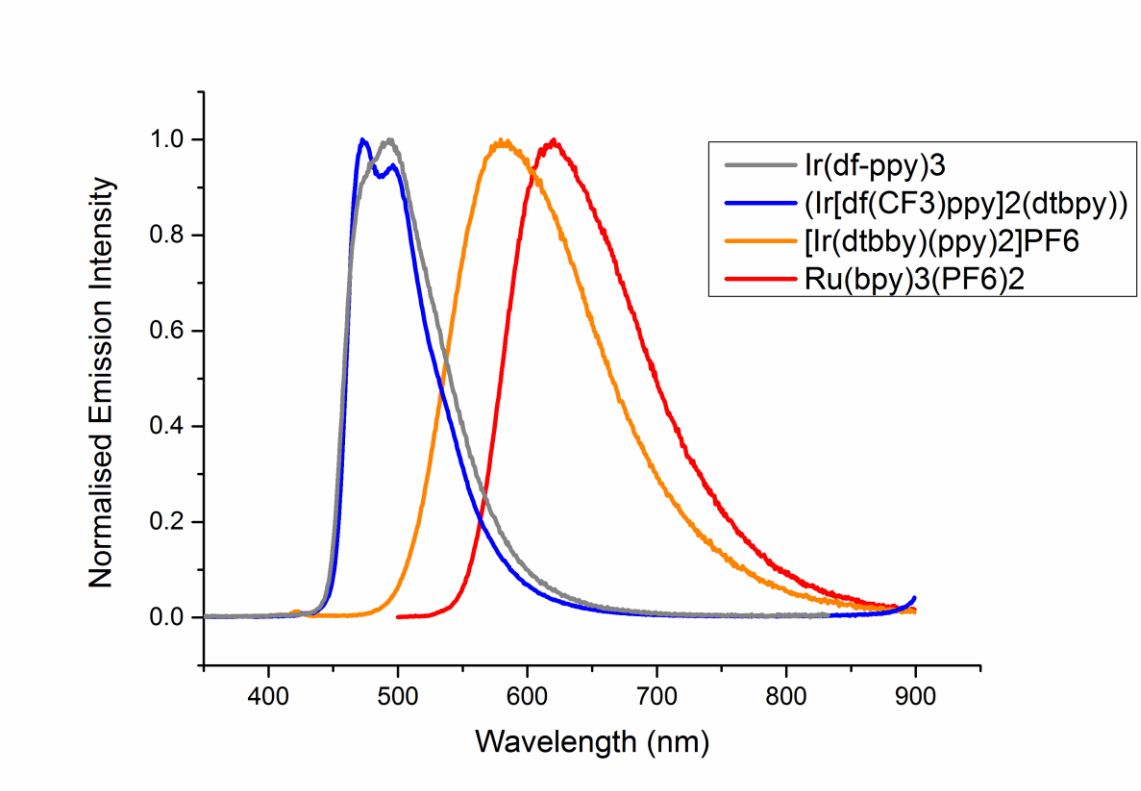

Figure 3.3: Photoluminescence spectra of 2 µM samples of $Ru(bpy)_3(PF_6)_2$, $Ir(dF\text{-}ppy)_3$, $(Ir[dF(CF_3)ppy]_2(dtbpy))PF_6$, and $[Ir(dtbbpy)(ppy)_2][PF_6]$

Table 3.1: The electrochemical and spectroscopic properties of the luminophores used in this study. [a] This is a shoulder; [b] Values from Lowry *et al.*[29]; [c] Values from Kerr *et al.*[30] (see bibliography). Electrochemical data from Figures 3.4, 3.6, 3.8, and 3.10 from chapter 3 and Figures 4.21, and 4.36 from chapter 4

	Electrochemistry		Absorbance	Photoluminescence
	E°red (V)	E°ox (V)	λabs (nm)	λmax (nm)
$Ru(bpy)_3(PF_6)_2$	-1.37, -1.57, -1.81	1.31	244, 253[a] 286, 420[a], 451	620
$[Ir(dtbbpy)(ppy)_2][PF_6]$	-1.51[b]	1.37	256, 303[a]	579
$Ir[dF(CF_3)ppy]_2(dt\text{-}bpy))PF_6$	-1.13	2.01	257, 294[a],376	472, (496)
$Ir(dF\text{-}ppy)_3$	-2.09[c]	1.25	237, 268, 341, 378[a]	493

3.3.2 Effect of rotation solely on the electrochemistry of the luminophore

Before the effect of rotation on the ECL intensity of various co-reactant ECL systems was investigated, the effect rotation has on the electrochemistry of both the luminophore and the co-reactant in each system was separately investigated.

As depicted in Figure 3.4, the linear scan voltammogram of 0.2 mM $[Ru(bpy)_3]^{2+}$ at an RDE in 0.1 M NBu_4PF_6 supporting electrolyte shows an increase in the Ru^{2+} oxidation limiting current as the electrode rotation rate was increased from 0 RPM to 3000 RPM. However, the limiting current was observed to drastically decrease when turbulent flow began to set in at rotation rates past 4000 RPM (data not shown). The increase of current at higher rotation rates occurs due to convective mass transport, not diffusion, now controlling the system. As the electrode rotates faster, the mass transport of molecules to the electrode surface increases and hence the limiting current becomes larger.

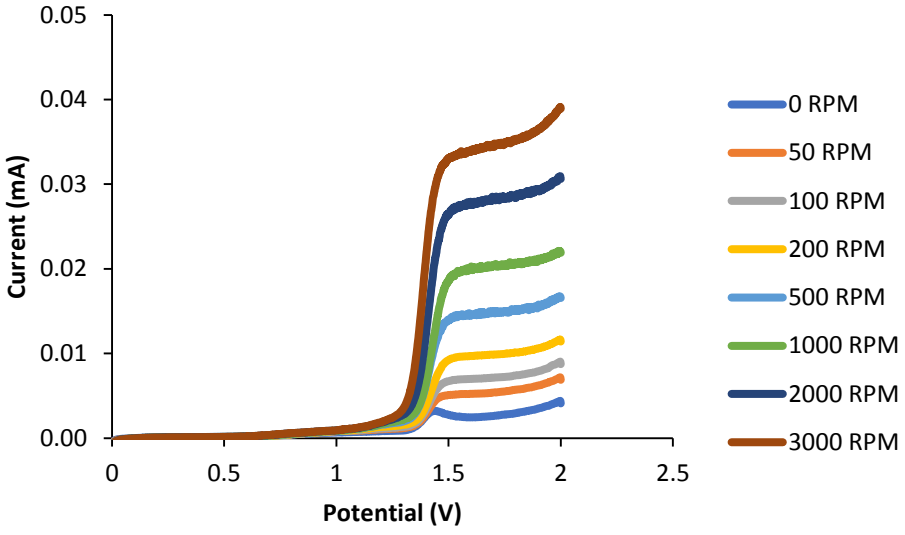

Figure 3.4: Voltammograms generated using 0.2 mM $Ru(bpy)_3(PF_6)_2$ in dry ACN with 0.1 M NBu_4PF_6 at various rotation rates (0 – 3000 RPM)

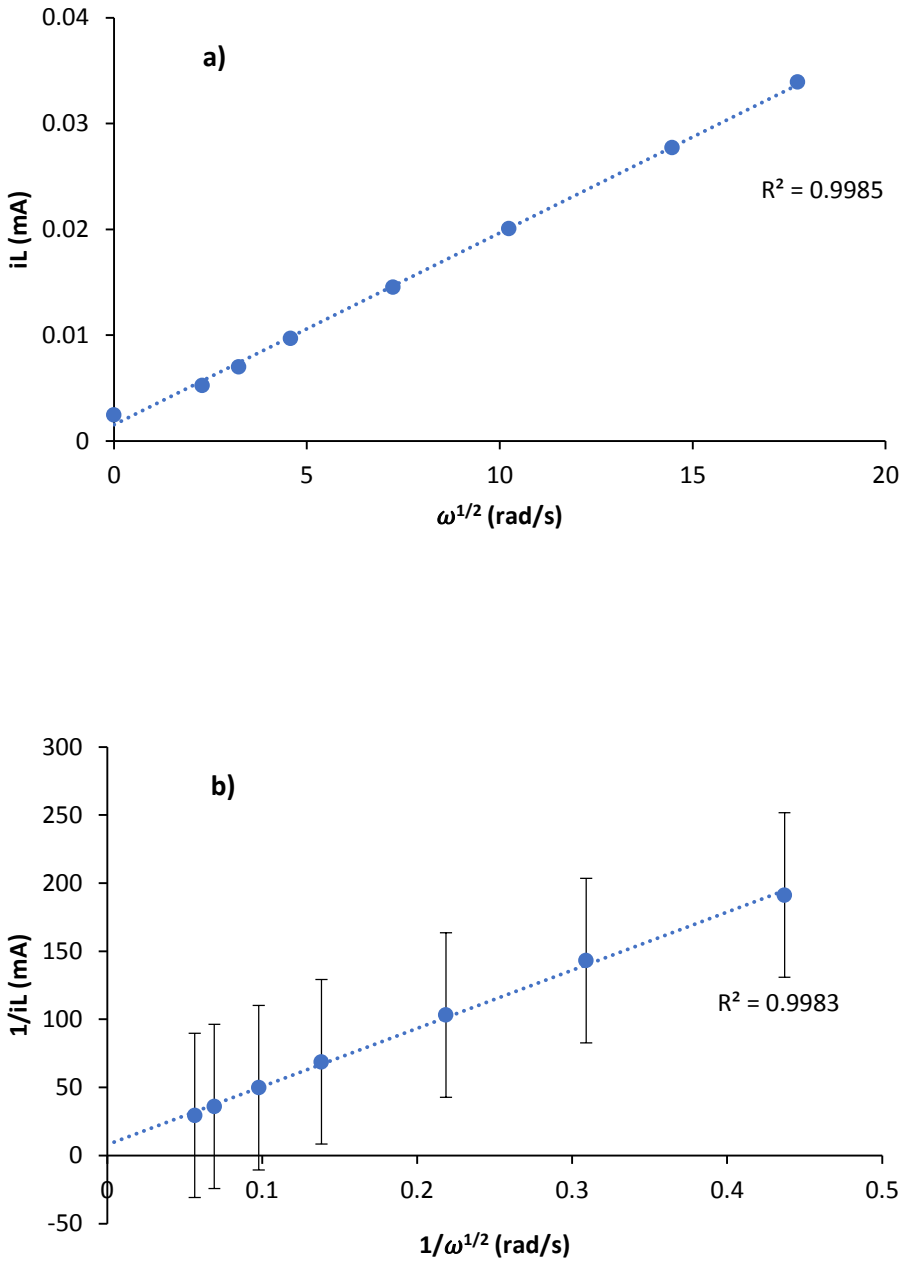

Figure 3.5: Levich (a) and Koutecky-Levich (b) plots of the currents generated at 1.6 V from 0.2 mM $Ru(bpy)_3(PF_6)_2$ in dry ACN with 0.1 M NBu_4PF_6 at various rotation rates (0 – 3000 RPM)

The limiting current in Figure 3.4 was then plotted against the square root of the rotation rate to obtain the Levich plot shown in Figure 3.5a. The plot shows the linear relationship between rotation rate and generated current where increasing the rotation rate of the electrode increases the limiting current. The reciprocal of the limiting current was then plotted against the reciprocal of the square root of electrode rotation rate ($1/\omega^{1/2}$) to obtain the Koutecky-Levich plot shown in Figure 3.5b, which yielded a y-intercept of 7.917 ± 1.815. Based on Equation 1.8, a zero y-intercept indicates that the system is controlled by mass transport, which is where the rotation rate notionally reaches infinity. The y-intercept of this system is not statistically different to zero hence the system is controlled by mass transport.

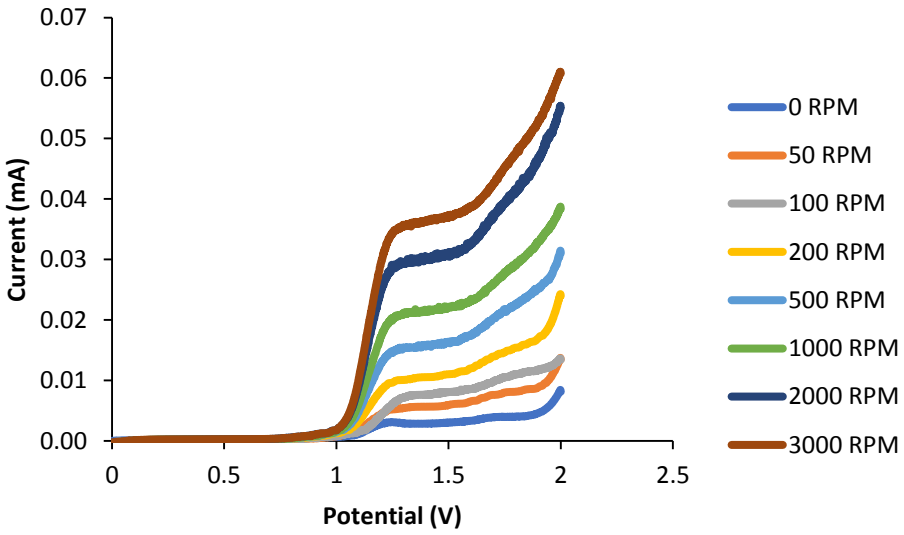

Figure 3.6: Voltammograms generated using 0.2 mM Ir(dF-ppy)$_3$ in dry ACN with 0.1 M NBu_4PF_6 at various rotation rates (0 – 3000 RPM)

Similar to Ru(bpy)$_3$(PF_6)$_2$, Figure 3.6 and Figure 3.7a show the same trend where the limiting current generated from the luminophore increases as the rotation rate of the electrode also increases when a solution containing 0.2 mM Ir(dF-ppy)$_3$ was examined. Taking the

limiting current values at 1.4 V, the Koutecky-Levich plot (Figure 3.7b) for $Ir(dF\text{-}ppy)_3$ indicate reversibility, i.e. no kinetic limitation, due to the plot yielding a y-intercept of 7.515 ± 1.383. Other processes (possibly ligand oxidation) are occurring at potentials beyond 1.4 V, but these were not investigated in this study.

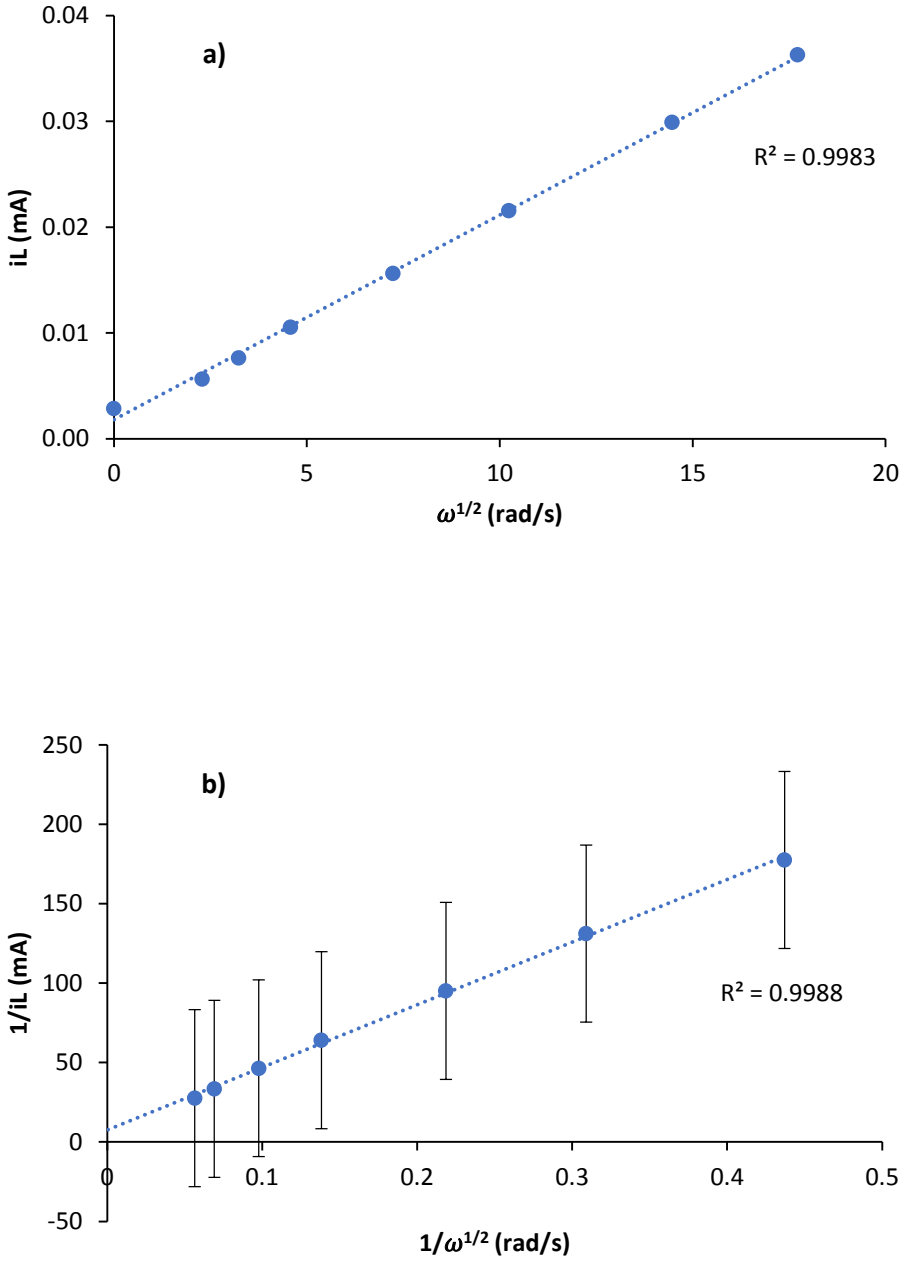

Figure 3.7: Levich (a) and Koutecky-Levich (b) plots of the currents generated at 1.4 V from 0.2 mM $Ir(dF\text{-}ppy)_3$ in dry ACN with 0.1 M NBu_4PF_6 at various RPMs (0 – 3000 RPM)

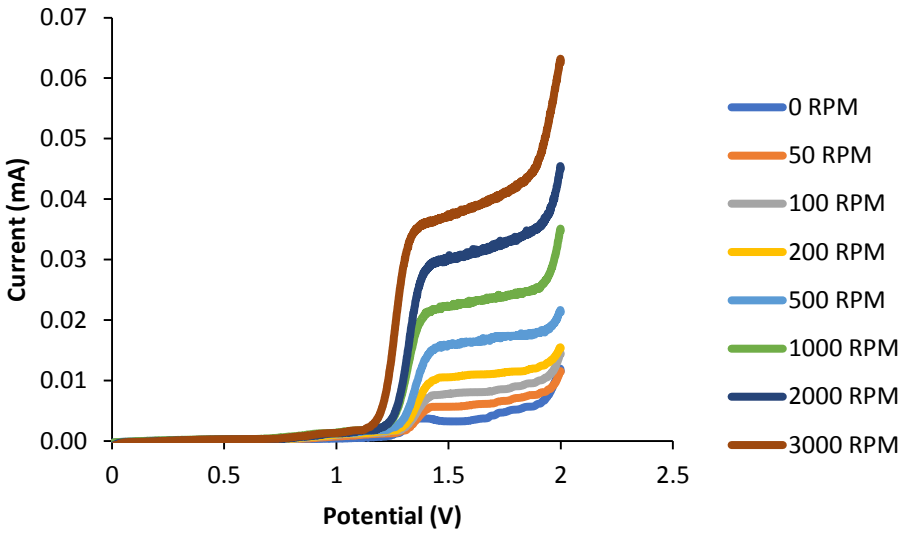

Figure 3.8: Voltammograms generated using 0.2 mM $[Ir(dtbbpy)(ppy)_2][PF_6]$ in dry ACN with 0.1 M NBu_4PF_6 at various rotation rates (0 – 3000 RPM)

Figure 3.8 and Figure 3.9a shows the same linear trend observed previously, where an increase of the limiting current occurs when the electrode rotation rate is increased when a solution containing 0.2 mM $[Ir(dtbbpy)(ppy)_2][PF_6]$ was examined under electrode rotation. At 1.5 V, $[Ir(dtbbpy)(ppy)_2][PF_6]$ without the presence of a co-reactant, is reversible and has no kinetic limitations. This is due to Koutecky-Levich plot (Figure 3.9b) yielding a y-intercept of 6.724 ± 1.158, which is statistically equal to zero. Other processes are occurring at potentials beyond 1.5 V, probably related to ligand oxidation, but these were not investigated in this study.

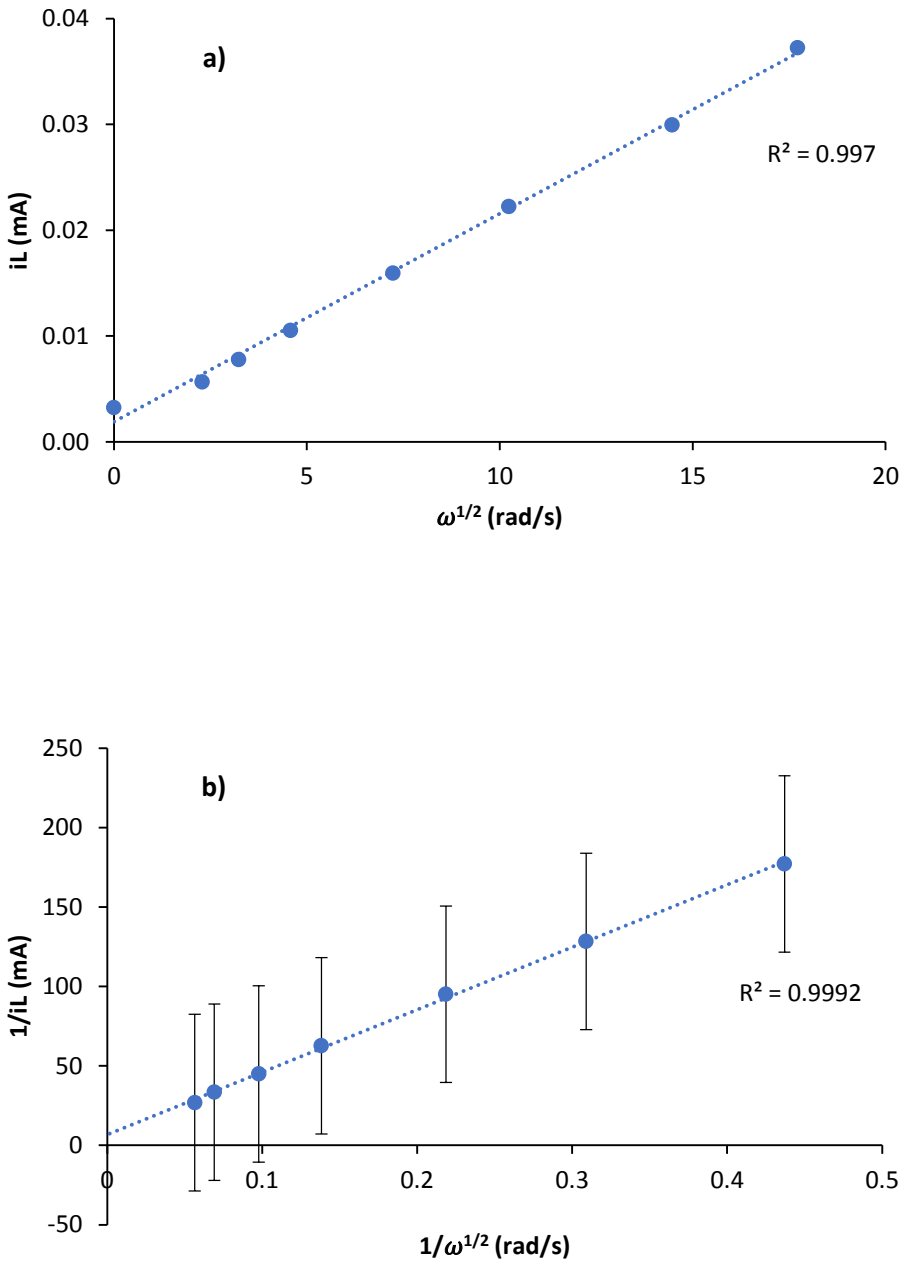

Figure 3.9: Levich (a) and Koutecky-Levich (b) plots of the currents generated at 1.5 V from 0.2 mM $[Ir(dtbbpy)(ppy)_2][PF_6]$ in dry ACN with 0.1 M NBu_4PF_6 at various rotation rates (0 – 3000 RPM)

The final luminophore used in this study, $(Ir[dF(CF_3)ppy]_2(dtbpy))PF_6$, also exhibits the same trend observed when each of the luminophores used in the study was examined under electrode rotation (Figure 3.10). The Levich plot (Figure 3.11a) shows a linear relationship where the limiting current increases with an increase of rotation rates. The Koutecky-Levich plot (Figure 3.11b) indicates that at 1.6 V, the oxidation of $(Ir[dF(CF_3)ppy]_2(dtbpy))PF_6$ without the presence of a co-reactant has kinetic limitations since the y-intercept of the Koutecky-Levich plot yielded a intercept of 29.049 ± 5.116, which is statistically greater than zero. Other processes (possibly ligand oxidation) are occurring at potentials beyond 1.6 V, but these were not investigated in this study.

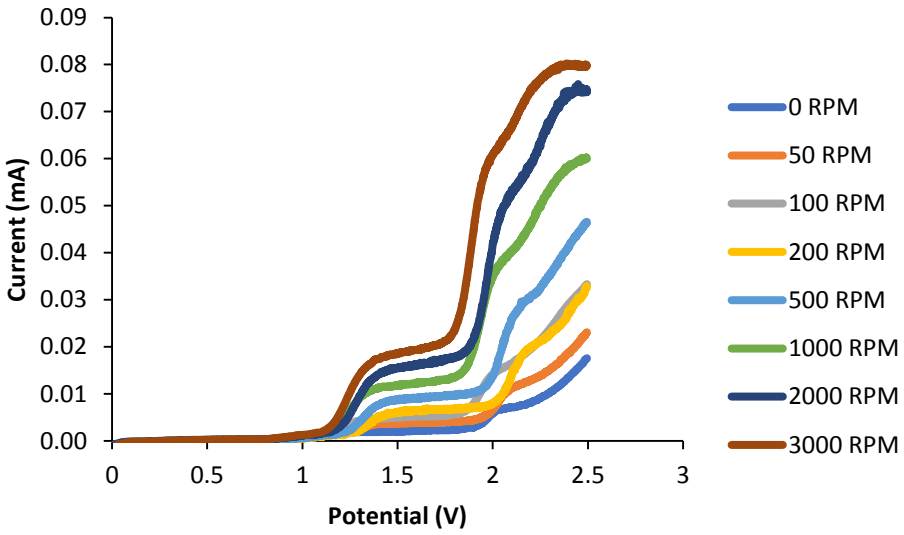

Figure 3.10: Voltammograms generated using 0.2 mM $(Ir[dF(CF_3)ppy]_2(dtbpy))PF_6$ in dry ACN with 0.1 M NBu_4PF_6 at various rotation rates (0 – 3000 RPM)

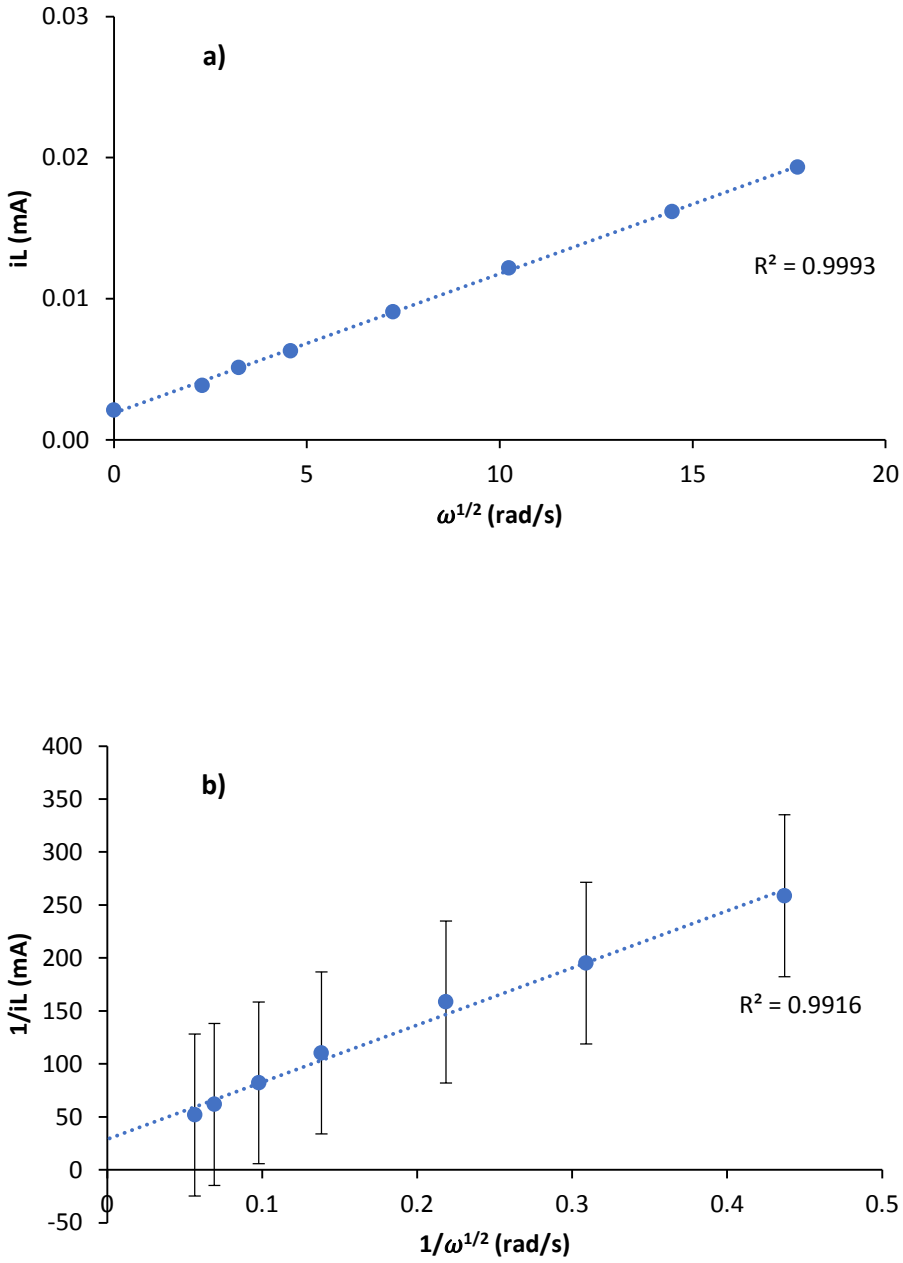

Figure 3.11: Levich (a) and Koutecky-Levich (b) plots of the currents generated at 1.6 V from 0.2 mM $(Ir[dF(CF_3)ppy]_2(dtbpy))PF_6$ in dry ACN with 0.1 M NBu_4PF_6 at various rotation rates (0 – 3000 RPM)

Table 3.2: Diffusion coefficients (D) and kinetic currents (i_k) of the luminophores (0.2 mM) and co-reactants (5 mM) examined in this study where Ir [1] = $Ir(dF\text{-}ppy)_3$, Ir [2] = $[Ir(dtbbpy)(ppy)_2][PF_6]$, and Ir[3] = $(Ir[dF(CF_3)ppy]_2(dtbpy)PF_6$

	$Ru(bpy)_3(PF_6)_2$	Ir [1]	Ir [2]	Ir [3]	TPA	DBAE
D (10^{-5} cm^2/s)	2.53	2.74	2.96	1.05	1.85	3.91
i_k (mA)	0.13	0.13	0.15	0.03	1.44	11.12

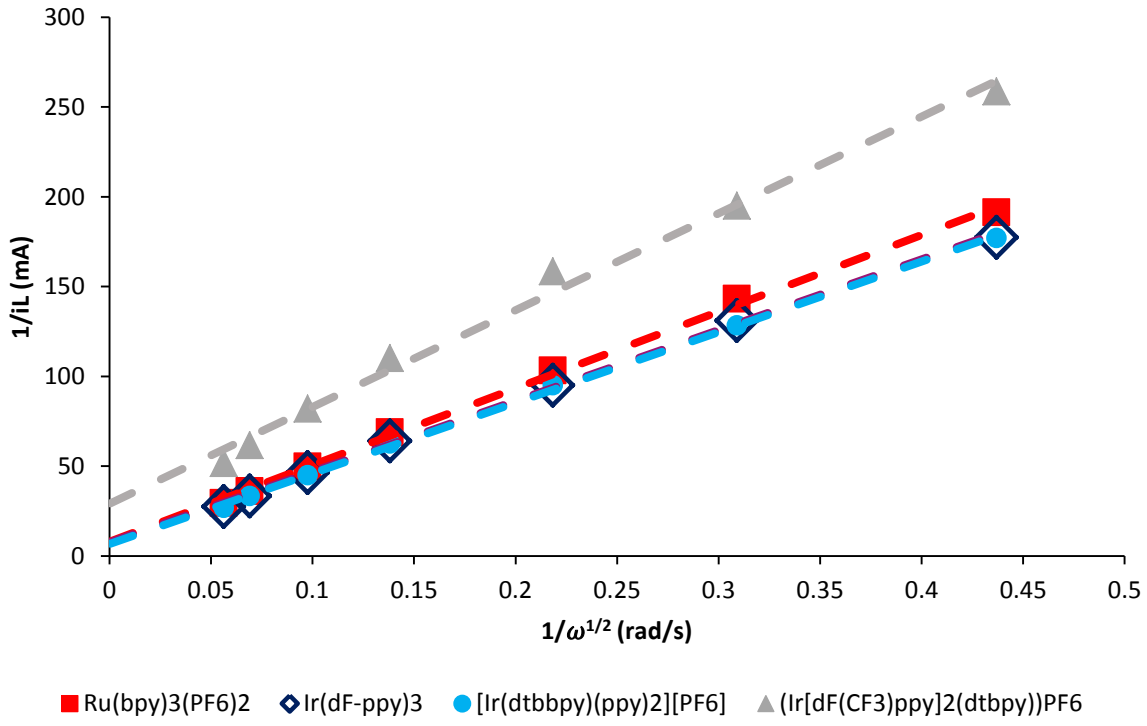

Figure 3.12: Koutecky-Levich studies of 0.2 mM $Ru(bpy)_3(PF_6)_2$, $Ir(dF\text{-}ppy)_3$, $(Ir[dF(CF_3)ppy]_2(dtbpy))PF_6$ and $[Ir(dtbbpy)(ppy)_2][PF_6]$ without the presence of a co-reactant under various rotation rates

Comparing the Koutecky-Levich plots (Figure 3.12) of the all the luminophores used in this study shows that the limiting current in all these systems are directly proportional to the electrode rotation rate and that each luminophore exhibits reversible kinetics, except for $(Ir[dF(CF_3)ppy]_2(dtbpy))PF_6$ which has sluggish heterogeneous kinetics as indicated by its larger y-intercept.

The diffusion coefficients (calculated using Eqn. 1.6) and the kinetic currents (evaluated from the Koutecky-Levich plot in each case) for the luminophores examined are displayed in Table 3.2. The diffusion coefficients of each luminophore do not vary too much when compared to each other, however the kinetic current of $(Ir[dF(CF_3)ppy]_2(dtbpy)PF_6$ is significantly lower than the other luminophores used in the study.

3.3.3 Effect of rotation rate on the electrochemistry of the co-reactant alone

After determining the effect rotation has on the electrochemistry of the luminophores that will be used in the study, the effect of rotation on the electrochemistry of TPA and DBAE (the co-reactants to be used in the study) was investigated. When a solution of 5 mM TPA and a solution of 5 mM DBAE (in an organic environment) was separately examined under the effect of electrode rotation, a trend similar to when the luminophores were studied previously was observed (Figure 3.13 and Figure 3.15). As the rotation rate increased, an increase of the limiting current of both TPA and DBAE was observed. The curvature in the Levich plot (Figure 3.14a) indicates that the electrochemical oxidation of TPA is under kinetic control at higher rotation rates. Unlike TPA, DBAE displays a linear Levich plot (Figure 3.16a) indicating that the electrochemical reaction is more reversible.

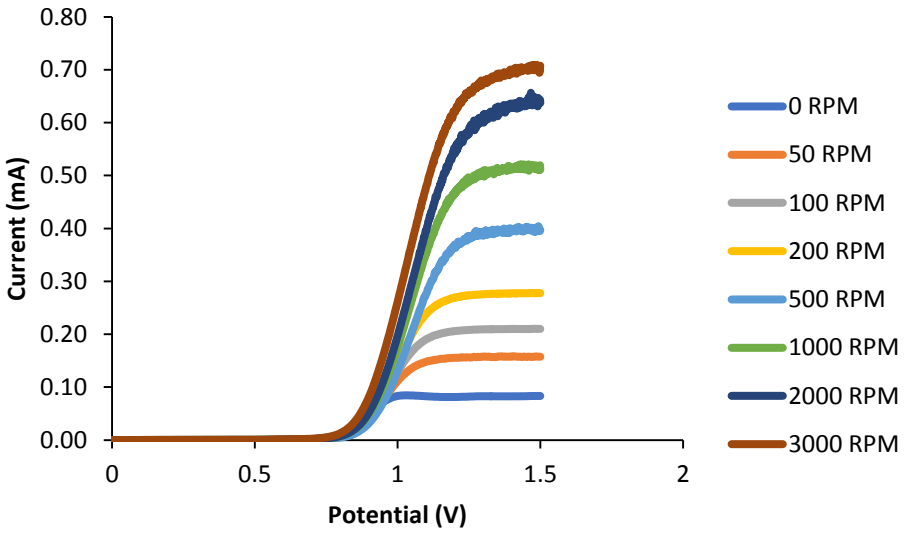

Figure 3.13: Voltammograms generated using 5 mM TPA in dry ACN with 0.1 M NBu_4PF_6 at various rotation rates (0 – 3000 RPM)

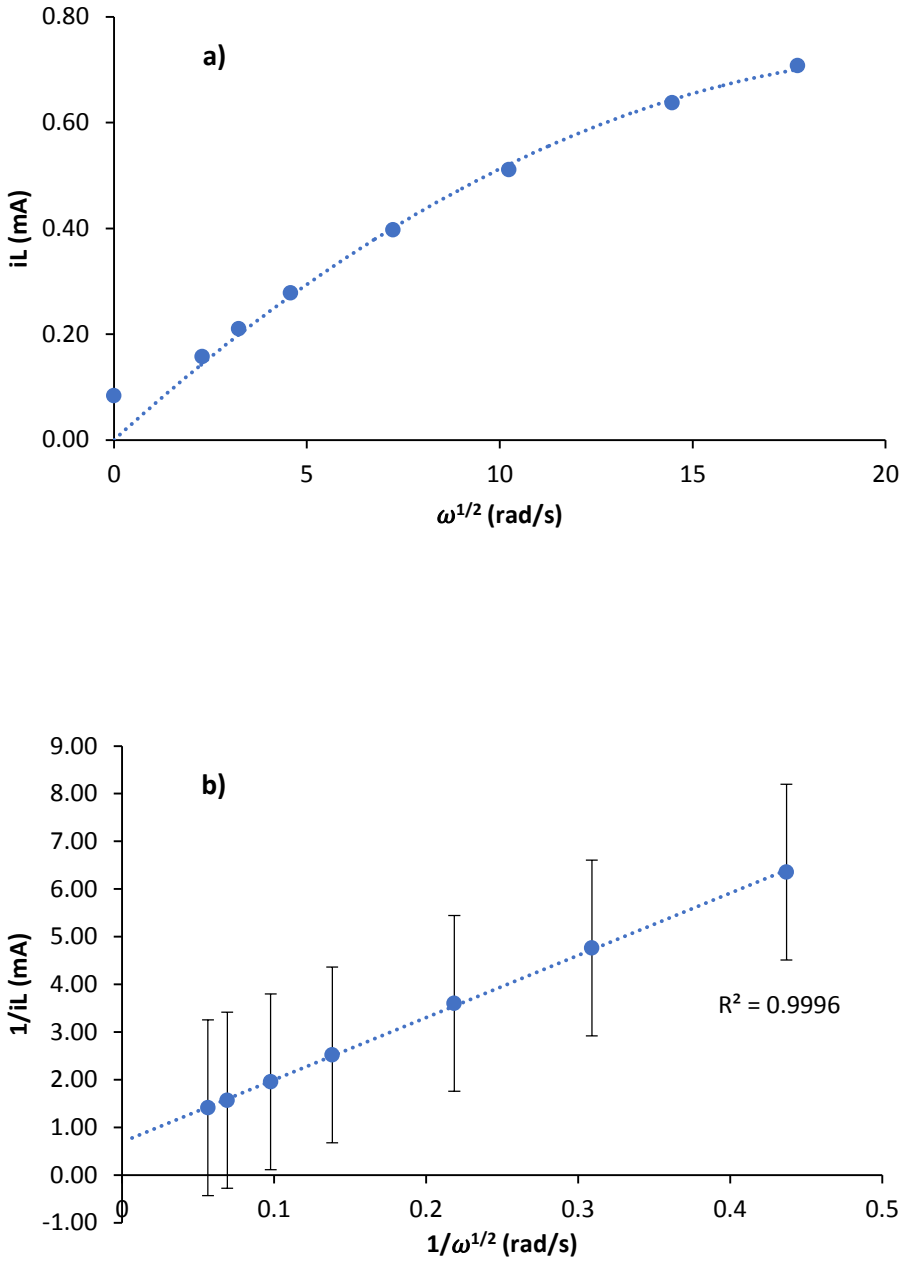

Figure 3.14: Levich (a) and Koutecky-Levich (b) plots of the currents generated at 1.5 V from 5 mM TPA in dry ACN with 0.1 M NBu_4PF_6 at various rotation rates (0 – 3000 RPM)

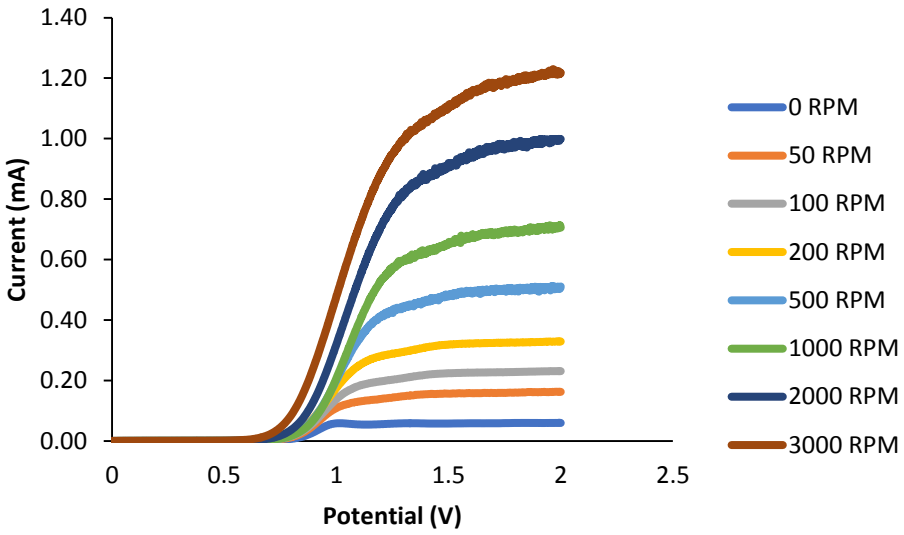

Figure 3.15: Voltammograms generated using 5 mM DBAE in dry ACN with 0.1 M NBu_4PF_6 at various rotation rates (0 – 3000 RPM)

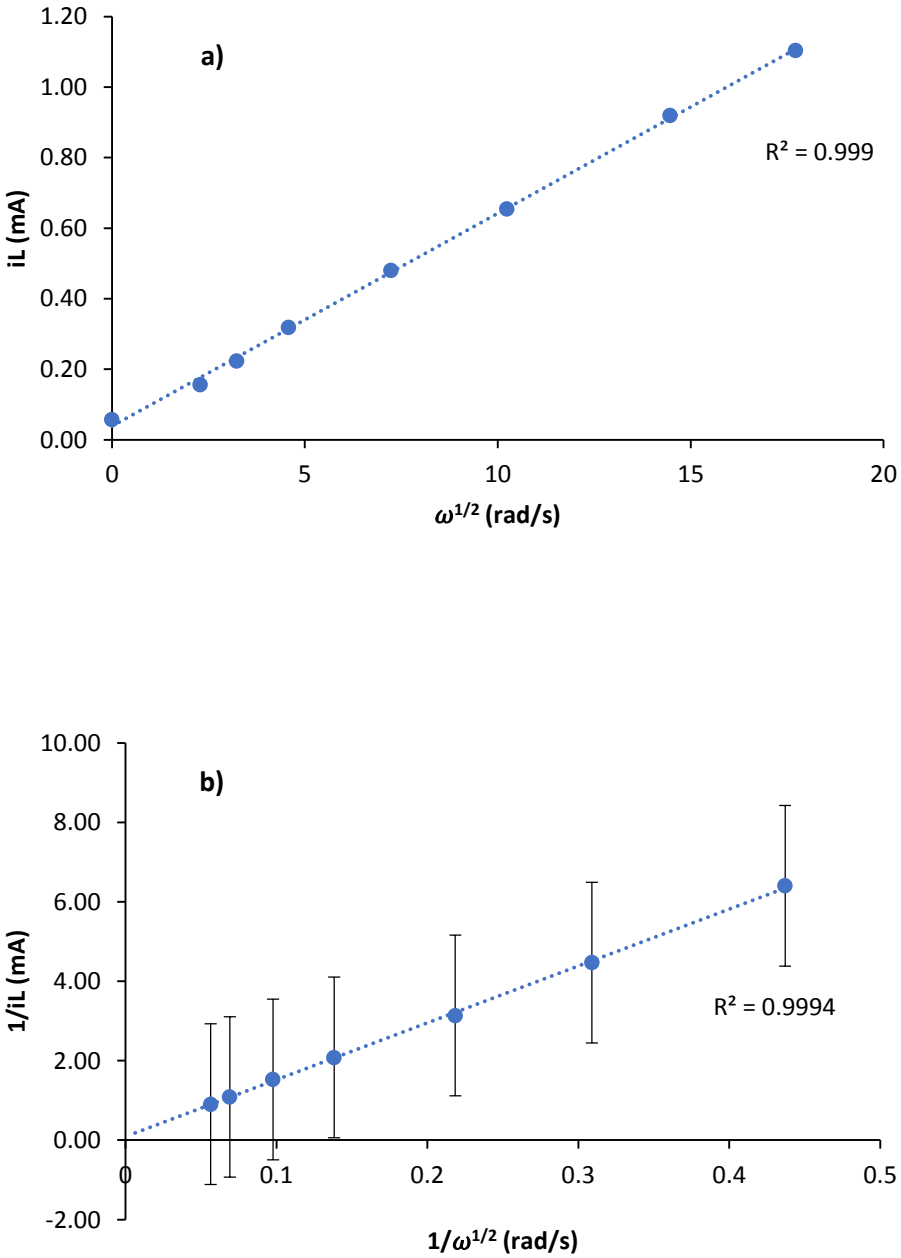

Figure 3.16: Levich (a) and Koutecky-Levich (b) plots of the currents generated at 1.5 V from 5 mM DBAE in dry ACN with 0.1 M NBu_4PF_6 at various rotation rates (0 – 3000 RPM)

Comparing the TPA and DBAE Koutecky-Levich studies to each other (Figure 3.17), it appears that TPA is more susceptible to sluggish kinetics than DBAE due to its larger y-intercept value. This may reflect differing stabilities between the $TPA^{\bullet+}$ and the $DBAE^{\bullet+}$. From the Koutecky-Levich plot it can be determined that the limiting current generated from TPA and DBAE when rotated is directly proportional to the rotation rate of the working electrode. The diffusion coefficients and the kinetic currents for the co-reactants examined are displayed in Table 3.2.

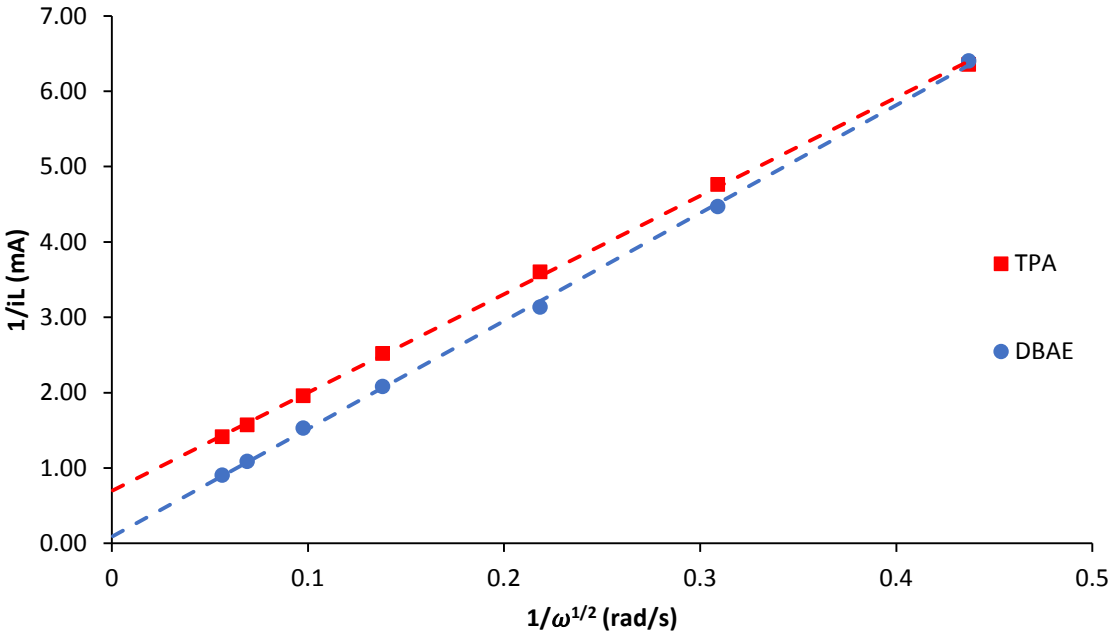

Figure 3.17: Koutecky-Levich studies of 5 mM TPA and DBAE in dry ACN with 0.1 M NBu_4PF_6 without the presence of a co-reactant under various rotation rates

3.3.4 Effect of rotation on co-reactant ECL intensity and currents in organic media

Now that the electrochemical behaviour of the luminophores and the co-reactants under rotation has been characterised, detailed rotation rate studies of the ECL intensities generated from the $Ru(bpy)_3(PF_6)_2$, $Ir(dF\text{-}ppy)_3$, $(Ir[dF(CF_3)ppy]_2(dtbpy))PF_6$ and $[Ir(dtbbpy)(ppy)_2][PF_6]$ co-reactant ECL systems (with TPA acting as the co-reactant) were performed. As expected, when a solution containing 0.2 mM $Ru(bpy)_3(PF_6)_2$ and 5 mM TPA was examined under the influence of rotation, an increase of the limiting current was observed with an increase of rotation rate (Figure 3.18). The current observed at 3000 RPM however appears to be 15% lower than expected on the basis of the trend in limiting currents in Figure 3.18; this may be due to the system entering slightly turbulent conditions at this rotation rate. The non-zero intercept in Figure 3.19, suggests a kinetic limitation to the current. In this case it probably reflects the second order kinetics of the reaction between Ru^{3+} and TPA.

It would be expected that the ECL intensities generated from the $Ru(bpy)_3(PF_6)_2$/TPA co-reactant ECL system should also increase with an increase of the rotation rate as the currents generated from the system increases with rotation; however an interesting phenomenon was observed instead. As depicted in Figure 3.20, an increase of ECL intensity is observed with rotation rate, but only up to approximately 1000 RPM (which will be referred to as the "critical RPM"), beyond which a steady decrease in ECL intensity was observed, despite the fact that the limiting current continued to increase. The corresponding Levich plot of the current and ECL intensities is shown in Figure 3.21.

This interesting phenomenon was also observed in the $[Ir(dtbbpy)(ppy)_2][PF_6]$/TPA, $(Ir[dF(CF_3)ppy]_2(dtbpy))PF_6$/TPA and $Ir(dF\text{-}ppy)_3$/TPA co-reactant ECL systems (Figures 3.18-3.33) where a decrease of ECL intensities with continual increase of the limiting current was observed at rotation rates faster than the systems' respective critical RPM. In some cases,

a non-steady-state ECL response was observed. The approx. critical RPMs and kinetic currents for each system are shown in Table 3.3.

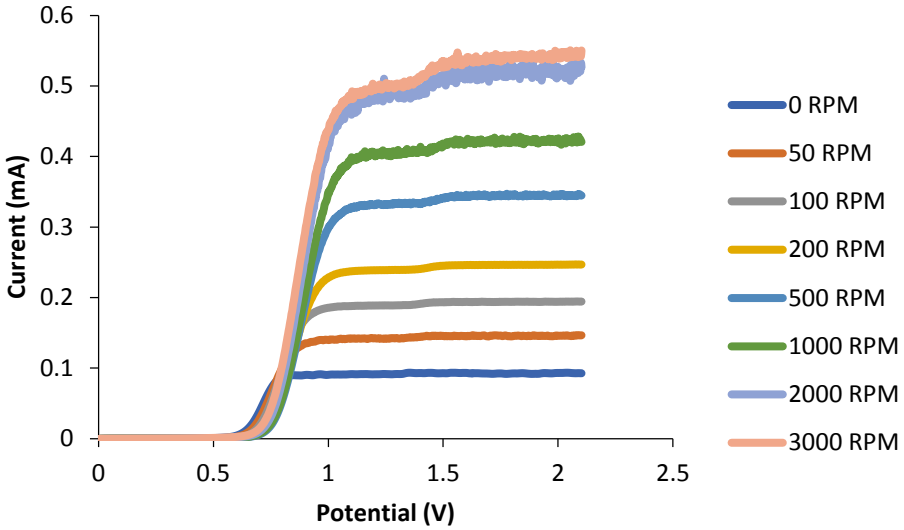

Figure 3.18: Voltammograms generated using the 0.2 mM $Ru(bpy)_3(PF_6)_2$/5 mM TPA co-reactant ECL system in dry ACN with 0.1 M NBu_4PF_6 at various rotation rates (0 – 3000 RPM)

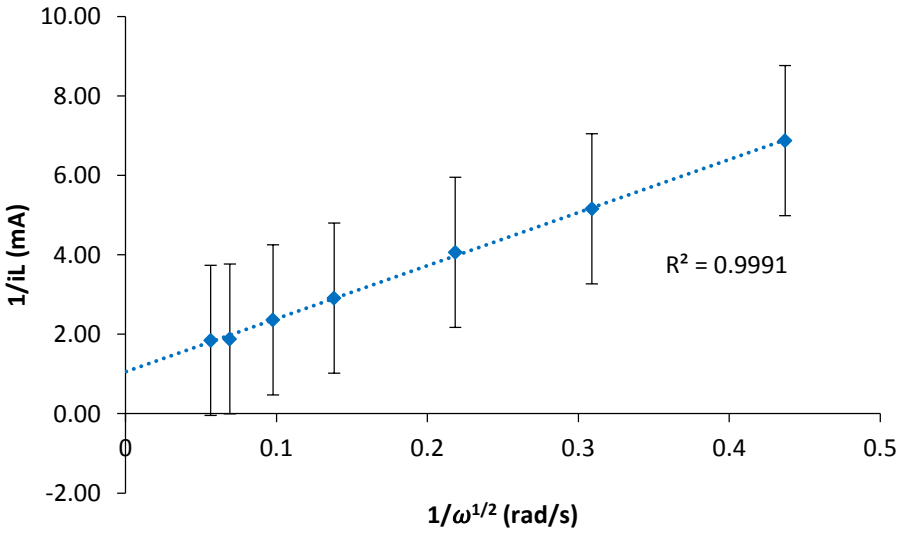

Figure 3.19: Koutecky-Levich plot of the currents generated at 1.5 V from the 0.2 mM $Ru(bpy)_3(PF_6)_2$/5 mM TPA co-reactant ECL system in dry ACN with 0.1 M NBu_4PF_6 at various RPMs (0 – 3000 RPM)

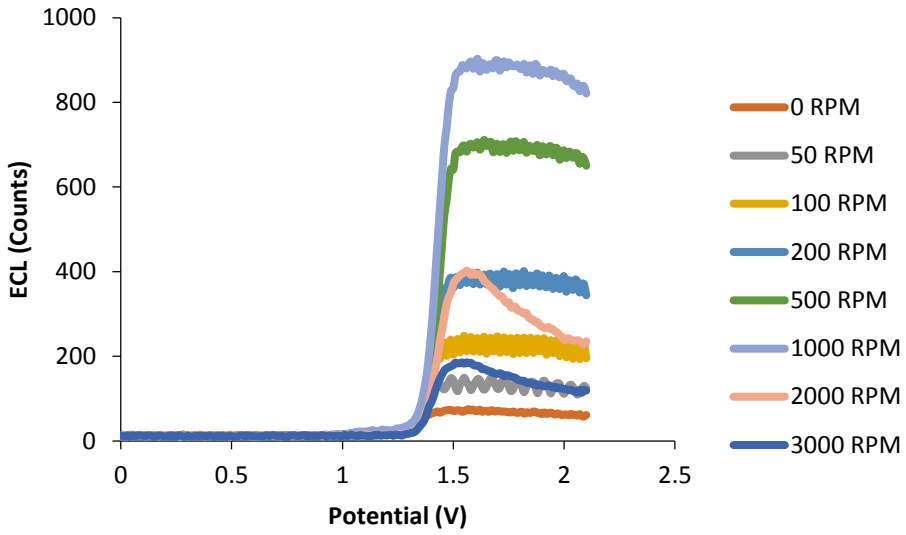

Figure 3.20: Voltammograms of the ECL intensities generated using the 0.2 mM $Ru(bpy)_3(PF_6)_2$/5 mM TPA co-reactant ECL system in dry ACN with 0.1 M NBu_4PF_6 at various rotation rates (0 – 3000 RPM)

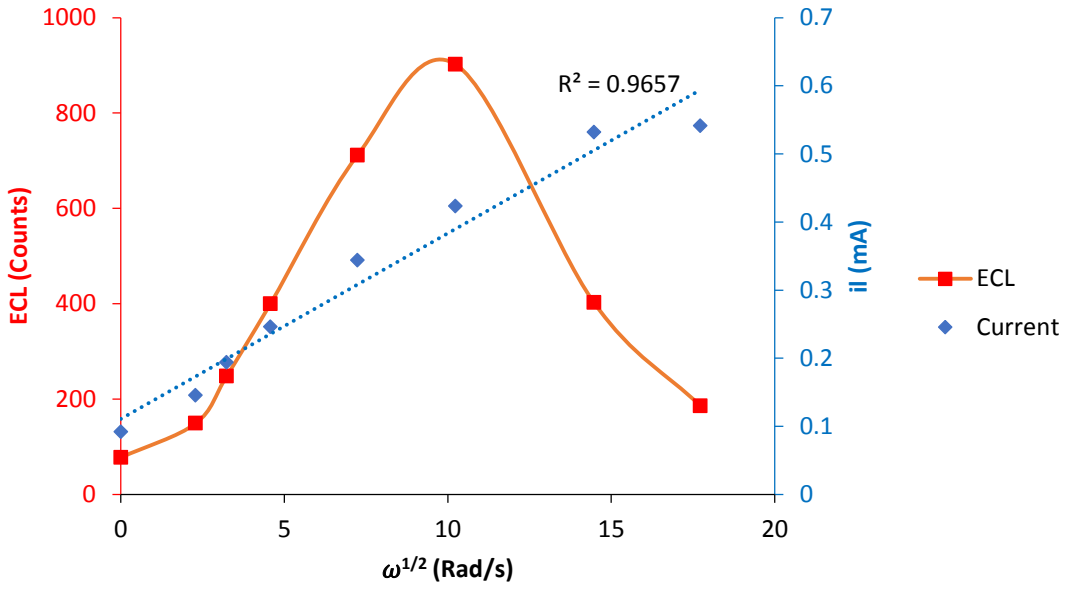

Figure 3.21: Levich plots of the current (blue plot, at 1.5 V) and ECL intensities (red plot, at 1.75 V) generated from the 0.2 mM $Ru(bpy)_3(PF_6)_2$/5 mM TPA co-reactant ECL system in dry ACN with 0.1 M NBu_4PF_6 at various rotation rates (0 – 3000 RPM) at 610 nm highlighting the decrease of ECL intensities past 1000 RPM (104.72 rad/s)

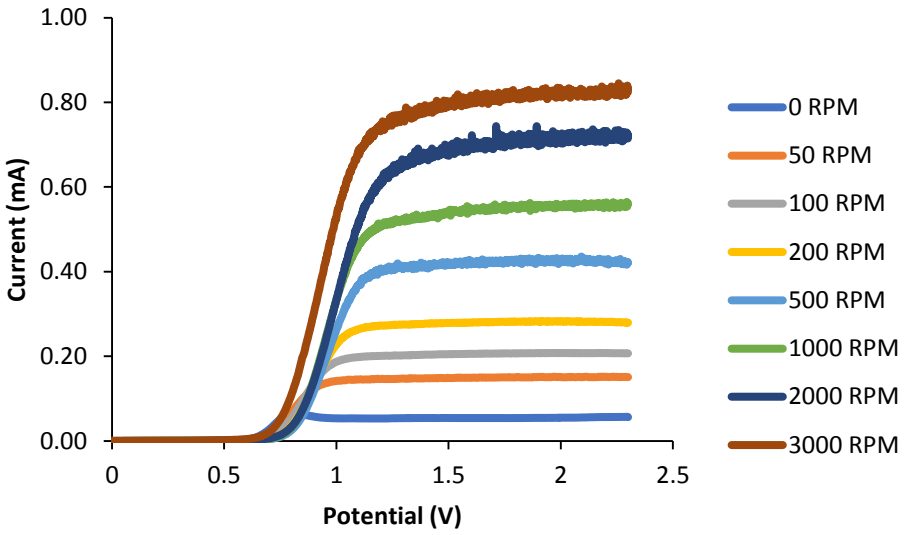

Figure 3.22: Voltammograms generated using the 0.2 mM $[Ir(dtbbpy)(ppy)_2][PF_6]$/5 mM TPA co-reactant ECL system in dry ACN with 0.1 M NBu_4PF_6 at various RPMs (0 – 3000 RPM)

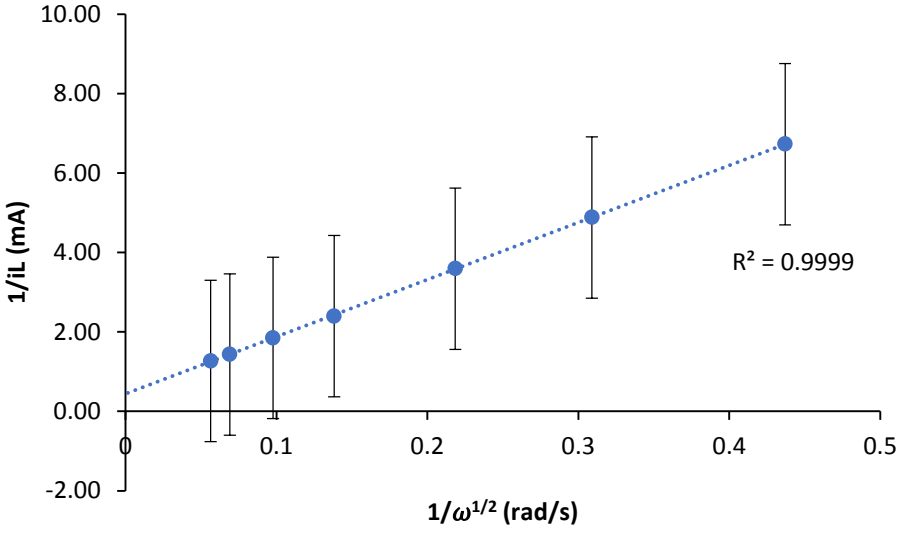

Figure 3.23: Koutecky-Levich plot of the currents generated at 1.5 V from the 0.2 mM $[Ir(dtbbpy)(ppy)_2][PF_6]$/5 mM TPA co-reactant ECL system in dry ACN with 0.1 M NBu_4PF_6 at various rotation rates (0 – 3000 RPM)

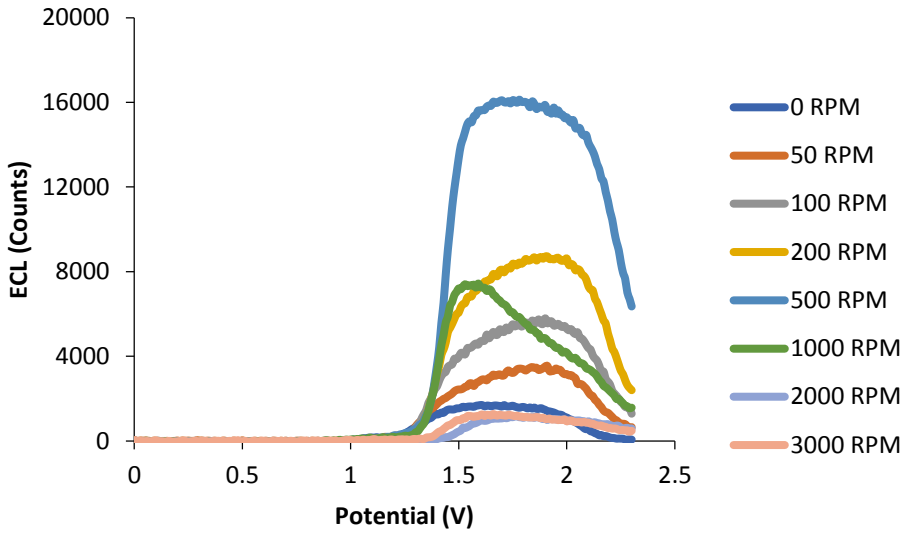

Figure 3.24: Voltammograms of the ECL intensities generated using the 0.2 mM $[Ir(dtbbpy)(ppy)_2][PF_6]$/5 mM TPA co-reactant ECL system in dry ACN with 0.1 M NBu_4PF_6 at various rotation rates (0 – 3000 RPM)

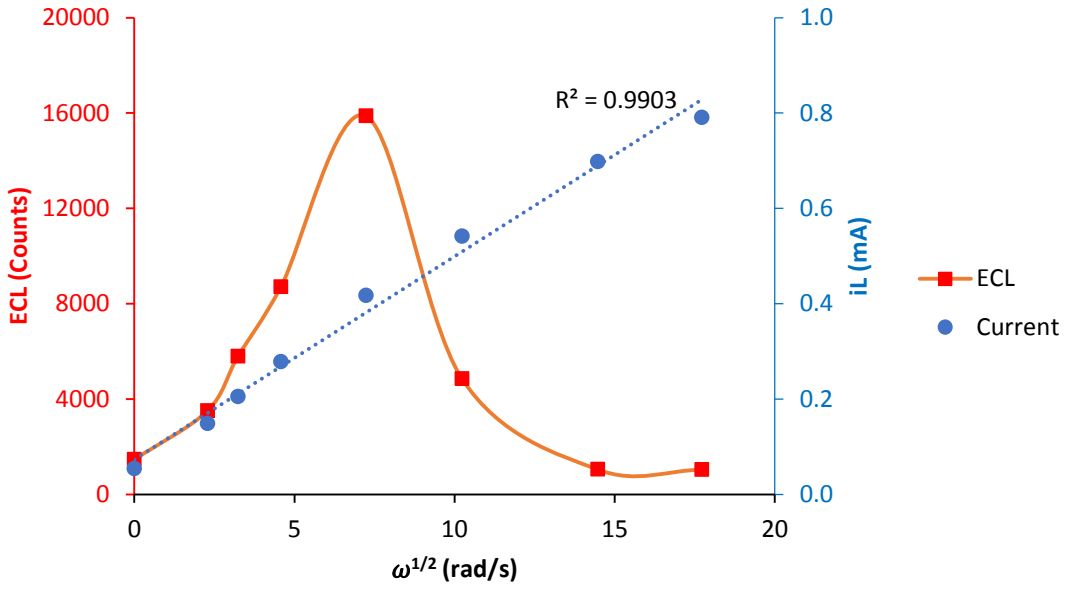

Figure 3.25: Levich plots of the current (blue plot, at 1.5 V) and the ECL intensities (red plot, at 1.9 V) generated from the 0.2 mM $[Ir(dtbbpy)(ppy)_2][PF_6]$/5 mM TPA co-reactant ECL system in dry ACN with 0.1 M NBu_4PF_6 at various rotation rates (0 – 3000 RPM) at 577 nm highlighting a decrease of ECL intensities past 500 RPM (52.36 rad/s)

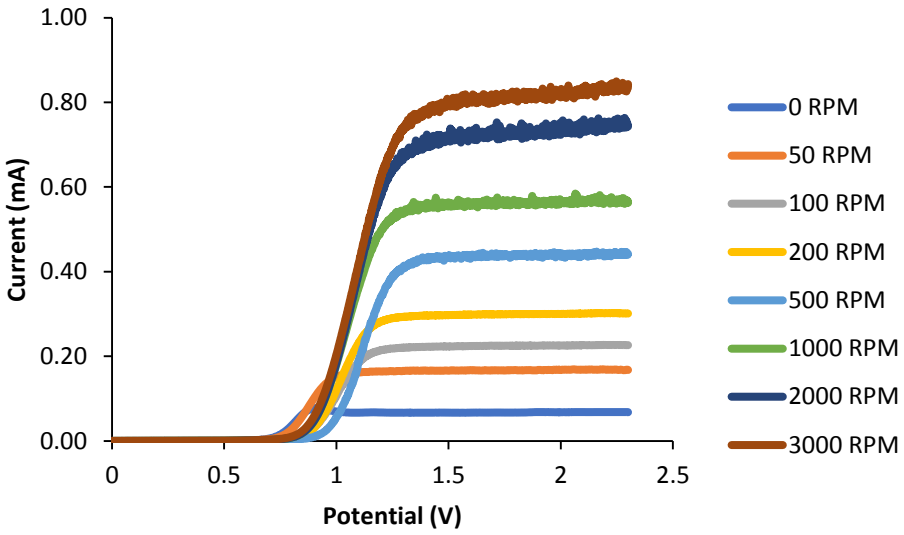

Figure 3.26: Voltammograms generated using the 0.2 mM ($Ir[dF(CF_3)ppy]_2(dtbpy))PF_6$ /5 mM TPA co-reactant ECL system in dry ACN with 0.1 M NBu_4PF_6 at various rotation rates (0 – 3000 RPM)

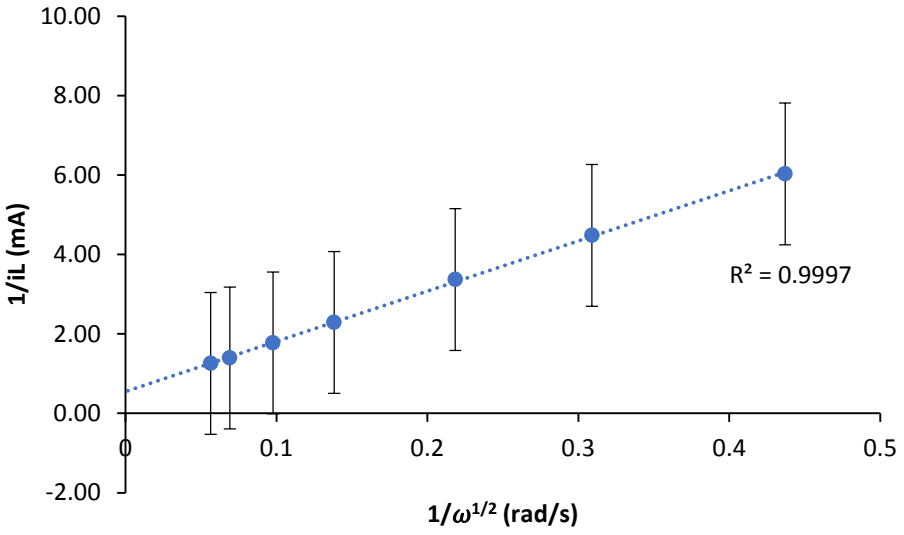

Figure 3.27: Koutecky-Levich plot of the currents generated at 1.5 V from the 0.2 mM ($Ir[dF(CF_3)ppy]_2(dtbpy))PF_6$/5 mM TPA co-reactant ECL system in dry ACN with 0.1 M NBu_4PF_6 at various rotation rates (0 – 3000 RPM)

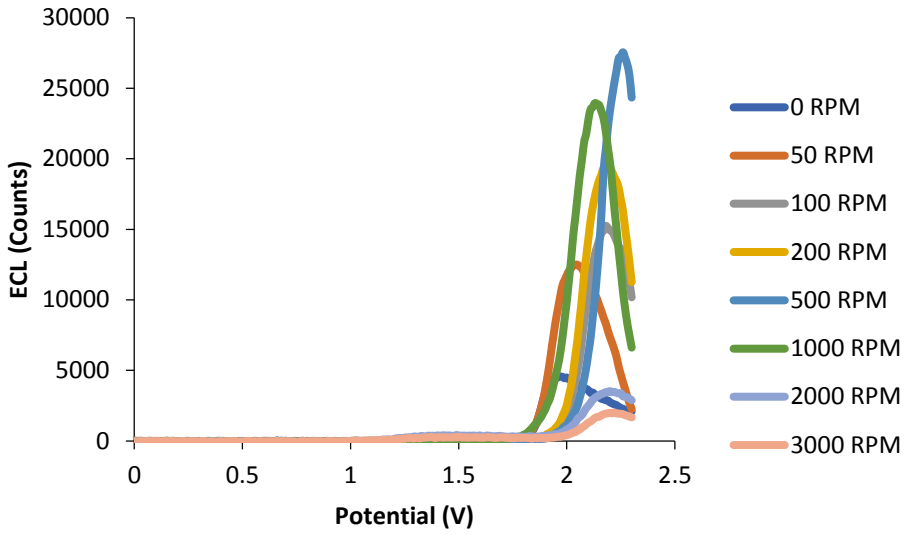

Figure 3.28: Voltammograms of the ECL intensities generated using the 0.2 mM (Ir[dF(CF_3)ppy]$_2$(dtbpy))PF_6 /5 mM TPA co-reactant ECL system in dry ACN with 0.1 M NBu_4PF_6 at various rotation rates (0 – 3000 RPM)

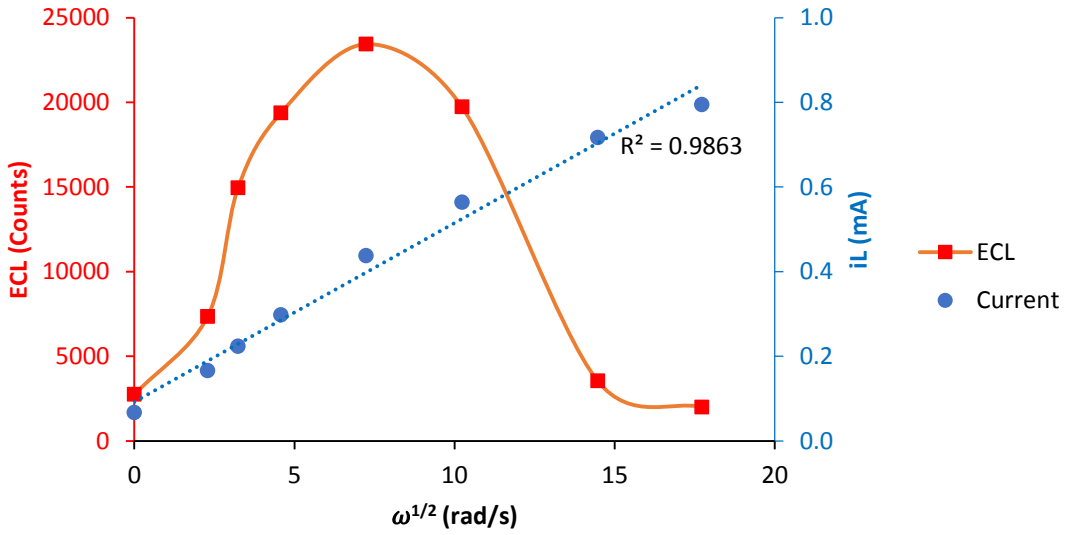

Figure 3.29: Levich plots of the current (blue plot, at 1.5 V) and the ECL intensities (red plot, at 2.2 V) generated from the 0.2 mM (Ir[dF(CF_3)ppy]$_2$(dtbpy))PF_6/5 mM TPA co-reactant ECL system in dry ACN with 0.1 M NBu_4PF_6 at various rotation rates (0 – 3000 RPM) at 470 nm highlighting a decrease of ECL intensities past 500 RPM (52.36 rad/s)

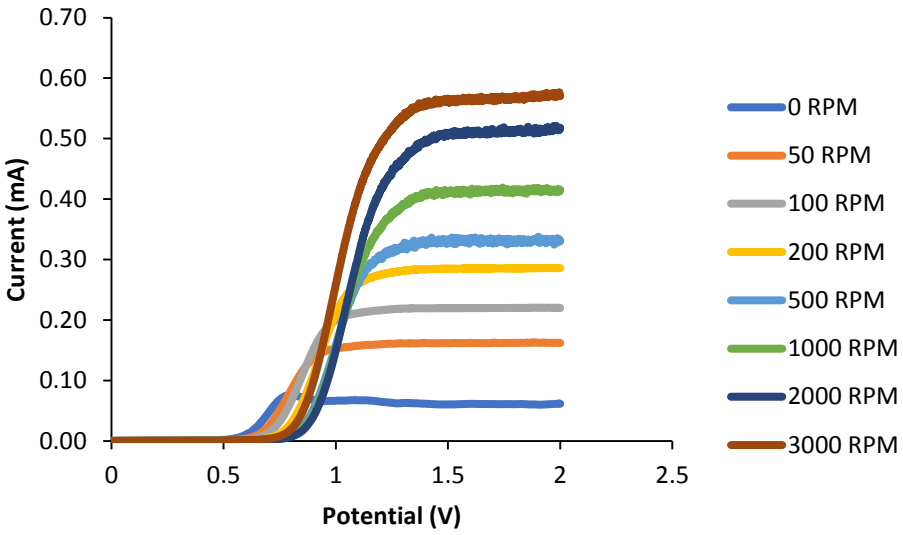

Figure 3.30: Voltammograms generated using the 0.2 mM $Ir(dF\text{-}ppy)_3$/5 mM TPA co-reactant ECL system in dry ACN with 0.1 M NBu_4PF_6 at various rotation rates (0 – 3000 RPM)

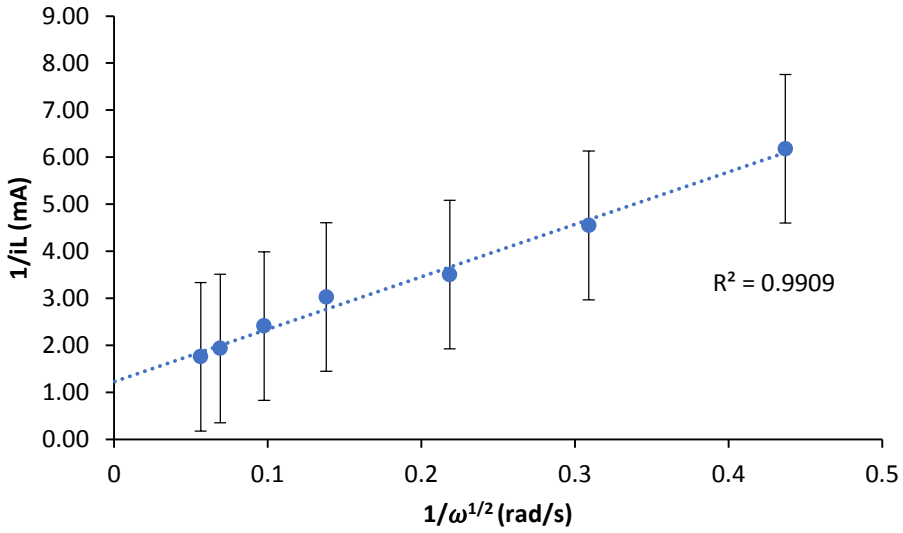

Figure 3.31: Koutecky-Levich plot of the currents generated at 1.5 V from the 0.2 mM $Ir(dF\text{-}ppy)_3$/5 mM TPA co-reactant ECL system in dry ACN with 0.1 M NBu_4PF_6 at various rotation rates (0 – 3000 RPM)

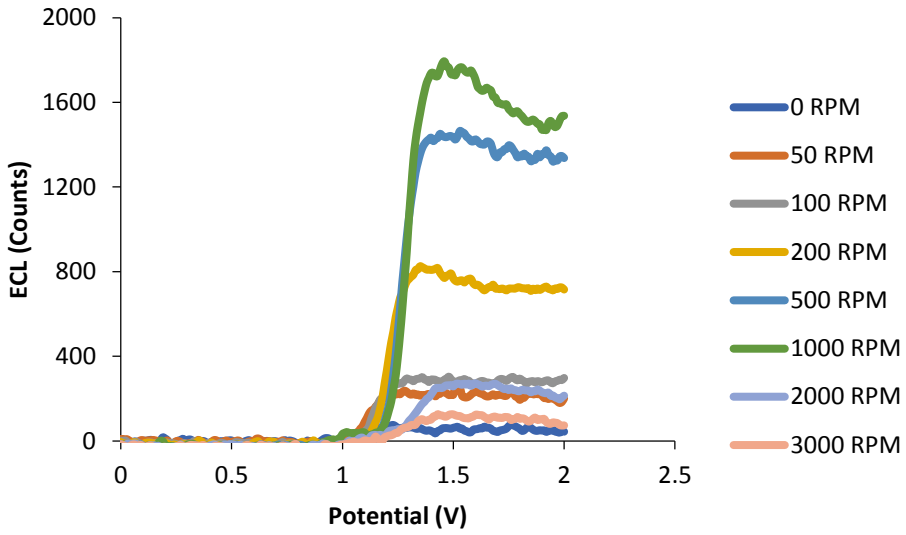

Figure 3.32: Voltammograms of the ECL intensities generated using the 0.2 mM Ir(dF-ppy)$_3$/5 mM TPA co-reactant ECL system in dry ACN with 0.1 M NBu_4PF_6 at various rotation rates (0 – 3000 RPM)

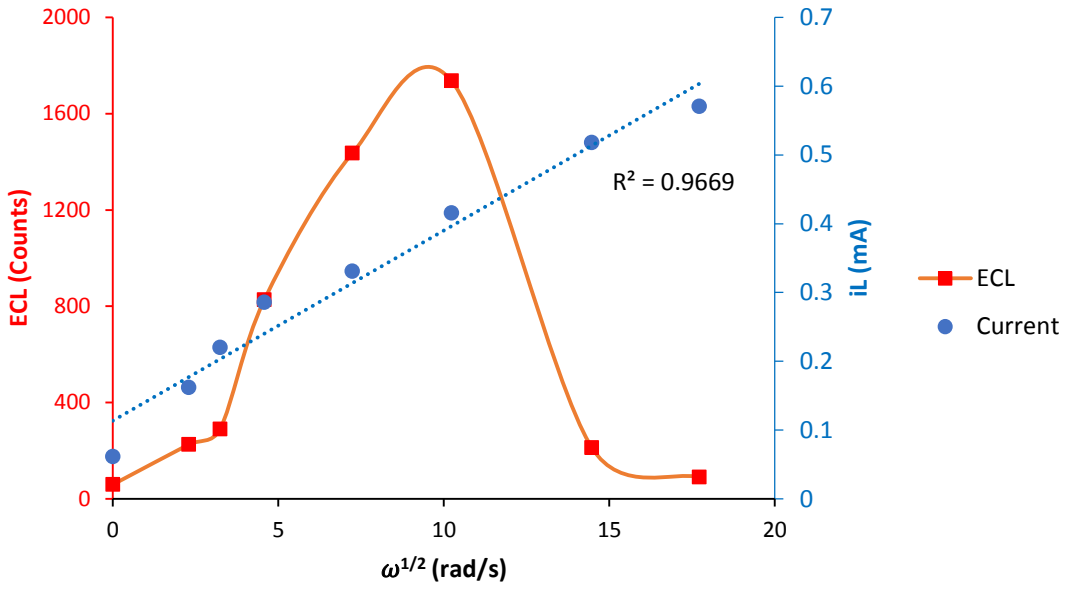

Figure 3.33: Levich plots of the current (blue plot, at 1.5 V) and the ECL intensities (red plot, at 1.4 V from the 0.2 mM Ir(dF-ppy)$_3$/5 mM TPA co-reactant ECL system in dry ACN with 0.1 M NBu_4PF_6 at various rotation rates (0 – 3000 RPM) at 500 nm highlighting the decrease of ECL intensities past 1000 RPM (104.72 rad/s)

Table 3.3: Approx. critical RPM and kinetic currents (i_k) of the 0.2 mM luminophore/5 mM TPA co-reactant ECL systems examined in this study

	$Ru(bpy)_3(PF_6)_2$	$Ir(dF\text{-}ppy)_3$	$[Ir(dtbbpy)(ppy)_2][PF_6]$	$(Ir[dF(CF_3)ppy]_2(dtbpy)PF_6$
Critical RPM	1000	1000	500	500
i_k (mA)	0.95	0.82	2.28	1.82

Koutecky-Levich studies of the limiting currents generated from each co-reactant ECL system under similar conditions (Figure 3.34) show that each system exhibits kinetic limitations to some extent. In regards to the limiting current, sluggish kinetics has a slightly greater effect on the $Ir(dF\text{-}ppy)_3$/TPA co-reactant ECL system compared to the other co-reactant ECL systems studied. As expected, there is a linear relationship between rotation rates and limiting current for each co-reactant ECL system under laminar conditions.

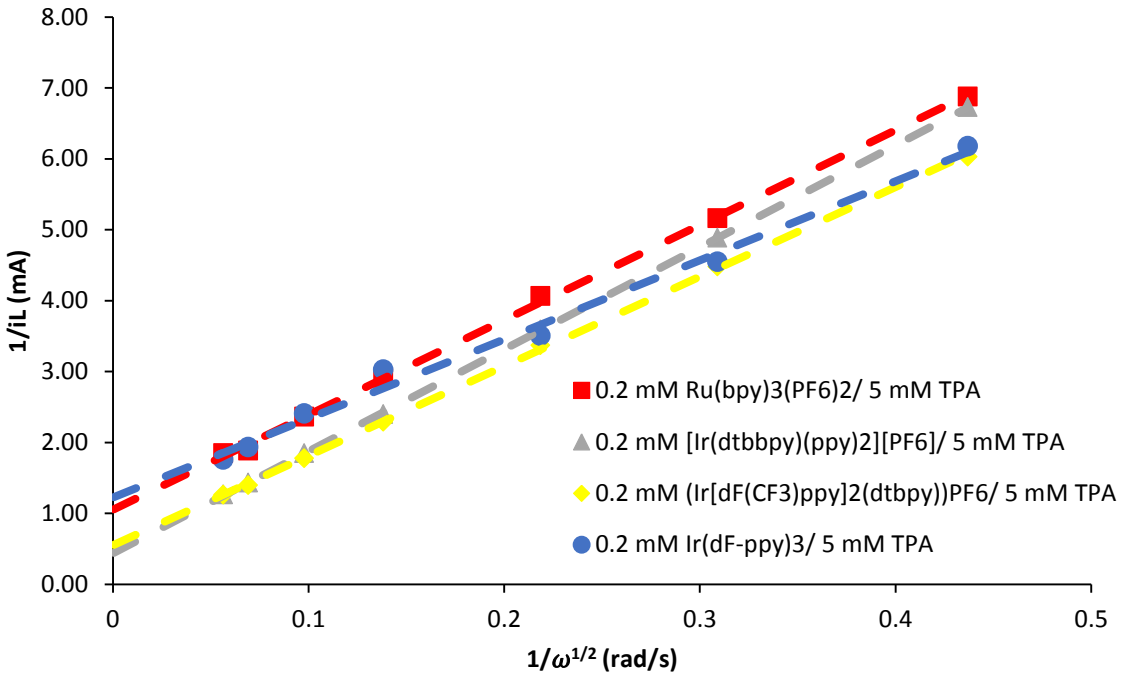

Figure 3.34: Koutecky-Levich studies of the currents generated from the 0.2 mM $Ru(bpy)_3(PF_6)_2$, $Ir(dF\text{-}ppy)_3$, $(Ir[dF(CF_3)ppy]_2(dtbpy))PF_6$ and $[Ir(dtbbpy)(ppy)_2][PF_6]$ co-reactant ECL systems in the presence of 5 mM TPA under various rotation rates

The decrease in ECL intensity observed at rotation rate higher than the critical RPM can be explained by the insufficient time (residence time, see reaction [3.5] (k_2)) for a radical cation spent near the electrode surface, leading to less light being generated from the luminophore.

$$[Ru(bpy)_3]^{2+} - e^- \rightarrow [Ru(bpy)_3]^{3+} \quad \textbf{[3.1]}$$

$$HTPA \rightleftharpoons TPA + H^+ \quad \textbf{[3.2]}$$

$$[Ru(bpy)_3]^{3+} + TPA \xrightarrow{k_1} [Ru(bpy)_3]^{2+} + TPA^{\bullet+} \quad \textbf{[3.3]}$$

$$TPA - e^- \rightarrow TPA^{\bullet+} \quad \textbf{[3.4]}$$

$$TPA^{\bullet+} \xrightarrow{k_2} TPA^{\bullet} + H^+ \quad \textbf{[3.5]}$$

$$[Ru(bpy)_3]^{3+} + TPA^{\bullet} \xrightarrow{k_3} [Ru(bpy)_3]^{2+}* + \text{other products} \quad \textbf{[3.6]}$$

$$[Ru(bpy)_3]^{2+}* \rightarrow [Ru(bpy)_3]^{2+} + h\nu \quad \textbf{[3.7]}$$

To put it simply, at the critical RPM the rate of removal of the radical cation is greater than the rate of the deprotonation step and therefore less of the strongly reducing $TPA^{\bullet}$ is around the electrode surface for it to interact with the oxidised form of the luminophore which would affect the ECL intensities generated. For this conjecture to be correct, varying the concentration of the co-reactant or varying the pH of the system should affect when this critical RPM takes place.

Alternatively, reaction [3.3] (k_1), where the oxidised $[Ru(bpy)_3]^{3+}$ state oxidises TPA to form $TPA^{\bullet+}$, could also be the cause of the critical RPM phenomena. If this conjecture is correct though, varying the concentration of the luminophore should affect when the critical

RPM takes place. Reaction [3.6] (k_3) is known to occur extremely fast so it is unlikely to be the cause of the critical RPM phenomena.

3.3.5 Effect of co-reactant and luminophore concentration on the critical RPM of the $Ru(bpy)_3(PF_6)_2$/TPA co-reactant ECL system

If our previous critical RPM hypothesis is correct, then altering the concentration of the co-reactant should have an effect on the critical RPM. Extrapolation of the Koutecky-Levich study (Figure 3.35) based on the limiting current from the linear scan voltammogram of a 0.2 mM $Ru(bpy)_3(PF_6)_2$ solution containing either 1 mM, 5 mM or 20 mM of TPA shows that increasing the co-reactant (TPA) concentration will result in faster kinetics. Once again at these lower and higher co-reactant concentrations a linear relationship between rotation rates and the currents generated is observed.

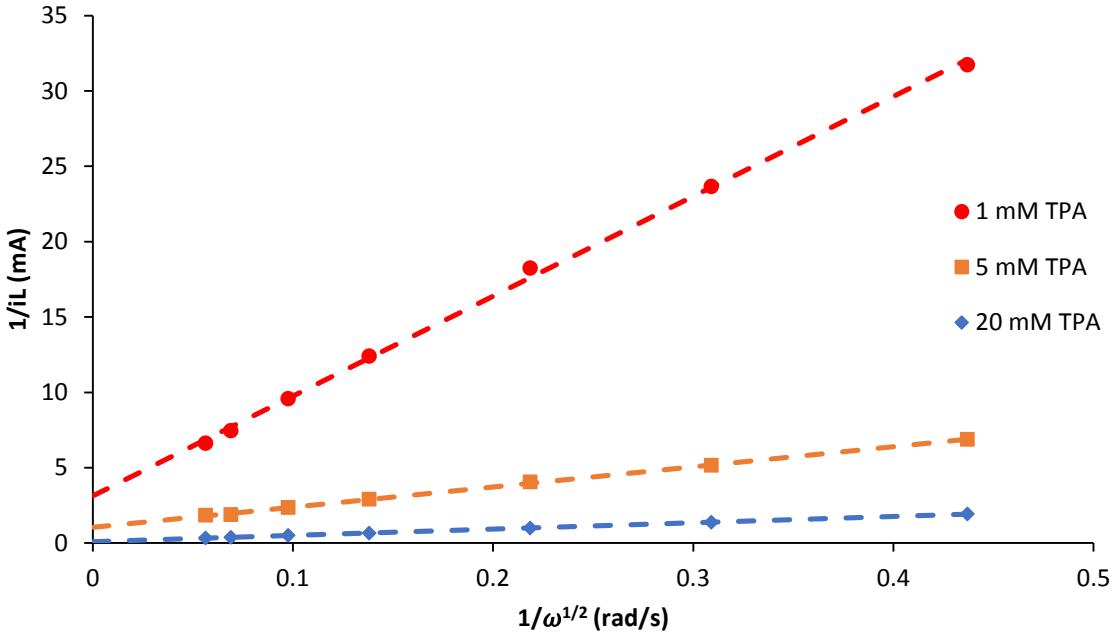

Figure 3.35: Koutecky-Levich studies of the currents generated from 0.2 mM $Ru(bpy)_3(PF_6)_2$ where 1mM (red), 5mM (orange) and 20 mM (blue) of TPA was used as the co-reactant in dry ACN with 0.1 M NBu_4PF_6 under rotation at various RPMs (0 – 3000 RPM) at 610 nm

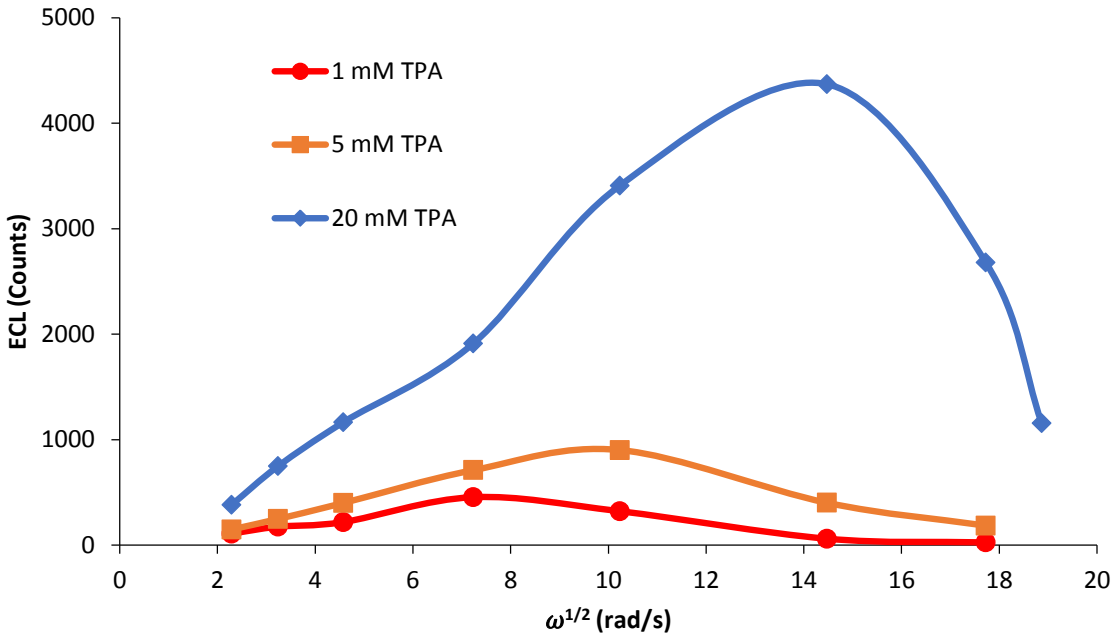

Figure 3.36: Levich plots of the peak ECL intensities generated from 0.2 mM $Ru(bpy)_3(PF_6)_2$ where 1mM (red), 5mM (orange) and 20 mM (blue) of TPA was used as the co-reactant in dry ACN with 0.1 M NBu_4PF_6 under rotation at various RPMs (0 – 3000 RPM) at 610 nm

The Levich plots of the ECL intensities generated from $Ru(bpy)_3(PF_6)_2$ solutions under electrode rotation (Figure 3.36) however does in fact show a shift in the observed critical RPM. A critical RPM of approx. 500 RPM (52.36 rad/s) takes place in the 0.2 mM $Ru(bpy)_3(PF_6)_2$/1 mM TPA co-reactant ECL system. A faster critical RPM of approx. 1000 RPM (104.72 rad/s) occurs in the 0.2 mM $Ru(bpy)_3(PF_6)_2$/5 mM TPA co-reactant ECL system while the 0.2 mM $Ru(bpy)_3(PF_6)_2$/20 mM TPA co-reactant ECL system exhibits the fastest critical RPM observed in the study occurring at approx. 2000 RPM (209.44 rad/s).

See supplementary information Figures S3-S6 for the voltammograms of the current and ECL intensities generated from the 0.2 mM $Ru(bpy)_3(PF_6)_2$/1 mM TPA and 0.2 mM $Ru(bpy)_3(PF_6)_2$/20 mM TPA co-reactant ECL systems and Figures 3.18 and 3.20 for the voltammograms generated from the 0.2 mM $Ru(bpy)_3(PF_6)_2$/5 mM TPA system.

A shift in the observed critical RPM in systems containing different concentrations of the co-reactant (TPA) supports our earlier hypothesis that at the critical RPM, the rate of removal of the radical cation is greater than the rate of the deprotonation step. Therefore less of the $TPA^{\bullet}$ strongly reducing intermediate is around the electrode surface for it to interact with the reduced form of the luminophore which would affect the ECL intensities generated. In systems containing higher concentrations of the co-reactant, there would be a greater amount of the radical cation present at the electrode surface and hence a faster electrode rotation speed is required to outpace the rate of the deprotonation step thereby increasing the critical RPM observed in the system. Simply put, with an increase of co-reactant concentrations in the system, an increase of the critical RPM of the system occurs, supporting our earlier hypothesis that the critical RPM phenomenon reflects the kinetics of reaction [3.5].

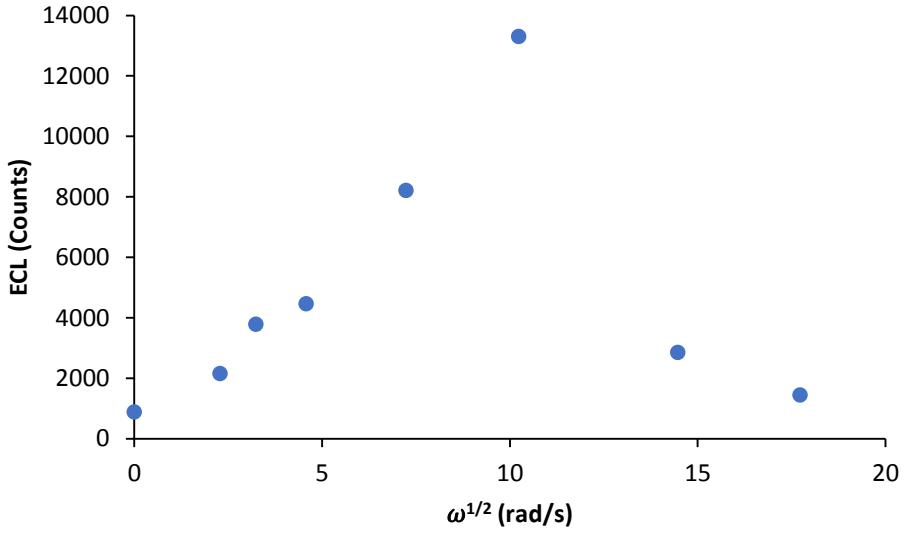

Figure 3.37: Levich plot of the ECL intensities generated at 2.0 V from the RPM study of the 0.05 mM $Ru(bpy)_3(PF_6)_2$/5 mM TPA co-reactant ECL system in dry ACN with 0.1 M NBu_4PF_6 at various RPMs (0 – 3000 RPM) at 610 nm

No difference of the critical RPM was observed however when the 0.2 mM $Ru(bpy)_3(PF_6)_2$/5 mM TPA (Figure 3.21, red plot) and the 0.05 mM $Ru(bpy)_3(PF_6)_2$/5 mM co-reactant ECL (Figure 3.37) systems were examined. In both systems the critical RPM occurred at approx. 1000 RPM (104.72 rad/s). See supplementary information Figures S7 and S8 for the voltammograms of the current and ECL intensities generated from the 0.05 mM $Ru(bpy)_3(PF_6)_2$/5 mM TPA co-reactant ECL system.

It can be stated that the concentration of the luminophore has no effect on where the critical RPM takes place in the system. This further supports our earlier hypothesis that the rate of removal of the radical cation is the cause of the critical RPM phenomena because if reaction [3.3] was the cause, then the break in the ECL intensities observed would be sensitive to the concentration of ruthenium which isn't the case.

3.3.6 Effect of pH on the critical RPM

To further investigate the critical RPM phenomena, a pH RPM study was performed on both the 0.2 mM $Ru(bpy)_3(PF_6)_2$/5 mM TPA and the 0.2 mM $Ru(bpy)_3(PF_6)_2$/5 mM DBAE co-reactant ECL systems at various pHs and rotation rates. Once again the critical RPM phenomena was observed in both co-reactant ECL systems and recorded at each pH level used in the study (Tables 3.4 and 3.5). Figure 3.38 shows that the pH of the system does in fact affect when the critical RPM occurs, supporting our earlier hypothesis that the cause of the reduced ECL intensities was due to the rate of removal of the radical co-reactant cation outpacing the rate of deprotonation.

Table 3.4: Critical RPMs of the 0.2 mM $Ru(bpy)_3(PF_6)_2$/5 mM TPA co-reactant ECL system at various pH levels

pH	10.49	9.94	9.22	8.65	7.72
Critical RPM	1000	975	925	875	825

Table 3.5: Critical RPMs of the 0.2 mM $Ru(bpy)_3(PF_6)_2$/5 mM DBAE co-reactant ECL system at various pH levels

pH	10.9	9.17	8.38	7.84	7.55
Critical RPM	1100	1025	1000	960	950

The lower (or more acidic) the pH of the system is, the lower the rotation rate to reach the critical RPM of the system is required. A more acidic environment would promote the rate of deprotonation which would explain why a shift towards slower critical RPM rates is observed at lower pHs. ECL intensities generated from both co-reactant ECL systems used in this study also significantly decreased at these lower pH levels.

The critical RPMs observed when DBAE was used as the co-reactant were faster than the critical RPMs observed when TPA was used at the same pH level. This indicates that higher rotations rates were required to remove the $DBAE^{\bullet+}$ from the electrode surface compared to the removal of the $TPA^{\bullet+}$ suggesting that the kinetics of the deprotonation of the $DBAE^{\bullet+}$ is faster than the deprotonation of the $TPA^{\bullet+}$.

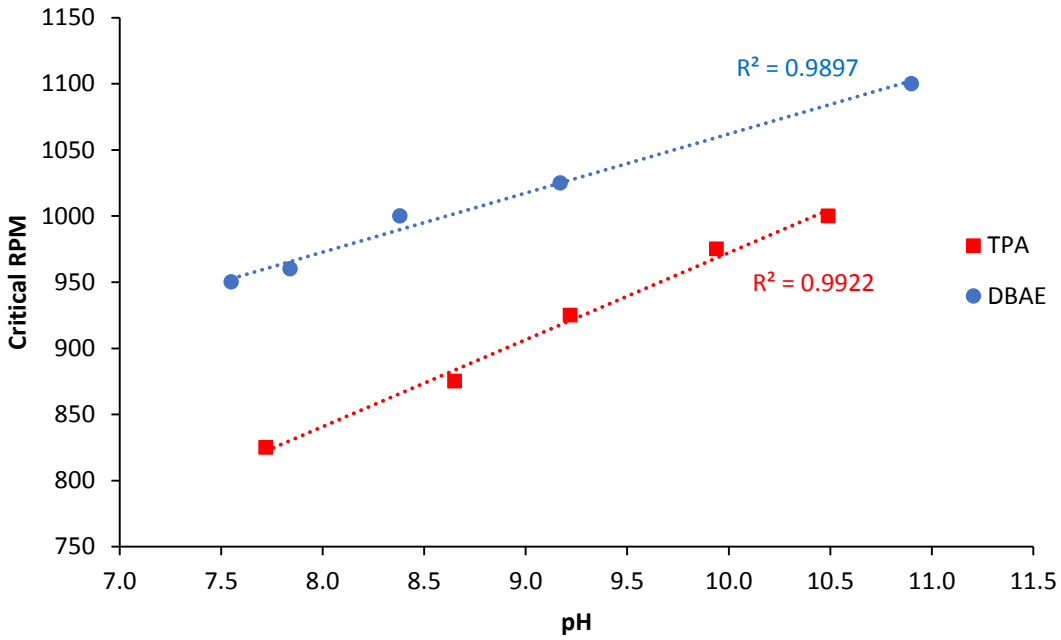

Figure 3.38: Plots of the critical RPMs of the 0.2 mM $Ru(bpy)_3(PF_6)_2$/5 mM TPA (red plot) and the 0.2 mM $Ru(bpy)_3(PF_6)_2$/5 mM DBAE (blue plot) co-reactant ECL systems in dry ACN with 0.1 M NBu_4PF_6 against the pH levels where the critical RPM occurs

3.3.7 Effect of rotation on co-reactant ECL intensities in an aqueous environment

Since all the previously mentioned studies where the critical RPM phenomena occurs were performed in an organic environment (ACN as the solvent and 0.1 M NBu_4PF_6 acting as the electrolyte in the system), we wanted to observe if the same critical RPM phenomena would occur in co-reactant ECL systems in an aqueous environment (0.1 M PBS at pH 7).

When a solution containing the 0.5 mM $[Ru(bpy)_3]^{2+}$/5 mM TPA co-reactant ECL system in an aqueous environment was examined under rotation, an increase in the peak limiting current was detected with the increase of rotation rate, similar to what was observed in rotated co-reactant ECL systems in organic environments (Figure 3.39). Once again a linear relationship between the currents generated and the rotation rate can be observed in the Koutecky-Levich plot (Figure 3.40). Extrapolation of the Koutecky-Levich plot (Figure 3.40) for this system back towards the y-axis suggests that the system at 1.1 V has sluggish kinetics.

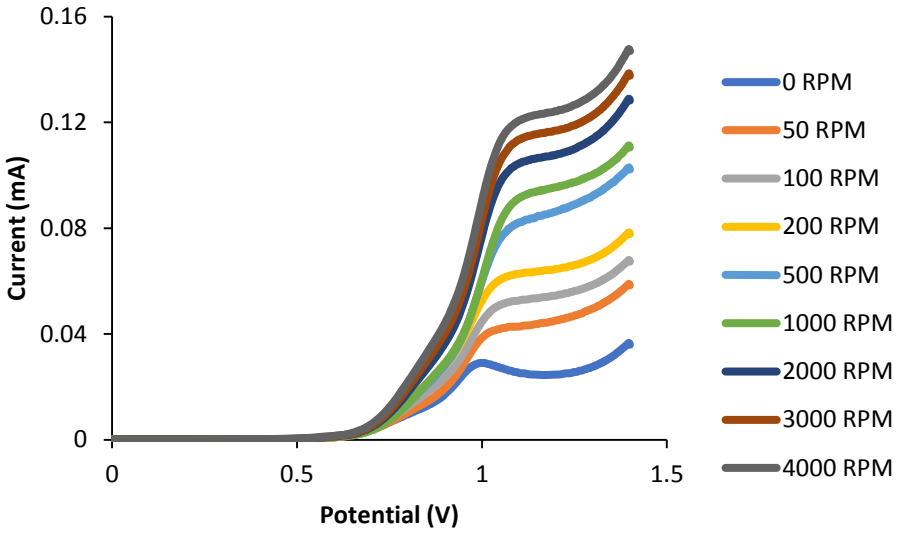

Figure 3.39: Voltammograms generated using the 0.5 mM $[Ru(bpy)_3]^{2+}$/5 mM TPA co-reactant ECL system in 0.1 M phosphate buffer (pH 7) at various rotation rates (0 – 4000 RPM)

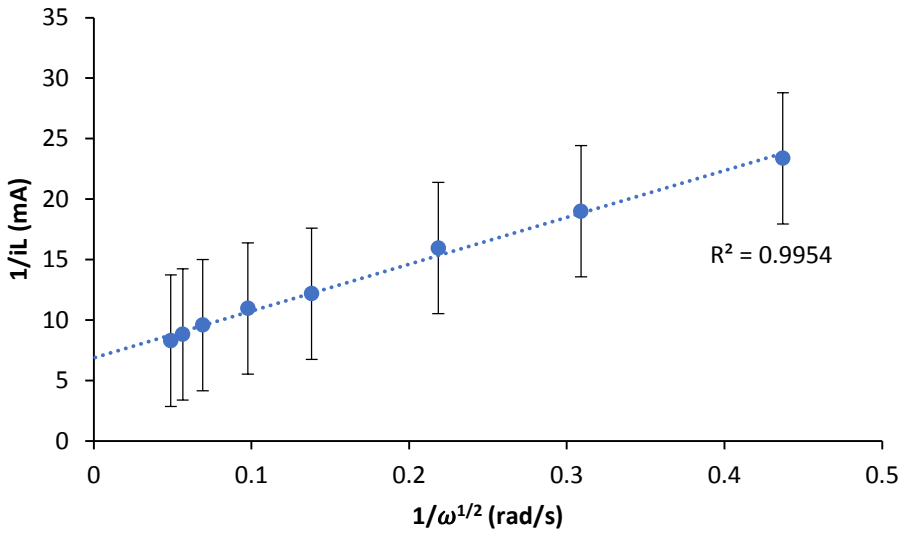

Figure 3.40: Koutecky-Levich plot of the currents generated at 1.1 V from the 0.5 mM $[Ru(bpy)_3]^{2+}$/5 mM TPA co-reactant ECL system in 0.1 M phosphate buffer (pH 7) at various rotation rates (0 – 4000 RPM)

Interestingly however, unlike what is observed in co-reactant ECL systems in organic environments, a critical RPM is not observed in this aqueous system (Figures 3.41 and 3.42). Like the current, as the rotation rate of the electrode increases, so does the ECL intensity.

The same trend where a critical RPM is not observed, while both the limiting current and ECL intensity increase with increase in rotation rate was again observed for the 0.1 mM $[Ru(bpy)_3]^{2+}$/10 mM DBAE (Figures 3.44-3.47) and the 0.1 mM $[Ru(bpy)_3]^{2+}$/10 mM TPA (Figures 3.49-3.52) co-reactant ECL systems in an aqueous environment. The Koutecky-Levich plot of the 0.1 mM $[Ru(bpy)_3]^{2+}$/10 mM TPA co-reactant ECL system (Figure 3.50) suggests the system has kinetic limitations. The non-linear Koutecky-Levich plot of the 0.1 mM $[Ru(bpy)_3]^{2+}$/10 mM DBAE co-reactant ECL system (Figure 3.45) suggests that the system is irreversable. See Figures 3.43, 3.48 and 3.53 for the 3D plots of the ECL intensity generated from the 0.5 mM $[Ru(bpy)_3]^{2+}$/5 mM TPA, 0.1 mM $[Ru(bpy)_3]^{2+}$/10 mM DBAE and the 0.1 mM $[Ru(bpy)_3]^{2+}$/10 mM TPA co-reactant ECL systems respectively under quiescent conditions (0 RPM) and under rotation (1000 RPM).

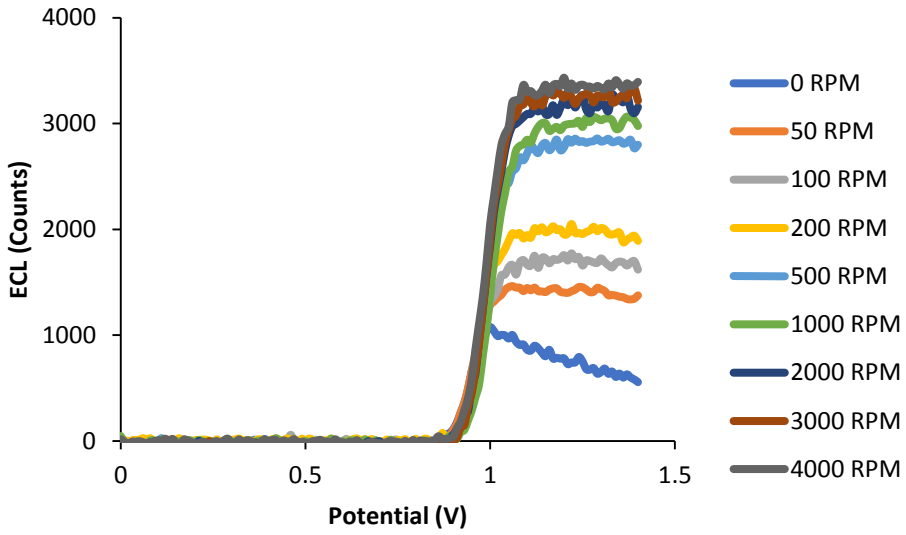

Figure 3.41: Voltammograms of the ECL intensities generated using the 0.5 mM $[Ru(bpy)_3]^{2+}$/5 mM TPA co-reactant ECL system in 0.1 M phosphate buffer (pH 7) at various rotation rates (0 – 4000 RPM)

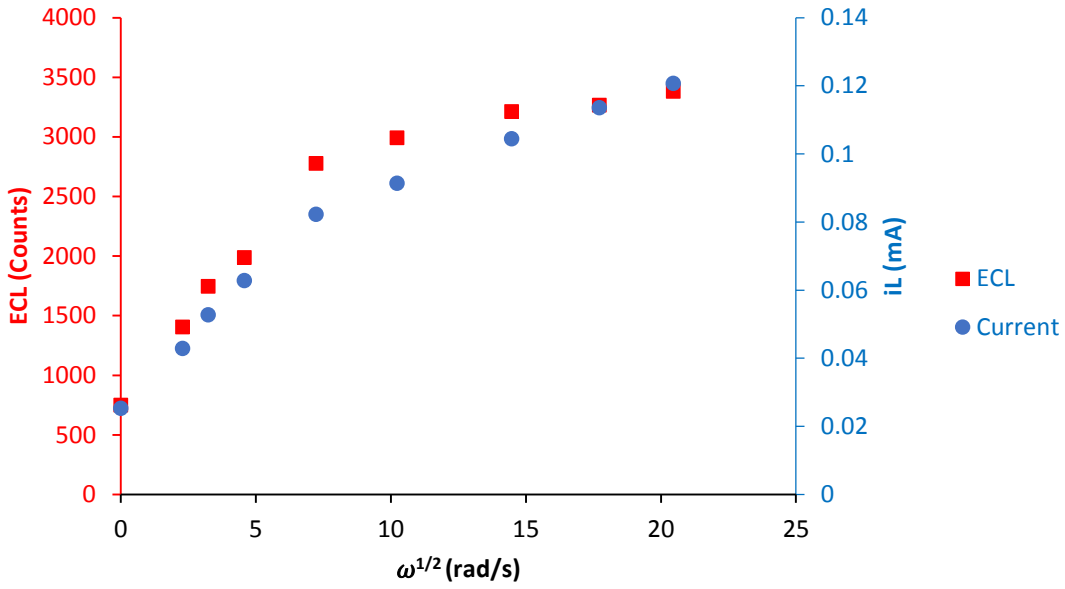

Figure 3.42: Levich plots of the current (blue plot, at 1.1 V) and ECL intensities (red plot, at 1.2 V) generated from the 0.5 mM $[Ru(bpy)_3]^{2+}$/5 mM TPA co-reactant ECL system in 0.1 M phosphate buffer (pH 7) at various rotation rates (0 – 4000 RPM) at 610 nm. The system has no critical RPM since an increase of both the current and ECL intensity is observed under rotation in an aqueous environment

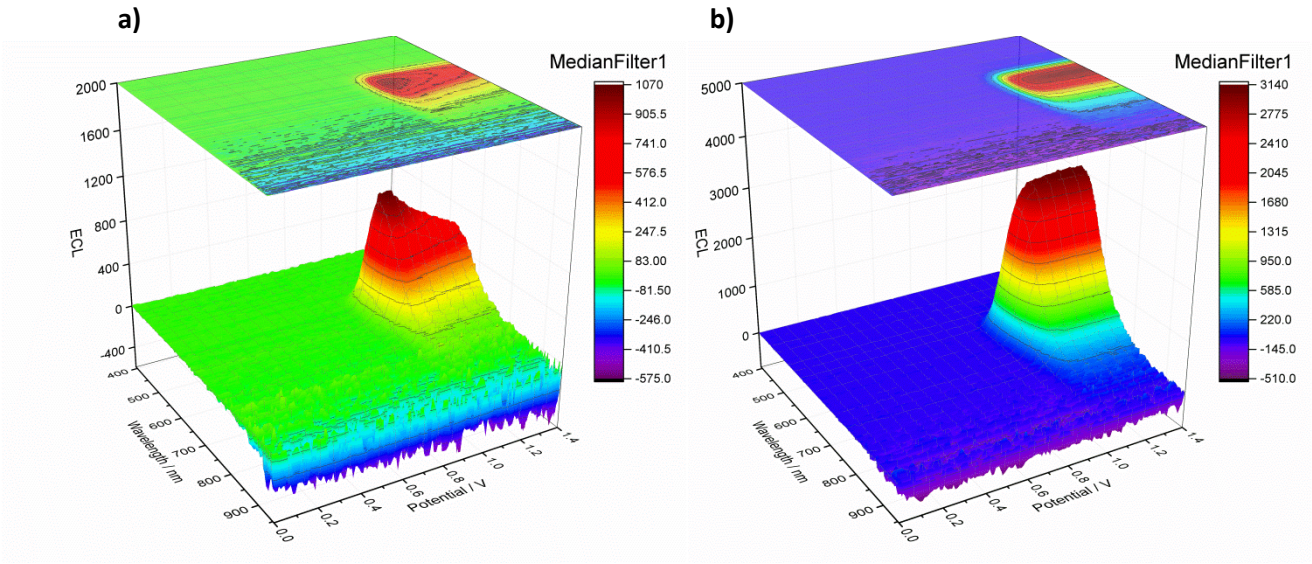

Figure 3.43: 3D plots of the ECL intensities generated from the 0.5 mM $[Ru(bpy)_3]^{2+}$/5 mM TPA co-reactant ECL system in 0.1 M phosphate buffer (pH 7) under rotation where a) shows the intensities generated under quiescent conditions (0 RPM) and b) represent the intensities generated under rotation (1000 RPM)

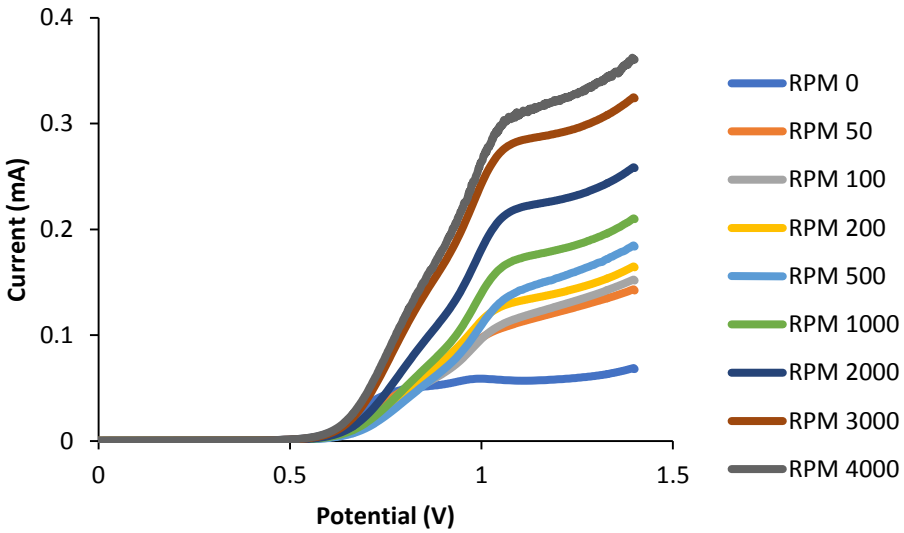

Figure 3.44: Voltammograms generated using the 0.1 mM $[Ru(bpy)_3]^{2+}$/10 mM DBAE co-reactant ECL system in 0.1 M phosphate buffer (pH 7) at various rotation rates (0 – 4000 RPM)

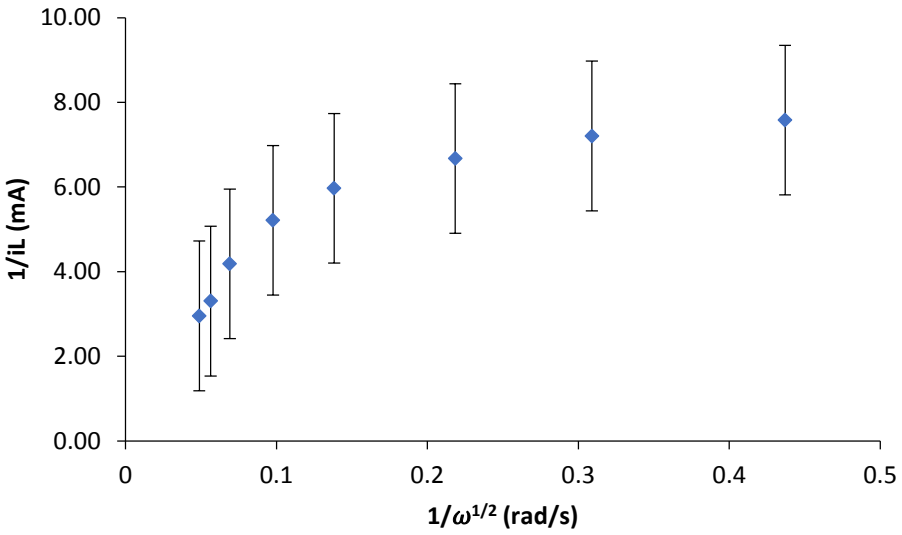

Figure 3.45: Koutecky-Levich plot of the currents generated at 1.3 V from the 0.1 mM $[Ru(bpy)_3]^{2+}$/10 mM DBAE co-reactant ECL system in 0.1 M phosphate buffer (pH 7) at various rotation rates (0 – 4000 RPM)

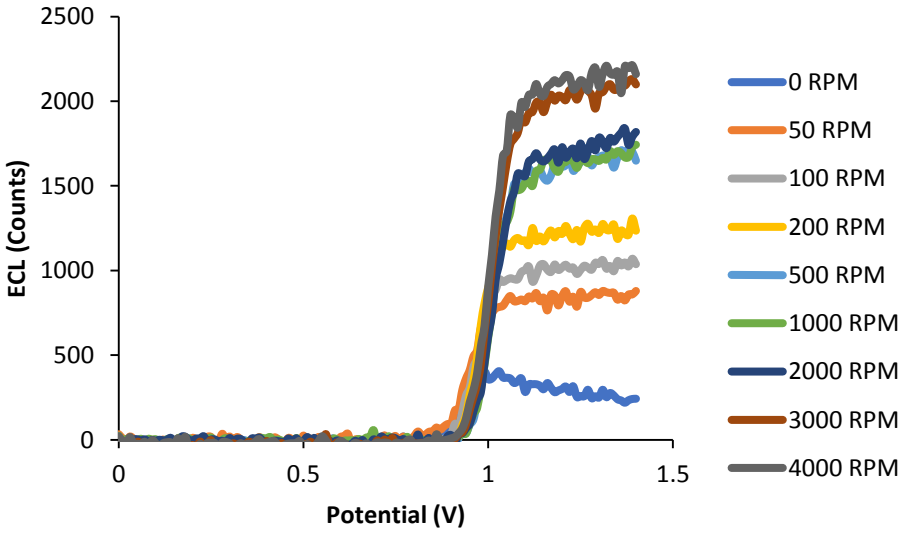

Figure 3.46: Voltammograms of the ECL intensities generated using the 0.1 mM $[Ru(bpy)_3]^{2+}$/10 mM DBAE co-reactant ECL system in 0.1 M phosphate buffer (pH 7) at various rotation rates (0 – 4000 RPM)

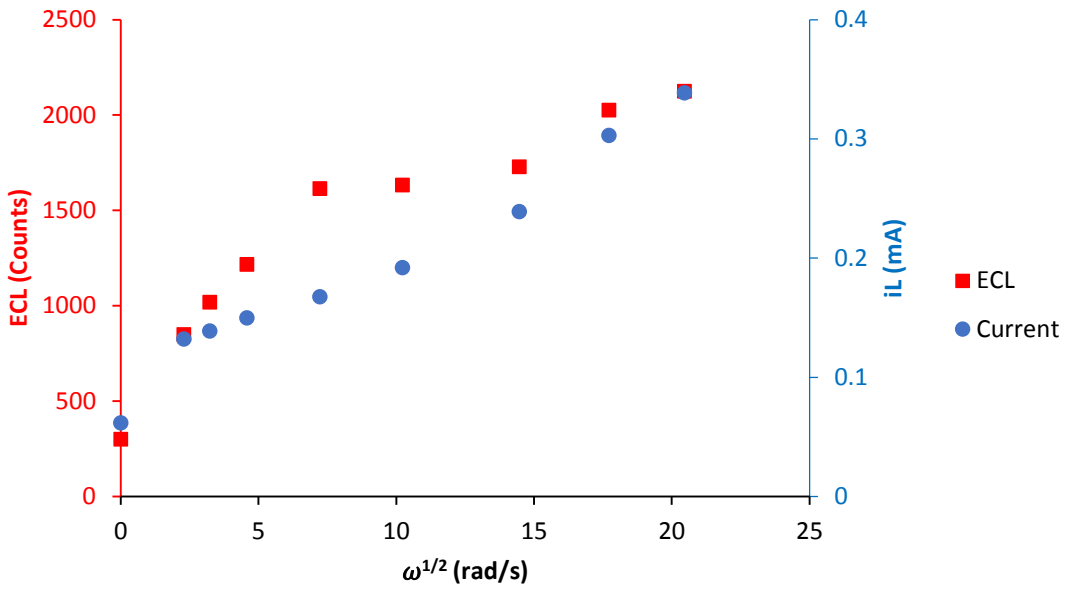

Figure 3.47: Levich plots of the current (blue plot, at 1.3 V) and ECL intensities (red plot, at 1.2 V) generated from the 0.1 mM $[Ru(bpy)_3]^{2+}$/10 mM DBAE co-reactant ECL system in 0.1 M phosphate buffer (pH 7) at various rotation rates (0 – 4000 RPM) at 610 nm. The system has no critical RPM since an increase of both the current and ECL intensity is observed under rotation

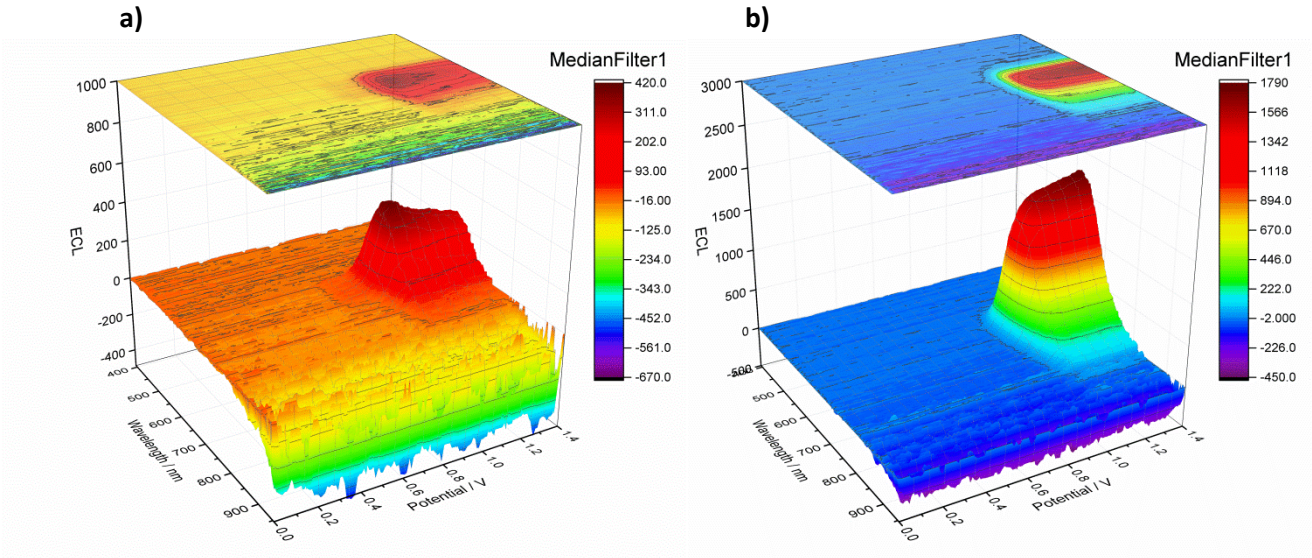

Figure 3.48: 3D plots of the ECL intensities generated from the 0.1 mM $[Ru(bpy)_3]^{2+}$/10 mM DBAE co-reactant ECL system in 0.1 M phosphate buffer under rotation where a) shows the intensities generated under quiescent conditions (0 RPM) and b) represent the intensities generated under rotation (1000 RPM)

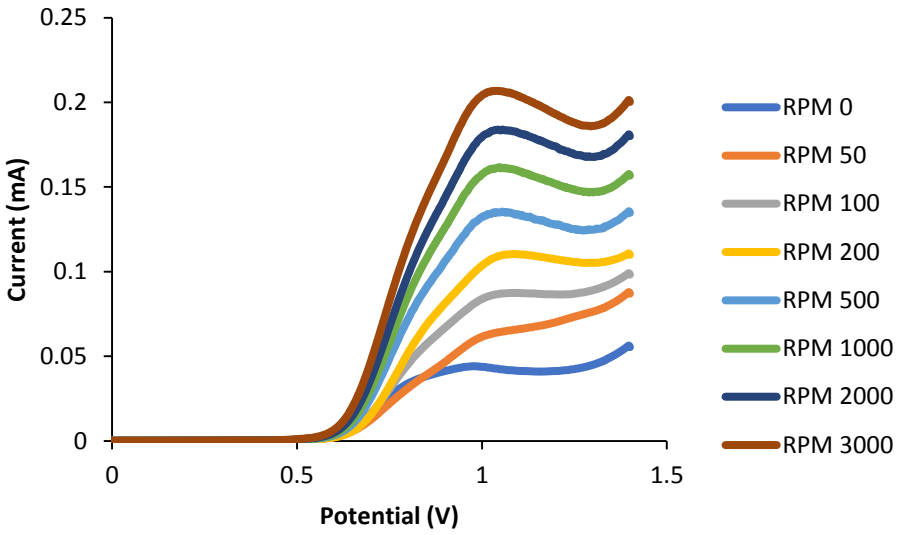

Figure 3.49: Voltammograms generated using the 0.1 mM $[Ru(bpy)_3]^{2+}$/10 mM TPA co-reactant ECL system in 0.1 M phosphate buffer (pH 7) at various rotation rates (0 – 3000 RPM)

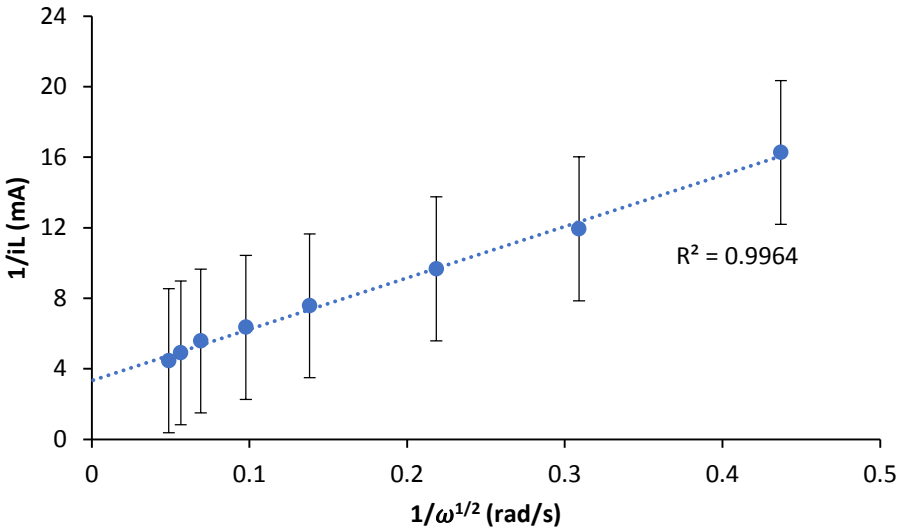

Figure 3.50: Koutecky-Levich plot of the currents generated at 1.0 V from the 0.1 mM $[Ru(bpy)_3]^{2+}$/10 mM TPA co-reactant ECL system in 0.1 M phosphate buffer (pH 7) at various rotation rates (0 – 3000 RPM)

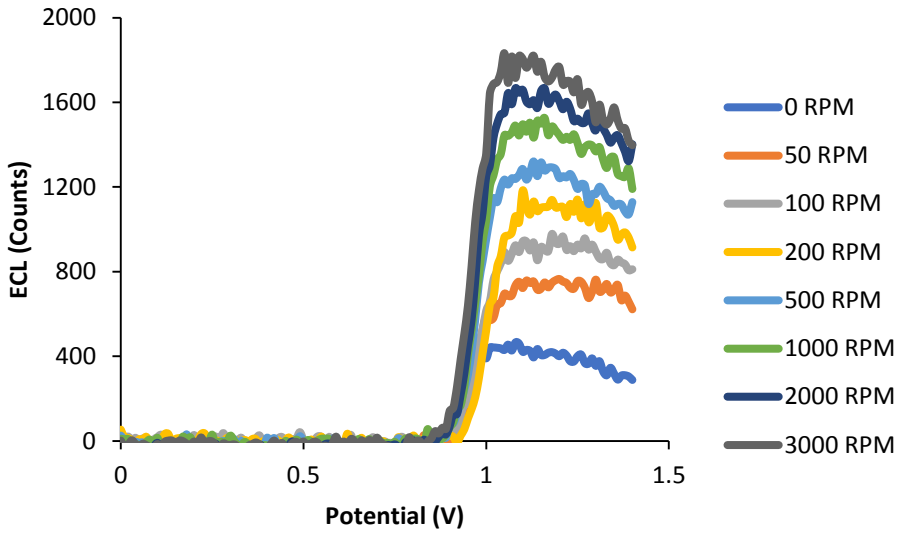

Figure 3.51: Voltammograms of the ECL intensities generated using the 0.1 mM $[Ru(bpy)_3]^{2+}$/10 mM TPA co-reactant ECL system in 0.1 M phosphate buffer (pH 7) at various rotation rates (0 – 3000 RPM)

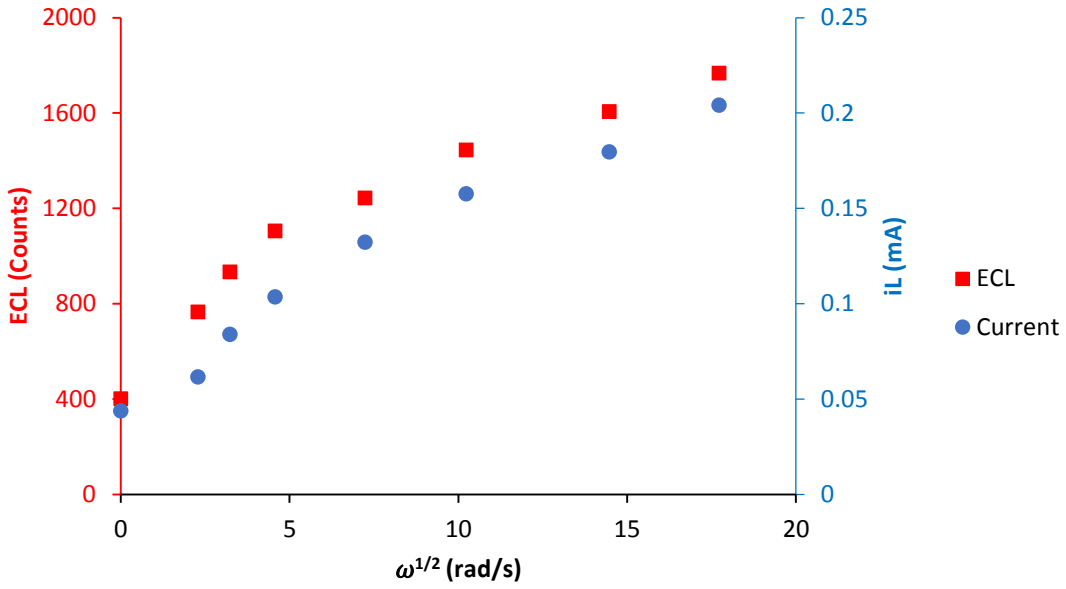

Figure 3.52: Levich plots of the current (blue plot, at 1.0 V) and ECL intensities (red plot, at 1.2 V) generated from the 0.1 mM $[Ru(bpy)_3]^{2+}$/10 mM TPA co-reactant ECL system in 0.1 M phosphate buffer (pH 7) at various rotation rates (0 – 3000 RPM) at 610 nm. The system has no critical RPM since an increase of both the current and ECL intensity is observed under rotation

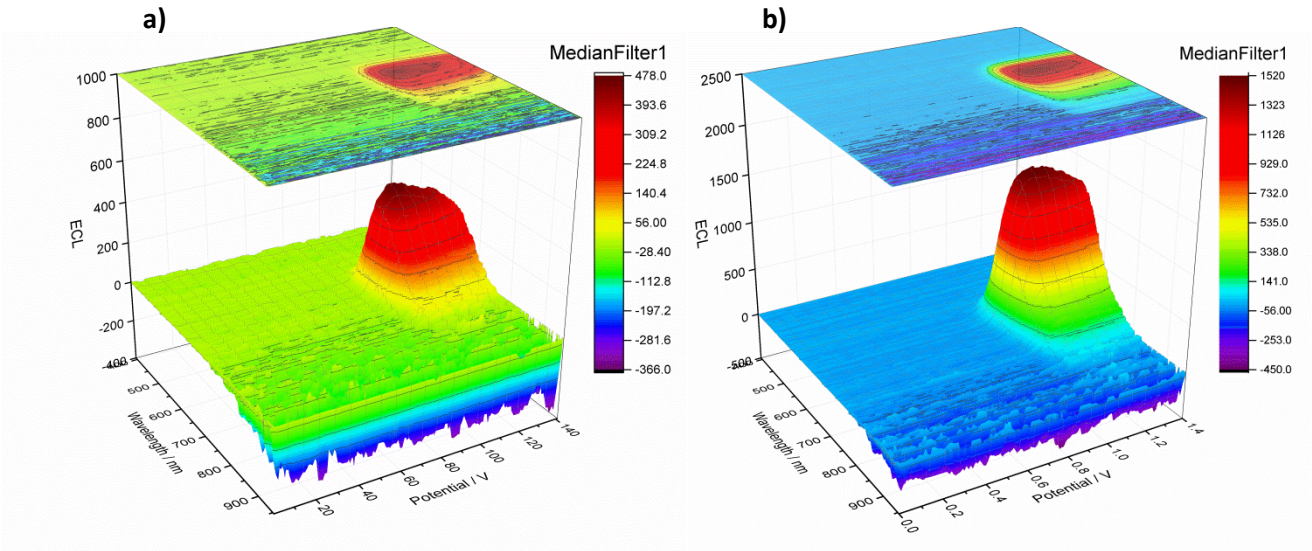

Figure 3.53: 3D plots of the ECL intensities generated from the 0.1 mM $[Ru(bpy)_3]^{2+}$/10 mM TPA co-reactant ECL system in 0.1 M phosphate buffer (pH 7) under rotation where a) shows the intensities generated under quiescent conditions (0 RPM) and b) represent the intensities generated under rotation (1000 RPM)

So why is the critical RPM phenomena observed in co-reactant ECL systems in organic environments while not occurring in co-reactant ECL systems in aqueous environments? The kinetics involved with the deprotonation of the co-reactant in an aqueous environment could differ significantly from the kinetics involved with the deprotonation step of the co-reactant in an organic environment. Further investigation of this phenomenon in the future will hopefully clarify this issue further.

3.4 Conclusion

We adapted a classic RDE apparatus for ECL measurements of various co-reactant ECL systems under conditions of electrode rotation. The results presented show that each co-reactant ECL system used in this study, in organic media (ACN with 0.1 M NBu_4PF_6 acting as supporting electrolyte) exhibits a "critical RPM" where a decrease of observed ECL intensities occurs while the limiting current continues to increase at rotation rates past the critical RPM. This occurs at the critical RPM when the residence time of the radical cation is less than the time required to react (deprotonate). The faster the rotation rate of the working electrode, the less time the radical cation spends near the electrode surface and as a direct result of this, less light can be produced from the luminophore. This may be an interesting new way to probe the kinetics of key steps in ECL mechanisms.

3.5 References

1 D. M. Hercules, *Science*, 1964, **145**, 808–809.

2 K. S. V Santhanam and A. J. Bard, *J. Am. Chem. Soc.*, 1965, **87**, 139–140.

3 R. T. Dufford, D. Nightingale and L. W. Gaddum, *J. Am. Chem. Soc.*, 1927, **49**, 1858–1864.

4 N. E. Tokel and A. J. Bard, *J. Am. Chem. Soc.*, 1972, **94**, 2862–2863.

5 I. Rubinstein and A. J. Bard, *J. Am. Chem. Soc.*, 1981, **103**, 512–516.

6 J. K. Leland and M. J. Powell, *J. Electrochem. Soc.*, 1990, **137**, 3127.

7 W. Miao, *Chem. Rev.*, 2008, **108**, 2506–2553.

8 L. Hu and G. Xu, *Chem. Soc. Rev.*, 2010, **39**, 3275–3304.

9 B. A. Gorman, P. S. Francis and N. W. Barnett, *Analyst*, 2006, **131**, 616–639.

10 K. E. Haapakka and J. J. Kankare, *Anal. Chim. Acta*, 1982, **138**, 253–262.

11 K. E. Haapakka, *Anal. Chim. Acta*, 1982, **139**, 229–236.

12 K. E. Haapakka and J. J. Kankare, *Anal. Chim. Acta*, 1982, **138**, 263–275.

13 V. J. Puglisi and A. J. Bard, *J. Electrochem. Soc.*, 1972, **119**, 833.

14 S. Karp, *J. Phys. Chem.*, 1968, **72**, 1082–1082.

15 S. Vesztergom, M. Ujvári and G. G. Láng, *Electrochem. commun.*, 2012, **19**, 1–4.

16 S. Vesztergom, M. Ujvári and G. G. Láng, *Electrochim. Acta*, 2013, **110**, 49–55.

17 S. Tsuneyasu, T. Ichikawa, K. Nakamura and N. Kobayashi, *ChemElectroChem*, 2017, **4**, 1731–1735.

18 J. T. Maloy, K. B. Prater and A. J. Bard, *J. Phys. Chem.*, 1968, **72**, 4348–4350.

19 L. S. Marcoux, R. N. Adams and S. W. Feldberg, *J. Phys. Chem.*, 1969, **73**, 2611–2614.

20 J. T. Maloy, K. B. Prater and A. J. Bard, *J. Am. Chem. Soc.*, 1971, **93**, 5959–5968.

21 J. T. Maloy and A. J. Bard, *J. Am. Chem. Soc.*, 1971, **93**, 5968–5981.

22 N. E. Tokel-Takvoryan, R. E. Hemingway and A. J. Bard, *J. Am. Chem. Soc.*, 1973, **95**, 6582–6589.

23 K. Boto and A. J. Bard, *J. Electroanal. Chem.*, 1975, **65**, 945–962.

24 J. Ludvik, F. Pragst and J. Volke, *J. Electroanal. Chem.*, 1984, **180**, 141–156.

25 R. J. Fealy and J. I. Goldsmith, *J. Phys. Chem. C*, 2012, **116**, 13133–13142.

26 J. Ludvik and J. Volke, *Electrochim. Acta*, 1990, **35**, 1983–1986.

27 J. Ludvík, *J. Solid State Electrochem.*, 2011, **15**, 2065–2081.

28 D. Juknelevicius, L. Mikoliunaite, A. Ramanaviciene and A. Ramanavicius, *Chem. Pap.*, 2017, **71**, 905–912.

29 M. S. Lowry, J. I. Goldsmith, J. D. Slinker, R. a Pascal, G. G. Malliaras, S. Bernhard and R. Rohl, *J. Mater.*, 2005, **17**, 5712–5719.

30 E. Kerr, E. H. Doeven, G. J. Barbante, C. F. Hogan, D. J. Bower, P. S. Donnelly, T. U. Connell and P. S. Francis, *Chem. Sci.*, 2015, **6**, 472–479.

Chapter 4: Rotating Ring-Disk Annihilation ECL

4.1 Introduction

ECL can be produced through two different mechanistic pathways: the annihilation and co-reactant pathways. In the annihilation pathway (reactions [4.1]-[4.4]), both the oxidised and reduced forms of the electroluminophore are generated at the electrode surface when a potential step or sweep is applied at the electrode. A ground and excited state of the luminophore are then formed from the interaction between the oxidised and reduced forms of the luminophore. This excited state then emits a photon in order for it to relax back to its ground state.

$$A \rightarrow A^{\bullet+} + e^{-} \quad \textbf{[4.1]}$$

$$A \rightarrow A^{\bullet-} - e^{-} \quad \textbf{[4.2]}$$

$$A^{\bullet+} + A^{\bullet-} \rightarrow A + A^{*} \quad \textbf{[4.3]}$$

$$A^{*} \rightarrow A + h\nu \quad \textbf{[4.4]}$$

Annihilation ECL experiments are typically performed using a single working electrode where potentials necessary for the generation of the reduced and oxidised species of a luminophore are applied sequentially. These electroactive species then react in the diffusion layer near the electrode surface to produce light. The annihilation pathway is an attractive ECL methodology due to its simplicity. However, since a single electrode is typically used; only a fraction of the electroactive species generated from the first half cycle is present in the next half cycle, making efficiency calculations difficult. ECL intensities are also affected by the diffusion of the reacting species near the electrode surface.[1–3]

The previous chapter described a method that incorporated the use of a rotating disk electrode (RDE) to improve the rate of mass transport in co-reactant ECL systems. To

maximise efficiency in annihilation ECL systems, a generator-collector electrode system in the form of a rotating ring disk electrode (RRDE) can be used, where the disk electrode generates either the oxidised or reduced form of the luminophore while the ring electrode simultaneously generates the other. Convective flow of bulk solution towards the centre of the disk electrode is induced by the rotation of the RRDE. Bulk solution containing the electroactive species formed at the disk electrode is then flung radially from the centre of the disk to the ring electrode via centrifugal forces where it can react with the electroactive species formed at the ring to generate steady-state annihilation ECL.[4,5]

While RRDEs have been extensively used to study the mechanisms of electrochemical reactions,[6–21] there have been only a handful of studies describing the study of annihilation ECL using an RRDE,[4,5,22–25] and none describing the study of mixed ECL systems with an RRDE.

The aim of this study was to build on the investigation in the previous chapter. Here, instead of investigating the effect electrode rotation has on co-reactant ECL intensities, we investigate the effect rotation has on the annihilation ECL intensities generated from several different annihilation ECL systems, and to determine what mechanistic and other insights night be gained from such a study.

4.2 Experimental

4.2.1 Chemicals and materials

Unless otherwise stated, deionised water (Sartorius Stedim biotech arium® pro VF Ultrapure Water System, 18.2 MΩ cm, Germany) and analytical grade reagents were used. Dry acetonitrile was distilled from CaH_2. Tris(2,2′-bipyridine)ruthenium(II) hexafluorophosphate ($Ru(bpy)_3(PF_6)_2$, 97%), [4,4′-*bis*(1,1-dimethylethyl)-2,2′-bipyridine-*N*1,*N*1′]*bis*[3,5-difluoro-2-[5-(trifluoromethyl)-2-pyridinyl-*N*]phenyl-C]Iridium(III) hexafluorophosphate ($(Ir[dF(CF_3)ppy]_2(dtbpy))PF_6$), tris[2-phenylpyridinato-C^2,N]iridium(III) ($Ir(ppy)_3$) and tetrabutylammonium hexafluorophosphate (NBu_4PF_6) were all purchased from Sigma-Aldrich (NSW, Australia). Structures for the luminophores used in this study are shown in Figure 4.1.

4.2.2 Photophysics

Characterisation of $Ru(bpy)_3(PF_6)_2$, $(Ir[dF(CF_3)ppy]_2(dtbpy))PF_6$ and $Ir(ppy)_3$ was performed by collecting absorption spectra using a Cary Series UV−visible spectrophotometer (Agilent) with a 1 cm path length quartz cuvette, 1 nm spectral bandwidth, 0.1 s signal averaging time, 0.25 nm data interval and a 150 nm/min scan rate. In this work, 0.02 mM samples of $Ru(bpy)_3(PF_6)_2$, $(Ir[dF(CF_3)ppy]_2(dtbpy))PF_6$ and $Ir(ppy)_3$ were prepared in distilled acetonitrile. A blank solvent was used to baseline (T100%) correct the spectrometer, while blocking the detector from the light-beam zero (T0%) corrected the spectrometer.

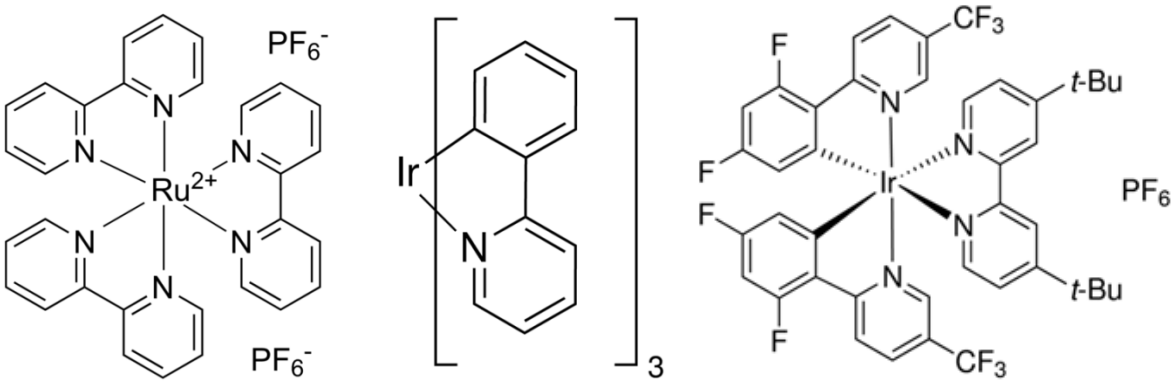

Figure 4.1 Luminophores used in this study from left to right: $Ru(bpy)_3(PF_6)_2$, $Ir(ppy)_3$, $(Ir[dF(CF_3)ppy]_2(dtbpy))PF_6$

Steady-state emission spectra were collected on a Nanolog (HORIBA Jobin Yvon IBH) spectrometer using a 1 cm four-sided quartz cuvette, 2 nm band pass and an increment of 1 nm. An integration time of 0.2 s was used for 0.02 mM solutions. To excite the complexes, a 450 W xenon-arc lamp was used, using a 1200 g/mm grating blazed at 330 nm excitation monochromator and a 1200 g/mm grating blazed at a 500 nm emission monochromator. A liquid nitrogen-cooled Symphony II (model SII-1LS-256-06) charged-coupled device was used to detect the light emission from these complexes. Long pass filters were used on the emission side to block the excitation scatter peaks and spectra were corrected for wavelength dependent variation in source intensity, gratings and detector response.

Lifetimes of 20 μM samples of the complexes in Figure 4.1 were measured using the time correlated single photon counting option on the spectrometer and correlated by a time-to-amplitude converter in forward TAC mode. A NanoLED laser (344 nm) was pulsed at 100 kHz. A FluoroHub counter was used to collect the signal. DAS6 software (HORIBA Jobin Yvon IBH) was used to analyse the data obtained. The luminescence decay curves were

fitted to either single or double exponential equations. Fitting of the curves was assessed by minimizing χ^2 (0.95-1.2) and visual inspection of the weighted residuals.

4.2.3 Electrochemistry and Electrochemiluminescence

Electrochemical experiments were performed using a PGSTAT12 AUTOLAB electrochemical potentiostat coupled with a BIPOT module (MEP Instruments, North Ryde, NSW, Australia) with Nova 2.1 software. Levich and Koutecky-Levich studies were performed with the use of a RRDE-3A Rotating Ring Disk Electrode Apparatus (ALS Co., Ltd, Japan). The electrochemical cell consisted of a glass cell with a quartz window base and Teflon cover with a spill tray. A conventional three-electrode configuration consisting of a 1 cm^2 silver-wire quasi reference electrode, a 1 cm^2 gold wire auxiliary electrode and a glassy-carbon rotating ring-disk working electrode (see Figure 4.2 for dimensions) consisting of a disk electrode (area = 0.13 cm^2) and ring electrode (area = 0.19 cm^2) shrouded in Teflon (ALS Co., Ltd, Japan) was used. The RRDE was polished on a felt pad containing 0.3 μm alumina slurry and rinsed with water and acetone. The RRDE was then dried under a steady stream of nitrogen (N_2).

Organic solutions of $Ru(bpy)_3(PF_6)_2$, $(Ir[dF(CF_3)ppy]_2(dtbpy))PF_6$ and $Ir(ppy)_3$ of varying concentrations were prepared in freshly distilled acetonitrile and 0.1 M NBu_4PF_6 added as supporting electrolyte. Oxygen was removed from the solutions by bubbling vigorously with N_2 for 10 min, followed by lightly blanketing the solution with N_2 during the experiments. Potentials were referenced against a Ag/Ag^+ wire quasi reference electrode. The surface of the rotating disk electrode was positioned at a reproducible distance (~2 mm) from the bottom of the cell for detection.

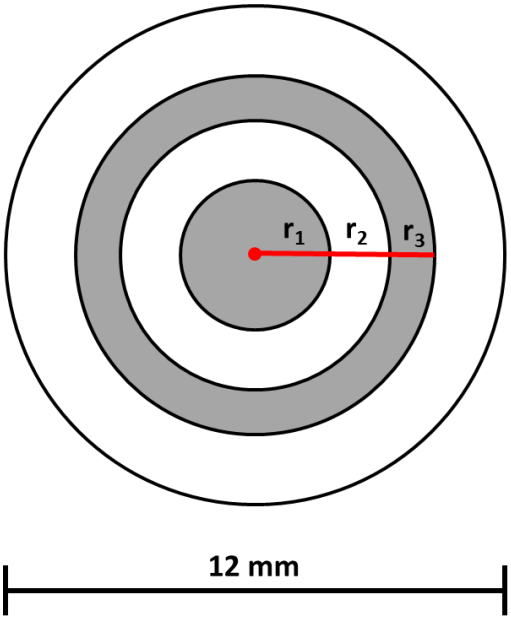

Figure 4.2: Glassy-carbon RRDE used in this study where: r_1 = 2 mm; r_2 = 2.5 mm; r_3 = 3.5 mm. Figure not to scale

Levich studies were performed by either using linear scan voltammetry (sweeping between 0 V and a variety of potentials) under various rotation rates at a scan rate of 0.01 V/s, or by holding the ring and disk electrodes at potentials where either reduction or oxidation occurs for 10 s, while the ECL signal was simultaneously recorded. ECL signals were detected using a QE65 Pro Spectrometer (Ocean Optics, model QEPB0931) with OceanView 1.6.7 software with an integration time of 1 s, coupled with a custom made fibre optic QP1000-025-SR-BX (Ocean Optics, China) inside a custom-built light-tight Faraday cage. The fibre optic was attached to a right-angled reflector coupled with a UV/VIS collimating lens (Ocean Optics, China) located directly underneath the electrochemical cell within a custom made cell holder (see supplementary information Figures S1 and S2).

4.3 Results and Discussion

4.3.1 Annihilation ECL from hold-sweep experiments under rotation

In the previous chapter, we showed that it is possible to elicit enhanced co-reactant ECL intensity under rotation using an RDE. However, to elicit annihilation ECL from a luminophore such as $Ru(bpy)_3(PF_6)_2$, both the oxidised and reduced forms of the luminophore are required. Using an RRDE, we can perform electrochemical experiments where either the oxidised or reduced form of the luminophore is generated at the ring while the other is formed at the disk. While the RRDE is rotating, the oxidised and reduced forms of the luminophore react with each other according to reaction [4.7] below; to produce a ring shaped ECL emission localised near the ring electrode.

The absorbance and photoluminescence spectra of the luminophores used in the study are shown in Figures 4.3 and 4.4 respectively. Figure 4.3 shows that the ruthenium complex has a significantly higher absorbance in the visible region of the spectrum, while Figure 4.4 illustrates the range of emission colours of the complexes used in the study. The electrochemical and spectroscopic properties of each complex is summarised in either Table 3.1 in chapter 3 or Table 4.1.

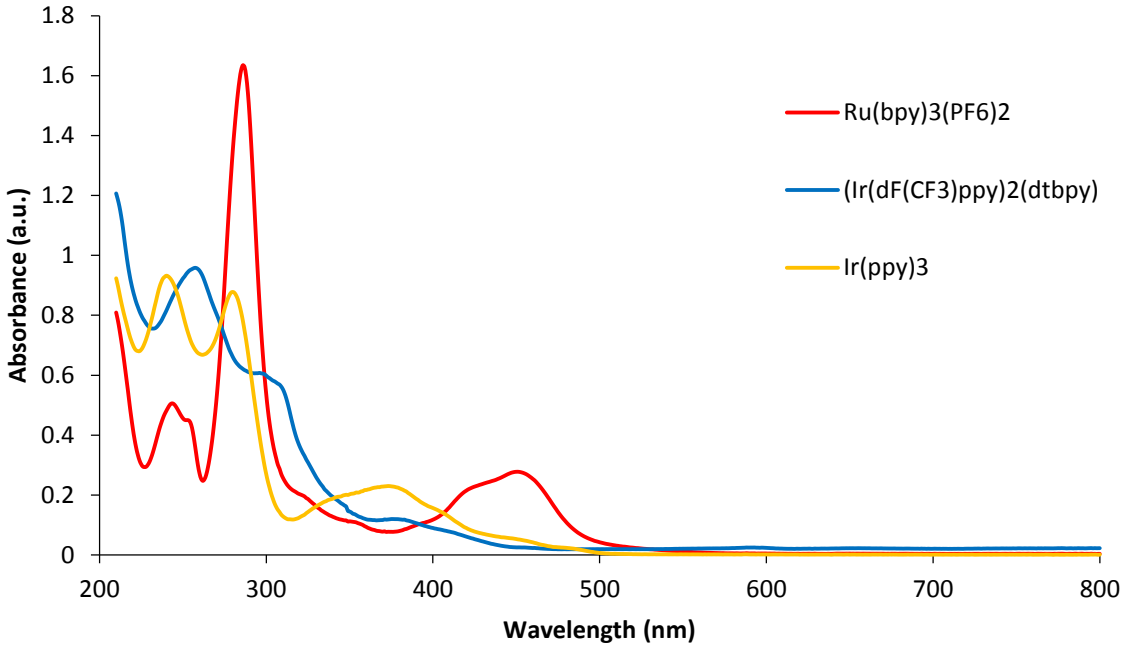

Figure 4.3: Absorbance spectra of 2 µM samples of $Ru(bpy)_3(PF_6)_2$, $Ir(ppy)_3$ and $(Ir[dF(CF_3)ppy]_2(dtbpy))PF_6$

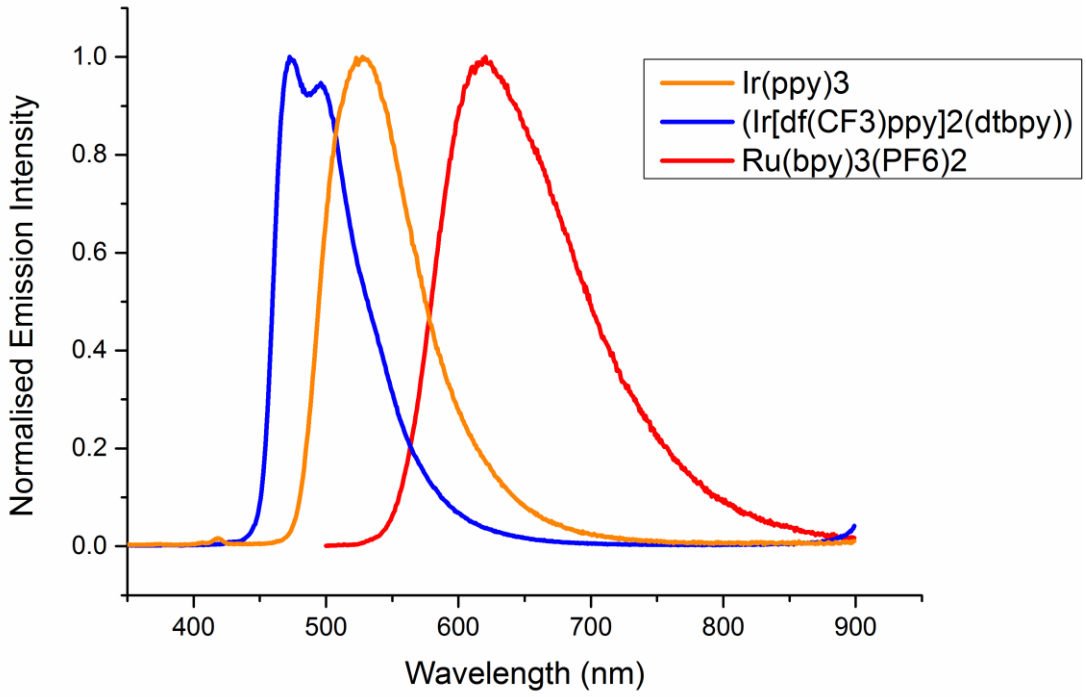

Figure 4.4: Photoluminescence spectra of 2 µM samples of $Ru(bpy)_3(PF_6)_2$, $Ir(ppy)_3$ and $(Ir[dF(CF_3)ppy]_2(dtbpy))PF_6$

Table 4.1: The electrochemical and spectroscopic properties of $Ir(ppy)_3$. [a] This is a shoulder. Electrochemical data from Figure 4.26. Refer to Table 3.1 in chapter 3 for the electrochemical and spectroscopic properties of $Ru(bpy)_3(PF_6)_2$ and $(Ir[dF(CF_3)ppy]_2(dtbpy))PF_6$

	Electrochemistry		Absorbance	Photoluminescence
	E°red (V)	E°ox (V)	λabs (nm)	λmax (nm)
$Ir(ppy)_3$	-2.34	0.73	240, 280, 348[a], 373	527

To elicit annihilation ECL from a solution containing 0.2 mM $Ru(bpy)_3(PF_6)_2$, the ring electrode was held at a potential approximately 10 mV more negative than the first reduction of the ruthenium complex, (as illustrated in Figure 4.5), in order to generate the reduced state of the luminophore according to reaction [4.5], while the ruthenium (II) oxidation (reaction [4.6]) potential region was scanned at the disk electrode simultaneously (Figure 4.5). Using this experimental setup we were able to not only generate annihilation ECL from $Ru(bpy)_3(PF_6)_2$ but also obtain rotating disk voltammograms of the currents and ECL intensities produced at various rotation rates and perform an RPM study (Figures 4.6 - 4.9).

$$Ru^{2+} + e^- \rightarrow Ru^+ \qquad \textbf{[4.5]}$$

$$Ru^{2+} \rightarrow Ru^{3+} + e^- \qquad \textbf{[4.6]}$$

$$Ru^+ + Ru^{3+} \xrightarrow{k_1} Ru^{2+} + Ru^{2+*} \qquad \textbf{[4.7]}$$

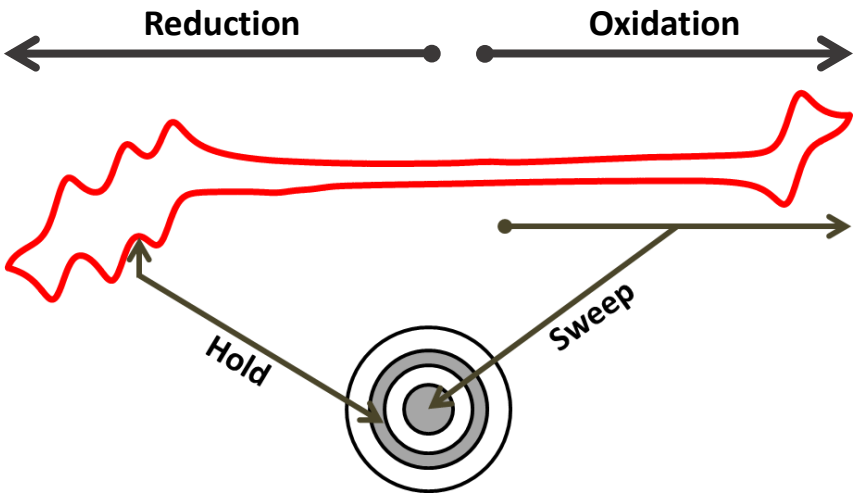

Figure 4.5: Representation of a hold-sweep annihilation ECL experiment of 0.2 mM $Ru(bpy)_3(PF_6)_2$ in dry ACN with 0.1 M NBu_4PF_6 using a RRDE where the first ruthenium reduction was held at -1.38 V at the ring electrode, while the potential was scanned from 0 V to 1.6 V at the disk electrode

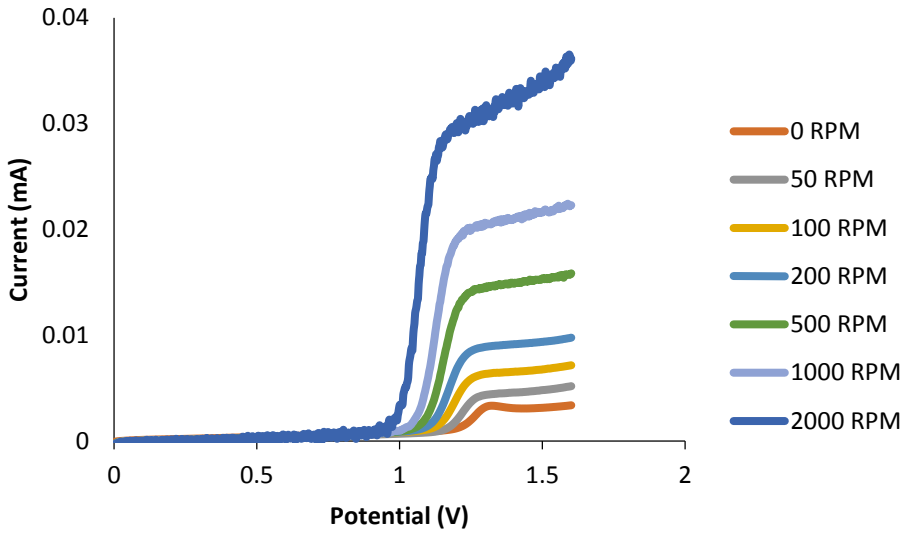

Figure 4.6: Voltammograms of the disk currents generated using 0.2 mM $Ru(bpy)_3(PF_6)_2$ in dry ACN with 0.1 M NBu_4PF_6 at various rotation rates (0 – 2000 RPM) where the first ruthenium reduction was held at -1.38 V at the ring electrode, while the potential was scanned from 0 V to 1.6 V at the disk electrode

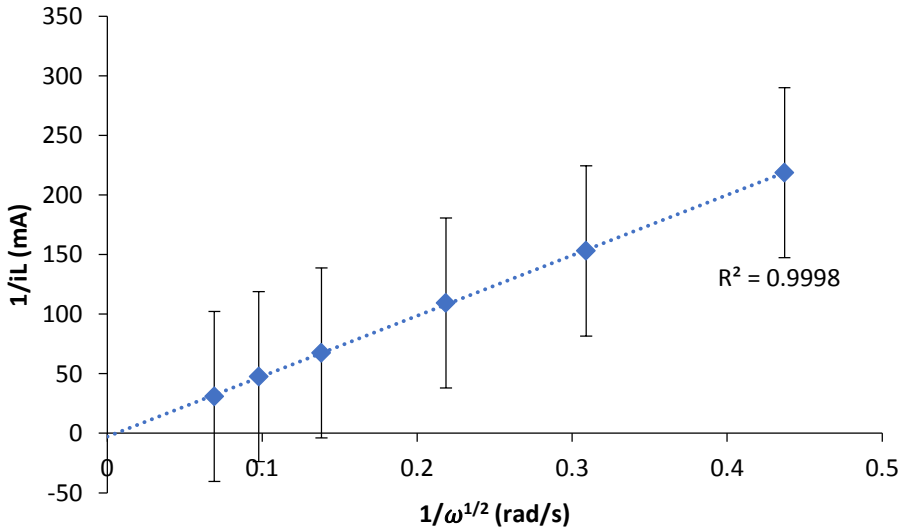

Figure 4.7: Koutecky-Levich plot of the currents generated at 1.4 V from 0.2 mM $Ru(bpy)_3(PF_6)_2$ in dry ACN with 0.1 M NBu_4PF_6 at various RPMs (0 – 2000 RPM) where the first ruthenium reduction was held at -1.38 V at the ring electrode, while the potential was scanned from 0 V to 1.6 V at the disk electrode

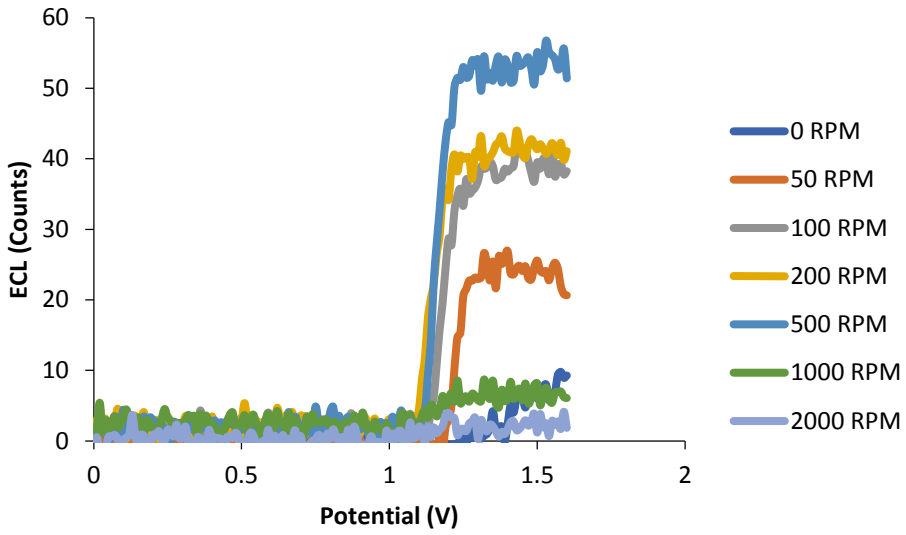

Figure 4.8: Voltammograms of the annhilation ECL intensities generated using 0.2 mM $Ru(bpy)_3(PF_6)_2$ in dry ACN with 0.1 M NBu_4PF_6 at various rotation rates (0 – 2000 RPM) where the first ruthenium reduction was held at -1.38 V at the ring electrode, while the potential was scanned from 0 V to 1.6 V at the disk electrode

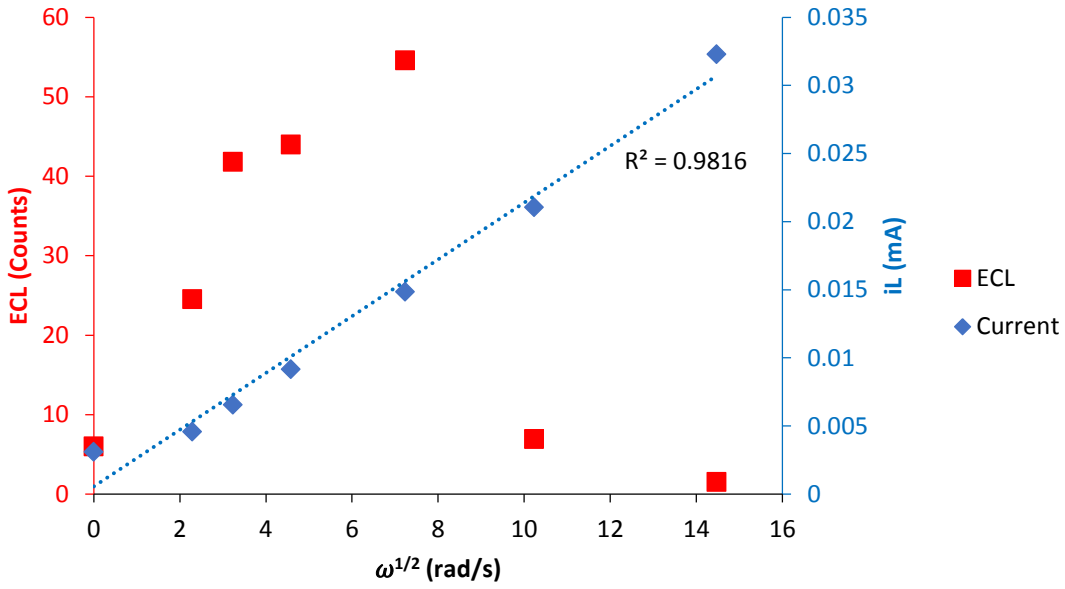

Figure 4.9: Levich plots of the current (blue plot, at 1.4 V) and ECL intensities (red plot, at 1.4 V) generated from 0.2 mM $Ru(bpy)_3(PF_6)_2$ in dry ACN with 0.1 M NBu_4PF_6 at various rotation rates (0 – 2000 RPM) at 610 nm highlighting the decrease of ECL intensities past 500 RPM (52.36 rad/s) when the first ruthenium reduction was held at -1.38 V at the ring electrode, while the potential was scanned from 0 V to 1.6 V at the disk electrode

Similar to what was observed when the co-reactant ECL systems was investigated under electrode rotation, Figures 4.6 and 4.7 show the continual increase of the observed limiting current of the system with the increase of the rotation rate of the electrode when the first ruthenium reduction is held at the ring while the ruthenium oxidation is swept at the disk. The linear relationship between the rotation rate and observed disk current, shown in Figure 4.7, was observed until 2000 RPM, after which non-steady state current was obtained, most likely caused by turbulent flow. However, we once again witness the interesting critical RPM phenomenon, where the observed ECL intensity increases with increased rotation rate until the critical RPM of the system (in this case approximately 500 RPM or 52.36 rad/s) was reached. A decrease of ECL intensity was then observed at rotation rates past the critical RPM while the continual increase of the limiting current past the critical RPM occurs (blue data in Figure 4.9).

$$Ru^{+} + e^{-} \rightarrow Ru \qquad \textbf{[4.8]}$$

$$Ru + Ru^{3+} \xrightarrow{k_2} Ru^{+} + Ru^{2+*} \qquad \textbf{[4.9]}$$

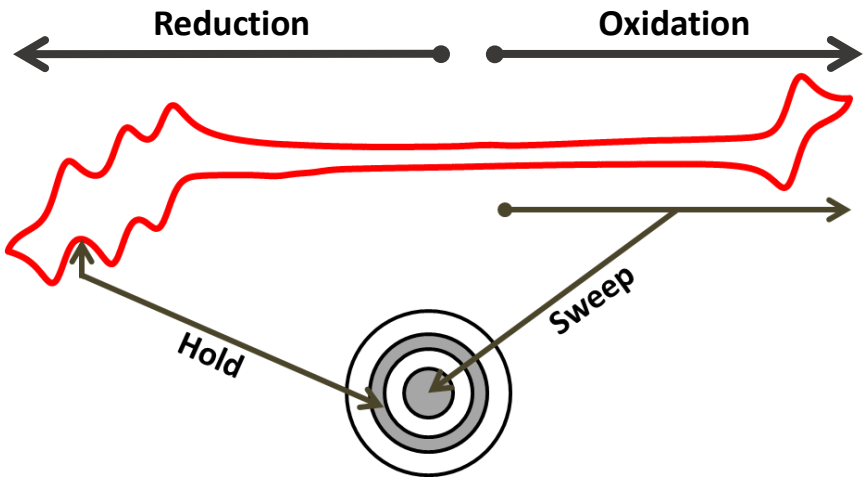

Figure 4.10: Representation of a hold-sweep annihilation ECL experiment of 0.2 mM $Ru(bpy)_3(PF_6)_2$ in dry ACN with 0.1 M NBu_4PF_6 using a RRDE where the second ruthenium reduction was held at -1.58 V at the ring electrode, while the potential was scanned from 0 V to 1.6 V at the disk

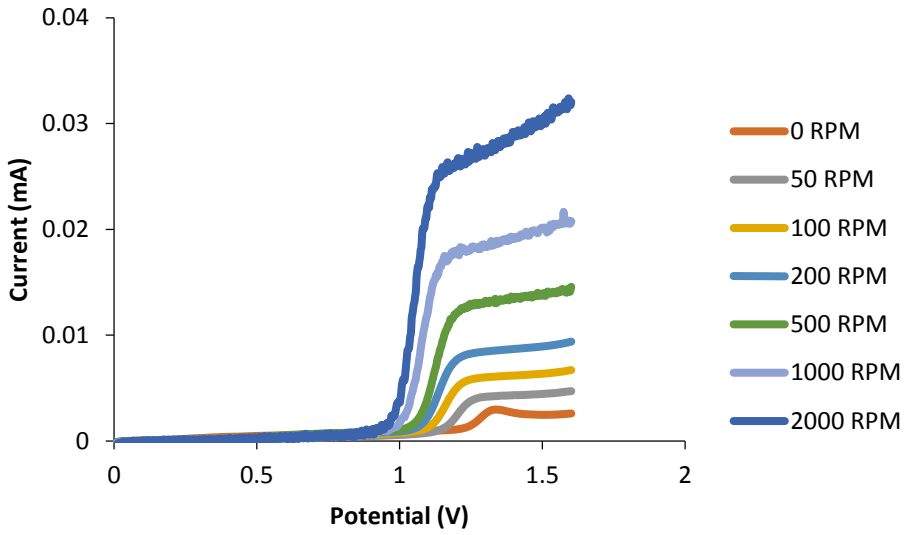

Figure 4.11: Voltammograms of the disk currents generated using 0.2 mM $Ru(bpy)_3(PF_6)_2$ in dry ACN with 0.1 M NBu_4PF_6 at various rotation rates (0 – 2000 RPM) where the second ruthenium reduction was held at -1.58 V at the ring electrode, while the potential was scanned from 0 V to 1.6 V at the disk electrode

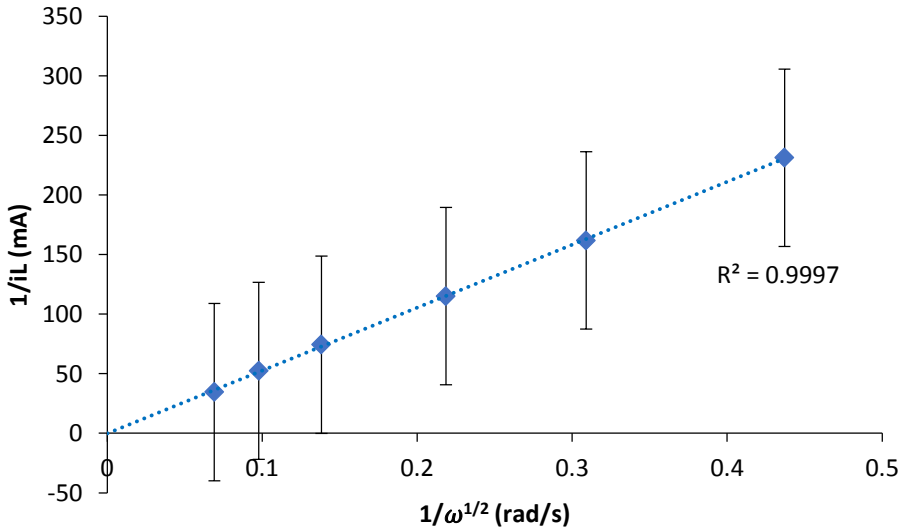

Figure 4.12: Koutecky-Levich plot of the currents generated at 1.4 V from 0.2 mM $Ru(bpy)_3(PF_6)_2$ in dry ACN with 0.1 M NBu_4PF_6 at various RPMs (0 – 2000 RPM) where the second ruthenium reduction was held at -1.58 V at the ring electrode, while the potential was scanned from 0 V to 1.6 V at the disk electrode

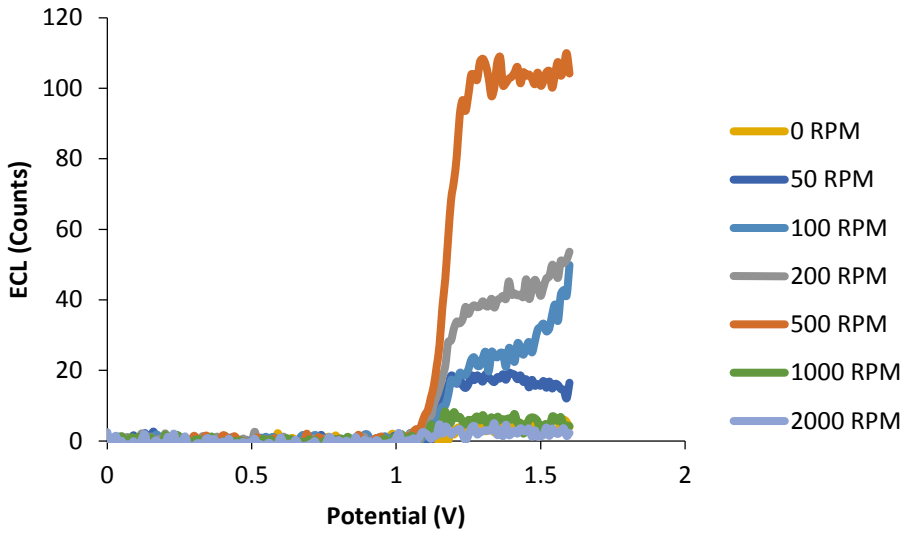

Figure 4.13: Voltammograms of the ECL intensities generated using 0.2 mM $Ru(bpy)_3(PF_6)_2$ in dry ACN with 0.1 M NBu_4PF_6 at various rotation rates (0 – 2000 RPM) where the second ruthenium reduction was held at -1.58 V at the ring electrode, while the potential was scanned from 0 V to 1.6 V at the disk electrode

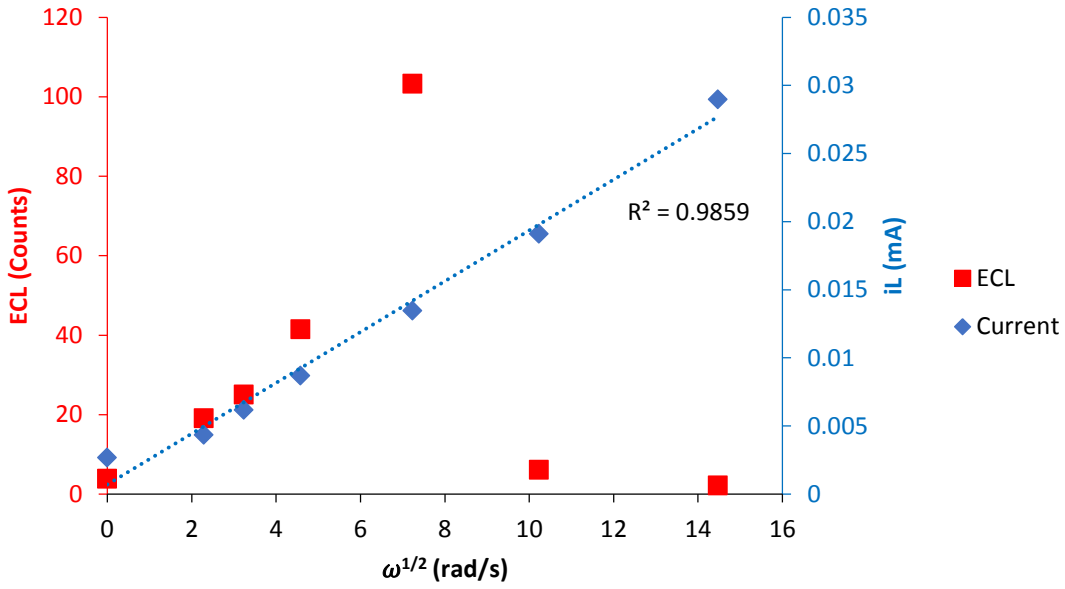

Figure 4.14: Levich plots of the current (blue plot, at 1.4 V) and ECL intensities (red plot, at 1.4 V) generated from 0.2 mM $Ru(bpy)_3(PF_6)_2$ in dry ACN with 0.1 M NBu_4PF_6 at various rotation rates (0 – 2000 RPM) at 610 nm highlighting the decrease of ECL intensities past 500 RPM (52.36 rad/s) when the second ruthenium reduction was held at -1.58 V at the ring electrode, while the potential was scanned from 0 V to 1.6 V at the disk electrode

When poising the ring potential approximately 10 mV more negative than the second reduction of the ruthenium complex (-1.58 V, reaction [4.8]), while an oxidation potential scan was simultaneously applied to the disk electrode (Figure 4.10), the limiting currents are unchanged and once again continue to increase with rotation rate over the full range, see Figures 4.11, 4.12 and 4.14 (blue plot). With the ECL responses, as annihilation reaction [4.8] becomes the dominant annihilation reaction, we again observe the intriguing critical RPM phenomena (Figure 4.13). A critical RPM of approx. 500 RPM/52.36 rad/s was observed in this system; see Figure 4.14, red plot. Overall these experiments elicited a 47% higher ECL intensity compared to when the first reduction of the ruthenium complex was held at the ring electrode under rotation.

$$Ru + e^- \rightarrow Ru^- \qquad \textbf{[4.10]}$$

$$Ru^- + Ru^{3+} \xrightarrow{k_3} Ru + Ru^{2+*} \qquad \textbf{[4.11]}$$

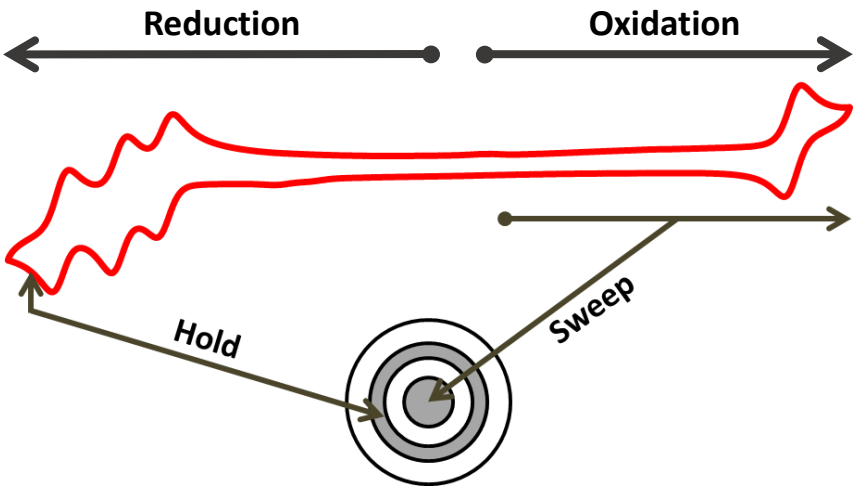

Figure 4.15: Representation of a hold-sweep annihilation ECL experiment of 0.2 mM $Ru(bpy)_3(PF_6)_2$ in dry ACN with 0.1 M NBu_4PF_6 using a RRDE where the third ruthenium reduction was held at -1.82 V at the ring electrode, while the potential was scanned from 0 V to 1.6 V at the disk electrode

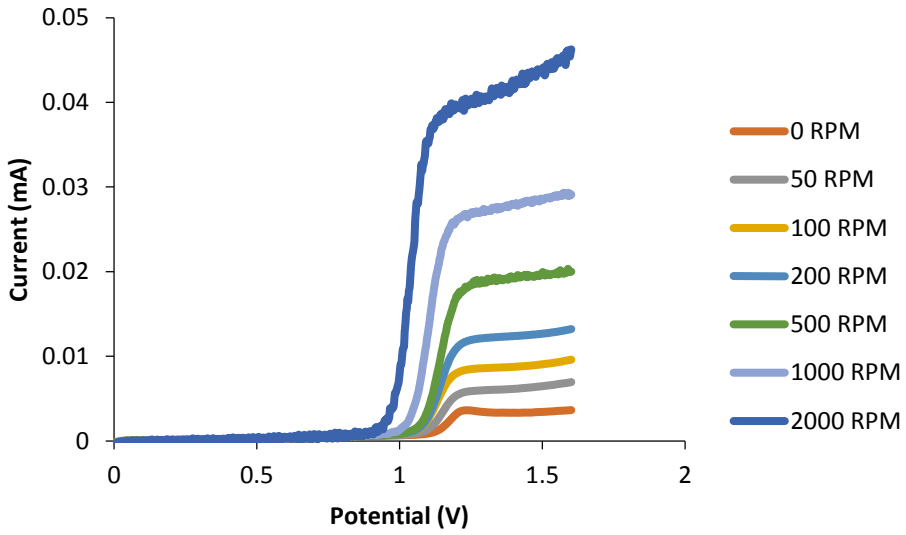

Figure 4.16: Voltammograms of the disk currents generated using 0.2 mM $Ru(bpy)_3(PF_6)_2$ in dry ACN with 0.1 M NBu_4PF_6 at various rotation rates (0 – 2000 RPM) where the third ruthenium reduction was held at -1.82 V at the ring electrode, while the potential was scanned from 0 V to 1.6 V at the disk electrode

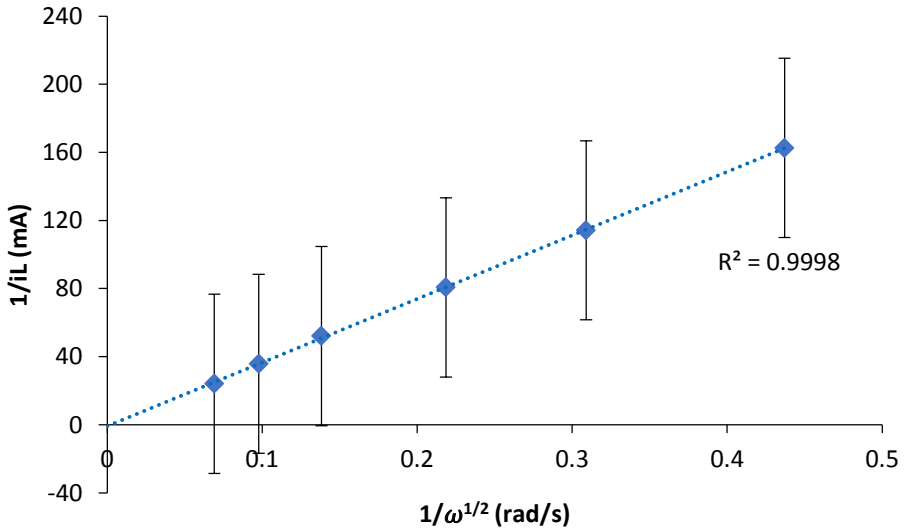

Figure 4.17: Koutecky-Levich plot of the currents generated at 1.4 V from 0.2 mM $Ru(bpy)_3(PF_6)_2$ in dry ACN with 0.1 M NBu_4PF_6 at various RPMs (0 – 2000 RPM) where the third ruthenium reduction was held at -1.82 V at the ring electrode, while the potential was scanned from 0 V to 1.6 V at the disk electrode

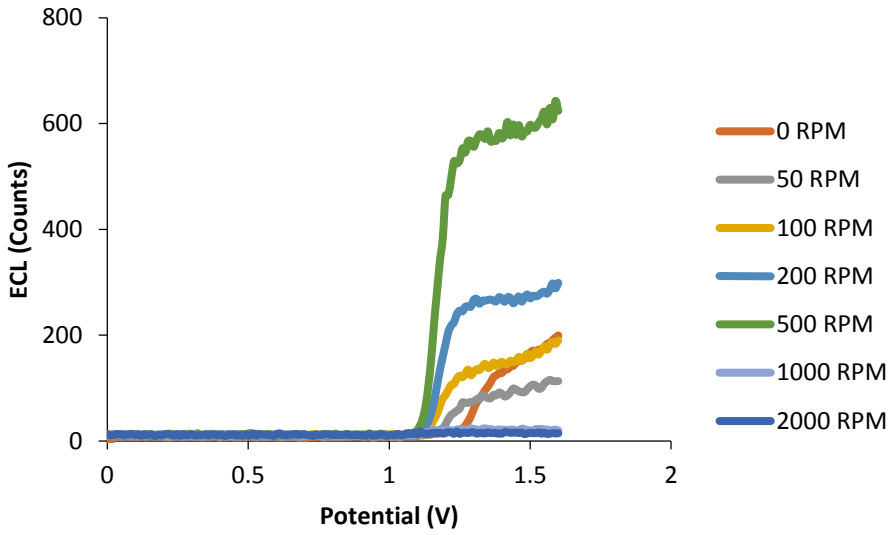

Figure 4.18: Voltammograms of the ECL intensities generated using 0.2 mM $Ru(bpy)_3(PF_6)_2$ in dry ACN with 0.1 M NBu_4PF_6 at various rotation rates (0 – 2000 RPM) where the third ruthenium reduction was held at -1.82 V at the ring electrode, while the potential was scanned from 0 V to 1.6 V at the disk electrode

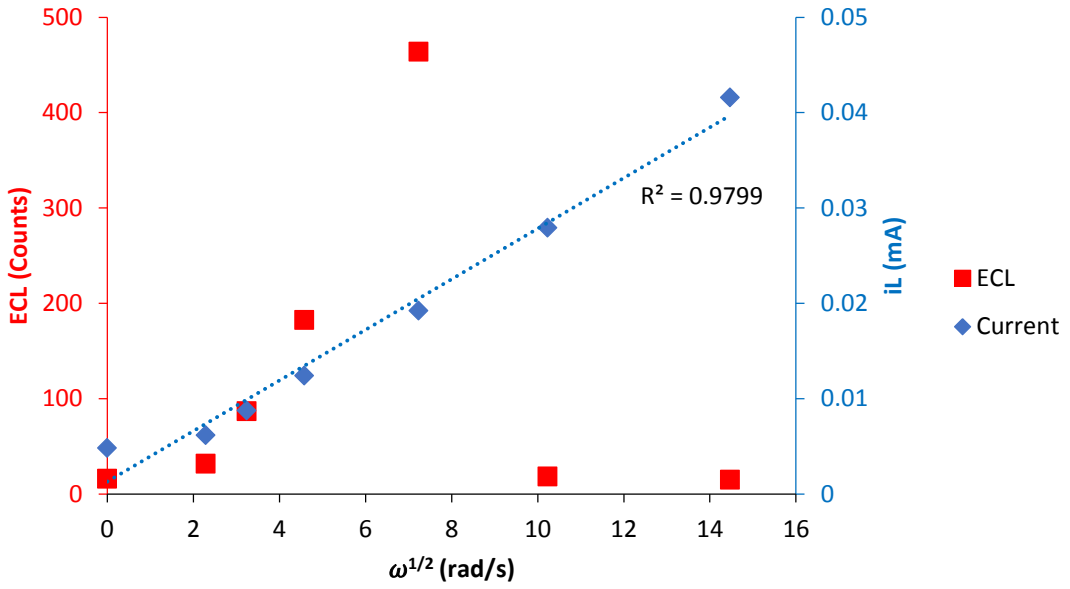

Figure 4.19: Levich plots of the current (blue plot, at 1.4 V) and ECL intensities (red plot, at 1.2 V) generated from 0.2 mM $Ru(bpy)_3(PF_6)_2$ in dry ACN with 0.1 M NBu_4PF_6 at various rotation rates (0 – 2000 RPM) at 610 nm highlighting the decrease of ECL intensities past 500 RPM (52.36 rad/s) when the third ruthenium reduction was held at -1.82 V at the ring electrode, while the potential was scanned from 0 V to 1.6 V at the disk electrode

When poising the ring potential approximately 10 mV more negative than the third reduction of the ruthenium complex (-1.82 V, reaction [4.10]), and a ruthenium oxidation scan was applied to the disk electrode (Figure 4.15), the critical RPM phenomena was once again observed (at approx. 500 RPM/52.36 rad/s) while the limiting current continues to increase at rotation rates faster than the system's critical RPM (Figures 4.16-4.19). This method generated 88% and 78% greater ECL intensity compared to that obtained when the first reduction (-1.38 V) and the second reduction (-1.58 V) of the ruthenium complex, respectively, was held at the ring electrode.

Next we tested the effect of reversing the location of the generation of the oxidised species. As depicted in Figure 4.20 below, we sought to sequentially trigger the three annihilation reactions [4.7], [4.9] and [4.11], by sweeping the ruthenium reductions at the disk while holding the ruthenium oxidation potential at the ring electrode. Yet again we witness the critical RPM phenomena where current increases (Figures 4.21, 4.22 and 4.24 (blue plot)) while ECL intensities begin to decrease past 500 RPM/52.36 rad/s (Figures 4.23 and 4.24 (red plot)). Compared to the other experimental configurations, this configuration generated 86% higher annihilation ECL intensity from $Ru(bpy)_3(PF_6)_2$ under rotation.

At rotation rates faster than 1000 RPM however, we believe O_2 begins to enter the system, this is illustrated by the large peak at -1.06 V that is usually attributed to O_2 in the voltammogram of the limiting current generated (Figure 4.21) when the electrode was rotated at speeds faster than 1000 RPM. If O_2 was quenching our emission as soon as we began to rotate the electrode, we would have observed a lower ECL intensity compared to results obtained at a stationary electrode, which does not occur in this case. The effect of O_2 on the disk current at 2000 RPM is significant.

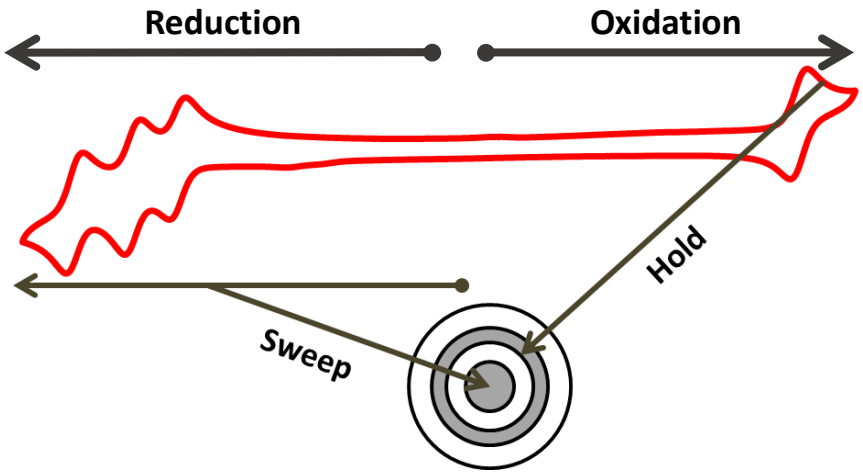

Figure 4.20: Representation of a hold-sweep annihilation ECL experiment of 0.2 mM $Ru(bpy)_3(PF_6)_2$ in dry ACN with 0.1 M NBu_4PF_6 using a RRDE where the ruthenium oxidation was held at 1.32 V at the ring electrode, while the potential was scanned from 0 V to -2.16 V at the disk electrode

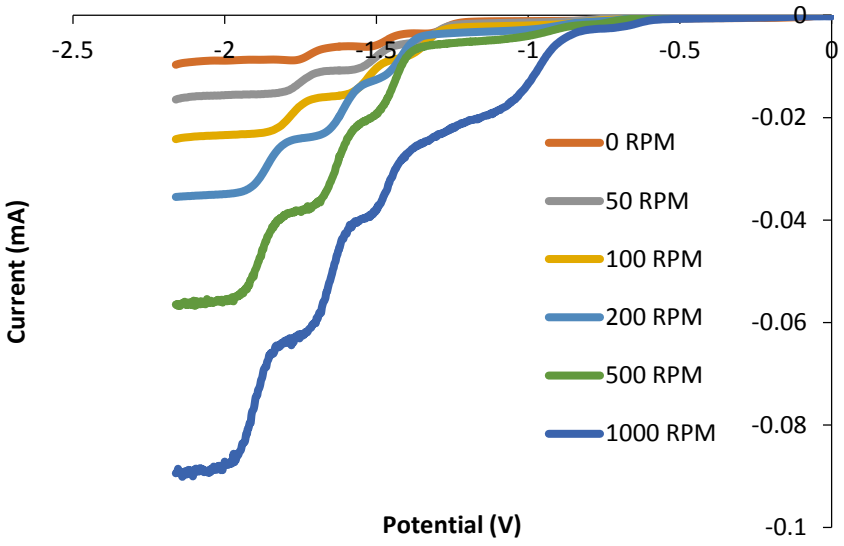

Figure 4.21: Voltammograms of the disk currents generated using 0.2 mM $Ru(bpy)_3(PF_6)_2$ in dry ACN with 0.1 M NBu_4PF_6 at various rotation rates (0 – 1000 RPM) where the ruthenium oxidation was held at 1.32 V at the ring electrode, while the potential was scanned from 0 V to -2.16 V at the disk electrode

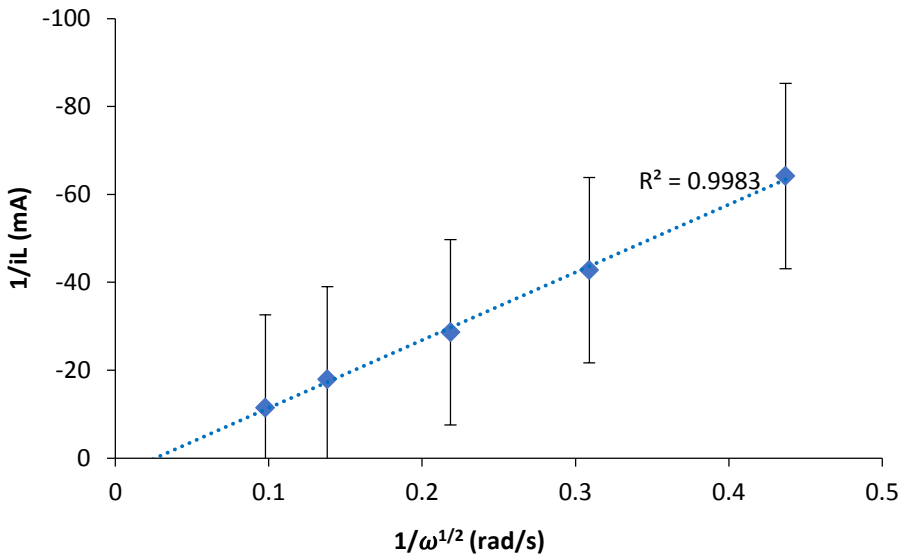

Figure 4.22: Koutecky-Levich plot of the currents generated at -2.0 V from 0.2 mM $Ru(bpy)_3(PF_6)_2$ in dry ACN with 0.1 M NBu_4PF_6 at various RPMs (0 – 1000 RPM) where the ruthenium oxidation was held at 1.32 V at the ring electrode, while the potential was scanned from 0 V to -2.16 V at the disk electrode

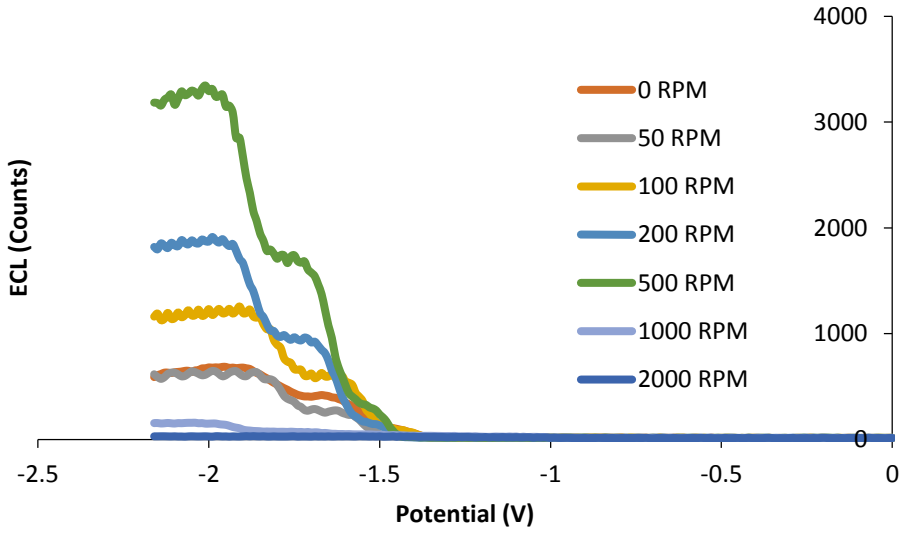

Figure 4.23: Voltammograms of the ECL intensities generated using 0.2 mM $Ru(bpy)_3(PF_6)_2$ in dry ACN with 0.1 M NBu_4PF_6 at various rotation rates (0 – 2000 RPM) where the ruthenium oxidation was held at 1.32 V at the ring electrode, while the potential was scanned from 0 V to -2.16 V at the disk electrode

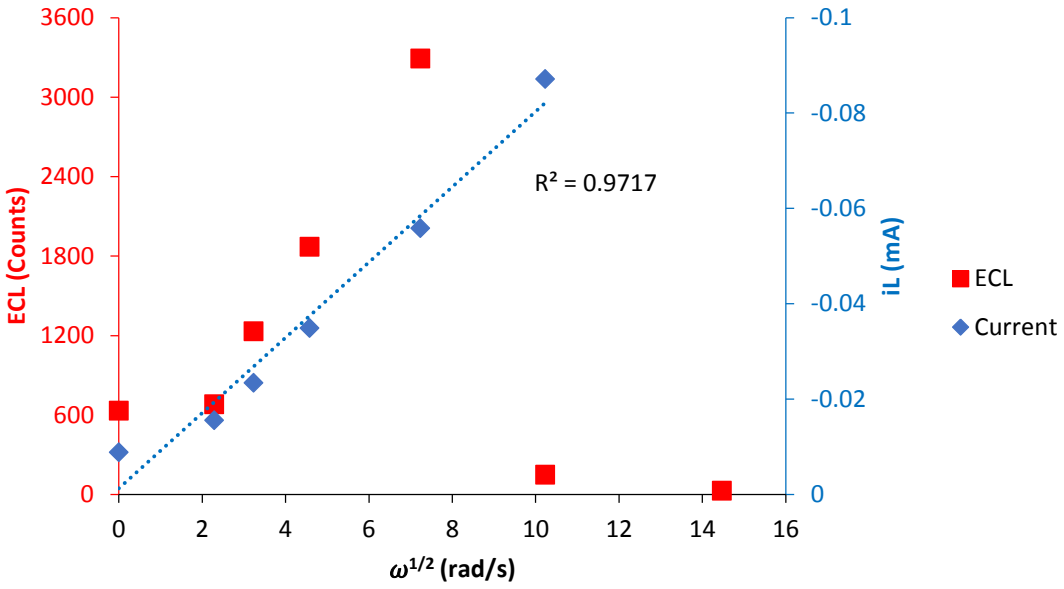

Figure 4.24: Levich plots of the current (blue plot, at -2.0 V) and ECL intensities (red plot, at -2.0 V) generated from 0.2 mM $Ru(bpy)_3(PF_6)_2$ in dry ACN with 0.1 M NBu_4PF_6 at various rotation rates (0 – 2000 RPM) at 610 nm highlighting the decrease of ECL intensities past 500 RPM (52.36 rad/s) when the ruthenium oxidation was held at 1.32 V at the ring electrode, while the potential was scanned from 0 V to -2.16 V at the disk electrode

It is important to be able to explain how the critical RPM phenomenon occurred in an annihilation ECL system without any co-reactant in the system. This can be similarly attributed to that already proposed in our RDE co-reactant ECL study. That is the rate of removal of the reduced species, Ru^+, Ru or Ru^- at the critical RPM is greater than that of the reaction rate for the generation of the Ru^{2+*} excited state, which results in lower ECL intensities observed at faster rotation rates.

With this knowledge, RPM studies were then performed on the $Ir(ppy)_3$ and the $(Ir[dF(CF_3)ppy]_2(dtbpy))PF_6$ annihilation ECL systems to observe if the critical RPM phenomenon takes place in other systems or if the phenomenon was exclusive to the $Ru(bpy)_3(PF_6)_2$ annihilation ECL system.

$$Ir(ppy)_3^- + Ir(ppy)_3^+ \xrightarrow{k_4} Ir(ppy)_3 + Ir(ppy)_3^* \quad \textbf{[4.12]}$$

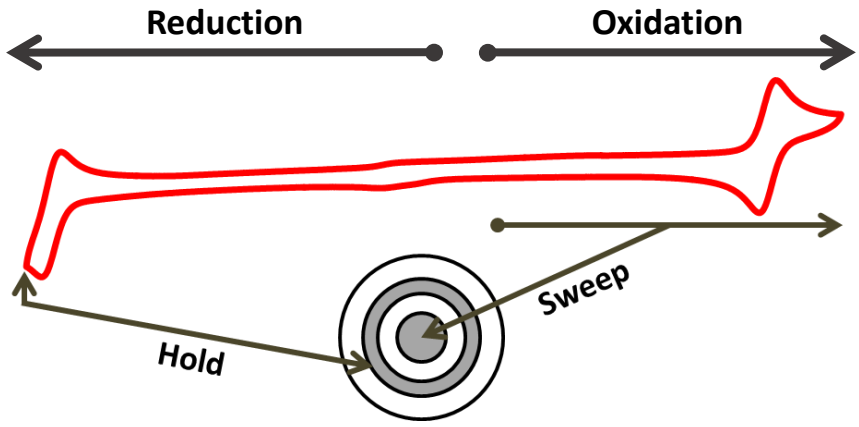

Figure 4.25: Representation of a hold-sweep annihilation ECL experiment of 0.2 mM $Ir(ppy)_3$ in dry ACN with 0.1 M NBu_4PF_6 using an RRDE, where the iridium reduction was held at -2.35 V at the ring electrode, while the potential was scanned from 0 V to 1.0 V at the disk electrode

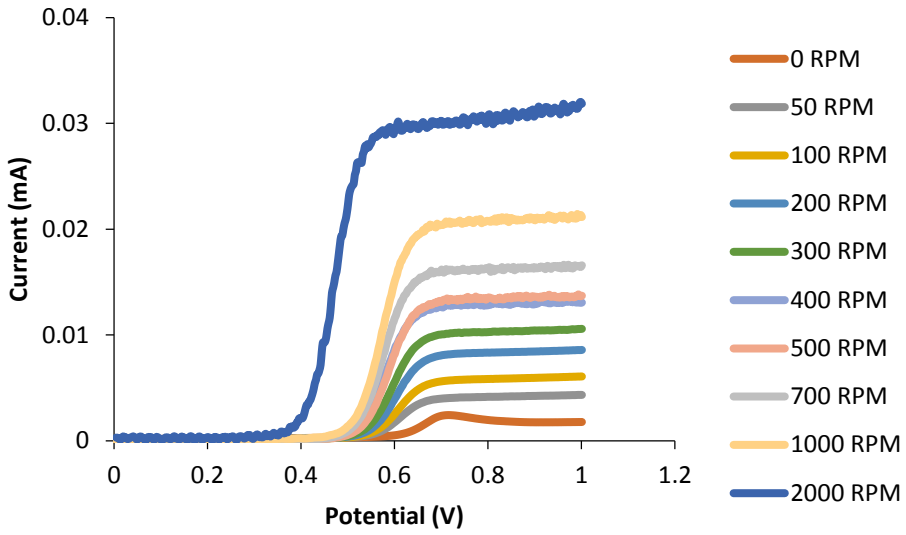

Figure 4.26: Voltammograms of the disk currents generated using 0.2 mM $Ir(ppy)_3$ in dry ACN with 0.1 M NBu_4PF_6 at various rotation rates (0 – 2000 RPM) where the iridium reduction was held at -2.35 V at the ring electrode, while the potential was scanned from 0 V to 1.0 V at the disk electrode

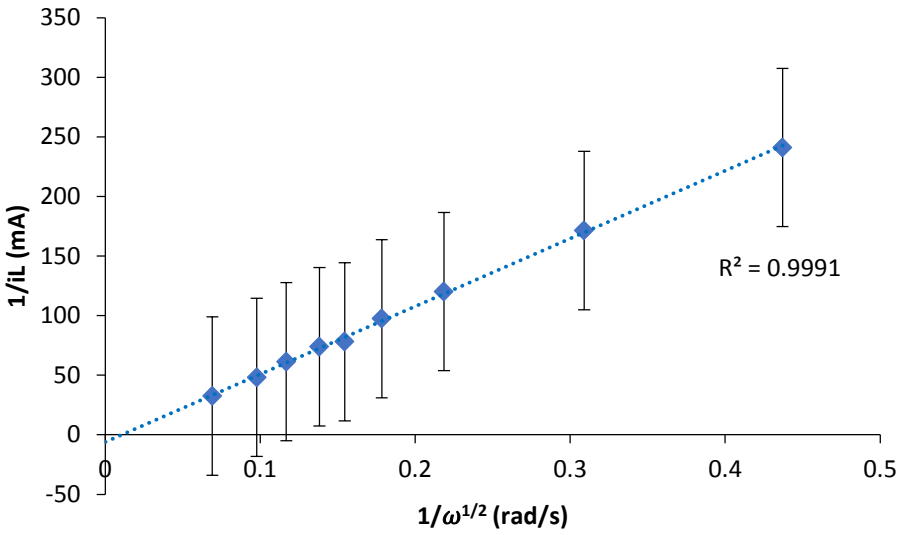

Figure 4.27: Koutecky-Levich plot of the currents generated at 0.8 V from 0.2 mM $Ir(ppy)_3$ in dry ACN with 0.1 M NBu_4PF_6 at various RPMs (0 – 2000 RPM) where the iridium reduction was held at -2.35 V at the ring electrode, while the potential was scanned from 0 V to 1.0 V at the disk electrode

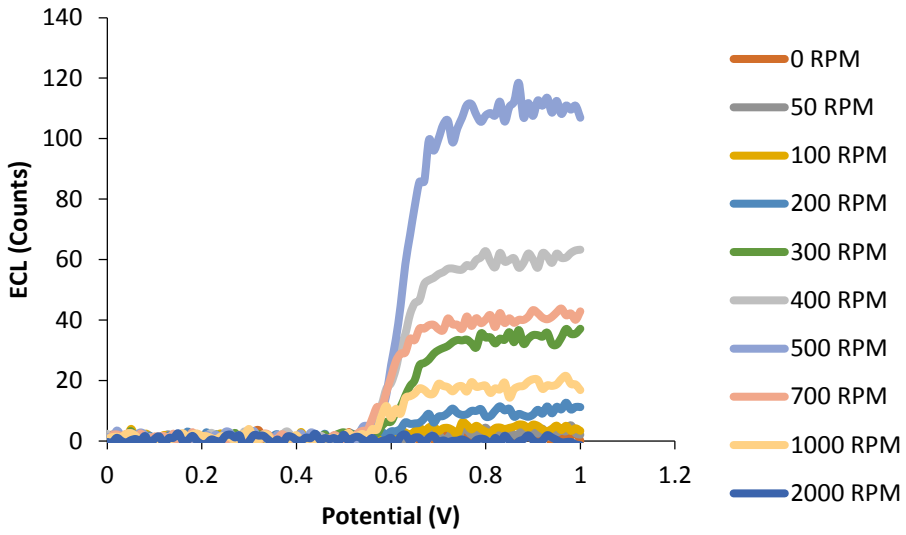

Figure 4.28: Voltammograms of the ECL intensities generated using 0.2 mM $Ir(ppy)_3$ in dry ACN with 0.1 M NBu_4PF_6 at various rotation rates (0 – 2000 RPM) where the iridium reduction was held at -2.35 V at the ring electrode, while the potential was scanned from 0 V to 1.0 V at the disk electrode

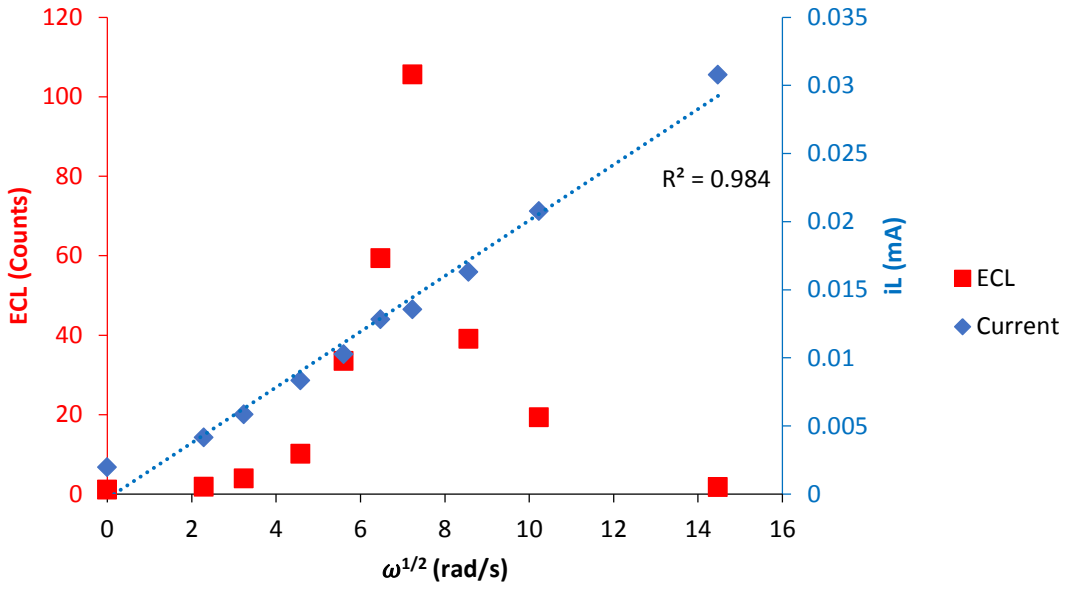

Figure 4.29: Levich plots of the current (blue plot, at 0.8 V) and ECL intensities (red plot, at 0.84 V) generated from 0.2 mM $Ir(ppy)_3$ in dry ACN with 0.1 M NBu_4PF_6 at various rotation rates (0 – 2000 RPM) at 520 nm highlighting the decrease of ECL intensities past 500 RPM (52.36 rad/s) when the iridium reduction was held at -2.35 V at the ring electrode, while the potential was scanned from 0 V to 1.0 V at the disk electrode

High annihilation ECL intensities from reaction [4.12] (0.2 mM $Ir(ppy)_3$) under rotation was achieved by reducing Ir^{3+} at -2.35 V at the ring electrode while the oxidation of $Ir(ppy)_3$ was achieved by simultaneously scanning the potential from 0 V to 1.0 V at the disk electrode (Figure 4.25). As the rotation rate increased, a linear increase of the limiting current was also observed (Figures 4.26, 4.27 and 4.29 (blue plot)). Similar to the $Ru(bpy)_3(PF_6)_2$ annihilation ECL system, we again observe a decrease in ECL intensity (Figures 4.28 and 4.29 (red plot)) past a critical RPM (approx. 500 RPM/52.36 rad/s). However, when the iridium reduction was swept at the disk electrode and the iridium oxidation was held at the ring instead, no $Ir(ppy)_3$ ECL emissions were detected. This might be due to the relative instability of $[Ir(ppy)_3]^-$.

$$[Ir(dF(CF_3)ppy)_2(dtbpy)] + [Ir(dF(CF_3)ppy)_2(dtbpy)]^{2+} \xrightarrow{k_5} [Ir(dF(CF_3)ppy)_2(dtbpy)]^{+} + [Ir(dF(CF_3)ppy)_2(dtbpy)]^{+*} \quad \textbf{[4.13]}$$

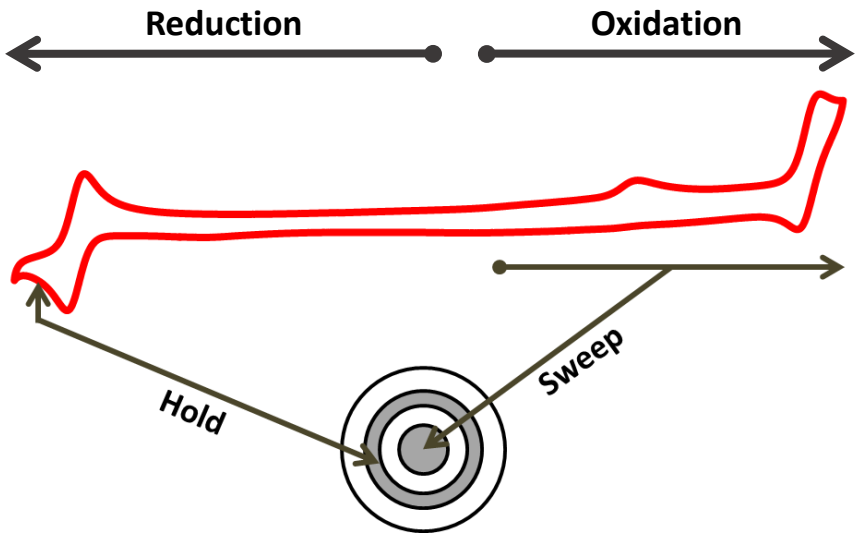

Figure 4.30: Representation of a hold-sweep annihilation ECL experiment of 0.4 mM $(Ir[dF(CF_3)ppy]_2(dtbpy))PF_6$ in dry ACN with 0.1 M NBu_4PF_6 using a RRDE where the $(Ir[dF(CF_3)ppy]_2(dtbpy))PF_6$ reduction was held at -1.14 V at the ring electrode, while the potential was scanned from 0 V to 2.30 V at the disk electrode

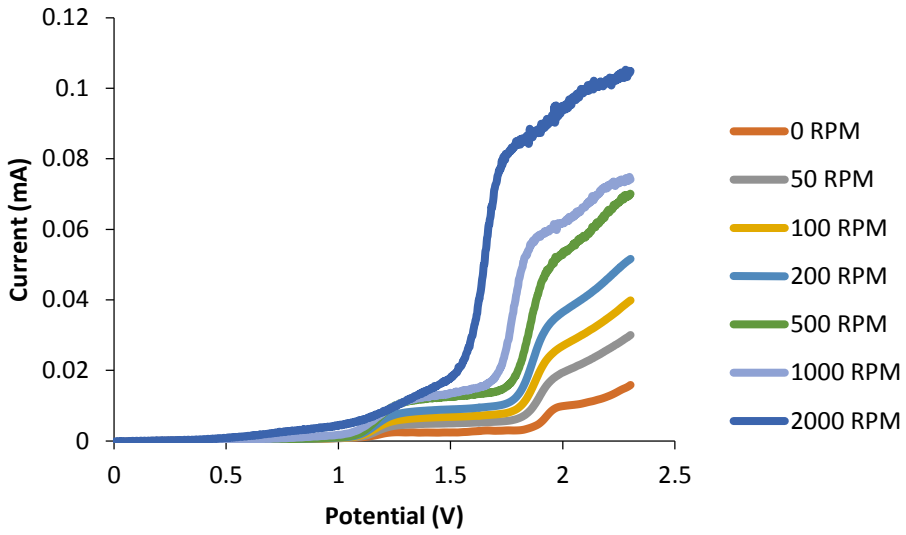

Figure 4.31: Voltammograms of the disk currents generated using 0.4 mM $(Ir[dF(CF_3)ppy]_2(dtbpy))PF_6$ in dry ACN with 0.1 M NBu_4PF_6 at various rotation rates (0 – 2000 RPM) where the $(Ir[dF(CF_3)ppy]_2(dtbpy))PF_6$ reduction was held at -1.14 V at the ring electrode, while the potential was scanned from 0 V to 2.30 V at the disk electrode

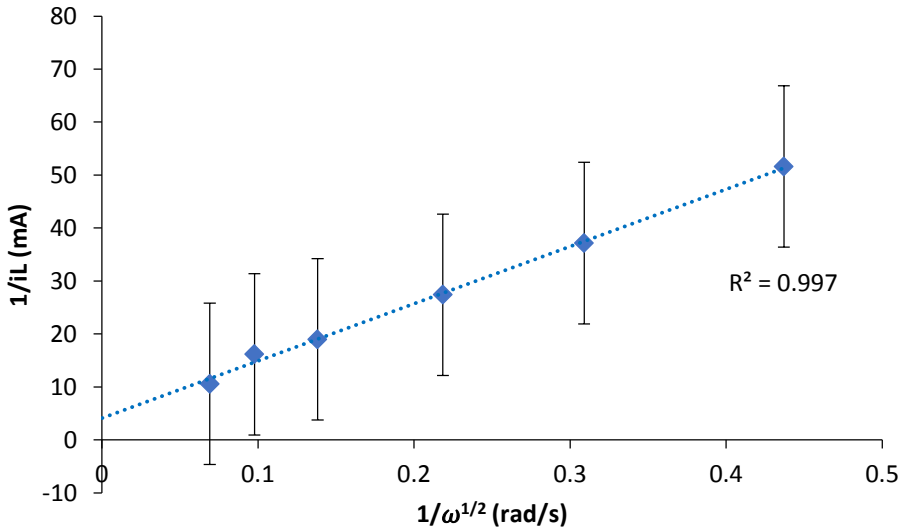

Figure 4.32: Koutecky-Levich plot of the currents generated at 0.8 V from 0.4 mM $(Ir[dF(CF_3)ppy]_2(dtbpy))PF_6$ in dry ACN with 0.1 M NBu_4PF_6 at various RPMs (0 – 2000 RPM) where the $(Ir[dF(CF_3)ppy]_2(dtbpy))PF_6$ reduction was held at -1.14 V at the ring electrode, while the potential was scanned from 0 V to 2.30 V at the disk electrode

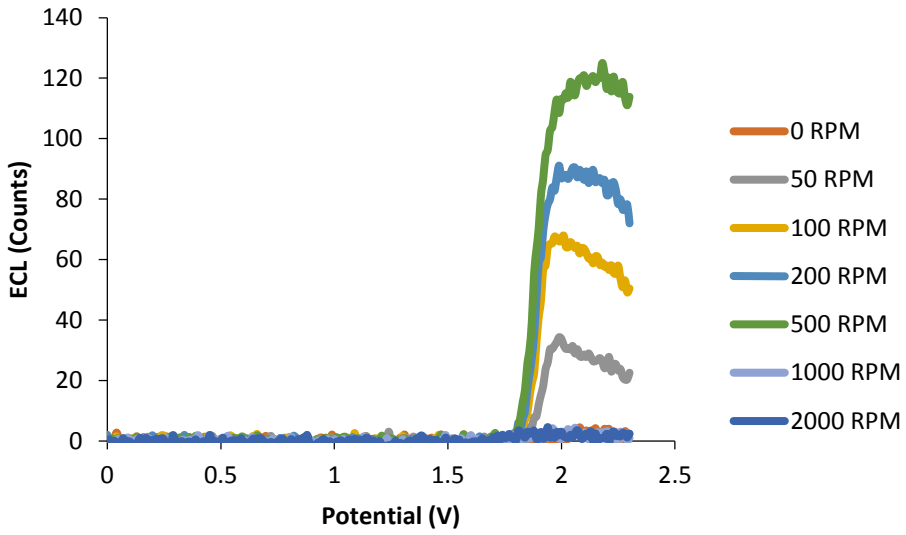

Figure 4.33: Voltammograms of the ECL intensities generated using 0.4 mM $(Ir[dF(CF_3)ppy]_2(dtbpy))PF_6$ in dry ACN with 0.1 M NBu_4PF_6 at various rotation rates (0 – 2000 RPM) where the $(Ir[dF(CF_3)ppy]_2(dtbpy))PF_6$ reduction was held at -1.14 V at the ring electrode, while the potential was scanned from 0 V to 2.30 V at the disk electrode

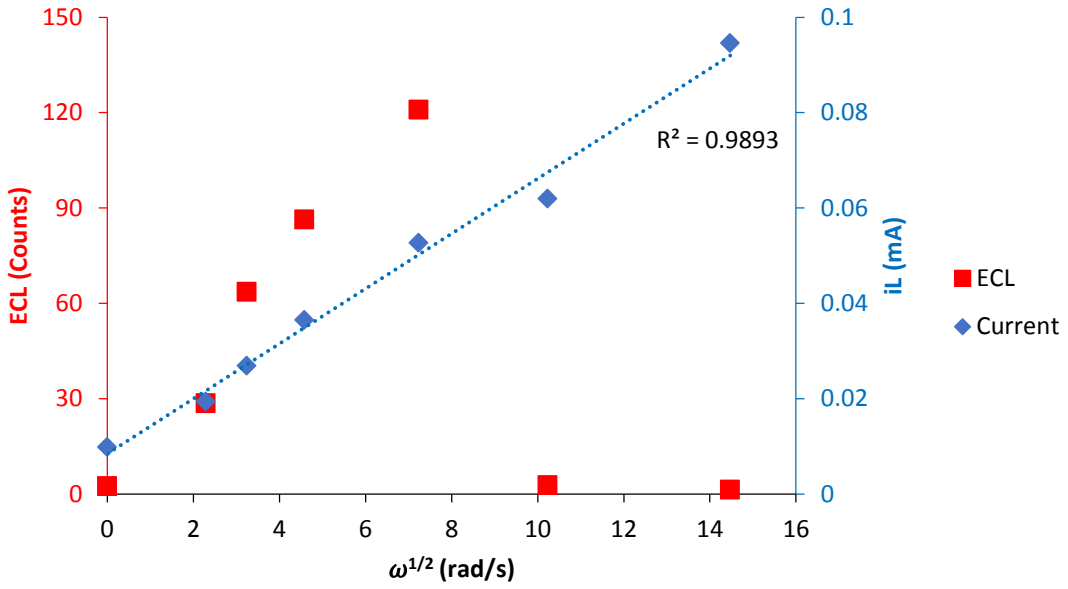

Figure 4.34: Levich plots of the current (blue plot, at 2.0 V) and ECL intensities (red plot, at 2.1 V) generated from 0.4 mM $(Ir[dF(CF_3)ppy]_2(dtbpy))PF_6$ in dry ACN with 0.1 M NBu_4PF_6 at various rotation rates (0 – 2000 RPM) at 470 nm highlighting the decrease of ECL intensities past 500 RPM (52.36 rad/s) when the $(Ir[dF(CF_3)ppy]_2(dtbpy))PF_6$ reduction was held at -1.14 V at the ring electrode, while the potential was scanned from 0 V to 2.30 V at the disk electrode

The effect of electrode rotation on annihilation ECL generated was examined using 0.4 mM $(Ir[dF(CF_3)ppy]_2(dtbpy))PF_6$. The corresponding reaction is shown in reaction [4.13]. In this experiment, the reduction of $(Ir[dF(CF_3)ppy]_2(dtbpy))PF_6$ was conducted by applying -1.14 V to the ring electrode, while the oxidation of $(Ir[dF(CF_3)ppy]_2(dtbpy))PF_6$ was achieved by simultaneously scanning the potential from 0 V to 2.3 V at the disk electrode. This is schematically shown in Figure 4.30.

The critical RPM phenomenon occurs yet again at approx. 500 RPM/52.36 rad/s (Figures 4.31-4.34). This phenomenon was repeated when the reduction was swept at the disk and the oxidation held at the ring instead (Figures 4.35- 4.39). Similar to when the $Ru(bpy)_3(PF_6)_2$ annihilation ECL system was examined when the reductions were swept at the disk, O_2 began to interfere in the system, as illustrated by the large peak at 0.8 V in Figure 4.36, which is attributed to O_2 reduction. However, it is important to note that ECL intensities did not decrease on rotation compared to the stationary electrode.

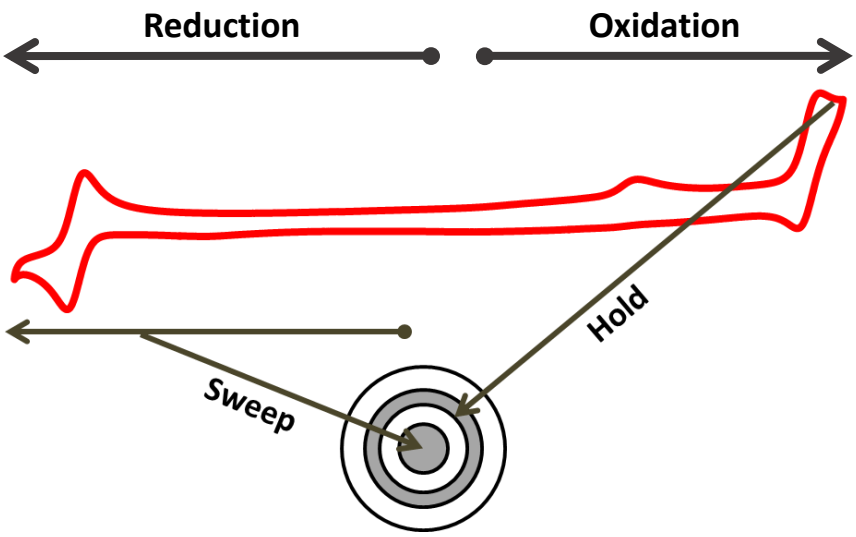

Figure 4.35: Representation of a hold-sweep annihilation ECL experiment of 0.4 mM $(Ir[dF(CF_3)ppy]_2(dtbpy))PF_6$ in dry ACN with 0.1 M NBu_4PF_6 using a RRDE where the $(Ir[dF(CF_3)ppy]_2(dtbpy))PF_6$ oxidation was held at 2.02 V at the ring electrode, while the potential was scanned from 0 V to -1.40 V at the disk electrode

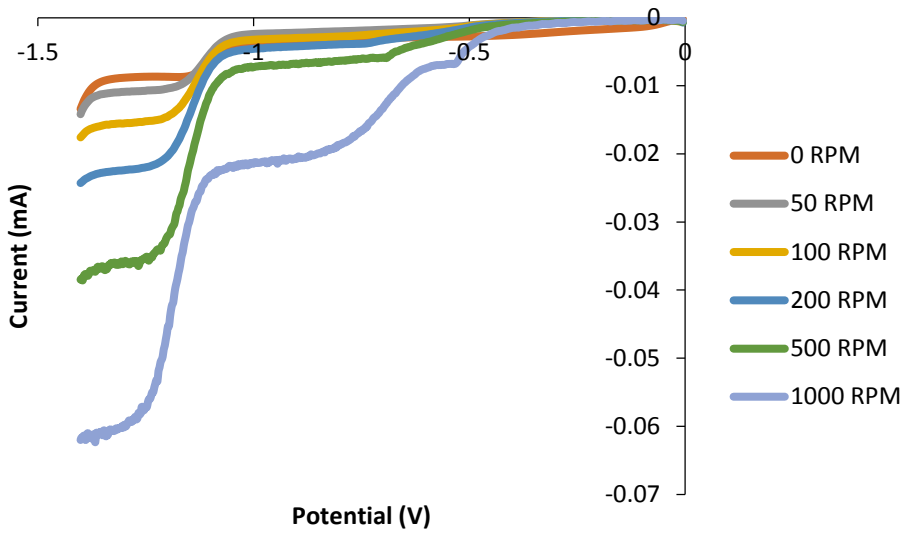

Figure 4.36: Voltammograms of the disk currents generated using 0.4 mM $(Ir[dF(CF_3)ppy]_2(dtbpy))PF_6$ in dry ACN with 0.1 M NBu_4PF_6 at various rotation rates (0 – 1000 RPM) where the $(Ir[dF(CF_3)ppy]_2(dtbpy))PF_6$ oxidation was held at 2.02 V at the ring electrode, while the potential was scanned from 0 V to -1.40 V at the disk electrode

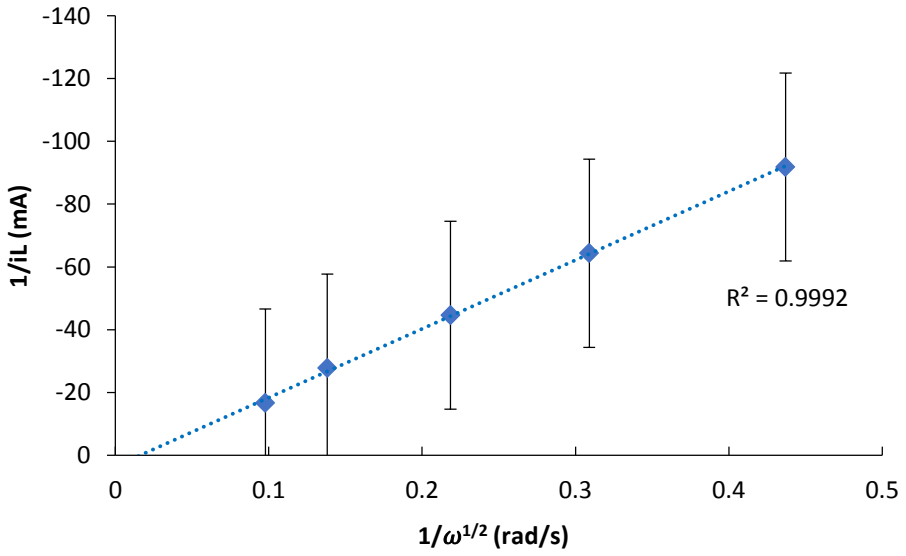

Figure 4.37: Koutecky-Levich plot of the currents generated at -1.3 V from 0.4 mM $(Ir[dF(CF_3)ppy]_2(dtbpy))PF_6$ in dry ACN with 0.1 M NBu_4PF_6 at various RPMs (0 – 1000 RPM) where the $(Ir[dF(CF_3)ppy]_2(dtbpy))PF_6$ oxidation was held at 2.02 V at the ring electrode, while the potential was scanned from 0 V to -1.40 V at the disk electrode

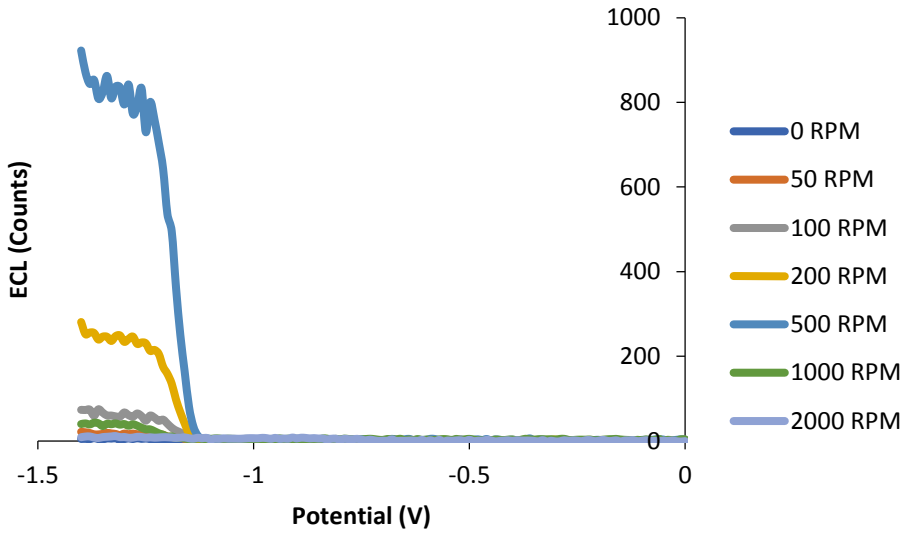

Figure 4.38: Voltammograms of the ECL intensities generated using 0.4 mM $(Ir[dF(CF_3)ppy]_2(dtbpy))PF_6$ in dry ACN with 0.1 M NBu_4PF_6 at various rotation rates (0 – 1000 RPM) where the $(Ir[dF(CF_3)ppy]_2(dtbpy))PF_6$ oxidation was held at 2.02 V at the ring electrode, while the potential was scanned from 0 V to -1.40 V at the disk electrode

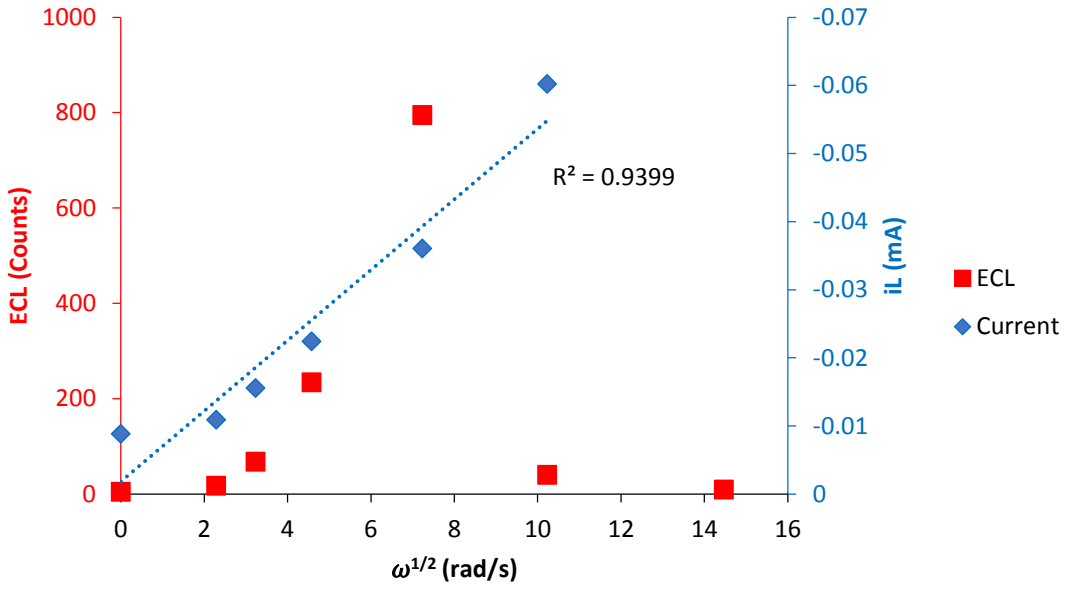

Figure 4.39: Levich plots of the current (blue plot, at -1.3 V) and ECL intensities (red plot, at -1.3 V) generated from 0.4 mM $(Ir[dF(CF_3)ppy]_2(dtbpy))PF_6$ in dry ACN with 0.1 M NBu_4PF_6 at various rotation rates (0 – 2000 RPM) at 470 nm highlighting the decrease of ECL intensities past 500 RPM (52.36 rad/s) when the $(Ir[dF(CF_3)ppy]_2(dtbpy))PF_6$ oxidation was held at 2.02 V at the ring electrode, while the potential was scanned from 0 V to -1.40 V at the disk electrode

4.3.2 Effect of electrode polarity on annihilation ECL intensity under rotation

The hold-sweep experiments described previously can produce voltammograms of both the current and ECL intensities generated from the luminophores used in our study as well as providing important qualitative information, such as redox potentials, about each system. However, there were a few drawbacks in our hold-sweep method, mainly the low ECL intensities that were produced as well the lengthy timescales required to complete each experiments. Due to these drawbacks, a new approach for the generation of annihilation ECL using a RRDE was developed. Instead of applying either a reduction scan or an oxidation scan, both an oxidation potential and a reduction potential will be held constant at the ring electrode and the disk electrode for 10 s, respectively, while the electrode is rotated during the experiment. We shall describe this as a "hold-hold experiment.

The effect of the electrode polarity in our hold-hold experiments on the annihilation ECL intensities generated from both $Ru(bpy)_3(PF_6)_2$ and $Ir(ppy)_3$ under rotation were then examined. We are interested in examining whether our annihilation ECL intensity would be enhanced by constantly reducing the luminophore at the ring, while simultaneously oxidising the luminophore at the disk electrode, or vice versa.

Figure 4.40 shows the effect of electrode polarity on the ECL intensity generated from the 0.2 mM $Ru(bpy)_3(PF_6)_2$ annihilation ECL system when the electrode was rotated at 600 RPM. Holding the oxidation at 1.32 V at the ring and while simultaneously holding the third reduction of the ruthenium complex at -1.82 V at the disk to produce reaction [4.11] (the orange spectrum), generates ECL intensities approximately seven times more intense than the intensities generated when the third reduction is held at the ring and the oxidation at the disk to produce reaction [4.11] (the blue spectrum).

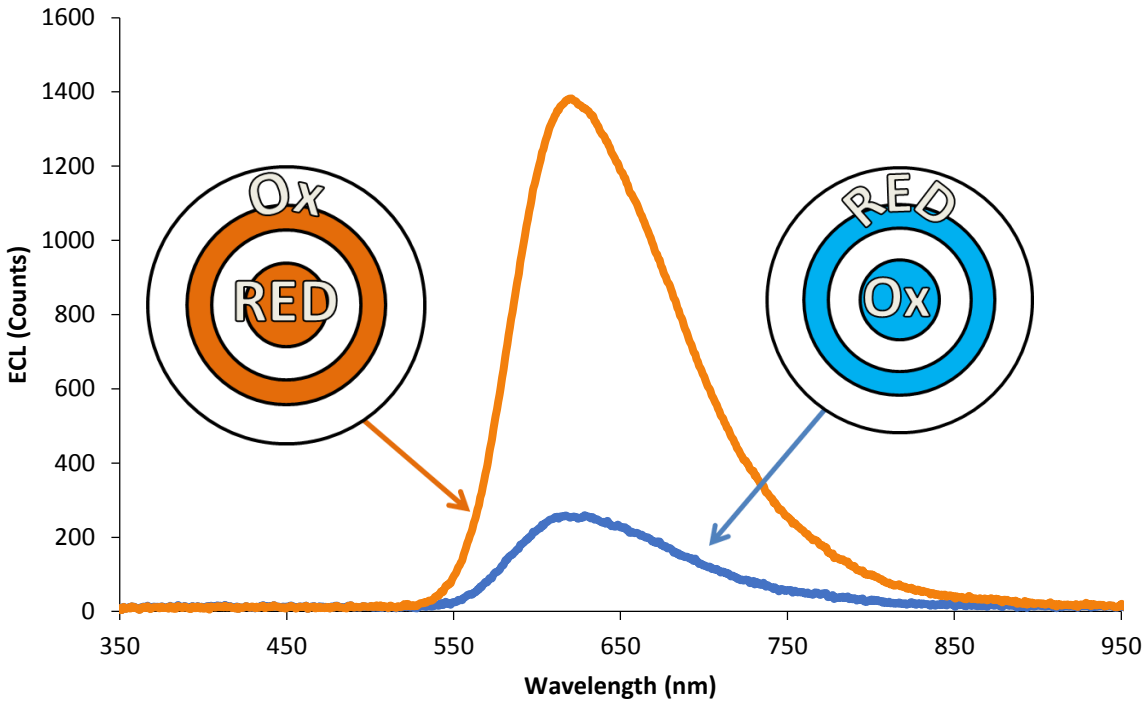

Figure 4.40: Spectra of the annihilation ECL generated from 0.2 mM $Ru(bpy)_3(PF_6)_2$ in dry ACN with 0.1 M NBu_4PF_6 under rotation at 600 RPM where the orange spectrum represents when the third reduction of the ruthenium complex was held at the disk electrode and the oxidation of the ruthenium complex was also held at the ring electrode while the blue spectrum represents when the third reduction of the ruthenium complex was held at the ring electrode and the oxidation of the ruthenium complex was also held at the disk electrode

Changing the order in which electrode polarity is investigated first revealed that holding the third reduction and oxidation at the disk and ring electrodes respectively always generates greater intensities compared to when the third reduction and oxidation were both held at the ring and disk electrodes respectively. Generating the Ru^- state at the disk and having it swept towards the ring electrode, where the Ru^{3+} state is generated, is the most efficient pathway for intense annihilation ECL emissions from $Ru(bpy)_3(PF_6)_2$.

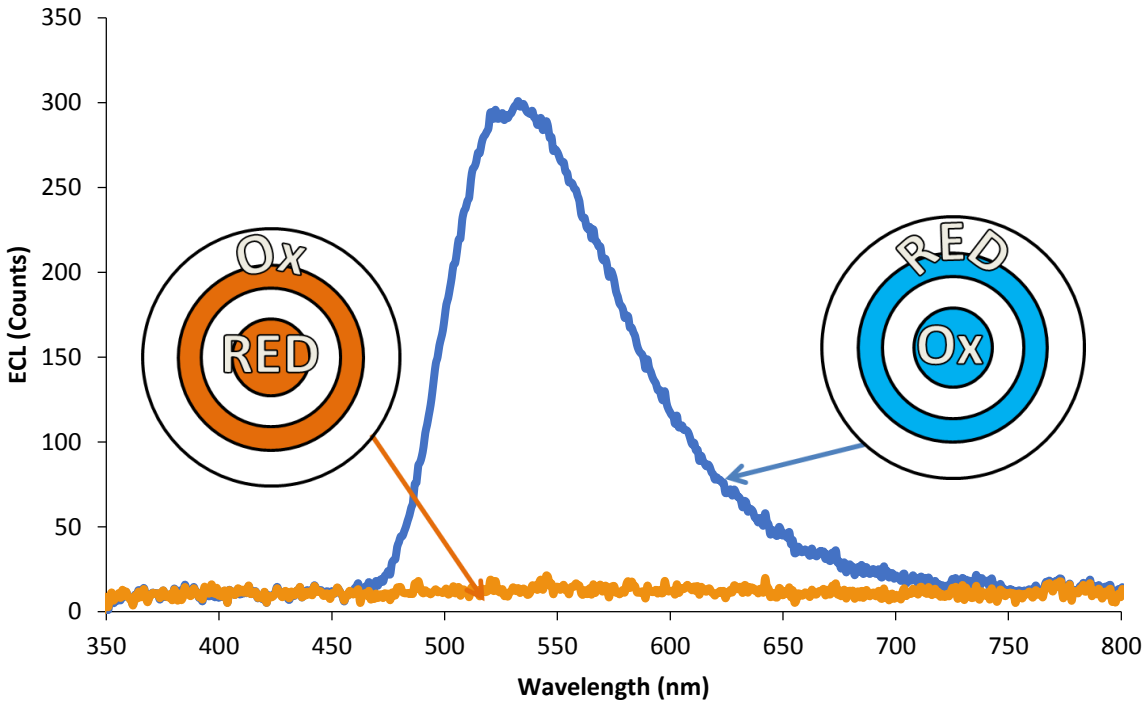

Figure 4.41: Spectra of the annihilation ECL generated from 0.2 mM $Ir(ppy)_3$ in dry ACN with 0.1 M $NBu4PF_6$ under rotation at 450 RPM where the orange spectrum represents when reduction of the iridium complex was held at the disk electrode and the oxidation of the iridium complex was also held at the ring electrode while the blue spectrum represents when the reduction of the iridium complex was held at the ring electrode and the oxidation of the iridium complex was also held at the disk electrode

However, ECL intensities from the 0.2 mM $Ir(ppy)_3$ annihilation ECL system only occurs when the iridium reduction was held at the ring while the iridium oxidation was held at the disk to produce reaction [4.12] (blue spectrum in Figure 4.41) when under electrode rotation (450 RPM). This clearly demonstrates that changing the polarity of the electrode in our hold-hold experiments has an enormous effect on the ECL intensities generated from these systems. This requires further investigation, but this is probably due to the relative stabilities of the oxidised and reduced species for each complex.

4.3.3 Detailed RPM studies from hold-hold experiments under rotation

Detailed RPM studies using the previously determined optimum electrode polarities for both the $Ru(bpy)_3(PF_6)_2$ and $Ir(ppy)_3$ annihilation ECL systems were then performed. Figure 4.42 describes a hold-hold experiment where a solution containing 0.2 mM $Ru(bpy)_3(PF_6)_2$ was examined under rotation to generate reaction [4.7], i.e.

$$Ru^{+} + Ru^{3+} \xrightarrow{k_1} Ru^{2+} + Ru^{2+*} \qquad \textbf{[4.7]}$$

The first reduction of the ruthenium complex was held at -1.38 V at the disk while the oxidation of the ruthenium complex was simultaneously held at 1.32 V at the ring electrode for 10 s.

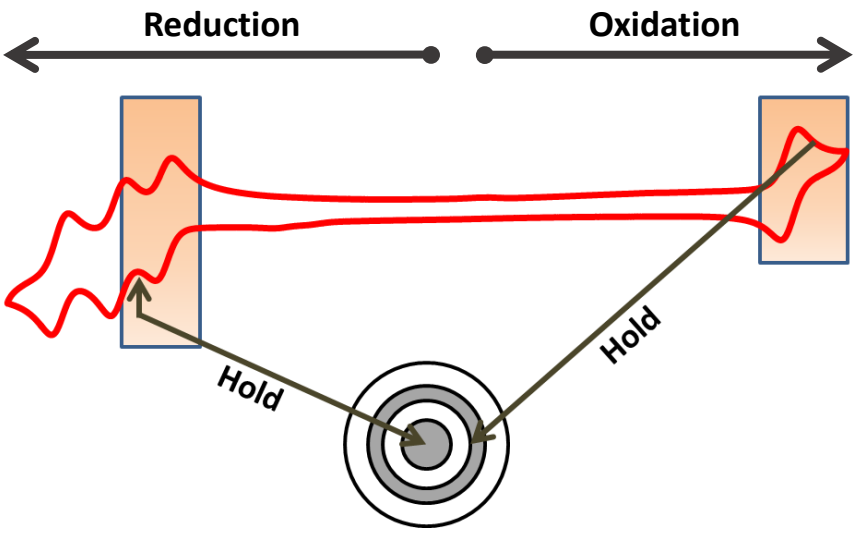

Figure 4.42: Representation of a hold-hold annihilation ECL experiment of 0.2 mM $Ru(bpy)_3(PF_6)_2$ in dry ACN with 0.1 M NBu_4PF_6 using a RRDE where the first ruthenium reduction was held at -1.38 V at the disk electrode, while the oxidation was simultaneously held at 1.32 V at the ring electrode

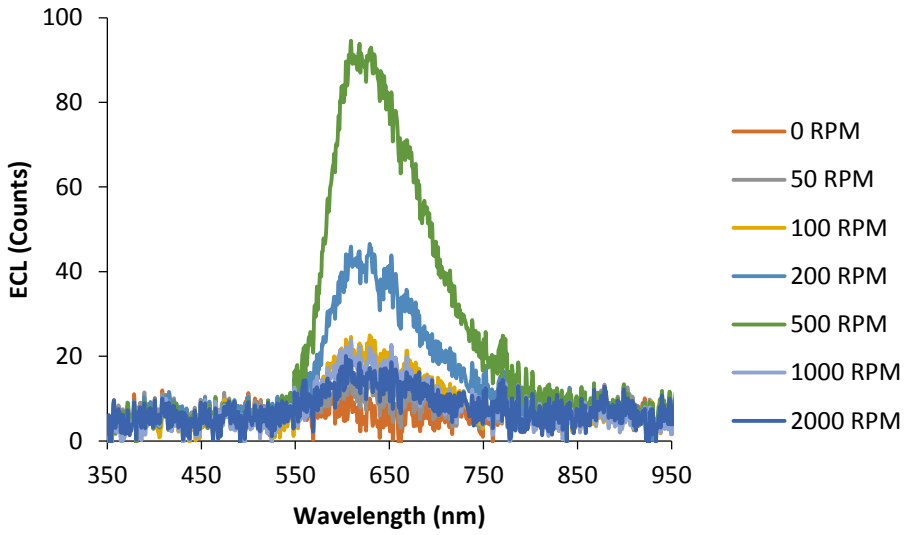

Figure 4.43: Spectra of the annihilation ECL generated from 0.2 mM $Ru(bpy)_3(PF_6)_2$ in dry ACN with 0.1 M NBu_4PF_6 at various rotation rates (0 – 2000 RPM) where the first ruthenium reduction was held at -1.38 V at the disk electrode, while the oxidation was simultaneously held at 1.32 V at the ring electrode for 10 s

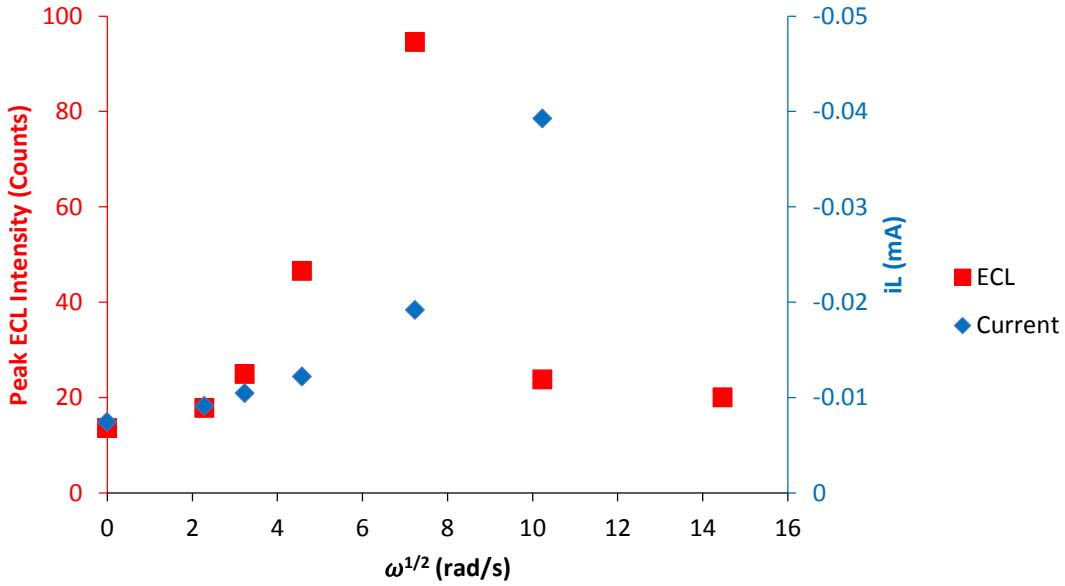

Figure 4.44: Levich plot of the peak annhilation ECL intensities (red) and the current (blue) generated from 0.2 mM $Ru(bpy)_3(PF_6)_2$ in dry ACN with 0.1 M NBu_4PF_6 at various rotation rates (0 – 2000 RPM) at 610 nm where the first ruthenium reduction was held at -1.38 V at the disk electrode, while the oxidation was simultaneously held at 1.32 V at the ring electrode for 10 s

Figure 4.43 shows that this new method does facilitate annihilation ECL emissions from $Ru(bpy)_3(PF_6)_2$ under rotation. Annihilation ECL intensities increased by approximately 42% when compared to the intensities generated from the same system when the hold-sweep experiment was used to hold the first ruthenium reduction at the ring, while an oxidation potential scan was applied at the disk (Figures 4.8 and 4.9).

The Levich study of the system (Figure 4.44) shows that once again the critical RPM phenomena occurs where an increase of ECL intensities are observed until the critical RPM is reached (approx. 500 RPM/52.36 rad/s). ECL intensities then decrease past this RPM. To obtain these increased ECL intensities from the hold-hold method however we must sacrifice the qualitative information we would obtain when we use the hold-sweep experiments.

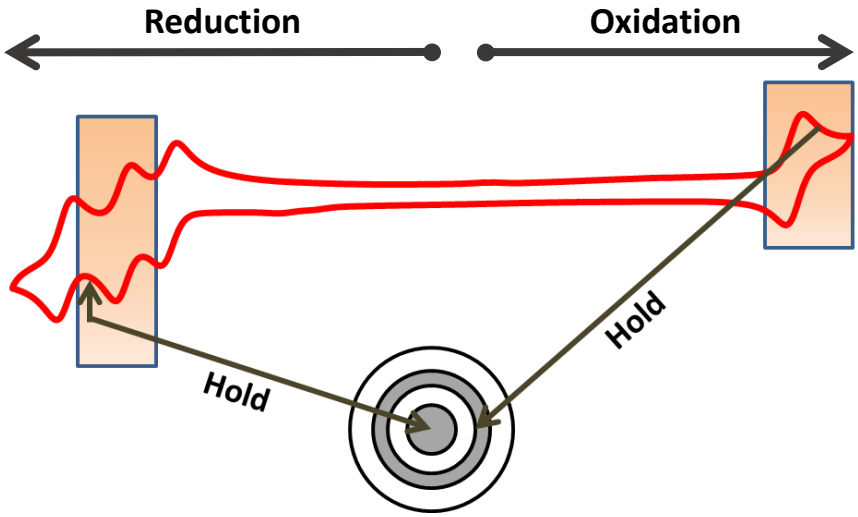

Figure 4.45: Representation of a hold-hold annihilation ECL experiment of 0.2 mM $Ru(bpy)_3(PF_6)_2$ in dry ACN with 0.1 M NBu_4PF_6 using a RRDE where the second ruthenium reduction was held at -1.58 V at the disk electrode, while the oxidation was simultaneously held at 1.32 V at the ring electrode

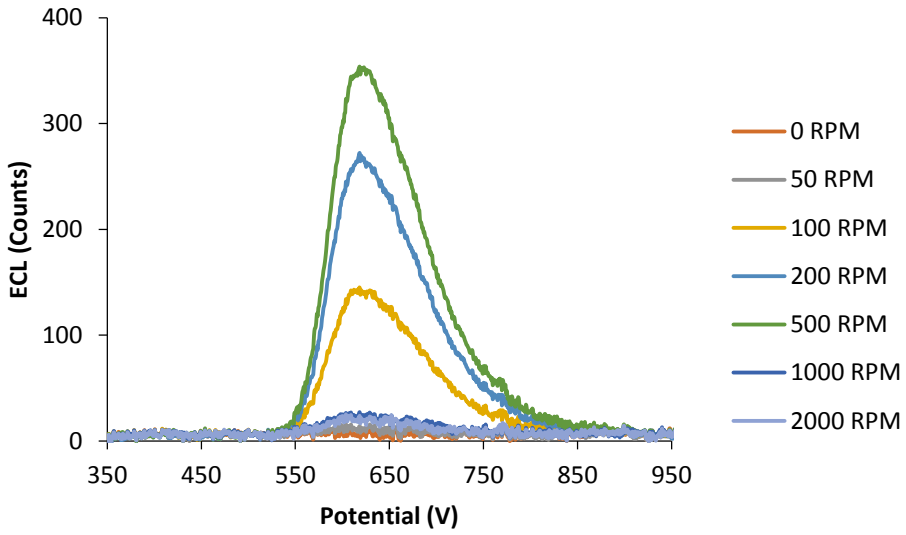

Figure 4.46: Spectra of the annihilation ECL generated from 0.2 mM $Ru(bpy)_3(PF_6)_2$ in dry ACN with 0.1 M NBu_4PF_6 at various rotation rates (0 – 2000 RPM) where the second ruthenium reduction was held at -1.58 V at the disk electrode, while the oxidation was simultaneously held at 1.32 V at the ring electrode 10 s

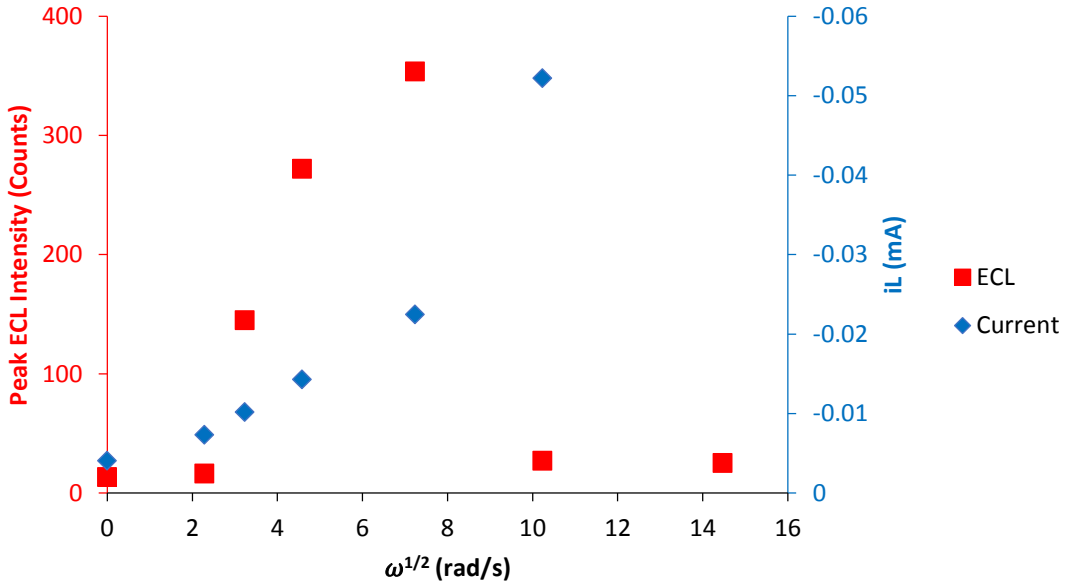

Figure 4.47: Levich plot of the peak annhilation ECL intensities (red) and the current (blue) generated from 0.2 mM $Ru(bpy)_3(PF_6)_2$ in dry ACN with 0.1 M NBu_4PF_6 at various rotation rates (0 – 2000 RPM) at 610 nm where the second ruthenium reduction was held at -1.58 V at the disk electrode, while the oxidation was simultaneously held at 1.32 V at the ring electrode 10 s

$$Ru + Ru^{3+} \overset{k_2}{\rightarrow} Ru^{+} + Ru^{2+*} \quad \textbf{[4.9]}$$

The annihilation ECL intensities from reaction [4.9] when using this new hold-hold method (Figure 4.46) where the second reduction of the ruthenium complex was held at -1.58 V at the disk and the oxidation held at 1.32 V at the ring under rotation (Figure 4.45) are almost three times greater than the intensities generated from the same system when the hold-sweep experiment was used. Again the system displays the critical RPM phenomena at about 550 RPM/57.60 rad/s highlighted by its Levich study in Figure 4.47.

$$Ru^{-} + Ru^{3+} \overset{k_3}{\rightarrow} Ru + Ru^{2+*} \quad \textbf{[4.11]}$$

For reaction [4.11], a more comprehensive RPM study (Figures 4.49 and 4.50) was performed to determine the exact RPM where the critical RPM of $Ru(bpy)_3(PF_6)_2$ takes place. To do this we held the third ruthenium reduction at the disk and the ruthenium oxidation at the ring (Figure 4.48). This detailed RPM study was performed on this system in particular since we previously determined that this system would generate the highest intensities of annihilation ECL due to the larger ΔG of the system (see Table 4.2) compared to the other two $Ru(bpy)_3(PF_6)_2$ systems.

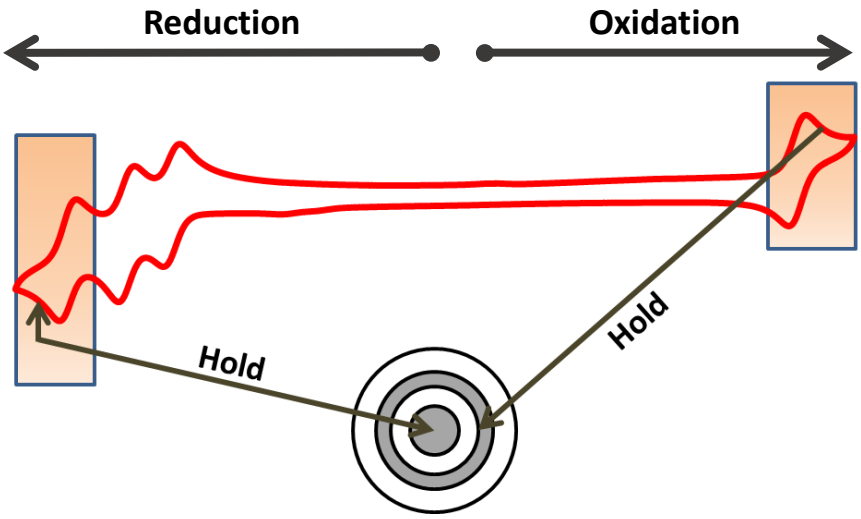

Figure 4.48: Representation of a hold-hold annihilation ECL experiment of 0.2 mM $Ru(bpy)_3(PF_6)_2$ in dry ACN with 0.1 M NBu_4PF_6 using a RRDE where the third ruthenium reduction was held at -1.82 V at the disk electrode, while the oxidation was simultaneously held at 1.32 V at the ring electrode

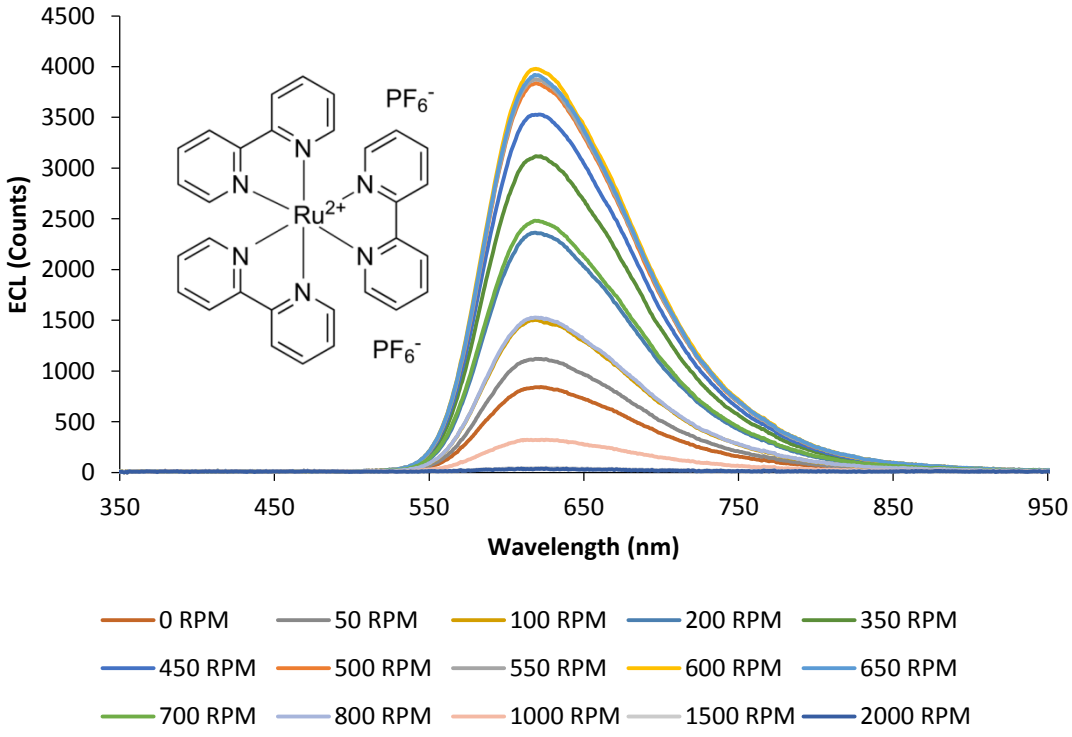

Figure 4.49: Spectra of the annihilation ECL generated from 0.2 mM $Ru(bpy)_3(PF_6)_2$ in dry ACN with 0.1 M NBu_4PF_6 at various rotation rates (0 – 2000 RPM) where the third ruthenium reduction was held at -1.82 V at the disk electrode, while the oxidation was simultaneously held at 1.32 V at the ring electrode for 10 s

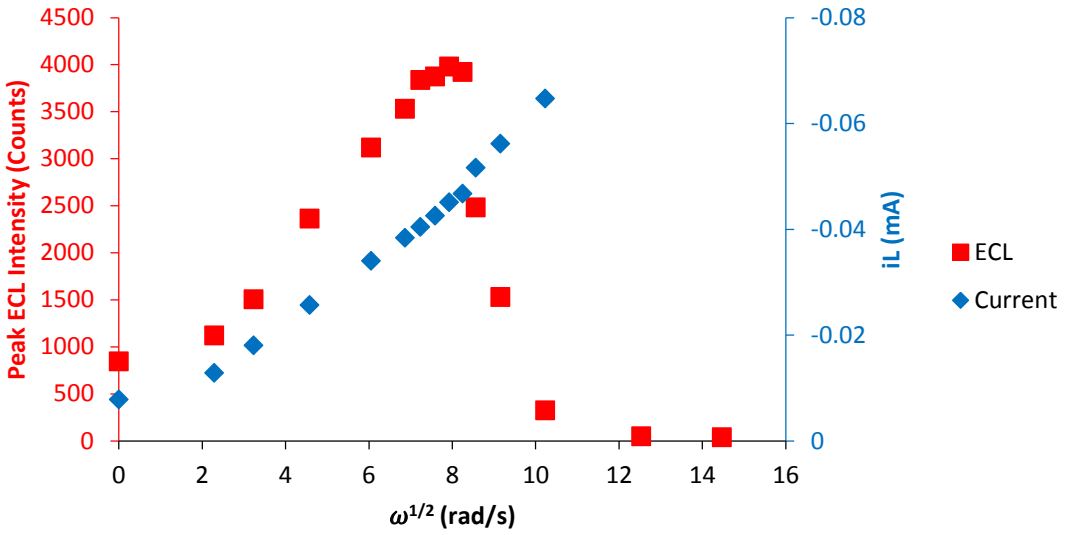

Figure 4.50: Levich plot of the peak annhilation ECL intensities (red) and the current (blue) generated from 0.2 mM $Ru(bpy)_3(PF_6)_2$ in dry ACN with 0.1 M NBu_4PF_6 at various rotation rates (0 – 2000 RPM) at 610 nm where the third ruthenium reduction was held at -1.82 V at the disk electrode, while the oxidation was simultaneously held at 1.32 V at the ring electrode for 10 s

The annihilation ECL intensities generated when the third ruthenium reduction is held at the disk and the oxidation held at the ring (Figure 4.49) are almost seven times greater than the intensities generated from the same system when the hold-sweep experiment was used to hold the third ruthenium reduction at the ring while sweeping the oxidation at the disk (Figure 4.18). The Levich study of the annihilation ECL intensities generated from 0.2 mM $Ru(bpy)_3(PF_6)_2$ (Figure 4.50) shows that the critical RPM of this system is approximately 625 RPM/65.45 rad/s.

Another detailed RPM study was then performed to determine the critical RPM of the $Ir(ppy)_3$ annihilation ECL system (reaction [4.12]) where the iridium reduction was held the ring while the iridium oxidation was held at the disk (Figure 4.51).

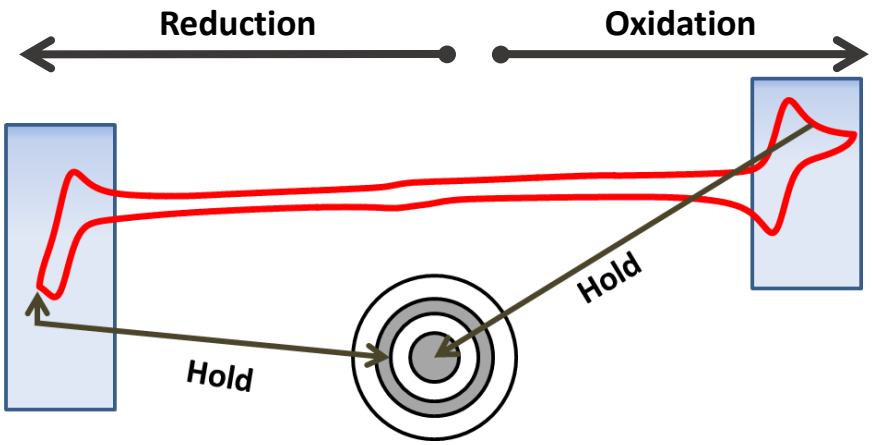

Figure 4.51: Representation of a hold-hold annihilation ECL experiment of 0.2 mM $Ir(ppy)_3$ in dry ACN with 0.1 M NBu_4PF_6 using a RRDE where the iridium reduction was held at -2.35 V at the ring electrode, while the oxidation was simultaneously held at 0.74 V at the disk electrode

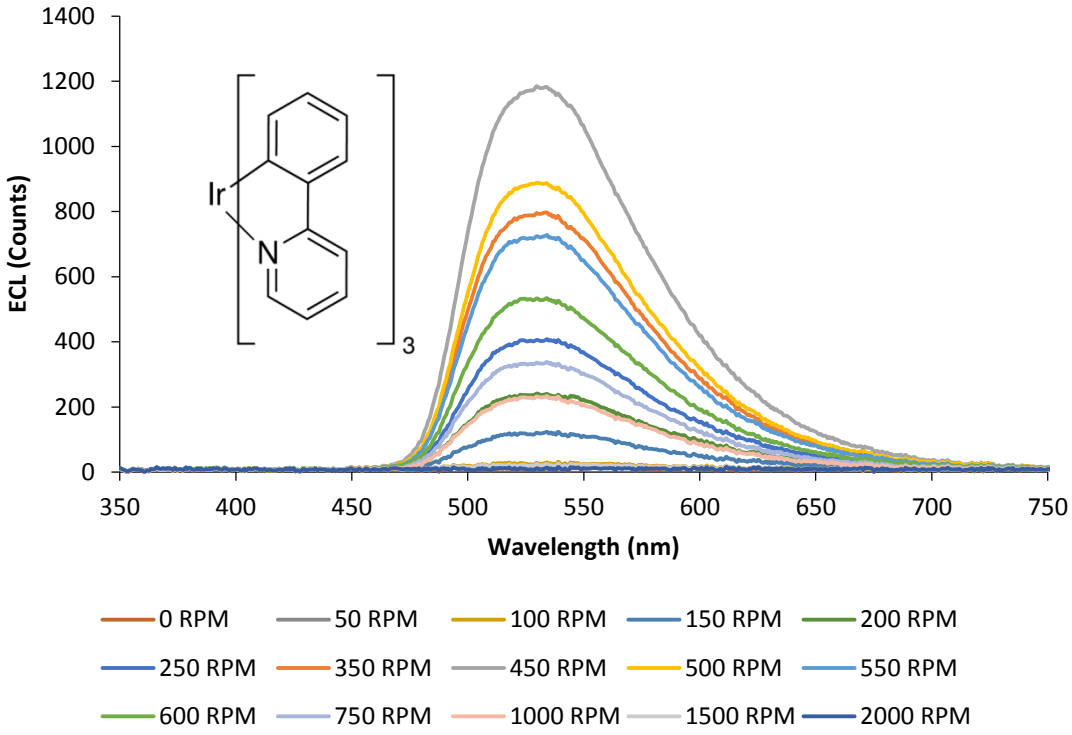

Figure 4.52: Spectra of the annihilation ECL generated from 0.2 mM $Ir(ppy)_3$ in dry ACN with 0.1 M NBu_4PF_6 at various rotation rates (0 – 2000 RPM) where the iridium reduction was held at -2.35 V at the ring electrode, while the oxidation was simultaneously held at 0.74 V at the disk electrode for 10 s

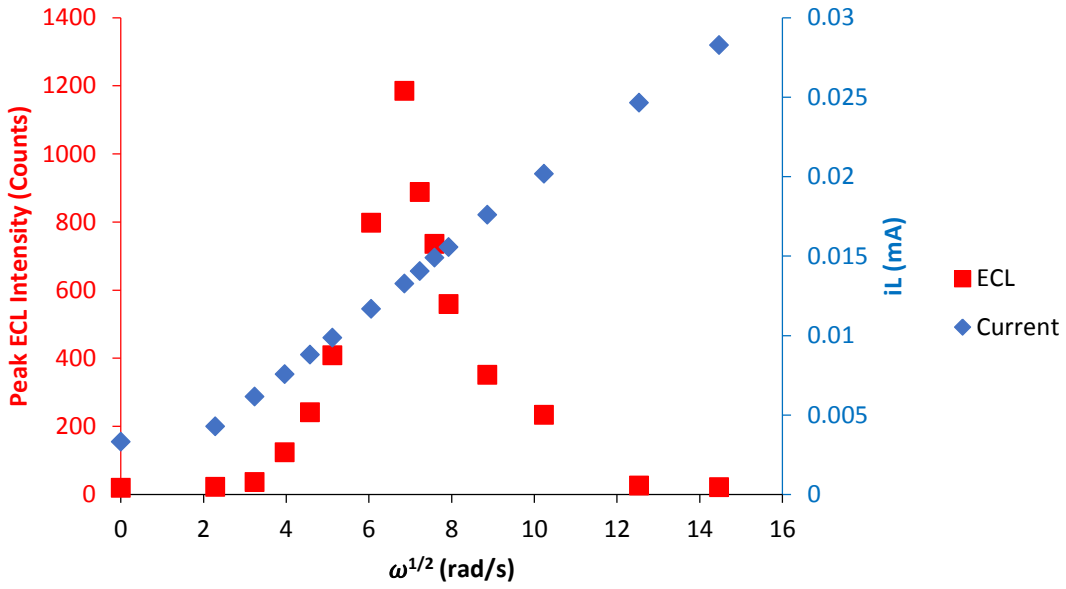

Figure 4.53: Levich plot of the peak annhilation ECL intensities (red) and the current (blue) generated from 0.2 mM $Ir(ppy)_3$ in dry ACN with 0.1 M NBu_4PF_6 at various rotation rates (0 – 2000 RPM) at 520 nm when the iridium reduction was held at -2.35 V at the ring electrode, while the oxidation was simultaneously held at 0.74 V at the disk electrode for 10 s

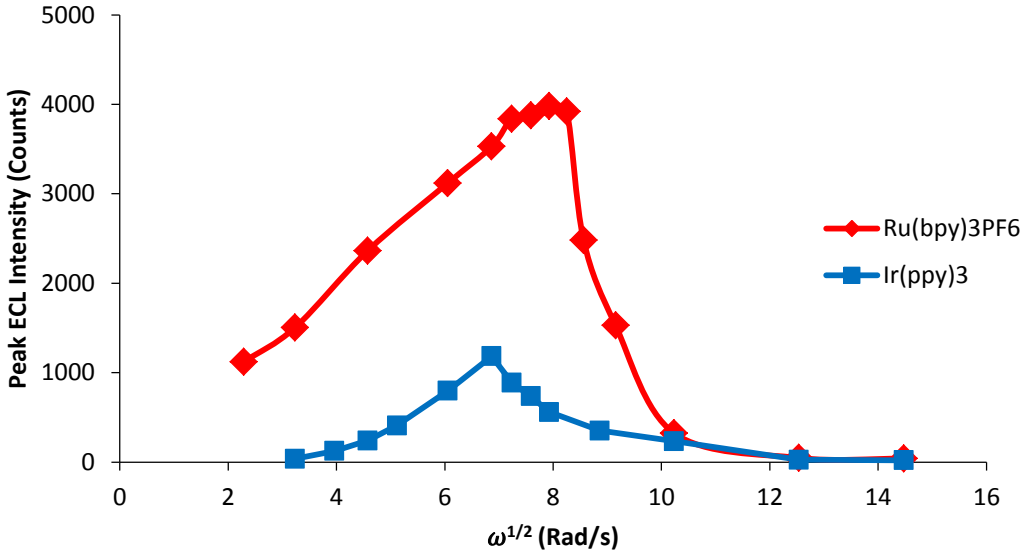

Figure 4.54: Levich plots of the peak annhilation ECL intensities generated from 0.2 mM $Ru(bpy)_3(PF_6)_2$ (red plot, when the third ruthenium reduction was held at -1.82 V at the disk electrode, while the oxidation was simultaneously held at 1.32 V at the ring electrode) and 0.2 mM $Ir(ppy)_3$ (blue plot, where the iridium reduction was held at -2.35 V at the ring electrode, while the oxidation was simultaneously held at 0.74 V at the disk electrode) in dry ACN with 0.1 M NBu_4PF_6 at various rotation rates, highlighting the difference in critical RPMs for each system

The annihilation ECL intensities generated when the iridium reduction is held at the ring and the oxidation held at the disk (Figure 4.52) are an order of magnitude greater than the intensities generated from the same system when the hold-sweep experiment was used to hold the iridium reduction at the ring while sweeping the oxidation at the disk (Figure 4.28). The Levich study of the annihilation ECL intensities generated from 0.2 mM $Ir(ppy)_3$ (Figure 4.53) shows that the critical RPM of this system occurs at 450 RPM/47.12 rad/s.

Interestingly, Figure 4.54 shows that the critical RPM observed in the $Ir(ppy)_3$ annihilation ECL system occurs at a slower RPM than that of the $Ru(bpy)_3(PF_6)_2$ system under similar conditions (approx. 450 RPM and 650 RPM respectively). Essentially, the $Ru(bpy)_3(PF_6)_2$ system requires a faster rotation rate, compared to $Ir(ppy)_3$, for the rate of removal of the reduced species to be greater than the rate of the reaction generating the excited species, resulting in the decline in ECL intensities observed at higher RPM.

While the phenomenon of decreased ECL intensity at rotation rates faster than the critical RPM during RRDE annihilation ECL has not been observed previously, interestingly however the phenomenon was predicted in an early paper by Allen Bard's group published in 1971.[4] In this paper, Maloy and Bard conducted finite element simulations which showed that the RRDE ECL intensity ought to increase with rotation rate up to a point. They predicted that at faster rotation rates, the species generated at the disk is swept past the doughnut shaped plume of ring-generated species before the annihilation reaction has time to occur, resulting in a decrease in ECL response at a high rotation rate, which is governed by the kinetics of the annihilation reaction:

$$Ru(red) + Ru(ox) \xrightarrow{k_{ann}} Ru^{*} + Ru \qquad \textbf{[4.14]}$$

The authors defined the dimensionless parameter XKCT (Eqn. 4.1) where *v* is the kinematic viscosity of the solvent (4.48 x 10^{-3} cm^2s^{-1} for acetonitrile), D is the diffusion coefficient of the luminophore and [Ru] is the concentration of the luminophore. Variations in this parameter determine the extent to which rotation competes with kinetics; and if ECL intensity (I_{ECL}) is plotted as a function of the square root of XKCT a maximum is predicted by simulations at $(XKCT)^{½} = 0.4$. We can use this prediction as a basis for obtaining kinetic information regarding ECL reactions.

$$XKCT = (\nu/_D)^{\frac{1}{3}} k_{ann} [Ru] \omega^{-1} \quad \textbf{Eqn. 4.1}$$

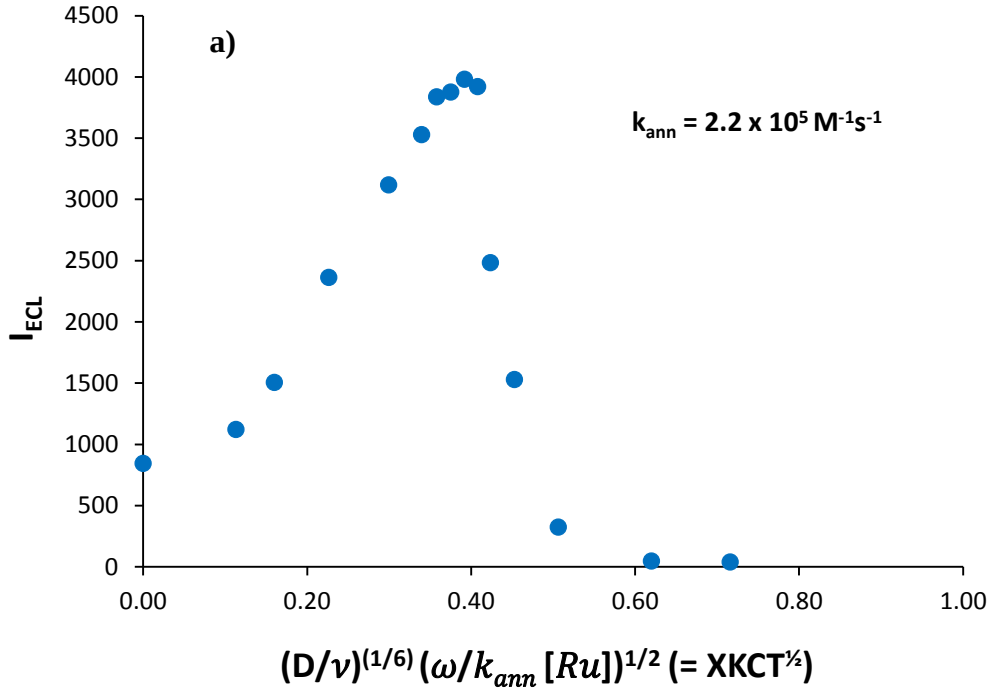

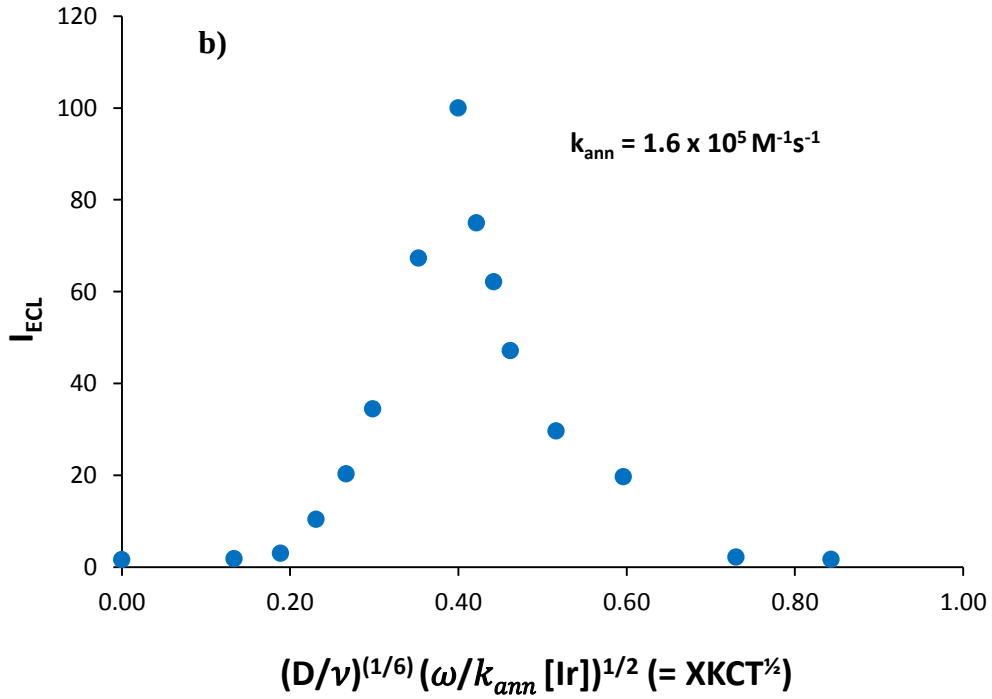

Figure 4.55: (a) Plot of ECL intensity for the third ruthenium reduction, as a function of the dimensionless parameter $(D/\nu)^{(1/6)}$ $(\omega/k_{ann}$ $[Ru])^{1/2}$ or sqrt(XKCT). (b) The same plot for the Ir^-/Ir^+ annihilation ECL reaction. These plots are used to estimate k_{ann} by varying the value of k_{ann} until the maximum value of sqrt(XKCT) = 0.4.[4]

Figure 4.55(a) shows the data for the rotation rate dependence of the annihilation reaction between Ru^{3+} and Ru^{-1} where k_{ann} has been set to a value such that the maximum at the graph lies at 0.4. Imposing this constraint on Eqn. 4.1 and substituting in the values of D and , yields a value of 2.2 x 105 $M^{-1}s^{-1}$ for (k_{ann}), the rate of reaction [4.11]. Similar analysis for the data relating to reactions [4.7] and [4.9] give values of 1.78 x 10^5 $M^{-1}s^{-1}$ and 1.96 x 10^5 $M^{-1}s^{-1}$ respectively. Table 4.2 reveals an upward trend in the kinetics of the annihilation reaction with the exergonicity calculated using the example of the Ru^{+}/Ru^{3+} annihilation ECL system:

$$-\Delta G_{ann} = e\left[E^o(Ru^{2+/3+}) - E^o(Ru^{2+/+})\right] - E_{es} = 2.68 - 2.05 = 0.58 \text{ eV}$$

Eqn. 4.2

Where 2.68 V is the difference between the two redox potentials, *e* is the elementary charge (= 1 eV/V) and E_{es} (2.05 eV) is the energy of the excited state product, estimated from the emission spectrum using the following equation:

$$E_{es} = \frac{hc}{\lambda_{max}}$$

Eqn. 4.3

This upward trend in the kinetics of the annihilation reaction with the exergonicity can be rationalised if we regard the ECL annihilation reactions as occurring in the so-called normal Marcus region where electron transfer rate increases with -ΔG.[26–28]

Table 4.2: Critical RPM and kinetic information for various annihilation ECL reactions

Annihilation Reaction	Critical RPM	k_{ann} ($M^{-1}s^{-1}$)	ΔG (eV)
$Ir^{+} + Ir^{-1} \rightarrow Ir^{*} + Ir$	450	1.60 x 10^5	-1.02
$Ru^{3+} + Ru^{+} \rightarrow Ru^{2+*} + Ru^{2+}$	500	1.78 x 10^5	-0.58
$Ru^{3+} + Ru^{0} \rightarrow Ru^{2+*} + Ru^{+}$	550	1.96 x 10^5	-0.83
$Ru^{3+} + Ru^{-1} \rightarrow Ru^{2+*} + Ru^{0}$	625	2.20 x 10^5	-1.07

Annihilation ECL kinetics are considered amongst the fastest known reactions of this type and might therefore be expected to approach the diffusion-controlled limit.[4] Therefore, it is instructive to compare the values obtained in this study with the maximum possible rate in acetonitrile based on the equation of Osborne and Porter,[29] where the viscosity (η) of acetonitrile is 790 kg m^{-3},[30] R is the universal gas constant and T is the temperature in Kelvin (298 K).

$$k = \frac{8RT}{1000\eta} \qquad \textbf{Eqn. 4.4}$$

Using Eqn. 4.4, a hypothetical rate of 2.2 x 10^{10} $M^{-1}s^{-1}$ is obtained, so the actual values of k_{ann} are surprisingly low compared to the maximum possible (diffusion-controlled) rate in this light. It should be noted that Maloy and Bard were unable to evaluate the kinetics of the diphenylanthracene ECL reaction in their study as they did not observe a maximum in their graph. They put this down to the kinetics being too fast relative to the maximum rotation rate available to them. While the range of rotation rates available to us was similar, due to more modern light detection instrumentation available now compared to the early 1970's, we were able to use a significantly lower concentration of the luminophore in order to reach higher XKCT values, see Eqn. 4.1.

Also predicted by this paper was the linear dependence of I_{ECL} on $\omega^{0.5}$ in the rising portion of the graph according to the equation:

$$I_{ECL} = 0.62\Phi_{ECL}ADCD^{\frac{2}{3}}\nu^{-\frac{1}{6}}\omega^{\frac{1}{2}} \qquad \textbf{Eqn. 4.5}$$

where Φ_{ECL} is the ECL efficiency, C is the concentration of the electroactive species, A the area of the electrode, D is the diffusion coefficient of the molecule or ion, ν is the kinematic viscosity of the solution and ω is the angular rotation rate of the working electrode.

This is essentially the analogous form of the Levich equation for ECL describing the dependence of ECL intensity, rather than current, on rotation rate. The results for the annihilation ECL reactions involving the first, second and third reductions of $Ru(bpy)_3^{2+}$ are plotted in Figure 4.56 below. As *A*, *D*, *C* and *ν* are identical for each system these data can be interpreted to as reflecting a higher ECL efficiency for the reactions with faster kinetics, see Table 4.2. Figure 4.57 shows the same plot for the Ir^-/Ir^+ annihilation ECL reaction. In this case a negative intercept and non-linearity is observed at low rotation rates (less than 450 RPM). This can be interpreted as a result of the instability of the Ir^- species as noted in Section 4.3.1. A similar conclusion was drawn by Bard and Maloy for the RRDE-ECL of diphenylanthracene in dimethylformamide.[4]

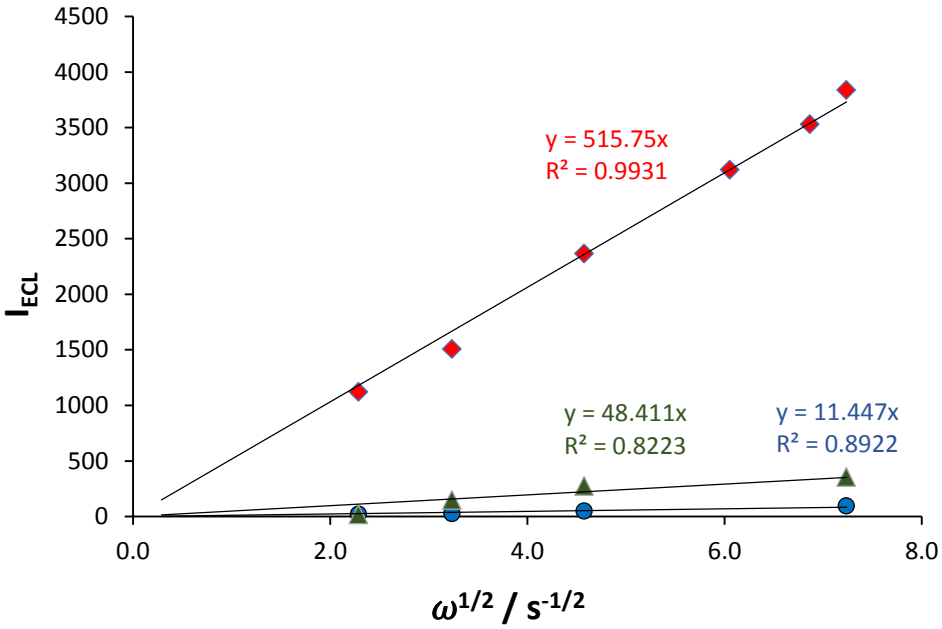

Figure 4.56: Dependence of ECL intensity on $\omega^{1/2}$ for the low rotation rates up to 2000 RPM for the Ru^{-1}/Ru^{3+}, Ru^0/Ru^{3+} and Ru^+/Ru^{3+} RRDE-annihilation ECL systems

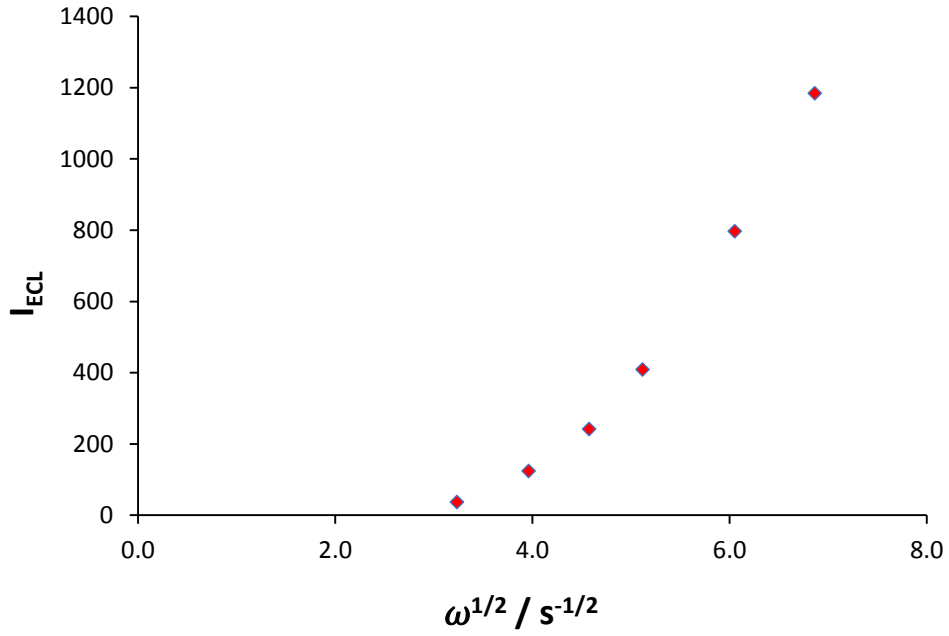

Figure 4.57: Dependence of ECL intensity on $\omega^{1/2}$ for the low rotation rates up to 2000 RPM for the Ir^{-}/Ir^{+} RRDE-annihilation ECL systems

4.3.4 Multiplexed annihilation ECL under rotation

After establishing that annihilation ECL from several luminophores could be achieved using an RRDE to generate the oxidised and reduced forms of the luminophore under rotation, we strived to achieve a multiplexed annihilation ECL system incorporating two of the previously studied luminophores, where either the potential corresponding to the oxidations or the reductions were scanned at the disk electrode while simultaneously holding the oxidation or reduction for one of the luminophores at the ring electrode to generate multiplexed emission.

This proved difficult however as we were only able to elicit ECL intensity from the $Ru(bpy)_3(PF_6)_2$/$Ir(ppy)_3$ annihilation ECL system when we held the third ruthenium reduction at the ring electrode, while simultaneously scanning the oxidation potentials of iridium and ruthenium at the disk electrode, as shown in Figure 4.58. Other configurations (i.e. (i) holding the ruthenium oxidation potential at the ring electrode, while sweeping the ruthenium and iridium reductions at the disk electrode, or (ii) holding the iridium reduction potential at the ring electrode while sweeping the ruthenium and iridium oxidations at the disk electrode), and other multiplexed systems (i.e. the $Ru(bpy)_3(PF_6)_2$/$(Ir[dF(CF_3)ppy]_2(dtbpy))PF_6$ multiplexed system) either did not emit ECL emissions or did not emit any detectable light intensity.

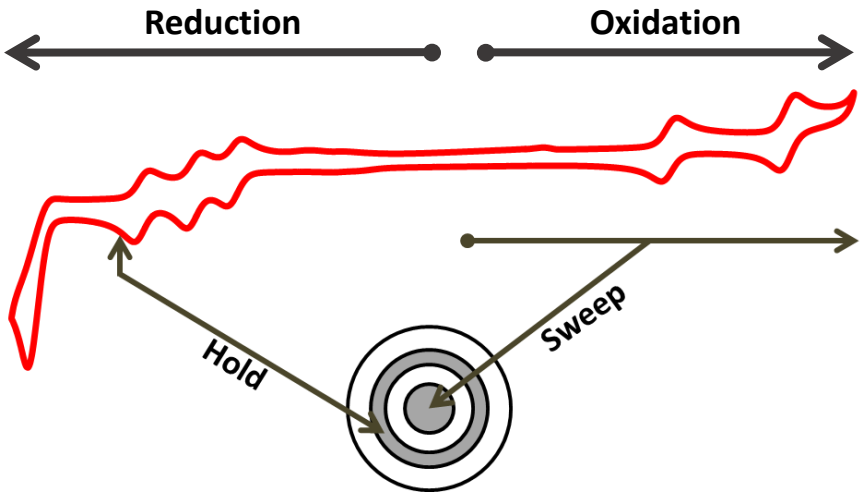

Figure 4.58: Representation of a hold-sweep annihilation ECL experiment of the 0.2 mM $Ru(bpy)_3(PF_6)_2$/0.2 mM $Ir(ppy)_3$ multiplexed annihilation ECL system in dry ACN with 0.1 M NBu_4PF_6 using a RRDE where the third ruthenium reduction was held at -1.82 V at the ring electrode, while the potential was scanned from 0 V to 1.50 V at the disk electrode

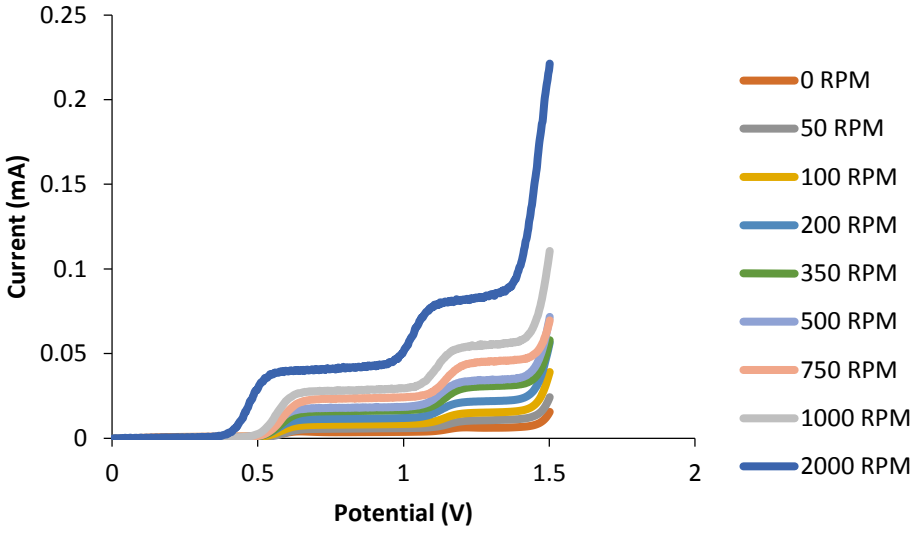

Figure 4.59: Voltammograms of the disk currents generated using a multiplexed solution containing 0.2 mM $Ru(bpy)_3(PF_6)_2$/0.2 mM $Ir(ppy)_3$ in dry ACN with 0.1 M NBu_4PF_6 at various RPMs (0 – 2000 RPM) where the third ruthenium reduction was held at -1.82 V at the ring electrode, while the potential was scanned from 0 V to 1.50 V at the disk electrode

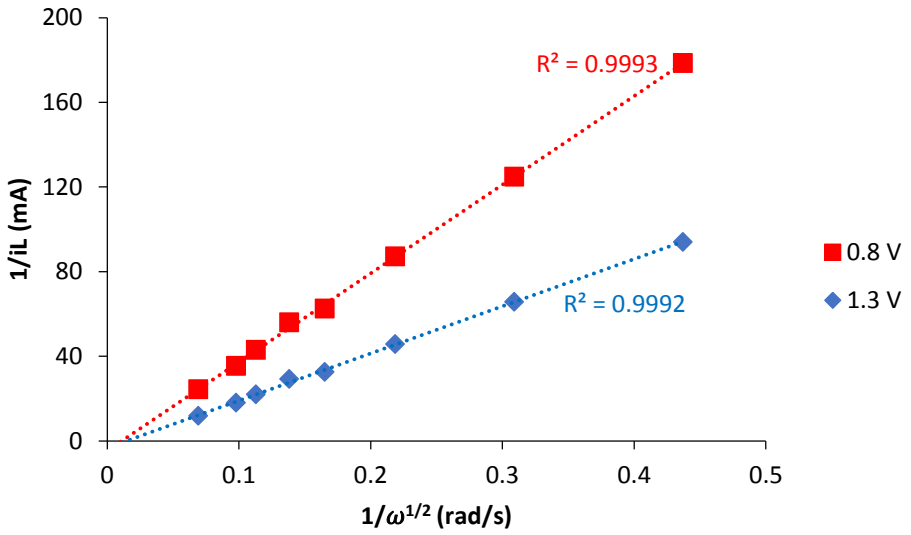

Figure 4.60: Koutecky-Levich plots of the currents generated at 0.8 V (red plot) and 1.3 V (blue plot) from a multiplexed solution containing 0.2 mM $Ru(bpy)_3(PF_6)_2$/0.2 mM $Ir(ppy)_3$ in dry ACN with 0.1 M NBu_4PF_6 at various RPMs (0 – 2000 RPM) where the third ruthenium reduction was held at -1.82 V at the ring electrode, while the potential was scanned from 0 V to 1.50 V at the disk electrode

Figure 4.59 shows two steady state current plateaus representing $Ir(ppy)_3$ (the first steady state current plateau) and $Ru(bpy)_3(PF_6)_2$ (the second steady state current plateau). Similar to when the luminophores were rotated separately, an increase of the limiting current occurs with the increase of rotation rate (Figure 4.60).

While the $Ru(bpy)_3(PF_6)_2$/$Ir(ppy)_3$ annihilation ECL system was the only multiplexed system to generate detectable ECL intensities using the hold-sweep method, no detectable iridium emission occurred at 520 nm. Interestingly however, at 610 nm (the wavelength where we should observe ECL emission from ruthenium), two emissive peaks at 0.8 V and 1.2 V are present (as seen in Figure 4.61). The 3D plot in Figure 4.63 shows this more clearly. At 610 nm, one emissive peak occurs at a potential where ruthenium emission is typically observed however the other emissive peak occurs at a potential where we typically observe the iridium emission.

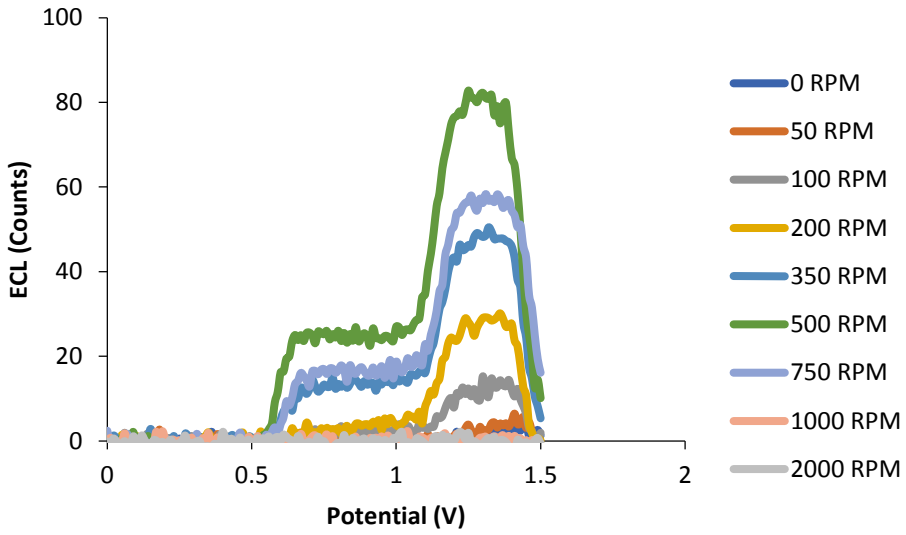

Figure 4.61: Voltammograms of the ECL intensities generated using a multiplexed solution containing 0.2 mM $Ru(bpy)_3(PF_6)_2$/0.2 mM $Ir(ppy)_3$ in dry ACN with 0.1 M NBu_4PF_6 at various RPMs (0 – 2000 RPM) where the third ruthenium reduction was held at -1.82 V at the ring electrode, while the potential was scanned from 0 V to 1.50 V at the disk electrode. Intensities observed at 610 nm.

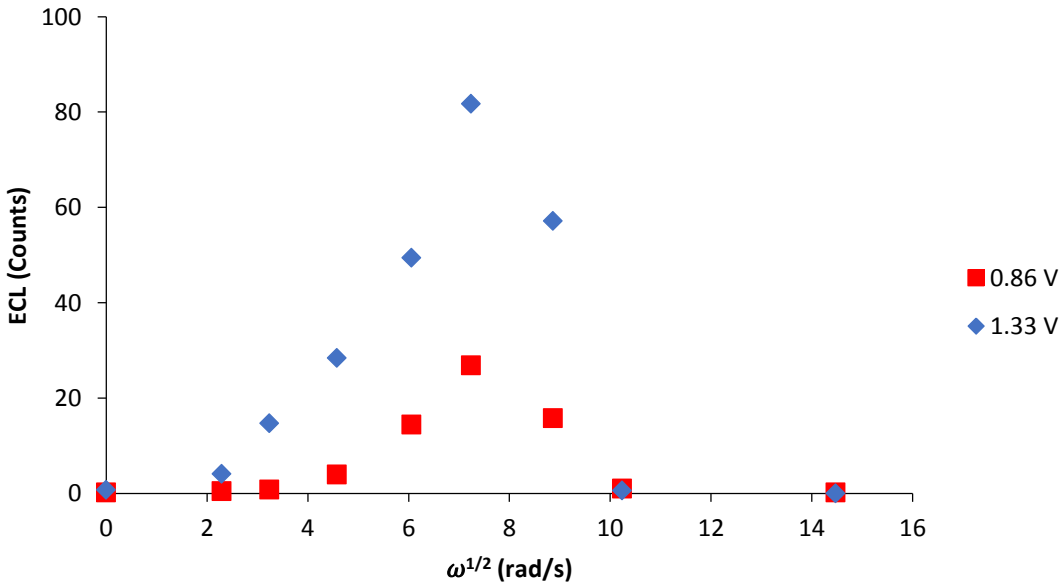

Figure 4.62: Levich plots ECL intensities generated at 0.86 V (red plot) and 1.33 V (blue plot) from a multiplexed solution containing 0.2 mM $Ru(bpy)_3(PF_6)_2$/0.2 mM $Ir(ppy)_3$ in dry ACN with 0.1 M NBu_4PF_6 at various RPMs (0 – 2000 RPM) where the third ruthenium reduction was held at -1.82 V at the ring electrode, while the potential was scanned from 0 V to 1.50 V at the disk electrode. Intensities observed at 610 nm

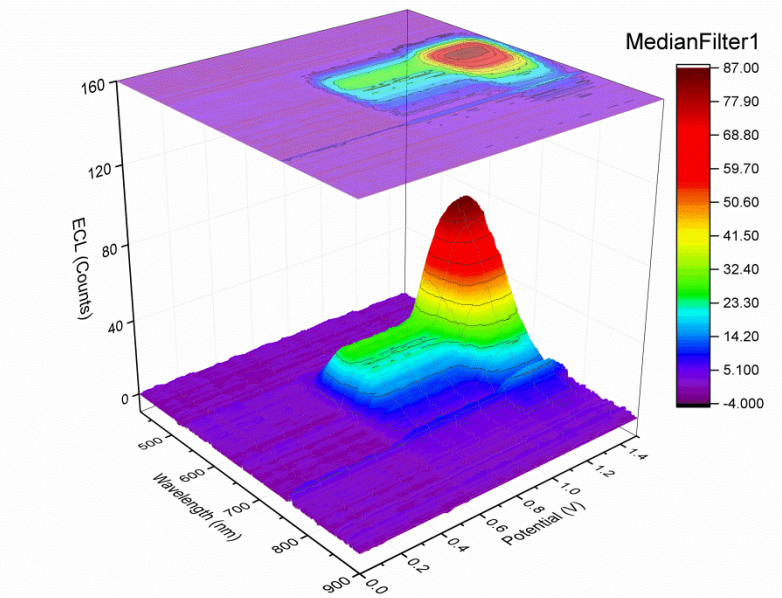

Figure 4.63: 3D plot of the ECL generated from a multiplexed solution containing 0.2 mM $Ru(bpy)_3(PF_6)_2$/0.2 mM $Ir(ppy)_3$ in dry ACN with 0.1 M NBu_4PF_6 at 500 RPM where the third ruthenium reduction was held at -1.82 V at the ring electrode, while the potential was scanned from 0 V to 1.50 V at the disk electrode

This was interesting as we did not observe the typical green emission that is synonymous with $Ir(ppy)_3$, instead a red emission is observed at this potential. The Levich plot (Figure 4.62) shows that the critical RPM phenomena occurs again at 0.86 V and 1.33 V, where an increase of ECL intensities (at both emitting potentials) under electrode rotation occurs until the critical RPM of the system (approximately 500 RPM/52.36 rad/s in this system) is reached. We then observe a decrease of both emissions at rotation rates past the critical RPM while the currents generated from the system continues to increase at rotation rates past the critical RPM.

In order to rule out energy transfer as the reason for the anomalous emission of red ECL at the Ir/Ir^+ redox potential, lifetime studies were performed (see Figure 4.64 and supplementary information Table S1). We can presume that no energy transfer (except possibly trivial energy transfer) occurs in our multiplex system when the third ruthenium

reduction was held at -1.82 V at the ring electrode, while the oxidation potential for iridium and ruthenium was swept from 0 V to 1.50 V at the disk electrode.

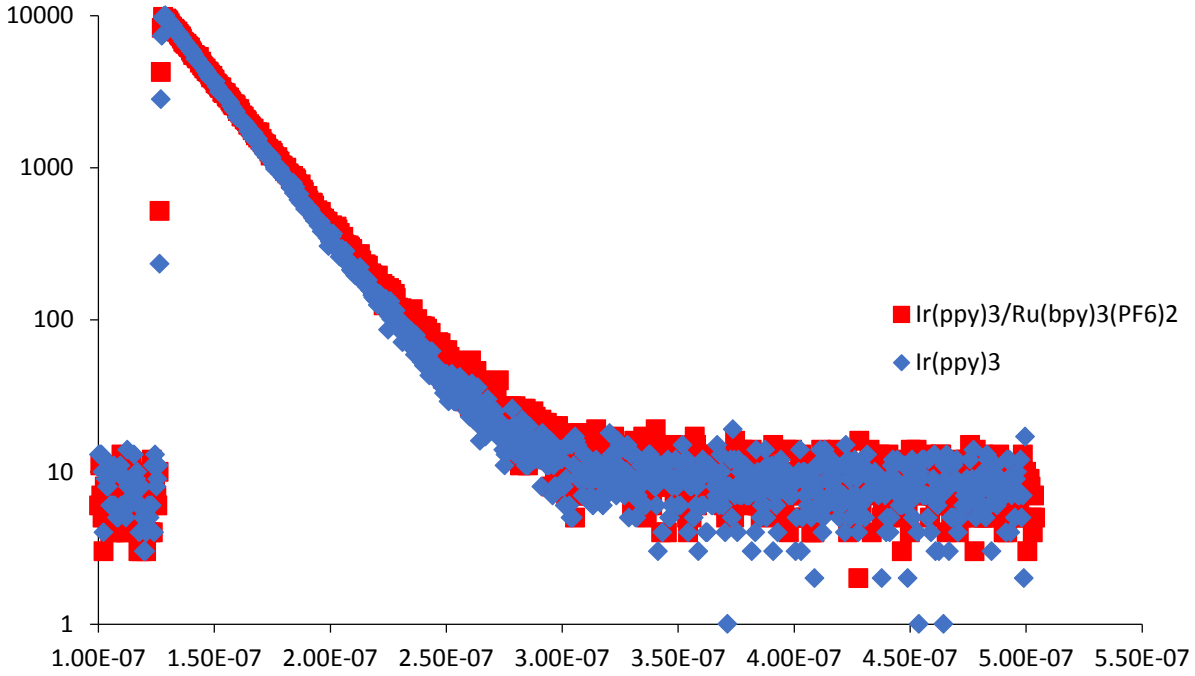

Figure 4.64: Luminescence decay curves of the $Ir(ppy)_3$ and the multiplexed $Ru(bpy)_3(PF_6)_2/Ir(ppy)_3$ annihilation ECL systems highlighting the trivial energy transfer occurring in the multiplexed system

As shown by the study in Section 4.3.2, both the $Ru(bpy)_3(PF_6)_2$ and $Ir(ppy)_3$ annihilation ECL systems prefer a particular electrode polarity to generate intense annihilation ECL emissions, we revisited the multiplexed $Ru(bpy)_3(PF_6)_2/Ir(ppy)_3$ ECL system to determine if we could not only achieve multiplexed emission (light emission from two luminophores in the same system), but also achieved tuneable ECL emission (either red or green emission) by varying the applied potentials at the ring and disk electrodes under rotation.

This proved difficult in terms of eliciting multiplexed ECL. As we previously determined that annihilation ECL from $Ir(ppy)_3$ could only occur when the iridium reduction was held at the ring and oxidation held at the disk, we could only use a single electrode polarity if we were to generate emissions from both $Ru(bpy)_3(PF_6)_2$ and $Ir(ppy)_3$. A careful balancing act of luminophore concentrations and applied potential were also required to elicit multiplexed ECL emissions under rotation using a RRDE (something that has not been reported in literature).

Incorporating information from previously published work on multiplexed ECL systems using stationary non-RRDE electrodes,[31,32] a new method was developed and performed on a multiplexed system containing 0.025 mM $Ru(bpy)_3(PF_6)_2$ and 0.25 mM $Ir(ppy)_3$ in dry ACN with 0.1 M NBu_4PF_6. A stationary, non-rotating RRDE was pulsed solely at the disk electrode between various different potential limits, defined by the redox potentials of the relevant processes, (see Figure 4.65 for values). These experiments were used to determine the optimal concentrations of each luminophore in this system for tuneable and detectable multiplexed ECL emissions.

Figure 4.65 shows green emission from our multiplexed system when the disk electrode was pulsed between -1.73 V and 1.4 V, red emission when the disk electrode was pulsed between -3.10 V and 0.77 V, and multiplexed emission when the disk electrode was pulsed between -2.90 V and 0.77 V. While the system was able to elicit tuneable multiplexed emissions using this new method, constant vigorous purging with nitrogen was required to elicit detectable ECL.

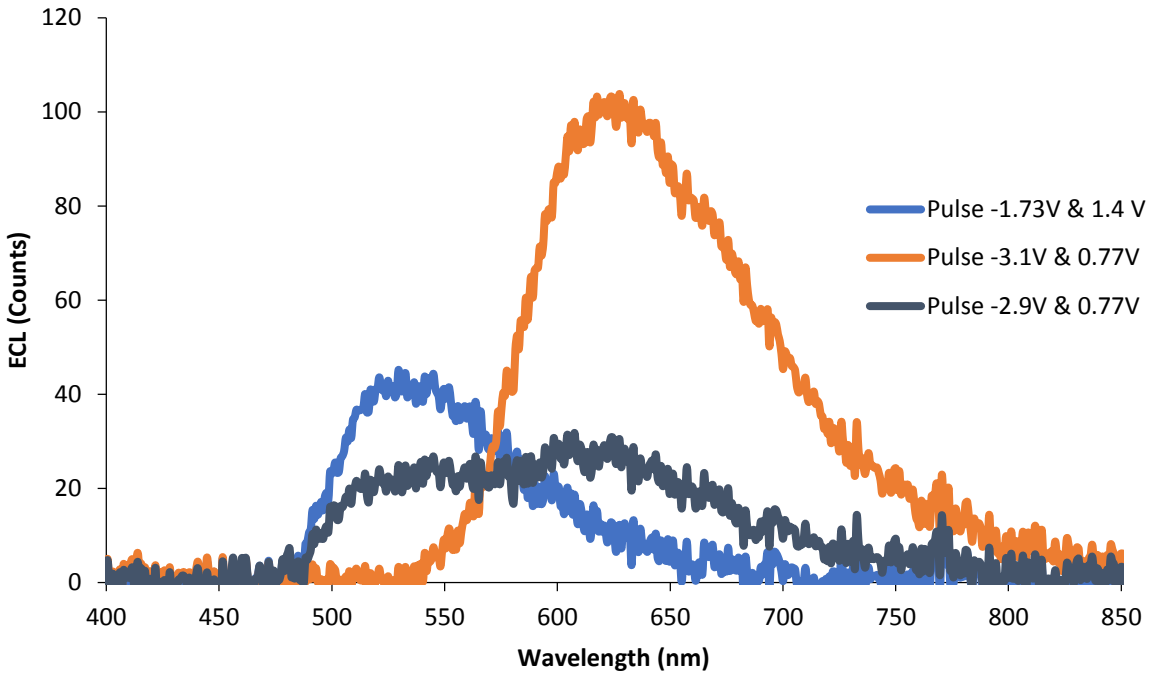

Figure 4.65: Spectra of the annihilation ECL generated from a multiplexed solution containing 0.025 mM $Ru(bpy)_3(PF_6)_2$/0.25 mM $Ir(ppy)_3$ in dry ACN with 0.1 M NBu_4PF_6 where a stationary non-rotating RRDE was pulsed solely at the disk electrode for 2 seconds between -1.73 V and 1.4 V (blue spectrum), -3.1 V and 0.77 V (orange spectrum) and -2.9 V and 0.77 V (purple spectrum)

Once we determined that the concentration of the luminophores used were able to elicit detectable multiplexed emissions, we then performed our hold-hold method on the 0.025 mM $Ru(bpy)_3(PF_6)_2$/0.25 mM $Ir(ppy)_3$ annihilation ECL system (Figure 4.66). Rotating the RRDE at 450 RPM (the critical RPM of the $Ir(ppy)_3$ annihilation ECL system where the greatest iridium ECL intensities was observed), green emission that is typically associated with $Ir(ppy)_3$ was detected (Figure 4.67) when the iridium oxidation was held at the ring and the iridium oxidation held at the disk (reaction [4.12]). No emission from $Ru(bpy)_3(PF_6)_2$ was observed at these parameters.

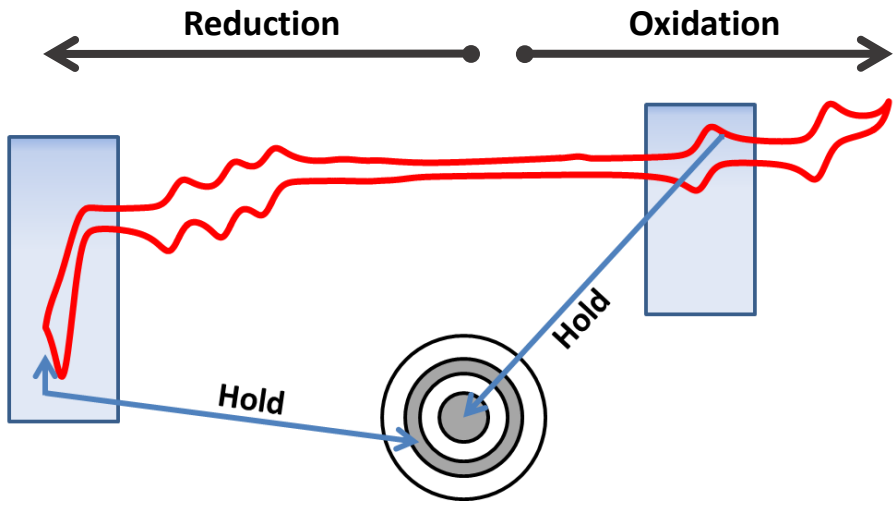

Figure 4.66: Representation of a hold-hold annihilation ECL experiment of the 0.025 mM $Ru(bpy)_3(PF_6)_2$/0.25 mM $Ir(ppy)_3$ multiplexed annihilation ECL system in dry ACN with 0.1 M NBu_4PF_6 using a RRDE where the ring electrode was held at -3.10 V while the disk electrode was simultaneously held at 0.77 V

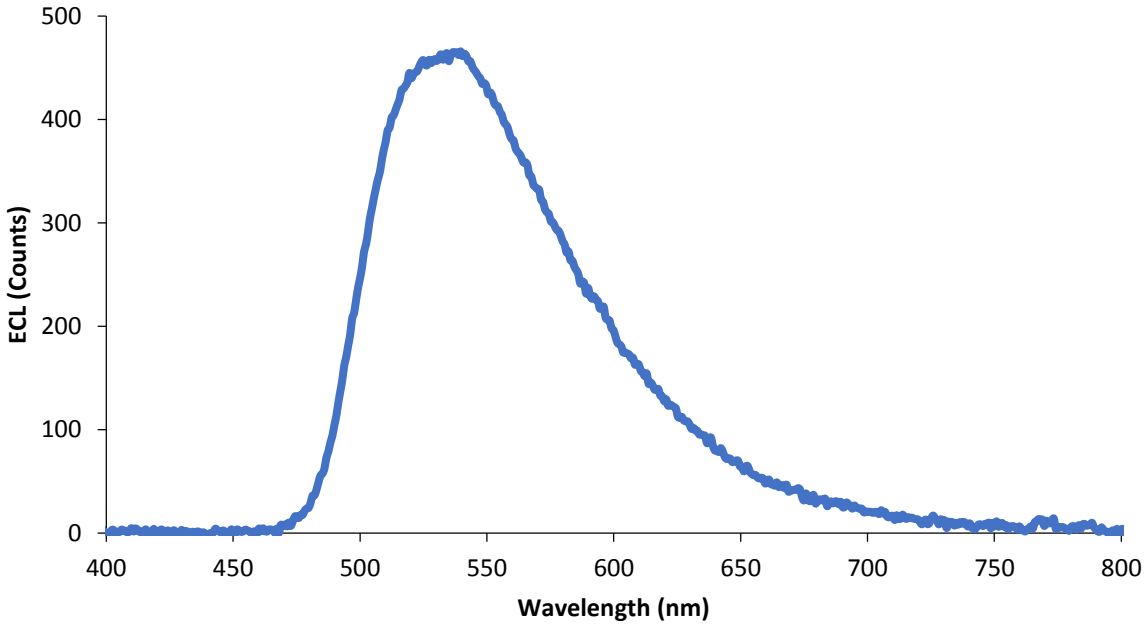

Figure 4.67: Spectrum of the annihilation ECL generated from a multiplexed solution containing 0.025 mM $Ru(bpy)_3(PF_6)_2$/0.25 mM $Ir(ppy)_3$ in dry ACN with 0.1 M NBu_4PF_6 where the ring electrode was held at -3.10 V while the disk electrode was simultaneously held at 0.77 V. The multiplexed system was rotated at the critical RPM of $Ir(ppy)_3$ (450 RPM)

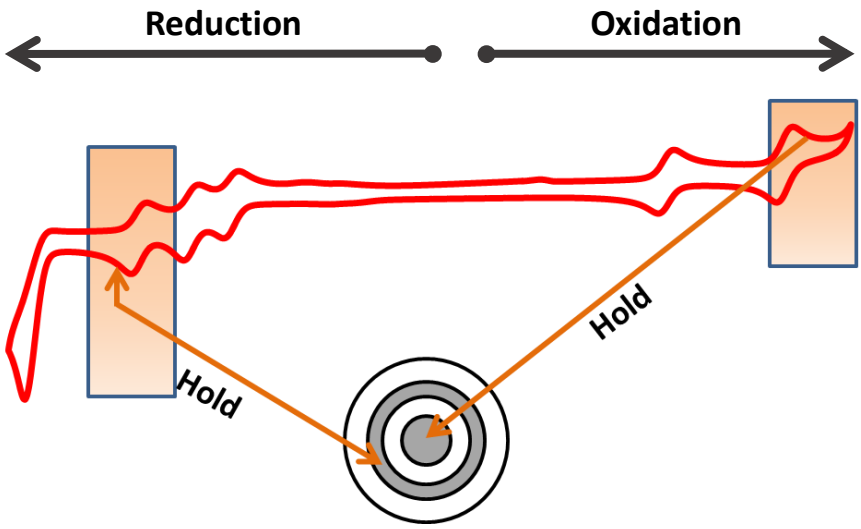

Figure 4.68: Representation of a hold-hold annihilation ECL experiment of the 0.025 mM $Ru(bpy)_3(PF_6)_2$/0.25 mM $Ir(ppy)_3$ multiplexed annihilation ECL system in dry ACN with 0.1 M NBu_4PF_6 using a RRDE where the ring electrode was held at -1.8 V while the disk electrode was simultaneously held at 1.4 V

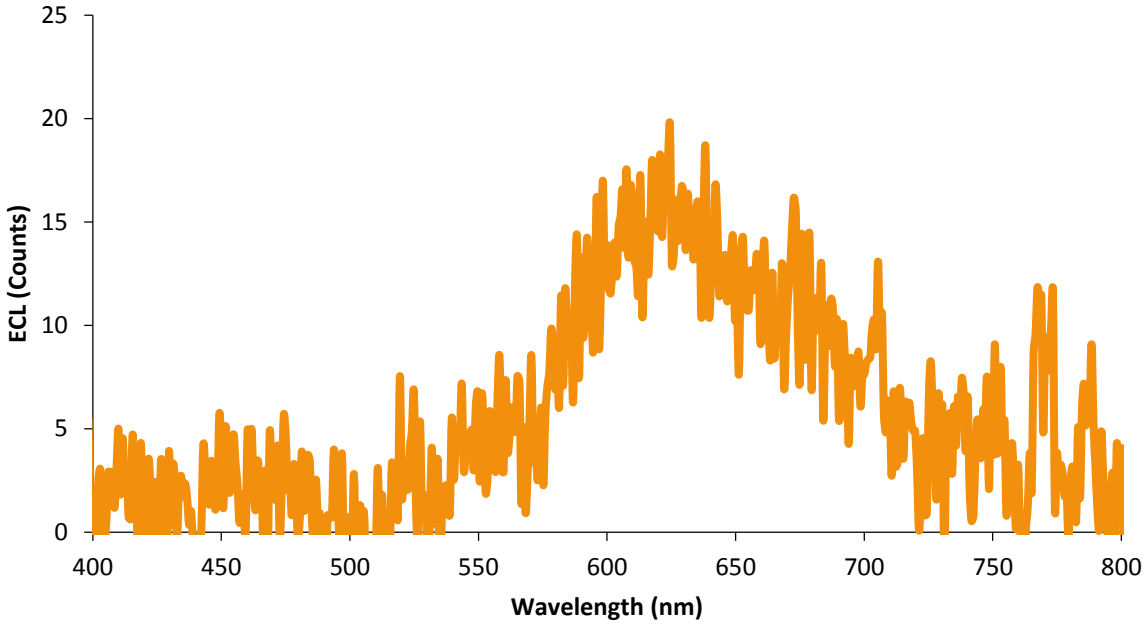

Figure 4.69: Spectra of the annihilation ECL generated from a multiplexed solution containing 0.025 mM $Ru(bpy)_3(PF_6)_2$/0.25 mM $Ir(ppy)_3$ in dry ACN with 0.1 M NBu_4PF_6 where the ring electrode was held at -1.8 V while the disk electrode was simultaneously held at 1.4 V. The multiplexed system was rotated at the critical RPM of $Ir(ppy)_3$ (450 RPM)

When the third ruthenium reduction potential at -1.8 V was held at the ring electrode, and the ruthenium oxidation potential at 1.4 V was held at the disk electrode to promote reaction [4.11] (Figure 4.68), the results obtained are shown in Figure 4.69. The low intensity red emission, attributed to $Ru(bpy)_3(PF_6)_2$, is due to the use of the less efficient electrode polarity (where the reduction is held at the ring while the oxidation is held at the disk) for $Ru(bpy)_3(PF_6)_2$ annihilation ECL emission since using the other electrode polarity (where the reduction is held at the disk while the oxidation is held at the ring) would not allow for the generation of multiplexed emissions (as no $Ir(ppy)_3$ emission occurred using the preferred electrode polarity of the $Ru(bpy)_3(PF_6)_2$ system). No emission from $Ir(ppy)_3$ was observed at these parameters.

Once we determined that we could selectively tune whichever coloured emission (green or red) under rotation, we set out to achieve multiplexed emission from both $Ru(bpy)_3(PF_6)_2$ and $Ir(ppy)_3$. To achieve such emissions, we held the iridium oxidation at 0.77 V at the disk electrode and held the ring electrode at -2.8 V, a potential that was between the iridium reduction and the third ruthenium reduction (Figure 4.70).

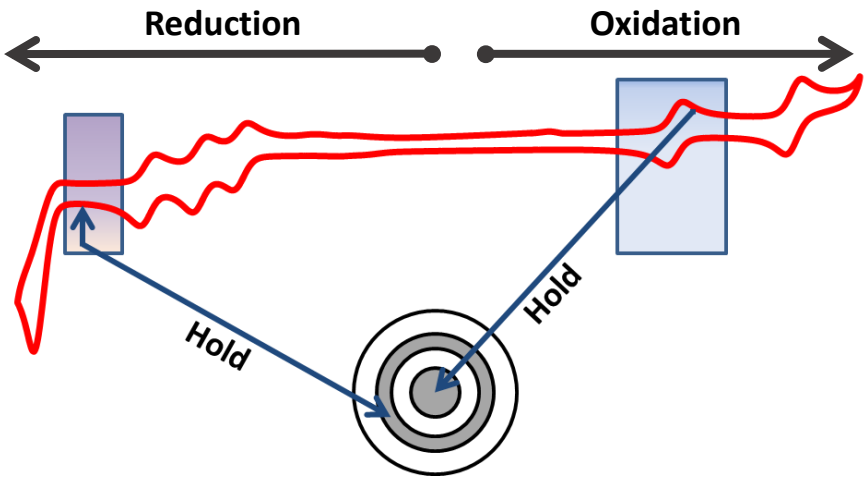

Figure 4.70: Representation of a hold-hold annihilation ECL experiment of the 0.025 mM $Ru(bpy)_3(PF_6)_2$/0.25 mM $Ir(ppy)_3$ multiplexed annihilation ECL system in dry ACN with 0.1 M NBu_4PF_6 using a RRDE where the ring electrode was held at -2.8 V while the disk electrode was simultaneously held at 0.77 V

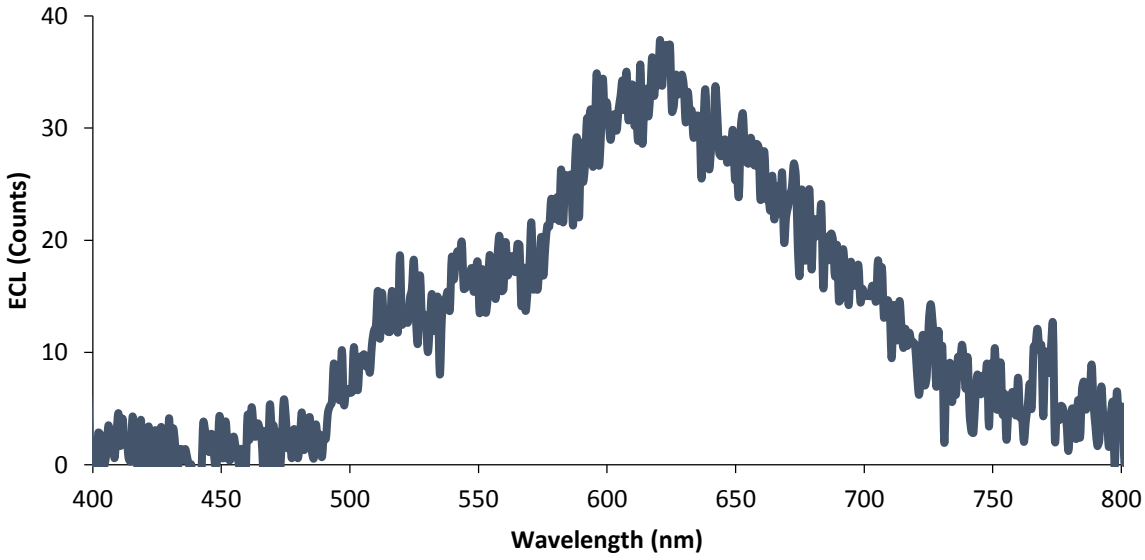

Figure 4.71: Spectra of the annihilation ECL generated from a multiplexed solution containing 0.025 mM $Ru(bpy)_3(PF_6)_2$/0.25 mM $Ir(ppy)_3$ in dry ACN with 0.1 M NBu_4PF_6 where the ring electrode was held at -2.8 V while the disk electrode was simultaneously held at 0.77 V. The multiplexed system was rotated at the critical RPM of $Ir(ppy)_3$ (450 RPM)

The spectrum in Figure 4.71 contains two peaks, one peak at 520 nm and another at 610 nm representing the green and red emissions from both $Ir(ppy)_3$ and $Ru(bpy)_3(PF_6)_2$, respectively, confirming that multiplexed annihilation ECL emission has occurred using the hold-hold method with an RRDE under rotation. Interestingly however, no multiplexed emissions were detected when the Ir^-/Ru^{3+} annihilation ECL system was examined under rotation.

Comparing the intensities generated from the hold-hold experiment with the intensities generated from when a stationary RRDE was pulsed solely at the disk electrode show an order of magnitude increase of $Ir(ppy)_3$ emissions when we selectively tune both systems to only emit green light. However, to observe this increase in $Ir(ppy)_3$ emissions, $Ru(bpy)_3(PF_6)_2$ emissions decrease when the hold-hold method is used compared to pulsing the stationary RRDE. The multiplexed ECL emissions observed from both methods were similar in intensity to each other, however, the hold-hold method under rotation did not require constant vigorous purging of nitrogen to generate multiplexed emission from both $Ir(ppy)_3$ and $Ru(bpy)_3(PF_6)_2$, unlike the pulsing method.

4.4 Conclusion

In conclusion, we observed increased current in annihilation ECL systems as we increase the rotation rate of the electrode. Increasing the rotation rate of the electrode does increase co-reactant and annihilation ECL intensities until we reach a critical RPM. At higher rotation rates past this critical value, we observed a decrease in ECL intensities. This was attributed to the rate of removal of the oxidised luminophore state (i.e. Ru^{+} in the $Ru(bpy)_3(PF_6)_2$ system) exceeding the rate of the key reaction in the annihilation pathway. Using the ECL intensity vs rotation rate data, we have assessed the kinetics of several annihilation ECL reactions, with reference to finite element simulations performed by Bard's group in 1971. The rate constants evaluated in this way varied with ΔG in agreement with the reactions being in the "normal" Marcus region. Interestingly the values of the rate constants were lower than might be expected. The electrode polarity of the RRDE also has a significant effect on the annihilation ECL intensity observed. Tuneable multiplexed emission from the $Ru(bpy)_3(PF)_6/Ir(ppy)_3$ annihilation ECL system was also achieved using an RRDE.

4.5 References

1 K. E. Haapakka and J. J. Kankare, *Anal. Chim. Acta*, 1982, **138**, 263–275.

2 K. E. Haapakka and J. J. Kankare, *Anal. Chim. Acta*, 1982, **138**, 253–262.

3 K. E. Haapakka, *Anal. Chim. Acta*, 1982, **139**, 229–236.

4 J. T. Maloy, K. B. Prater and A. J. Bard, *J. Am. Chem. Soc.*, 1971, **93**, 5959–5968.

5 J. T. Maloy and A. J. Bard, *J. Am. Chem. Soc.*, 1971, **93**, 5968–5981.

6 S. Vesztergom, M. Ujvári and G. G. Láng, *Electrochem. commun.*, 2012, **19**, 1–4.

7 S. Vesztergom and G. G. Lang, *Instrum. Sci. Technol.*, 2013, **41**, 82–95.

8 T. Lopes, J. Chlistunoff, J.-M. Sansiñena and F. H. Garzon, *Int. J. Hydrogen Energy*, 2012, **37**, 5202–5207.

9 J. L. Reyes-Rodríguez, F. Godínez-Salomón, M. A. Leyva and O. Solorza-Feria, *Int. J. Hydrogen Energy*, 2013, **38**, 12634–12639.

10 K. Ono, Y. Yasuda, K. Sekizawa, N. Takeuchi, T. Yoshida and M. Sudoh, *Electrochim. Acta*, 2013, **97**, 58–65.

11 S. Vesztergom, M. Ujvári and G. G. Láng, *Electrochim. Acta*, 2013, **110**, 49–55.

12 S. Tsuneyasu, K. Ichihara, K. Nakamura and N. Kobayashi, *Phys. Chem. Chem. Phys.*, 2016, **18**, 16317–16324.

13 S. Tsuneyasu, T. Ichikawa, K. Nakamura and N. Kobayashi, *ChemElectroChem*, 2017, **4**, 1731–1735.

14 A. Damjanovic, M. A. Genshaw and J. O. Bockris, *J. Phys. Chem.*, 1966, **70**, 3761–3762.

15 M. A. Genshaw, A. Damjanovic and J. O. Bockris, *J. Phys. Chem.*, 1967, **71**, 3722–3731.

16 A. Damjanovic, M. A. Genshaw and J. O. Bockris, *J. Electrochem. Soc.* , 1967, **114**, 466–472.

17 A. Damjanovic, M. A. Genshaw and J. O. Bockris, *J. Electrochem. Soc.*, 1967, **114**, 1107–1112.

18 L. S. Marcoux, R. N. Adams and S. W. Feldberg, *J. Phys. Chem.*, 1969, **73**, 2611–2614.

19 P. Krishnan, T.-H. Yang, S. G. Advani and A. K. Prasad, *J. Power Sources*, 2008, **182**, 106–111.

20 F. Jaouen, *J. Phys. Chem. C*, 2009, **113**, 15433–15443.

21 R. J. Fealy and J. I. Goldsmith, *J. Phys. Chem. C*, 2012, **116**, 13133–13142.

22 J. T. Maloy, K. B. Prater and A. J. Bard, *J. Phys. Chem.*, 1968, **72**, 4348–4350.

23 J. T. Maloy, *Comput. Chem. Instrum.*, 1972, **2**, 241–260.

24 N. E. Tokel-Takvoryan, R. E. Hemingway and A. J. Bard, *J. Am. Chem. Soc.*, 1973, **95**, 6582–6589.

25 K. Boto and A. J. Bard, *J. Electroanal. Chem.*, 1975, **65**, 945–962.

26 R. A. Marcus, *J. Chem. Phys.*, 1956, **24**, 966–978.

27 R. A. Marcus, *J. Chem. Phys.*, 1965, **43**, 2654–2657.

28 R. A. Marcus and N. Sutin, *Biochim. Biophys. Acta - Rev. Bioenerg.*, 1985, **811**, 265–322.

29 A. D. Osborne and G. Porter, *Proc. Roy. Soc., Ser. A*, 1953, **220**, 104.

30 C. Wohlfarth, in *Viscosity of Pure Organic Liquids and Binary Liquid Mixtures*, ed. M. D. Lechner, Springer Berlin Heidelberg, Berlin, Heidelberg, 2017, pp. 41–41.

31 E. Kerr, E. H. Doeven, G. J. Barbante, C. F. Hogan, D. J. Bower, P. S. Donnelly, T. U. Connell and P. S. Francis, *Chem. Sci.*, 2015, **6**, 472–479.

32 E. Kerr, E. H. Doeven, G. J. Barbante, C. F. Hogan, D. J. Hayne, P. S. Donnelly and P. S. Francis, *Chem. Sci.*, 2016, **7**, 5271–5279.

Chapter 5: Conclusions and Future Work

5.1 Conclusions

The overarching aim of the work described in this thesis was to explore new aspects of the phenomenon of electrogenerated chemiluminescence (ECL). The work addresses both fundamental issues, such as the investigation of the electron transfer kinetics of annihilation ECL reactions; and applied aspects, such as the development of new methodologies for bioanalytical ECL. Novel instrumentation was developed and innovative new approaches to conducting ECL measurements were developed. For example, rotating disk (RDE) and rotating ring disk (RRDE) apparatus were combined with ECL in unusual ways; and ECL-based analysis was streamlined by demonstrating that certain commonly used buffers could double as ECL co-reactants.

The work presented in Chapter 2 examined four so-called 'Good' buffers that possess aliphatic tertiary amine/ethanolamine groups as alternative, non-toxic co-reactants for $[Ru(bpy)_3]^{2+}$ ECL, with the prospect of simultaneously serving as the pH buffer and electrolyte within the aqueous environment. The results revealed these buffers could indeed be employed as multitasking reagents in ECL-based assays, using $[Ru(bpy)_3]^{2+}$ as the luminophore, over a wide pH range. Although the biological buffers give lower ECL intensities compared with TPA, this is compensated for by ease of sample preparation due to their higher aqueous solubility and the overall simplicity advantage of requiring fewer reagents. Moreover, their lower volatility and considerably lower toxicity allow for a safer and more environmentally friendly analysis and waste disposal. Therefore, although these buffers are not likely to replace traditional ECL co-reactants such as TPA, they do provide a useful alternative for certain applications where very low detection limits are not required.

The work presented in chapters 3 and 4 demonstrated the adaptation of RDE/RRDE methods for ECL measurements. This is a very unusual approach to ECL research which has only occasionally been explored in the past, however we showed that such measurements can offer great insights into the key steps of ECL mechanisms. Figure 5.1 shows the visible annihilation ECL emission of $Ru(bpy)_3(PF_6)_2$ under RRDE rotation. Detailed rotation rate studies were performed on the ECL generated from various co-reactant and annihilation ECL systems under rotation in organic media. The results presented showed that each annihilation and co-reactant ECL system studied, exhibited an unexpected phenomenon, a "critical RPM" where ECL intensities began to decrease although the limiting current continued to increase with rotation rate. In co-reactant ECL systems, observed ECL intensities decrease at rotation rates faster than the critical RPM due to the residence time of the radical cation of the co-reactant becoming so short that a key step in the ECL mechanism does not have time to occur. The faster the rotation rate of the working electrode, the less time the radical cation spends near the electrode surface where it can deprotonate and react with the oxidised luminophore.

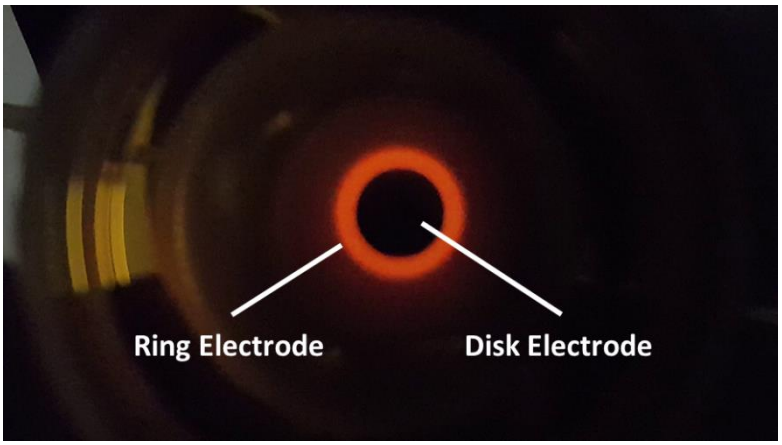

Figure 5.1: Light emission (at 2.0 V) from 0.2 mM $Ru(bpy)_3(PF_6)_2$ (in dry ACN with 0.1 M NBu_4PF_6) using a rotating ring disk electrode (rotating at 500 RPM). The ruthenium oxidation was held at the ring electrode and the ruthenium reductions were swept at the disk.

Similarly, in the annihilation ECL systems studied using rotating ring disk electrodes, a decrease in ECL intensity was observed at rotation rates faster than a critical RPM. This was attributed to the rate of removal of the oxidised luminophore state from the vicinity of the electrode surface before it had time to react with the reduced form of the luminophore. Thus, in both cases the rotation rate at which the maximum ECL intensity is obtained offers an insight into the kinetics of one of the key ECL reactions. Interestingly, while this phenomenon has never been previously observed, it was predicted on the basis of finite element simulations conducted by Bard's group in 1971.[1] In fact, using the calculations described in that paper we were able to estimate the rate constants for several annihilation ECL reactions.

Another interesting aspect of this work was the significant effect of the electrode polarity (i.e. whether the reduced or oxidised partner was generated at the ring or disk), of the RRDE on the annihilation ECL intensities observed from several systems. Also, for the first time, multiplexed annihilation ECL was generated from a RRDE system under rotation. Tuneable ECL was demonstrated from a mixture of $Ru(bpy)_3(PF_6)_2$ and $Ir(ppy)_3$.

5.2 Future Work

While we proposed four Good buffers that can serve as the co-reactant, buffer and electrolyte in ECL systems, there are over ten more buffers that could be investigated in the same way. Taking a step further, substituting these buffers as alternatives to other co-reactants in a wide range of ECL applications (i.e. immunoassay and DNA probe-based applications) can be further explored.

As there has been very little reported work on ECL emissions generated under rotation, further study on a wide range of co-reactant and annihilation ECL systems under rotation is required. More experiments are needed to help further understand the critical RPM phenomenon that occurs in the systems studied in chapters 3 and 4. It would desirable to expand this work to more co-reactant and annihilation ECL systems. Finite element simulations have come a long way since 1971, it would be of great interest to repeat the calculations of Bard *et al.* using modern methods and to expand them to co-reactant systems. This would facilitate the easy extraction of key kinetic parameters from ECL data conducted under conditions of electrode rotation. In particular, this might provide insights into unexplained aspects of the phenomenon, such as the apparent absence of a critical RPM in aqueous media.

Finally, more work to optimise and explore the tuneable multicolour ECL generated from rotated multiplexed ECL systems could lead to new fundamental insights and spur the development of new applications such as the measurement of biomarkers in immunodiagnostic testing.

5.3 References

1 J. T. Maloy, K. B. Prater and A. J. Bard, *J. Am. Chem. Soc.*, 1971, **93**, 5959–5968.

Supplementary

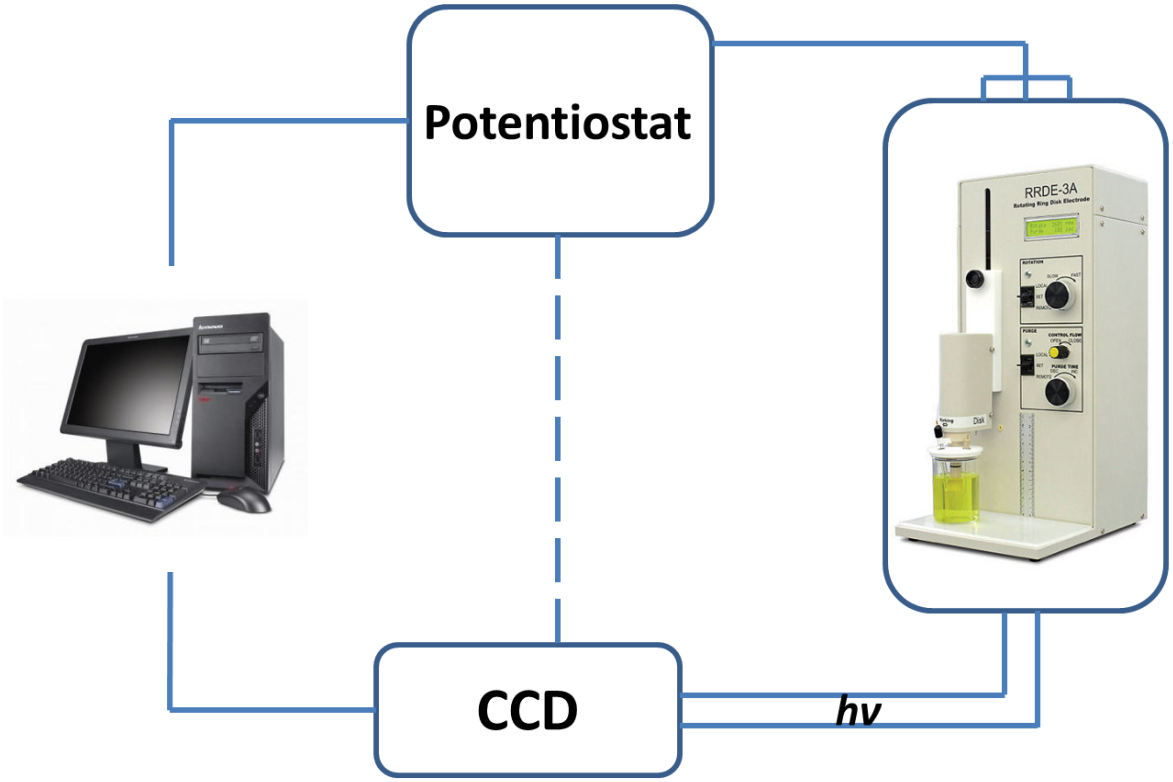

Figure S1: Simplified schematic of the RDE setup for ECL detection. The RDE sat inside a custom made dark box connected to a potentiostat, a custom made cell holder placed under the RDE was connected to a CCD via a fibre optic which sat directly underneath the electrochemical cell. The potentiostat (using software on the PC) would trigger the CCD to start capturing as soon as the potentiostat applied a potential

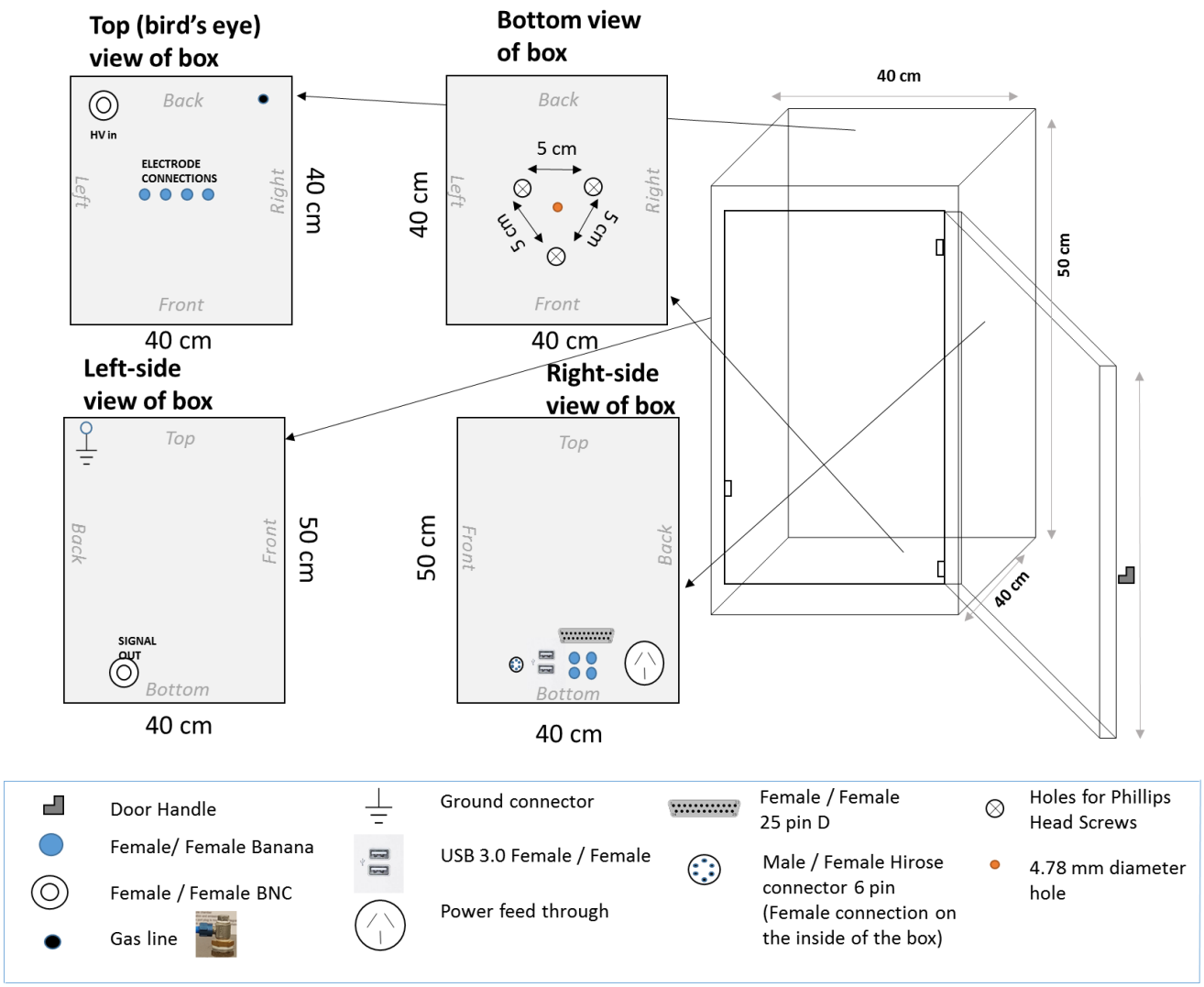

Figure S2: Schematic for the custom made light-tight faraday cage required to perform ECL experiments with an RDE/RRDE

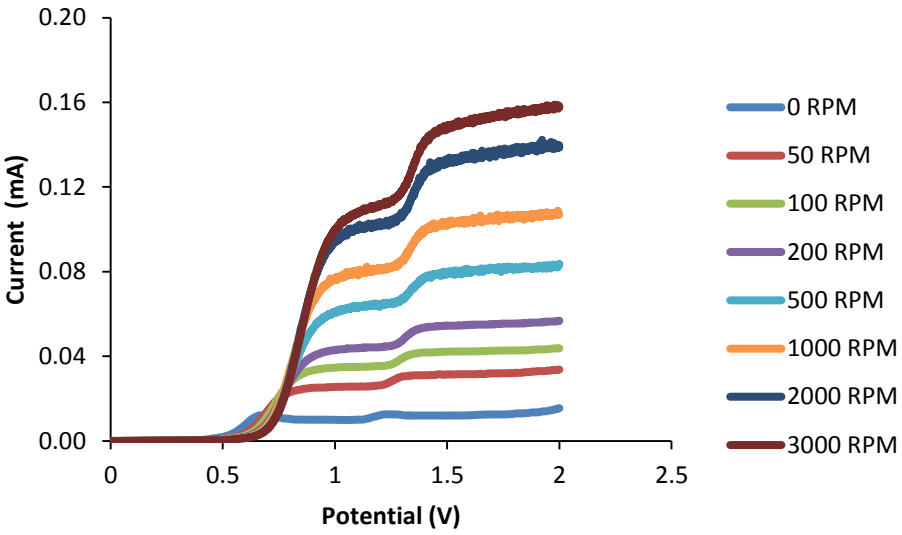

Figure S3: Voltammograms generated using the 0.2 mM $Ru(bpy)_3(PF_6)_2$/1 mM TPA co-reactant ECL system in dry ACN with 0.1 M NBu_4PF_6 at various rotation rates (0 – 3000 RPM)

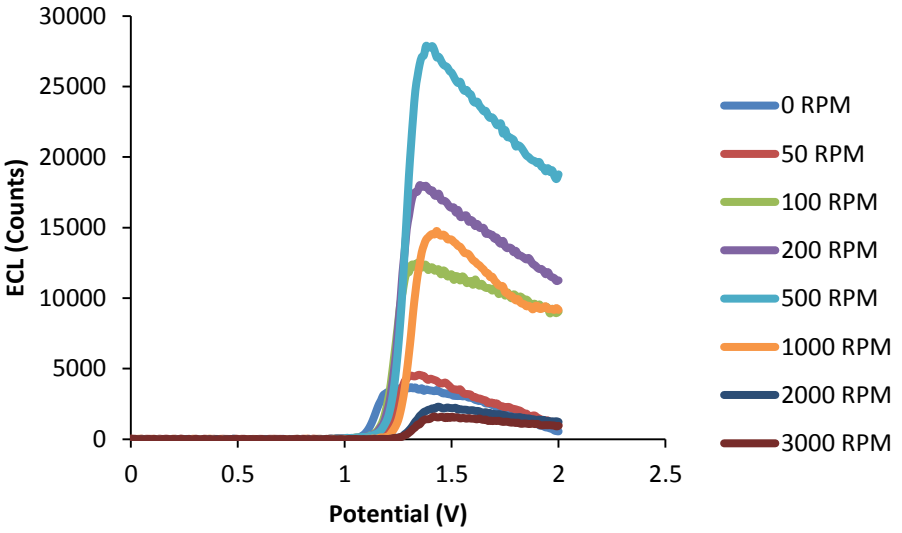

Figure S4: Voltammograms of the ECL intensities generated using the 0.2 mM $Ru(bpy)_3(PF_6)_2$/1 mM TPA co-reactant ECL system in dry ACN with 0.1 M NBu_4PF_6 at various rotation rates (0 – 3000 RPM)

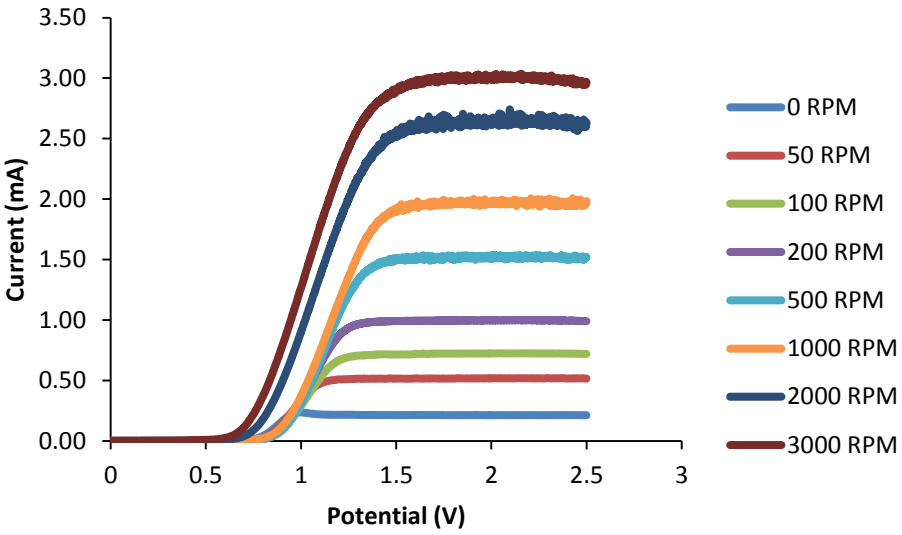

Figure S5: Voltammograms generated using the 0.2 mM $Ru(bpy)_3(PF_6)_2$/20 mM TPA co-reactant ECL system in dry ACN with 0.1 M NBu_4PF_6 at various rotation rates (0 – 3000 RPM)

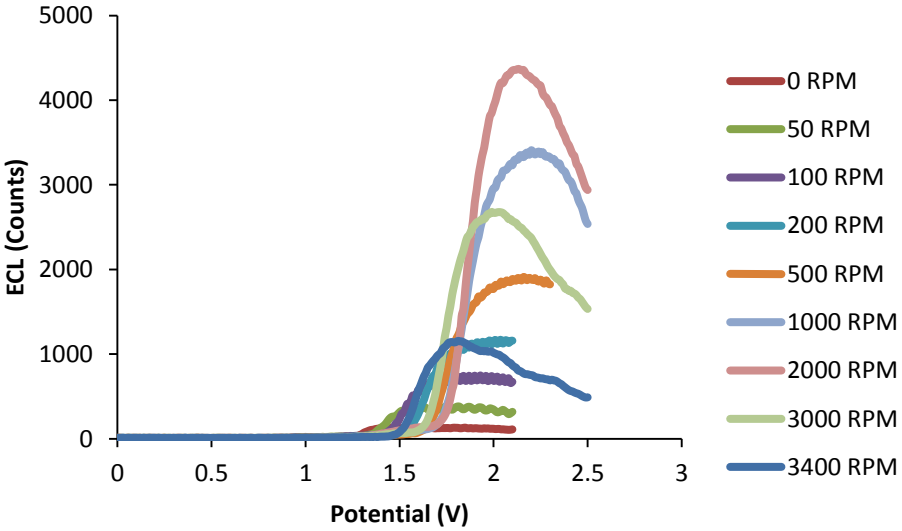

Figure S6: Voltammograms of the ECL intensities generated using the 0.2 mM $Ru(bpy)_3(PF_6)_2$/20 mM TPA co-reactant ECL system in dry ACN with 0.1 M NBu_4PF_6 at various rotation rates (0 – 3400 RPM)

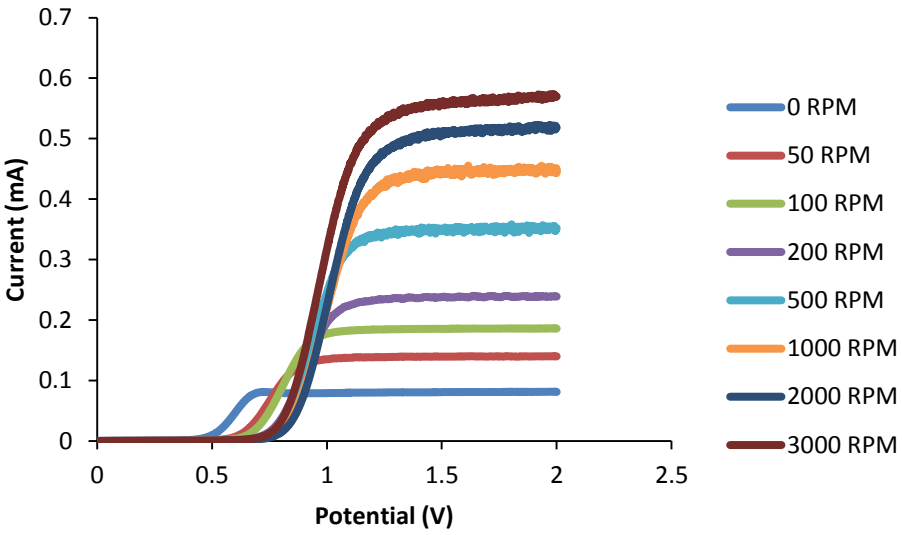

Figure S7: Voltammograms generated using the 0.05 mM $Ru(bpy)_3(PF_6)_2$/5 mM TPA co-reactant ECL system in dry ACN with 0.1 M NBu_4PF_6 at various rotation rates (0 – 3000 RPM)

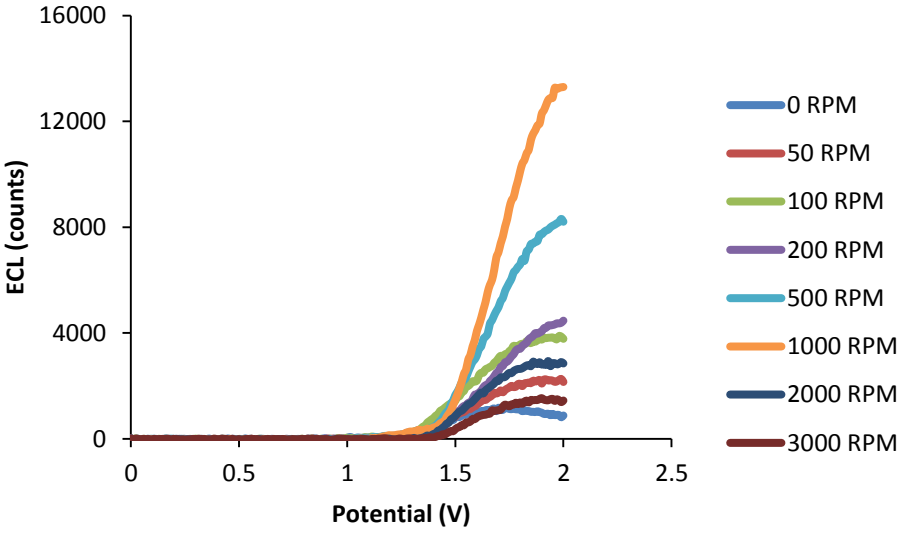

Figure S8: Voltammograms of the ECL intensities generated using the 0.05 mM $Ru(bpy)_3(PF_6)_2$/5 mM TPA co-reactant ECL system in dry ACN with 0.1 M NBu_4PF_6 at various rotation rates (0 – 3000 RPM)

Table S1: Average lifetimes of both the $Ir(ppy)_3$ and the multiplexed $Ru(bpy)_3(PF_6)_2/Ir(ppy)_3$ annihilation ECL systems. Average lifetime was calculated using $t_{av} = \Sigma B_i T_i^2 / \Sigma B_i T_i$ where t_{av} is the average lifetime, T_i is the lifetime obtained from the pre-exponential fitting and B_i is the pre-exponential factor for lifetime T_i

Compounds	Lifetime (μs)
Ru-Ir Multiplex	0.023
$Ir(ppy)_3$	0.022